

## REVIEW ARTICLE

# Extrinsic Magnetotransport Phenomena in Ferromagnetic Oxides

M Ziese <sup>‡</sup>

Department of Physics and Astronomy, University of Sheffield, Sheffield S3 7RH,  
United Kingdom

E-mail: ziese@physik.uni-leipzig.de

**Abstract.** Magnetic oxides show a variety of extrinsic magnetotransport phenomena: grain-boundary-, tunnelling- and domain-wall magnetoresistance. In view of these phenomena the role of some magnetic oxides is outstanding: these are believed to be half-metallic having only one spin-subband at the Fermi level. These fully spin-polarized oxides have great potential for applications in spin-electronic devices and have, accordingly, attracted an intense research activity in recent years.

This review is focused on extrinsic magnetotransport effects in ferromagnetic oxides. It consists of two parts; the second part is devoted to an overview of experimental data and theoretical models for extrinsic magnetotransport phenomena. Here a critical discussion of domain-wall scattering is given. Results on surfacial and interfacial magnetism in oxides are presented. Spin-polarized tunnelling in ferromagnetic junctions is reviewed and grain-boundary magnetoresistance is interpreted within a model of spin-polarized tunnelling through natural oxide barriers. The situation in ferromagnetic oxides is compared with data and models for conventional ferromagnets. The first part of the review summarizes basic material properties, especially data on the spin-polarization and evidence for half-metallicity. Furthermore, intrinsic conduction mechanisms are discussed. An outlook on the further development of oxide spin-electronics concludes this review.

PACS numbers: 72.20.My, 72.25.-b, 75.50.Cc

Submitted to: *Rep. Prog. Phys.*

<sup>‡</sup> Present address: Department of Superconductivity and Magnetism, University of Leipzig, Linnéstrasse 5, 04103 Leipzig, Germany

## Contents

<b>1</b>	<b>Introduction</b>	<b>4</b>
<b>Part 1: Preliminaries: Materials and intrinsic magnetotransport properties</b>		<b>7</b>
<b>2</b>	<b>Materials, half-metallicity and spin-polarization</b>	<b>7</b>
2.1	Overview of the materials . . . . .	7
2.2	Spin-polarization and half-metallicity . . . . .	11
<b>3</b>	<b>Intrinsic conductivity and optical properties</b>	<b>16</b>
3.1	$\text{SrRuO}_3$ . . . . .	18
3.2	$\text{Tl}_2\text{Mn}_2\text{O}_7$ . . . . .	20
3.3	$\text{CrO}_2$ . . . . .	22
3.4	$\text{La}_{0.7}\text{A}_{0.3}\text{MnO}_3$ . . . . .	24
3.4.1	Resistivity and phase diagram. . . . .	24
3.4.2	Theoretical models. . . . .	26
3.4.3	Optical properties. . . . .	38
3.5	$\text{Sr}_2\text{FeMoO}_6$ . . . . .	39
3.6	$\text{Fe}_3\text{O}_4$ . . . . .	42
<b>4</b>	<b>Intrinsic magnetoresistance</b>	<b>44</b>
4.1	$\text{SrRuO}_3$ . . . . .	44
4.2	$\text{Tl}_2\text{Mn}_2\text{O}_7$ . . . . .	44
4.3	$\text{CrO}_2$ . . . . .	45
4.4	$\text{La}_{0.7}\text{A}_{0.3}\text{MnO}_3$ . . . . .	46
4.4.1	Colossal magnetoresistance. . . . .	46
4.4.2	Anisotropic magnetoresistance. . . . .	48
4.5	$\text{Fe}_3\text{O}_4$ . . . . .	49
<b>Part 2: Extrinsic magnetotransport phenomena</b>		<b>51</b>
<b>5</b>	<b>Domain-wall scattering</b>	<b>51</b>
5.1	Elemental ferromagnets . . . . .	51
5.2	Magnetic oxides . . . . .	56
<b>6</b>	<b>Surface and interface properties</b>	<b>60</b>
6.1	Oxide-vacuum interface . . . . .	60
6.2	Theoretical results . . . . .	63
6.3	Oxide-metal interface . . . . .	66
6.4	Ferromagnet-superconductor hybrids . . . . .	67
6.5	Exchange biasing, multilayers and GMR . . . . .	70
6.6	Oxide-semiconductor interfaces . . . . .	72

<b>7</b>	<b>Ferromagnetic tunnelling junctions</b>	<b>72</b>
7.1	Basic theory . . . . .	72
7.2	Model systems . . . . .	75
7.3	Temperature and voltage dependence . . . . .	77
7.4	Oxide tunnelling junctions . . . . .	80
7.5	Barriers and band-structure . . . . .	88
7.6	Current-induced switching of the magnetization . . . . .	92
7.7	Intrinsic tunnelling in layered manganites . . . . .	94
<b>8</b>	<b>Grain-boundary junctions</b>	<b>95</b>
8.1	Basic theory: granular metals . . . . .	96
8.2	Experimental data on grain-boundary junctions . . . . .	99
8.2.1	Are polycrystalline manganite samples classical granular metals? . . . . .	99
8.2.2	Polycrystalline materials. . . . .	99
8.2.3	Bi-crystal junctions. . . . .	103
8.2.4	Step-edge junctions. . . . .	103
8.2.5	Laser-patterned junctions. . . . .	105
8.3	General characteristics and models . . . . .	105
8.4	Other ferromagnetic oxides . . . . .	113
8.4.1	Polycrystalline material. . . . .	113
8.4.2	Controlled defect structures. . . . .	115
<b>9</b>	<b>Summary, Conclusions and Outlook</b>	<b>116</b>
	<b>References</b>	<b>119</b>

## 1. Introduction

Although the study of magnetoresistance in ferromagnets started as early as 1857 with the measurements of anisotropic magnetoresistance in nickel and iron by William Thomson (Lord Kelvin), recent years have witnessed a tremendous interest into magnetotransport phenomena in magnetic oxides. Studies were stimulated by the discovery of “colossal magnetoresistance” (CMR) in ferromagnetic perovskites of the type  $\text{La}_{1-x}\text{Sr}_x\text{MnO}_3$ . The so-called manganites display a rich phase diagram as a function of temperature, magnetic field and doping that is due to the intricate interplay of charge, spin, orbital and lattice degrees of freedom. Colossal magnetoresistance is found on a magnetic field scale of several Teslas being not very appealing for applications. Accordingly, many research groups focused on the investigation of extrinsic magnetoresistance effects found in various magnetic oxides, since these promised a large magnetoresistance ratio in low magnetic fields. To a large extent this research is driven by the rapid increase of data storage density in magnetic storage devices. Since read heads for hard disks employ magnetoresistive read-out techniques, progressive miniaturization of sensors requires materials or heterostructures with increasing magnetoresistive effect. The development of hard disk storage media is currently very rapid with a doubling of storage density about every nine months. Therefore, the need for more efficient magnetoresistive sensors will persist in the future. It has to be clear that room temperature performance is the most vital criterion in judging new magnetoresistive materials.

In this review intrinsic and extrinsic magnetoresistive effects are distinguished. Whereas intrinsic effects are found in the bulk of the ferromagnetic material and are determined by material parameters, extrinsic effects are only found at defect structures, in suitable artificial heterostructures and devices. This distinction is not unique, since impurity scattering plays a vital role in some of the effects and is per se an extrinsic effect.

Extrinsic magnetotransport effects in ferromagnetic oxides fall into three broad classes, namely grain-boundary magnetoresistance, spin-polarized transport in ferromagnetic tunnelling junctions and domain-wall magnetoresistance. It was realized that manganite samples containing a large number of extended defects such as grain boundaries display a huge low field magnetoresistance much larger than the intrinsic magnetoresistance (Hwang *et al* 1996, Gupta *et al* 1996). Various samples have been studied, namely polycrystalline ceramics and films, pressed powders, single grain boundaries on bi-crystal substrates, scratched substrates, step-edge and laser-patterned junctions. The extrinsic effect therefore appears under various names such as grain-boundary magnetoresistance, junction magnetoresistance (JMR) and powder magnetoresistance (PMR). However, the basic physical mechanism behind these phenomena appears to be the same. This mechanism is likely to be spin-polarized tunnelling, although a final consensus on the interpretation of grain boundary magnetoresistance has not yet been reached; this conclusion links

the investigations of transport properties near extended defects to another class of extrinsic magnetoresistance: spin-polarized tunnelling in heterostructures. Such a heterostructure consists of two ferromagnetic layers separated by an insulating layer. The tunnelling current is found to depend sensitively on the relative magnetization direction in the ferromagnetic electrodes. This is related to the spin-dependent density of states at the Fermi level. It is useful to define a spin-polarization at the Fermi level that quantifies the spin-imbalance in itinerant ferromagnets; the elemental ferromagnets Fe, Co and Ni have spin-polarizations of 45%, 42% and 31%, respectively. Spin-polarized tunnelling in a thin film heterostructure and the basic theory was first discussed by Julliere (1975). However, an even earlier work on magnetic tunnelling junctions using manganite electrodes was reported by van den Brom and Volger (1968). Early experiments yielded only small magnetoresistive effects and the reproducibility of the junctions was poor. A breakthrough was achieved by the work of Moodera *et al* (1995) reporting magnetoresistance ratios in excess of 20% in permalloy/ $\text{Al}_2\text{O}_3$ /CoFe junctions at low temperature in agreement with Julliere's model; at room temperature effects of about 10% were recorded. Experimental work on manganite tunnelling junctions started at about the same time (Sun *et al* 1996). These studies were stimulated by band-structure calculations that indicated the half-metallic nature of ferromagnetic manganite oxides.

The concept of a half-metal was introduced by de Groot *et al* (1983) motivated by band-structure calculations of Mn-based Heusler alloys; a half-metal is defined as having a metallic density of states in one of the spin channels and a gap in the density of states in the other spin channel; within any reasonable definition of spin-polarization this corresponds to a spin-polarization value of 100%. The concept of spin-polarization is central to the theory of spin-polarized tunnelling; the only parameters entering Julliere's model for the tunnelling magnetoresistance are the spin-polarizations of the ferromagnetic electrodes; in the case of half-metallic metals the magnetoresistance ratio is expected to reach 100%. This is intuitively clear, since in the absence of spin-flips, a tunnelling current cannot flow between half-metallic electrodes with antiparallel magnetization directions, since there is no density of states at the Fermi level of the other electrode into which electrons could be tunnelling. Therefore, spin-polarized tunnelling in heterostructures using half-metallic electrodes is promising for applications and, at the same time, theoretically challenging, since the dependence of the tunnelling current on the band structure and barrier properties is not yet fully understood. The first experiments on manganite-insulator-manganite tunnelling junctions showed large magnetotunnelling effects at low temperatures (Lu *et al* 1996). The magnetoresistance ratio, however, decreases rapidly with temperature. A future experimental challenge is the achievement of a huge room temperature magnetoresistance in magnetic oxide heterostructures. Apart from the manganites,  $\text{CrO}_2$ , magnetite ( $\text{Fe}_3\text{O}_4$ ) and  $\text{Sr}_2\text{MoFeO}_6$  are suspected to be half-metallic magnets and are investigated in view of device applications.

A long-standing problem is the question of the magnetoresistance of a domain wall.

Within a domain the magnetization vector and therefore the majority and minority currents have spatially independent orientations. Accordingly, when charge carriers cross a domain wall, majority electrons may end up in the minority channel and vice versa leading to an additional magnetoresistance. An obvious measure of the scattering efficiency of a domain wall is the ratio between the time of passage through the domain wall and the precession period of the spin around the exchange field. In the adiabatic limit scattering effects are likely to be small, whereas these are expected to become appreciable in the ballistic regime.

This review is divided into two parts. The first part starts with a brief overview over the materials as well as the definition and measurement of the spin-polarization in section 2. Section 3 deals with the temperature dependent resistivity and the optical conductivity, whereas the intrinsic magnetoresistance is analyzed in section 4. These sections were included in order to elucidate the basic models for magnetotransport in the relevant oxides and to facilitate comparison with and identification of extrinsic magnetotransport phenomena. The presentation is restricted to a discussion of resistivity as the basic transport coefficient and does not include other valuable transport coefficients such as thermopower, Hall effect, etc. This is due to space limitations and the idea to use this review as a handbook in the evaluation of resistivity behaviours encountered in studies of magnetic oxides. In the second part extrinsic magnetotransport phenomena are reviewed. An overview of recent developments in the study of domain-wall scattering in both elemental ferromagnets and the manganites is given in section 5. Section 6 presents a discussion of various interface properties between magnetic oxides and normal metals, superconductors and conventional ferromagnets. Sections 7 and 8 contain the main experimental data and theoretical models relating to spin-polarized tunnelling and grain-boundary magnetoresistance, respectively. In the section on spin-polarized tunnelling appropriate room is given to the discussion of recent results for tunnelling junctions made from elemental ferromagnets in order to constitute background information for the discussion of the oxide magnets. The discussion of grain-boundary magnetoresistance concentrates on magnetic oxides, since grain-boundaries of elemental ferromagnets do not form junctions with tunnelling-like characteristics. In section 9 a summary of significant results and an outlook into the budding field of spin-electronics is given.

The bulk of recent investigations on the magnetotransport properties of oxides deals with CMR materials. The number of publications on this subject grows exponentially and it is virtually impossible to write a fully comprehensive review. Therefore, it might be helpful to point out some review articles on related topics. An excellent and extensive review on the physical properties of mixed-valence manganites was written by Coey, Viret and von Molnár (1999); this review is mainly focused on intrinsic properties. Two further extensive reviews on intrinsic conduction mechanisms by Dagotto, Hotta and Moreo (2001) and Nagaev (2001) focused on phase separation and the magnetopurity theory, respectively. Short reviews on experimental work and the basic theory of colossal magnetoresistance were published by Ramirez (1997), Fontcuberta (1999) and Tokura

and Tomioka (1999). Jaime and Salamon (1999) discussed intrinsic transport properties of the manganites and Lyanda-Geller *et al* (2001) Hall effect studies. The broad field of metal-insulator transitions was addressed by Imada, Fujimori and Tokura (1998). An overview of investigations on extrinsic magnetoresistance was compiled by Gupta and Sun (1999). A review of theoretical studies of double exchange systems was given by Furukawa (1998). Ziese (2000a) reviewed recent developments of oxide spin-electronics. A review on spin-dependent transport in magnetic nanostructures covering a few results on oxides was given by Ansermet (1998). Readers interested in spin-polarized tunnelling in conventional metallic systems are referred to Moodera and Mathon (1999). A comprehensive survey of spintronics can be found in the book “Spin Electronics” edited by M Ziese and M J Thornton.

## **Preliminaries: Materials and intrinsic magnetotransport properties**

### **2. Materials, half-metallicity and spin-polarization**

#### *2.1. Overview of the materials*

Ferro- and ferrimagnetic oxides that are thought to be half-metallic are the most interesting class of materials for the study of extrinsic magnetotransport phenomena. In this section the definitions of half-metallicity and spin-polarization are reviewed; some measurements of the spin-polarization using various techniques are discussed and compared. First, however, a brief overview of materials is given (crystal structures are shown in figure 1):

- (i) The colossal magnetoresistance manganites of the form  $\text{RE}_{1-x}\text{A}_x\text{MnO}_3$  have attracted most of the research efforts. RE stands for a rare earth ion such as La, Nd, Pr or Gd and A denotes a divalent ion such as Ca, Sr or Ba. The manganites crystallize in the perovskite structure, see figure 1a. Depending on doping, these compounds show a complex magnetic phase diagram, see Coey *et al* (1999). Ferromagnetism is found in the doping range  $0.15 < x < 0.5$  and, in view of an understanding of extrinsic magnetotransport, this review will be restricted to the discussion of the magnetic and transport properties of manganites in this range. The highest Curie temperatures are found in the archetypal compound  $\text{La}_{1-x}\text{A}_x\text{MnO}_3$  at a doping level  $x \sim 1/3$  with  $T_C$  of 270 K (Ca substitution), 360 K (Sr) and 330 K (Ba). The manganites show a metal-insulator transition accompanying the ferromagnetic transition. Ferromagnetic order in the mixed-valence manganites is induced by the double exchange mechanism proposed by Zener (1951). The intrinsic resistivity and magnetoresistance will be discussed in later sections. Replacing Mn by Co, Ni, Fe, ... leads to related families of oxides, see Goodenough and Longo. Especially the cobaltites show an appreciable magnetoresistance, see e.g. Yamaguchi *et al* (1995) for single crystal work. These oxides will not be discussed here, since extrinsic magnetoresistance effects have not

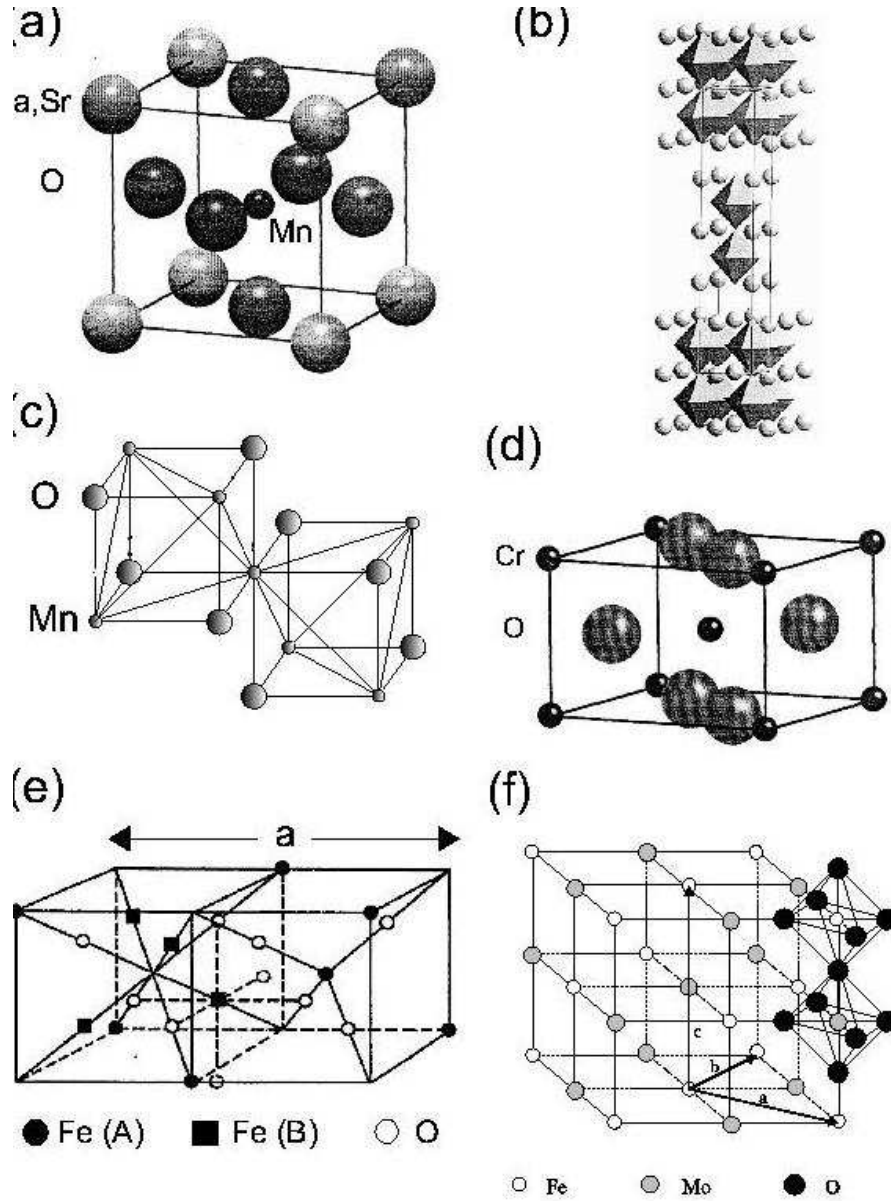


**Figure 1.** Crystal structures of the most important oxides discussed in this review: (a) perovskite structure ( $\text{La}_{0.7}\text{Sr}_{0.3}\text{MnO}_3$ ), (b)  $n = 2$  Ruddlesden-Popper phase ( $\text{La}_{1.2}\text{Sr}_{1.8}\text{Mn}_2\text{O}_7$ ,  $\text{MnO}_6$  octahedra are shaded, La/Sr ions are drawn as spheres), (c) pyrochlore structure ( $\text{Ti}_2\text{Mn}_2\text{O}_7$ ); (d) rutile structure ( $\text{CrO}_2$ ), (e) inverse spinel structure ( $\text{Fe}_3\text{O}_4$ , for clarity only a quarter of the unit cell is shown) and (f) double perovskite structure ( $\text{Sr}_2\text{FeMoO}_6$ ).

been studied in these.

- (ii) The Ruddlesden-Popper family of compounds  $(\text{RE}, \text{A})_{n+1}\text{Mn}_n\text{O}_{3n+1}$  (Moritomo *et al* 1996, Kimura *et al* 1996, Battle *et al* 1996, 1998) crystallize in a tetragonal structure consisting of vertex sharing  $\text{MnO}_6$  octahedra infinitely extending in the  $ab$ -plane and having a thickness of  $n$  octahedra along the  $c$ -axis, see figure 1b. Neighbouring layers are separated by a rock-salt layer consisting of  $(\text{RE}, \text{A})_2\text{O}_2$ . The manganites



can be regarded as the  $n = \infty$  member of the Ruddlesden-Popper series. The  $n = 1$  member  $\text{La}_{0.5}\text{Sr}_{1.5}\text{MnO}_4$  shows charge ordering on the Mn sublattice, but a significant magnetoresistance was not observed (Sternlieb *et al* 1996). A colossal magnetoresistance near the Curie temperature of 126 K was found, however, in the  $n = 2$  compound  $\text{La}_{1.2}\text{Sr}_{1.8}\text{Mn}_2\text{O}_7$  (Moritomo *et al* 1996). This compound is metallic at low temperatures and semiconducting at higher temperatures similar to the CMR materials. The  $n = 2$  compound  $\text{Nd}_{1+2x}\text{Sr}_{2-2x}\text{Mn}_2\text{O}_7$  shows a large magnetoresistance, but ferromagnetism was reported to be absent (Battle *et al* 1996). The Ruddlesden-Popper compounds have low Curie temperatures not exceeding 150 K and are, for this reason, not especially interesting for the fabrication of devices. The  $n = 2$  compound  $\text{La}_{2-2x}\text{Sr}_{1+2x}\text{Mn}_2\text{O}_7$ , however, shows an interesting anisotropy in the magnetoresistance that might be related to an intrinsic tunnelling effect. This is further discussed in section 7.

- (iii)  $\text{Tl}_2\text{Mn}_2\text{O}_7$  crystallizes in the pyrochlore structure (figure 1c); this compound also shows a metal insulator-transition and a large intrinsic magnetoresistance (Shimakawa *et al* 1996, 1997) near the Curie temperature of about 140 K. In contrast to the manganites, however, the carrier density is low and the ferromagnetism arises from the super-exchange interaction between  $\text{Mn}^{4+}$  ions. Majumdar and Littlewood (1998a, 1998b) developed a model for the magnetotransport properties of the pyrochlore based on the assumption of a low density electron gas coupled to spin fluctuations. The transport properties of  $\text{Tl}_2\text{Mn}_2\text{O}_7$  will be discussed in more detail in section 3.
- (iv)  $\text{CrO}_2$  is a ferromagnet with a Curie temperature of about 390 K. It crystallizes in the rutile structure, see figure 1d. This oxide is metallic both above and below the Curie temperature; the resistivity and magnetoresistance are discussed in later sections.
- (v) Magnetite,  $\text{Fe}_3\text{O}_4$ , is a ferrimagnetic oxide crystallizing in the inverse spinel structure (figure 1e) and has the highest Curie temperature,  $T_C = 858$  K, of the magnetic oxides discussed here. It is therefore often viewed as an ideal candidate for room temperature applications. The temperature dependence of the resistivity is quite complex, changing from semiconducting to metallic behaviour slightly above room temperature and back to semiconducting behaviour near the Curie temperature. The low temperature resistivity and magnetoresistance will be discussed in later sections.
- (vi)  $\text{Sr}_2\text{FeMoO}_6$  and  $\text{Sr}_2\text{FeReO}_6$  are double perovskite ferromagnets with comparatively high Curie temperatures of about 420 K and 400 K, respectively (Kobayashi *et al* 1998, 1999, Manako *et al* 1999). The structure is obtained by doubling the perovskite unit cell, see figure 1f. Cation pairs (Fe,Mo), (Fe,Re) order in a rock-salt-like fashion. These compounds were investigated in the sixties and seventies (Longo and Ward 1961, Sleight *et al* 1962, 1972, Abe *et al* 1973); interest in these has been revived, since band-structure calculations indicated a half-metallic state (Kobayashi

*et al* 1998, 1999). Often a metallic behaviour of the resistivity is observed (Manako *et al* 1999, Kobayashi *et al* 1999, Asano *et al* 1999); the resistivity, however, depends sensitively on the preparation conditions such as annealing and film growth parameters and semiconducting behaviour is sometimes reported (Kobayashi *et al* 1999, Asano *et al* 1999). The magnetic and transport properties will be further discussed in section 3.

- (vii)  $\text{SrRuO}_3$  is a metal that undergoes a ferromagnetic transition at 165 K (Callaghan *et al* 1966, Longo *et al* 1968, Cao *et al* 1997). It crystallizes in an orthorhombic structure.  $\text{SrRuO}_3$  is regarded as a strongly-correlated  $d$ -band metal (Klein *et al* 1996, Cao *et al* 1997, Fujioka *et al* 1997, Okamoto *et al* 1999) that falls into the class of “bad metals” (Emery and Kivelson 1995). A “bad metal” is defined as having an unsaturated resistivity with positive temperature coefficient that exceeds the Ioffe-Regel limit. The ferromagnetism in  $\text{SrRuO}_3$  is of itinerant character. The intrinsic resistivity and magnetoresistance will be discussed in this review in order to facilitate comparison with the other magnetic oxides.
- (viii) There are reports on the resistivity and magnetoresistance of  $\text{CaCu}_3\text{Mn}_4\text{O}_{12}$  (Zeng *et al* 1999) with  $T_C$  of 355 K,  $\text{Na}_{0.5}\text{Ca}_{0.5}\text{Cu}_{2.5}\text{Mn}_{4.5}\text{O}_{12}$  (Zeng *et al* 1998) with  $T_C$  of 340 K as well as  $\text{TbCu}_3\text{Mn}_4\text{O}_{12}$  ( $T_C = 430$  K) and  $\text{CaCu}_{1.5}\text{Mn}_{5.5}\text{O}_{12}$  (Troyanchuk *et al* 1998). Whereas Zeng *et al* (1998, 1999) describe the compounds as ferromagnetic, Troyanchuk *et al* (1998) interpret magnetization data as consistent with ferrimagnetic order. All compounds show a gradual decrease of the magnetoresistance in large applied fields from some 10% at low temperature to zero above  $T_C$ . Since these compounds are not important in device fabrication, these will not be further discussed in this review.
- (ix) The chalcogenides  $\text{Fe}_{1-x}\text{Cu}_x\text{Cr}_2\text{S}_4$  show a moderate magnetoresistance near the Curie temperature (Ramirez *et al* 1997, Yang *et al* 2000). Theoretical studies of the electronic structure indicate a half-metallic nature with a gap in the minority density of states (Park *et al* 1999). Since this review is focused on oxides, the interested reader is referred to the original reports.
- (x) Stimulated by the intense research on both giant and colossal magnetoresistance, there have been reports on magnetoresistive phenomena in various compounds that do not fall in the classes described above. Here only three reports are mentioned, namely the observation of a large positive magnetoresistance in  $\text{Ag}_2\text{Se}$  and  $\text{Ag}_2\text{Te}$  (Xu *et al* 1997, Chuprakov and Dahmen 1998) as well as in the ferromagnetic multilayer  $\text{LaMn}_2\text{Ge}_2$  (Mallik *et al* 1997). A discussion of these compounds is beyond the scope of this review.
- (xi) At the end of this list of materials and compounds the case of  $\text{GdI}_2$  should be mentioned.  $\text{GdI}_2$  shows a ferromagnetic transition close to room temperature; this transition is accompanied by a metal-insulator transition and negative colossal magnetoresistance, see Ahn *et al* (2000). This observation is especially intriguing, since  $\text{GdI}_2$  is nominally isoelectronic to the superconductor  $\text{NbSe}_2$ . In the

colossal magnetoresistance manganites the situation is similar: substitution of the magnetically active Mn by Cu leads from ferromagnetism in  $\text{La}_{1-x}\text{Sr}_x\text{MnO}_3$  to superconductivity in  $\text{La}_{2-x}\text{Sr}_x\text{CuO}_4$ . It would be interesting to search for similar trends in other material classes that might establish an underlying generic pattern.

## 2.2. Spin-polarization and half-metallicity

A quantity of fundamental interest for both basic physics and device applications is the degree of spin-polarization  $P$  at the Fermi level. The band-structure of ferromagnets is spin-dependent and two subbands are found for majority (carrier spin directed parallel to the magnetization) and minority (spin antiparallel to the magnetization) carriers, respectively (see Chikazumi 1997). The schematic density of states of a strong ferromagnet is shown in figure 2(a); here the majority  $d$  bands are completely filled. In the case of an itinerant ferromagnet, within a two-band model, the spin-polarization is often defined as the normalized difference of the majority ( $n_\uparrow$ ) and minority ( $n_\downarrow$ ) density of states at the Fermi level, thus

$$P_n = \frac{n_\uparrow - n_\downarrow}{n_\uparrow + n_\downarrow}. \quad (1)$$

This definition is somehow related to the definition of the magnetization as the difference between the integrated majority and minority carrier density,  $M = \mu_B \int (n_\uparrow - n_\downarrow) dE$ , and often a scaling  $P(T) \propto M(T)$  is expected. The spin-polarization defined in this way might be probed by spin-polarized photoemission.

However, as pointed out by Mazin (1999), the definition of spin-polarization is by no means unique. Often transport properties are of interest, especially for applications. In a ferromagnet the majority and minority carriers can be regarded as two parallel transport channels, see Mott (1936), Campbell and Fert (1982), and a definition of the spin-polarization in terms of the majority ( $J_\uparrow$ ) and minority ( $J_\downarrow$ ) current densities seems more appropriate. Within classical Boltzmann transport theory,  $J_{\uparrow(\downarrow)} \propto \langle nv^2 \rangle_{\uparrow(\downarrow)} \tau_{\uparrow(\downarrow)}$ , where  $\langle \dots \rangle$  denotes a Fermi-surface average and  $\tau_{\uparrow(\downarrow)}$  the relaxation times for majority and minority carriers, respectively. Assuming a spin-independent relaxation time, one finds

$$P_J = \frac{J_\uparrow - J_\downarrow}{J_\uparrow + J_\downarrow} = \frac{\langle nv^2 \rangle_\uparrow - \langle nv^2 \rangle_\downarrow}{\langle nv^2 \rangle_\uparrow + \langle nv^2 \rangle_\downarrow}. \quad (2)$$

This definition is fundamentally different from the definition in terms of the carrier densities. In the case of Ni and Fe, Mazin (1999) showed that within local spin density approximation (LSDA) calculations, these definitions lead to significantly different values of the spin-polarization.

Within the two-current model, the spin-polarization defined by the majority and minority currents can be simply related to the majority ( $\rho_\uparrow$ ) and minority ( $\rho_\downarrow$ ) resistivities:

$$P_J = \frac{\rho_\downarrow - \rho_\uparrow}{\rho_\downarrow + \rho_\uparrow}. \quad (3)$$

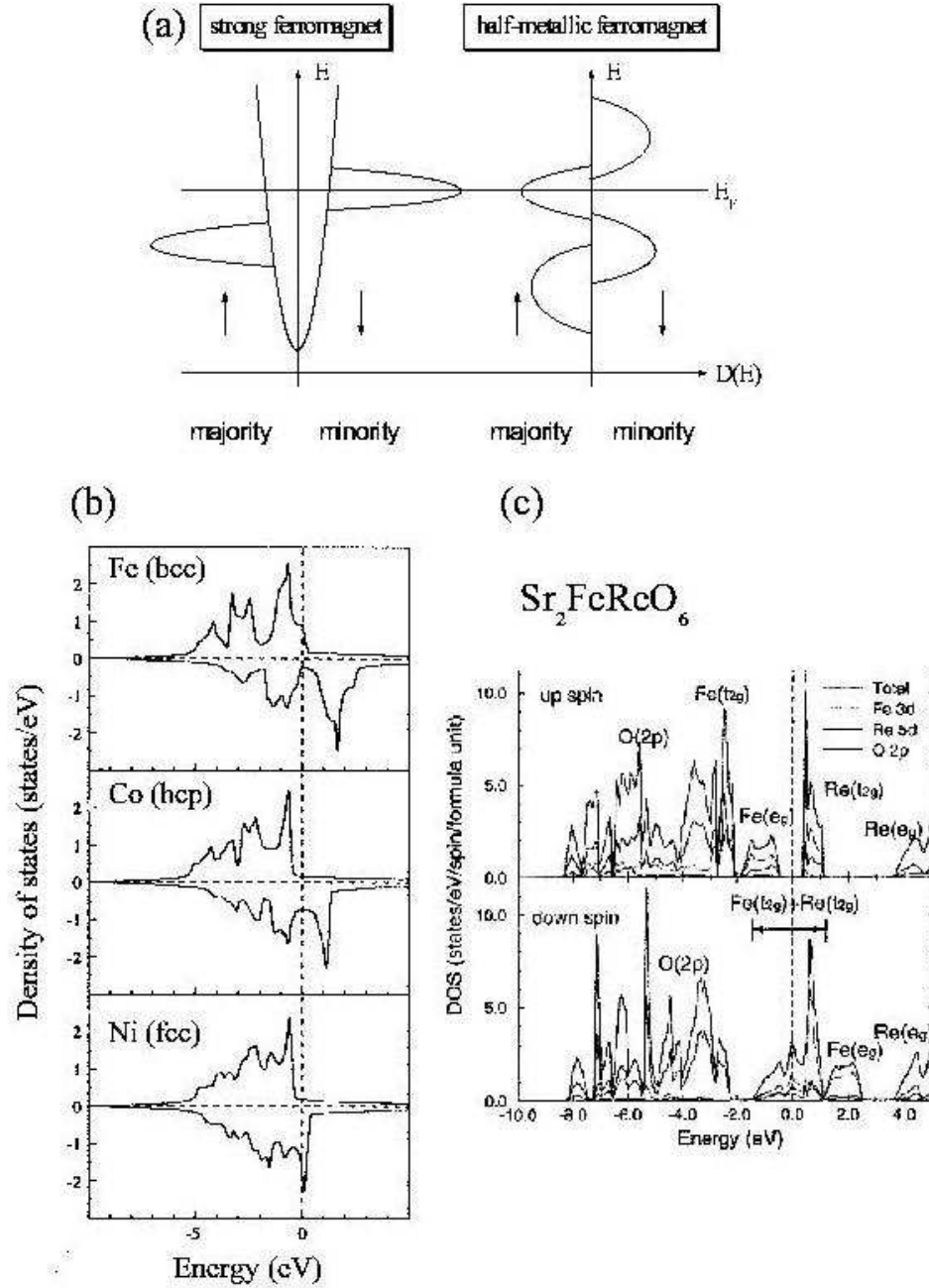


**Figure 2.** (a) Schematic density of states of a strong ferromagnet and a half-metallic ferromagnet. (b) Density of states of the elemental ferromagnets Fe, Co and Ni. Co and Ni are strong ferromagnets, Fe is a weak ferromagnet and shows a significant *d* state contribution in the majority spin channel. Adapted from Coey (2001). (c) Density of states of  $\text{Sr}_2\text{FeReO}_6$  as determined by calculations within the local density approximation (LDA).  $\text{Sr}_2\text{FeReO}_6$  is a half-metallic ferromagnet with a gap in the majority density of states. Adapted from Kobayashi *et al* (1999).

The channel resistivities can be determined at low temperature from deviations of Matthiesen's rule (Fert and Campbell 1968, Campbell and Fert 1982). These depend on the impurities present in the metal and consequently the spin-polarization can be tuned by alloying. According to Campbell and Fert (1982) the ratio of the intrinsic

resistivities  $\mu = \rho_{\downarrow}/\rho_{\uparrow}$  characteristic for the host material is  $\mu \simeq 3.6$  in Ni and  $\mu \simeq 1$  in Fe. This yields spin-polarization values  $P_J \simeq 0.56$  (Ni) and  $P_J \simeq 0$  (Fe). In contrast, the spin-polarization values at the Fermi level as calculated by Mazin (1999) are  $P_J \simeq 0$  (Ni) and  $P_J \simeq 0.2$  (Fe). Ziese (2000b) and Zhao *et al* (2001) tried to develop bulk probes for half-metallicity in  $\text{La}_{0.7}\text{Ca}_{0.3}\text{MnO}_3$  using the anisotropic magnetoresistance and the temperature dependence of the resistivity, respectively. Both experiments were consistent with a half-metallic character of the compound.

The archetypal experiments capable of determining the transport spin-polarization are spin-polarized tunnelling between ferromagnetic contacts and dynamic conductance of superconductor-ferromagnet contacts. Mazin (1999) analyzed transport through a superconductor-ferromagnet contact. In the case of ballistic transport without a barrier, the current through the contact is proportional to  $\langle nv \rangle$ ; thus, the ballistic spin-polarization is defined by

$$P_v = \frac{\langle nv \rangle_{\uparrow} - \langle nv \rangle_{\downarrow}}{\langle nv \rangle_{\uparrow} + \langle nv \rangle_{\downarrow}} \quad (4)$$

and does not agree with the spin-polarization Eq. (2) defined via the currents. If a specular barrier is present, the tunnelling current depends in a more complex way on both the Fermi velocity and the barrier transparency, and the measured spin-polarization does not agree with any of the definitions introduced so far. This analysis shows that experimental values obtained with different techniques relate to different definitions of the spin-polarization that need not necessarily agree.

The concept of half-metallicity was introduced by de Groot *et al* (1983) on the basis of band-structure calculations of Heusler alloys. These calculations showed a gap in the density of states of minority carriers. Half-metallicity is an independent particle concept and the inclusion of many-body-effects leads to the appearance of non-quasiparticle states extending down to the Fermi level, see Irkhin and Katsnel'son (1994). The density of states of a half-metallic ferromagnet as obtained within an independent particle calculation is schematically shown in figure 2(b). In this case, the spin-polarization is  $P = 1$  within any reasonable definition. In subsequent work it was found that  $\text{Fe}_3\text{O}_4$  ( $P = -1$ , Yanase and Siratori 1984, de Groot and Buschow 1986, Pénicaud *et al* 1992, Yanase and Hamada 1999),  $\text{CrO}_2$  ( $P = 1$ , Lewis *et al* 1997) and  $\text{La}_{0.7}\text{Sr}_{0.3}\text{MnO}_3$  ( $P = 1$ , Pickett and Singh 1996, de Boer *et al* 1997, Livesay *et al* 1999) are half-metallic magnets.

Here, some data on the spin-polarization of elemental as well as oxide magnets are summarized. The spin-polarization was determined by ferromagnet-insulator-ferromagnet (FIF) tunnelling, ferromagnet-insulator-superconductor (FIS) tunnelling, Andreev reflection (AR) at a superconductor-ferromagnet interface, spin-polarized photoemission (SPES) and two-dimensional angular correlation of electron-positron radiation (2D-ACAR). Here, only spin-polarization measurements using Andreev reflection will be discussed in greater detail; ferromagnetic tunnelling junctions are discussed in section 7. For a discussion of ferromagnet-insulator-superconductor tunnelling, spin-polarized photoemission and 2D-ACAR, the reader is referred to the

standard literature (Meservey and Tedrow 1994, Eib and Alvarado 1976, West 1995).

Electron transport through a normal metal-superconductor interface for energies below the superconducting gap  $\Delta$  is possible through Andreev reflection. An electron incident from the normal metal forms a pair with another electron of opposite momentum and spin and enters the superconductor as a Cooper pair, while a hole is reflected. This leads to a conductivity enhancement by a factor of two at small voltages. At large bias voltages, transport is dominated by quasiparticle injection and the conductance approaches the normal state conductance  $G_n$ . In the case of a ferromagnet-superconductor interface, Andreev reflection is suppressed, since not every majority electron finds a minority electron with appropriate momentum to form a Cooper pair. It is evident that the zero bias conductance should vanish in the case of a half-metallic ferromagnet. It was shown (Soulen *et al* 1998, Osofsky *et al* 1999) that the conductance of a ferromagnet-superconductor interface at zero temperature is given by

$$\frac{1}{G_n} \frac{dI}{dV} = 2(1 - |P_v|) \quad eV \ll \Delta \quad (5)$$

with the spin-polarization  $P_v$  as defined above. Thus, from the suppression of the conductance at zero bias the spin-polarization  $P_v$  can be determined. This method is not sensitive to the sign of the spin-polarization. A similar method was proposed and tested on elemental ferromagnets by Upadhyay *et al* (1998).

Results of spin-polarization measurements from FIF- and FIS-measurements, Andreev reflection and spin-polarized photoemission are summarized in table 1 for the elemental magnets Fe, Co, Ni, Gd, Tb, Dy, Ho, Er and Tm as well as for the oxide magnets  $\text{La}_{0.7}\text{Sr}_{0.3}\text{MnO}_3$ ,  $\text{CrO}_2$ ,  $\text{Fe}_3\text{O}_4$  and  $\text{SrRuO}_3$ . Data for alloys can be found in Meservey *et al* (1976), Paraskevopoulos *et al* (1977) obtained by the FIS-technique and in Nadgorny *et al* (2000) using Andreev reflection. Although the data show some scatter, it is clear that  $\text{CrO}_2$  and  $\text{La}_{0.7}\text{Sr}_{0.3}\text{MnO}_3$  have a spin-polarization much larger than that of elemental ferromagnets. The situation is not clear for  $\text{Fe}_3\text{O}_4$ , especially since it is not possible to perform Andreev reflection measurements due to the insulating nature of magnetite at low temperatures.

Note that the spin-polarization of Fe, Co and Ni as determined from FIS and FIF measurements is positive. From the band-structure, see figure 2, a negative value is expected for Co and Ni and is indeed found in spin-polarized photoemission studies. This discrepancy might be related to the type of bonding at the ferromagnet-insulator interface or to interfacial scattering and will be discussed in greater detail in section 7. Monsma and Parkin (2000b) reported an ageing of the spin-polarization of Ni films as observed in tunnelling studies and related it to chemical processes at the Ni- $\text{Al}_2\text{O}_3$  interface; this observation might explain the discrepancy between their data and the classical values of Tedrow and Meservey (1971, 1973).

Livesay *et al* (1998, 1999) used 2D-ACAR in order to determine the projection of the momentum density and spin density of a  $\text{La}_{0.7}\text{Sr}_{0.3}\text{MnO}_3$  crystal along [001]. This yields information on the Fermi surface topology. Experimental results are in good

**Table 1.** Spin-polarization as determined from ferromagnet-insulator-ferromagnet (FIF), ferromagnet-insulator-superconductor (FIS) tunnelling, Andreev reflection (AR) and spin resolved photoemission spectroscopy (SPES) for elemental ferromagnets and oxide magnets. For FIF and FIS measurements an  $\text{Al}_2\text{O}_3$  barrier was used. The Andreev reflection technique is not sensitive to the sign of the spin-polarization. All values were measured at low temperatures, i.e. 4.2 K or below, except for the SPES value of Ni that was measured at room temperature. The photoemission result for  $\text{CrO}_2$  by Kamper *et al* (1987) was obtained 2 eV below the Fermi level. The abbreviations in brackets indicate the reference with MPT80 (Meservey *et al* 1980), MP00 (Monsma and Parkin 2000a), WG00a (Worledge and Geballe 2000a), WG00b (Worledge and Geballe 2000b), M98 (Miyazaki *et al* 1998), M95 (Moodera *et al* 1995), Ji01 (Ji *et al* 2001), V97 (Viret *et al* 1997a), S99 (Seneor *et al* 1999), U98 (Upadhyay *et al* 1998), S98 (Soulen *et al* 1998), S95 (Sinkovic 1995), R95 (Rampe *et al* 1995), EA76 (Eib and Alvarado 1976), P98 (Park *et al* 1998a), B69 (Busch *et al* 1969), K87 (Kamper *et al* 1987) and A75 (Alvarado *et al* 1975).

Compound	FIS	FIF	AR	SPES
Fe	+0.45 (MP00)	+0.35 (M98)	–	+0.40 (S95)
Co	+0.42 (MP00)	+0.34 (M95)	0.37 (U98)	–0.4 (R95)
Ni	+0.31 (MP00)	–	0.32 (U98)	–0.3 (EA76)
Gd	+0.13 (MPT80)	–	–	+0.05 (B69)
Tb	+0.06 (MPT80)	–	–	–
Dy	+0.06 (MPT80)	–	–	–
Ho	+0.07 (MPT80)	–	–	–
Er	+0.05 (MPT80)	–	–	–
Tm	+0.03 (MPT80)	–	–	–
$\text{La}_{0.7}\text{Sr}_{0.3}\text{MnO}_3$	+0.70 (WG00a)	+0.83 (V97)	0.8 (S98)	+0.9 (P98)
$\text{CrO}_2$	–	–	0.9 (S98)	+1.0 (K87)
$\text{CrO}_2$	–	–	0.96 (Ji01)	–
$\text{Fe}_3\text{O}_4$	–	–0.5 (S99)	–	–0.4 (A75)
$\text{SrRuO}_3$	–0.095 (WG00b)	–	–	–

agreement with band-structure calculations. Figure 3(a) shows the radial anisotropy of the [001]-projected momentum density. The measurements are consistent with two Fermi-surface sheets, namely an electron-like sheet centered at the  $\Gamma$  point and hole-like sheets centered at the R points. The [001]-integrated spin density is shown in figure 3(b). The white areas indicate positive spin-polarization; these are located in the hole-like Fermi-surface cuboids at the R points in agreement with their origin in the manganese  $d$ -bands. These data indicate the complex nature of the spin-polarization in the manganites.

In conclusion of this section on half-metallic magnets a remark on the saturation magnetization is added. A stoichiometric, ordered half-metallic ferromagnet or ferrimagnet must have a saturation moment being an integral number of the Bohr magneton  $\mu_B$ , since the number of electrons per formula unit is an integer and the number of spin up (or spin down) electrons is also integral due to the gap in either the majority or the minority band. This argument can be extended to non-stoichiometric

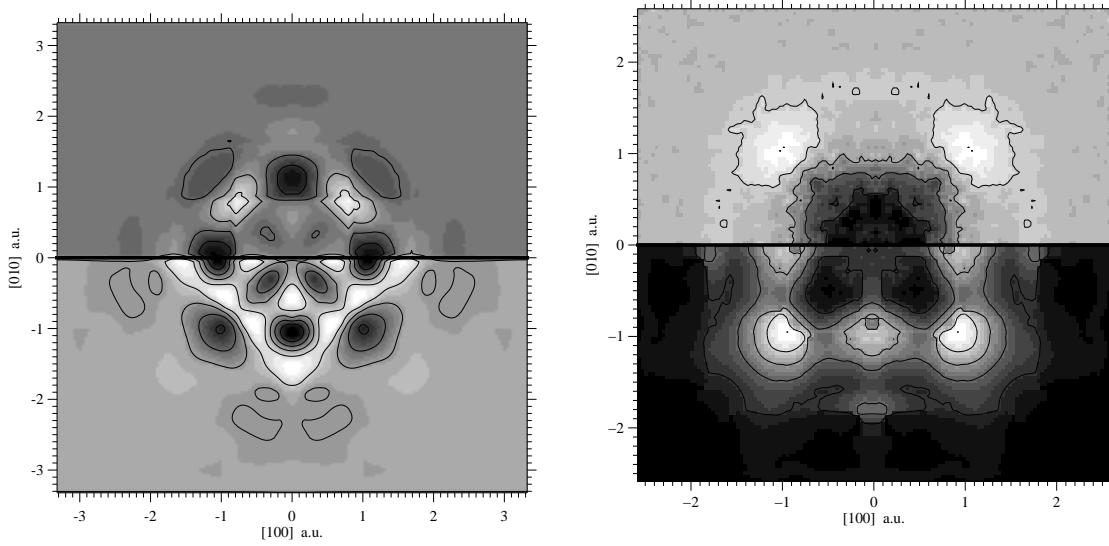


**Figure 3.** (a) Radial anisotropy of the [001]-projected momentum density of a  $\text{La}_{0.7}\text{Sr}_{0.3}\text{MnO}_3$  crystal, coming from experiment (top) and band-structure calculation (bottom). Reproduced from Livesay *et al* (1999). (b) The spin density in momentum space as seen by the positron, integrated along the [001] direction from the experiment (top) and band-structure calculation (bottom). White areas indicate positive spin-polarization. Unpublished, by courtesy of S B Dugdale.

ferromagnets that accordingly should have a saturation moment equal to the spin-only moment of the ferromagnetically coupled ions. In agreement with this rule, the saturation moments are close to  $2\mu_B$  in  $\text{CrO}_2$  ( $\text{Cr}^{4+}$ ,  $3d^2$ ),  $4\mu_B$  in  $\text{Fe}_3\text{O}_4$  ( $\text{Fe}^{2+}$ ,  $3d^6$ ) and  $3.7\mu_B$  in  $\text{La}_{0.7}\text{A}_{0.3}\text{MnO}_3$  (mixture of  $\text{Mn}^{3+}$ ,  $3d^4$  and  $\text{Mn}^{4+}$ ,  $3d^3$ ).

### 3. Intrinsic conductivity and optical properties

As already discussed in section 2, different exchange and transport mechanisms can be found in magnetic oxides. In this section, the temperature dependent resistivity and the optical conductivity are discussed and compared to recent theoretical models. The discussion starts with the itinerant ferromagnet  $\text{SrRuO}_3$ , then turns to a brief review of the super-exchange ferromagnet  $\text{Tl}_2\text{Mn}_2\text{O}_7$  before presenting data and models for the double exchange systems  $\text{La}_{0.7}\text{A}_{0.3}\text{MnO}_3$  and  $\text{CrO}_2$ . This is followed by a brief discussion of the double perovskite  $\text{Sr}_2\text{MoFeO}_6$  which seems to be an itinerant ferromagnet. At the end of this section the transport properties of magnetite are analyzed; magnetite is a strongly correlated ferrimagnet with significant polaronic effects and represents a class of its own. Since the resistivity depends sensitively on grain boundaries, see later sections, it is important to perform resistivity measurements on high quality single crystals and epitaxial films. Since research activity in recent years mainly focused on the colossal magnetoresistance perovskites, the bulk of this section will be devoted to this system.

Apart from the specific mechanisms relating to the individual systems, the issue of a minimal conductivity has re-emerged. This is due to the fact that many metallic



oxides such as the ferromagnetic compounds discussed here as well as high temperature superconductors apparently violate the Ioffe-Regel limit (Ioffe and Regel 1960, see also Mott 1978). This concept is based on the idea that the mean free path  $\ell$  cannot be smaller than the interatomic spacing  $a$ . In order to fix ideas, a simple estimate that should be valid for SrRuO<sub>3</sub> in the paramagnetic phase can be made. SrRuO<sub>3</sub> is particularly interesting, since Shubnikov-de Haas oscillations have been observed at low temperatures indicating Fermi-liquid behaviour (Mackenzie *et al* 1998). Assuming a typical metallic carrier density  $n \sim 5 \times 10^{27} \text{ m}^{-3}$ , a Fermi velocity  $v_F \sim 10^5 \text{ m/s}$  (Allen *et al* 1996) and an interatomic distance  $a \sim 2.5 \text{ \AA}$ , one finds from Drude theory a maximal resistivity

$$\rho_{\text{max}} \sim \frac{mv_F}{ne^2a} \sim 300 \mu\Omega\text{cm}. \quad (6)$$

SrRuO<sub>3</sub> displays at room temperature a resistivity of about  $200 \mu\Omega\text{cm}$  already close to the estimated saturation value. Allen *et al* (1996) measured the resistivity of a SrRuO<sub>3</sub> single crystal and found a linear dependence between room temperature and 1000 K without any sign of saturation up to a resistivity value of  $300 \mu\Omega\text{cm}$ . Other ferromagnetic oxides discussed here also show resistivities of the same order of magnitude without any tendency to saturation.

This behaviour is distinctly different from the resistivity curves found in A-15 compounds such as Nb<sub>3</sub>Sn which show an apparent saturation towards a value  $\rho_{\text{max}} \simeq 150 \mu\Omega\text{cm}$  (Wiesmann *et al* 1977). Fisk and Webb (1976) interpreted this resistivity saturation in terms of a saturation of the mean free path towards the interatomic distance in accordance with the Ioffe-Regel limit. The lack of saturation seen in many oxides motivated Emery and Kivelson (1995) to introduce the term “bad metal” meaning a system with a positive resistivity coefficient,  $d\rho/dT > 0$ , and a mean free path at high temperature smaller than the interatomic distance. These authors speculated that such systems could not be described within a Fermi-liquid picture with weak scattering.

A solution to this problem was indicated by Millis *et al* (1999) investigating electrons coupled to classical phonons with an arbitrary strong coupling. The resistivity was calculated within dynamical mean field theory. These calculations show a linear temperature dependence of the resistivity at small coupling and a linear temperature dependence with a non-zero offset at large coupling constants; these features are reminiscent of the saturation behaviour in A-15 compounds. However, a comparison of the numerical results to second order perturbation calculations shows that at strong electron-phonon couplings, the scattering rate increases with temperature at a rate much smaller than that given by perturbation theory. This indicates that the term “saturation” is a misnomer and that the apparent violation of the Ioffe-Regel limit is not per se a remarkable feature. Actually, at high temperatures classical diffusion might be expected leading to a linear temperature dependence of the resistivity according to the Einstein relation

$$\rho = \frac{kT}{ne^2D}, \quad (7)$$

where  $D$  denotes the diffusion constant.

Although the debate on a minimal metallic conductivity is certainly not exhausted, the apparent violation of the Ioffe-Regel limit in certain oxides with strongly coupled electron-phonon systems might not be an experimental smoking gun in regard to exotic transport theories.

### 3.1. $\text{SrRuO}_3$

$\text{SrRuO}_3$  is a strongly-correlated ferromagnetic  $d$ -band metal. The Curie temperature in the bulk is 165 K; for thin films reduced Curie temperatures of 150 K were observed possibly due to strain effects (Klein *et al* 1996). Magnetization measurements on single crystals (Cao *et al* 1997) showed a magnetic moment of about  $1.5\mu_B$  per  $\text{Ru}^{4+}$  ion. Within an ionic model, the fivefold degeneracy of the Ru ( $4d^4$ ) states is split by the octahedral crystalline field due to the O ions into two-thirds occupied  $t_{2g}$  and empty  $e_g$  levels. Thus,  $\text{Ru}^{4+}$  is in a low spin state with an ideal value of the magnetic moment of  $2\mu_B$ . The magnetization does not reach this ideal limit indicating the itinerant character of the ferromagnetism.

The zero field resistivity was found to increase proportional to  $T^2$  at low temperatures below about 10 K followed by a further steep increase up to the ferromagnetic Curie temperature that is marked by a change in slope. Above  $T_C$ , the resistivity continues to increase linearly with temperature, see figure 4. The resistivity increases strongly from residual resistivity values of about  $4\mu\Omega\text{cm}$  in high quality films to about  $200\mu\Omega\text{cm}$  at room temperature. Klein *et al* (1996) reported anomalously strong spin-scattering as evidenced by a resistivity derivative  $d\rho/dT$  of  $\text{SrRuO}_3$  being much larger than that of iron; these authors speculated that this might be related to the “bad metal” property.

Band-structure calculations show a gap of about 0.3 eV in the majority density of states that is only 20 mRy above the Fermi level (Mazin and Singh 1997, Santi and Jarlborg 1997). Thus,  $\text{SrRuO}_3$  is close to being a half-metal; Mazin and Singh (1997) pointed out that this nearly half-metallic character is important for understanding the transport properties.

Measurements of the optical conductivity indicate deviations from Fermi-liquid behaviour. Kostic *et al* (1998) measured  $\sigma(\omega)$  for temperatures between 40 K and 250 K. At low temperatures the real part of the optical conductivity was found to decrease with frequency as  $\omega^{-1/2}$ , a behaviour that is difficult to reconcile with standard Fermi-liquid theory predicting  $\Re(\sigma) \propto \omega^{-2}$  at comparable frequencies. At higher temperatures the low frequency conductivity was actually found to increase with frequency indicating the opening of an optical gap in contrast with the general characteristics of metals. Accordingly, Kostic *et al* (1998) concluded that  $\text{SrRuO}_3$  shows non-Fermi-liquid behaviour and derived frequency dependent scattering times and effective masses. This work was extended by Dodge *et al* (2000) who employed terahertz time-domain and far-infrared spectroscopy to measure the conductivity over

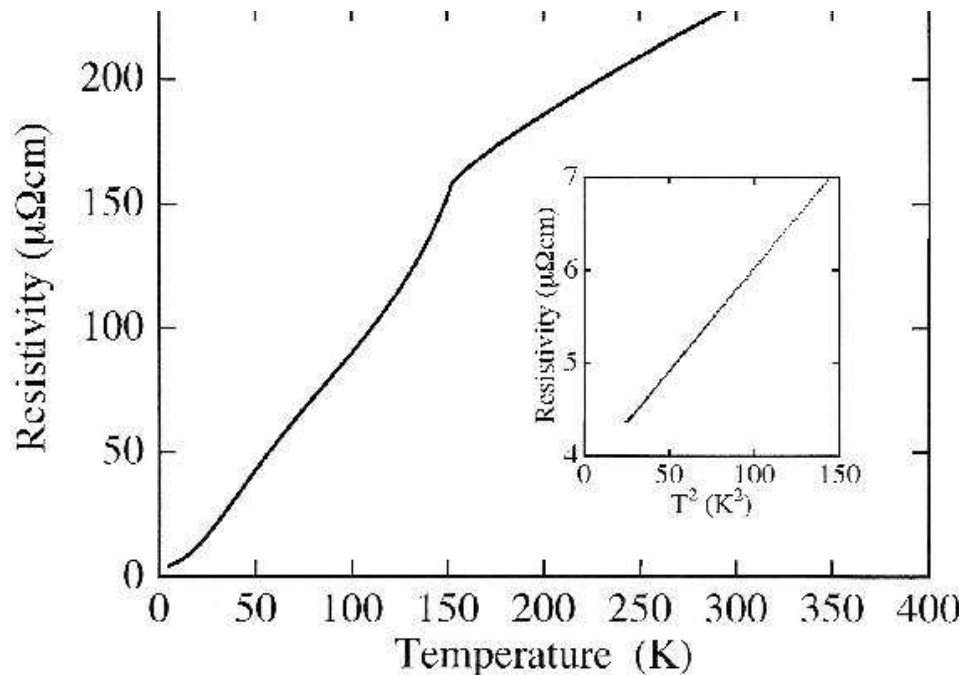


**Figure 4.** Resistivity of a high quality SrRuO<sub>3</sub> film grown on 2° miscut SrTiO<sub>3</sub>. The inset shows that there is a  $T^2$  scattering rate below about 10 K. Reproduced from Mackenzie *et al* (1998).

three decades in frequency. The results can be analyzed with a conductivity  $\sigma(\omega) \propto (\tau^{-1} + i\omega)^{-\alpha}$  yielding an exponent  $\alpha \simeq 0.4$  in contrast to the Drude result  $\alpha = 1$ . The authors conclude that SrRuO<sub>3</sub> displays non-Fermi liquid behaviour in the temperature  $5 \text{ K} \leq T < 95 \text{ K}$  and investigated frequency regime. At still lower energies, however, the observation of Shubnikov-de Haas oscillations in the resistivity of SrRuO<sub>3</sub> films at 35 mK by Mackenzie *et al* (1998) strongly suggests a ground state that is actually a Fermi-liquid. Accordingly, the Fermi-liquid state in SrRuO<sub>3</sub> might display some fragility leading to a breakdown of this concept at energies much lower than in conventional metals. The carrier mean free path was estimated by Kostic *et al* (1998) using the measured scattering times and Fermi velocities derived from band-structure calculations. At 145 K, the mean free path for majority and minority carriers was found to be about 0.6 nm and 1.2 nm, respectively. These values are comparable to the size of the unit cell and clearly show that SrRuO<sub>3</sub> is a “bad metal”.

Mazin and Singh (1997) argued that there is a strong coupling between electrons, phonons and magnons that probably produces significant spin-flip scattering. Furthermore, the Fermi-surface has a complex topology with electron- and hole-like sheets in each spin channel. Assuming electron-phonon and electron-paramagnon scattering Mazin and Singh (1997) argued that the resistivity is linear in temperature at high temperatures with the coefficient proportional to the sum of the coupling constants. The coupling constants derived from resistivity and specific heat data are in reasonable agreement in support of the above picture. The change in slope of the resistivity while

warming through the Curie temperature is explained by a change from electron-magnon scattering to electron-paramagnon scattering, the latter having a weaker coupling. The quadratic temperature dependence of the resistivity at low temperatures is due to electron-magnon scattering, again with an extraordinary large coupling constant. In summary, the transport properties of  $\text{SrRuO}_3$  can be qualitatively understood on the basis of band-structure calculations and Boltzmann transport-theory. This is in agreement with the general results by Millis *et al* (1999) on the resistivity of a metal with strong electron-phonon coupling, see above.

### 3.2. $\text{Tl}_2\text{Mn}_2\text{O}_7$

The pyrochlore  $\text{Tl}_2\text{Mn}_2\text{O}_7$  has a Curie temperature of about 140 K with a saturation magnetic moment of  $3\mu_B$  per formula unit corresponding to a ferromagnetic ordering of the  $\text{Mn}^{4+}$  ions (Shimakawa *et al* 1997). The transport and magnetotransport properties are similar to the CMR manganites, namely: metallic transport below  $T_C$  crossing over to semiconducting behaviour above  $T_C$ ; near the Curie temperature a large magnetoresistance is seen. Typical resistivity data are shown in figure 5(b). These properties make the pyrochlore interesting in comparison to the manganites, since they, especially the large magnetoresistance, do not seem to arise from a double exchange mechanism (Shimakawa *et al* 1997, Kwei *et al* 1997, Majumdar and Littlewood 1998a, 1998b, Imai *et al* 2000).

The carrier density of  $\text{Tl}_2\text{Mn}_2\text{O}_7$  is small of the order of 0.001-0.005 per formula unit (Shimakawa *et al* 1996, Raju *et al* 1994) and depends on temperature and magnetic field (Imai *et al* 2000), see figure 5(a). This carrier density is supposed to be too small to give rise to significant double exchange effects. X-ray and neutron diffraction studies did not indicate any structural changes near the Curie temperature (Shimakawa *et al* 1997), thus ruling out any spin-lattice or charge-lattice coupling. The compound does not show any significant Jahn-Teller distortion in accordance with the idea that manganese is in a  $\text{Mn}^{4+}$  ionization state which is not Jahn-Teller active. A comparison of the magnetic and transport properties of  $\text{A}_2\text{Mn}_2\text{O}_7$  pyrochlores with  $\text{A} = \text{Y}, \text{Lu}, \text{In}$  and  $\text{Tl}$  shows ferromagnetic order for all compounds with the Curie temperature varying from 15 K ( $\text{Y}_2\text{Mn}_2\text{O}_7$  and  $\text{Lu}_2\text{Mn}_2\text{O}_7$ ) to 140 K ( $\text{In}_2\text{Mn}_2\text{O}_7$  and  $\text{Tl}_2\text{Mn}_2\text{O}_7$ ). Apart from  $\text{Tl}_2\text{Mn}_2\text{O}_7$  all compounds are insulators. The ferromagnetic ordering was interpreted within a super-exchange model. According to the Goodenough-Kanamori rules (Kanamori 1958, Goodenough 1955, 1958) the super-exchange interaction between  $\text{Mn}^{4+}$  ions via oxygen ions is antiferromagnetic for a bond angle of  $180^\circ$  and ferromagnetic for a  $90^\circ$  bond angle. The bond angle is near  $133^\circ$  in the pyrochlores and therefore in the crossover region. From the empirical expression

$$J = J_{90^\circ} \sin^2 \phi + J_{180^\circ} \cos^2 \phi, \quad (8)$$

where  $\phi$  denotes the bonding angle, and using values for  $\text{Cr}^{3+}$  (supposed to be similar to  $\text{Mn}^{4+}$ ),  $4S(S+1)J_{90^\circ}/k = 380$  K,  $4S(S+1)J_{180^\circ}/k = -420$  K, Shimakawa *et al* (1999) estimated a small, but positive ferromagnetic super-exchange coupling between

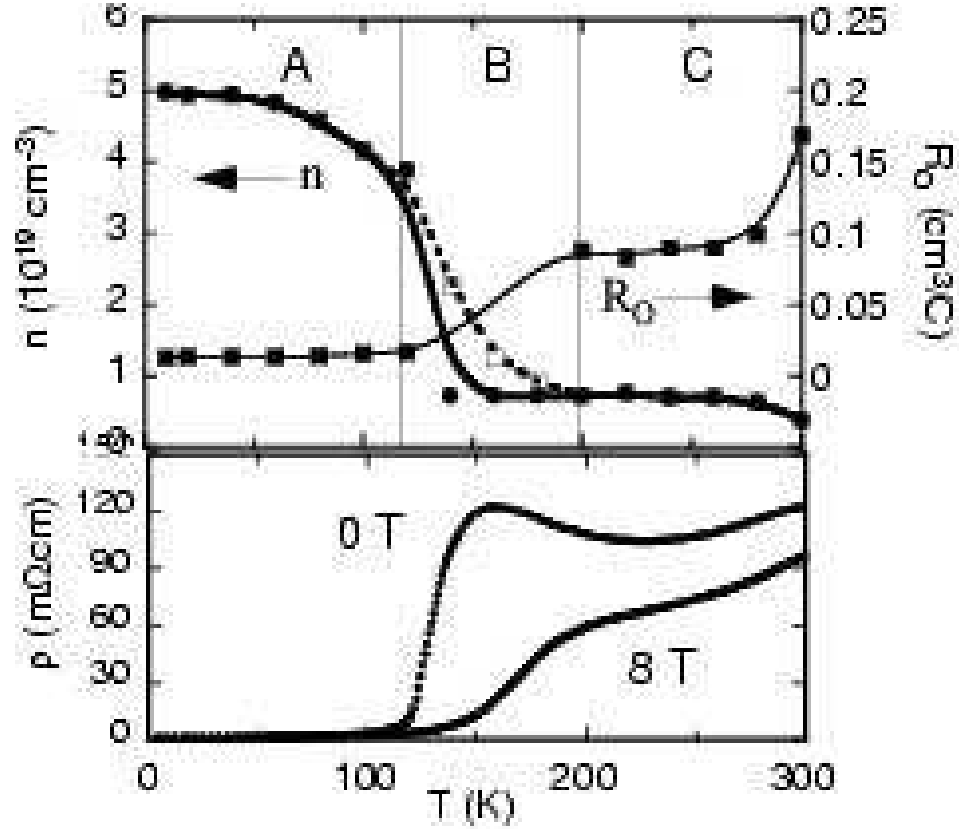


**Figure 5.** (a) Temperature dependence of the ordinary Hall coefficient,  $R_0$ , (right axis) and the free-electron carrier density,  $n$ , (left axis) of a polycrystalline  $\text{Tl}_2\text{Mn}_2\text{O}_7$  sample. Closed circles represent the zero field carrier density and open squares the carrier density measured at 8 T. Lines are guides for the eye. (b) The electrical resistivity of the same sample measured as a function of temperature in zero magnetic field and at 8 T. Reproduced from Imai *et al* (2000).

the  $\text{Mn}^{4+}$  ions.  $S = 3/2$  denotes the  $\text{Mn}^{4+}$  spin. This is supposed to lead to the small Curie temperature in  $\text{Y}_2\text{Mn}_2\text{O}_7$  and  $\text{Lu}_2\text{Mn}_2\text{O}_7$ . Electronic band-structure calculations using the LSDA+U method showed insulating behaviour for  $\text{Y}_2\text{Mn}_2\text{O}_7$  and  $\text{In}_2\text{Mn}_2\text{O}_7$  and metallic behaviour for  $\text{Tl}_2\text{Mn}_2\text{O}_7$  (Shimakawa *et al* 1999). Hybridisation between the  $\text{In}(5s)$ ,  $\text{O}(2p)$  and  $\text{Mn}(3d)$  states in  $\text{In}_2\text{Mn}_2\text{O}_7$  and the  $\text{Tl}(6s)$ ,  $\text{O}(2p)$  and  $\text{Mn}(3d)$  states in  $\text{Tl}_2\text{Mn}_2\text{O}_7$  was observed and interpreted as promoting the ferromagnetism, thus leading to the high Curie temperature of these compounds. The hybridized  $\text{Tl}(6s)$ ,  $\text{O}(2p)$  and  $\text{Mn}(3d)$  minority spin band crosses the Fermi level and overlaps with the valence band. Accordingly, a small free-electron like pocket is created at the  $\Gamma$  point. These electrons dominate the transport properties, since the up-spin holes near the  $\Gamma$  point have a very large mass. Band-structure calculations by Singh (1997) using the linearized augmented plane wave (LAPW) method yielded similar results. Highly spin-differentiated transport with dominantly minority carriers results. Thus, in the case of the pyrochlore one has itinerant carriers of mainly  $\text{Tl-O}$  character interacting with the

localized  $\text{Mn}^{4+}$  moments.

Majumdar and Littlewood (1998a, 1998b) proposed a model of a low density electron gas coupled to spin fluctuations to account for the properties of  $\text{Tl}_2\text{Mn}_2\text{O}_7$ . The low carrier density leads to large spin-disorder scattering within an itinerant model in agreement with the experimental results in the metallic phase. Above  $T_C$  spin polarons are formed with a strongly field dependent binding energy; the resistivity in this regime is semiconducting in agreement with experiment. This model was supported by Martínez *et al* (1999) and Alonso *et al* (1999) through measurements of the magnetic and magnetotransport properties as a function of carrier density in  $\text{Tl}_2\text{Mn}_{2-x}\text{Ru}_x\text{O}_7$  and  $\text{Tl}_{2-x}\text{Bi}_x\text{Mn}_2\text{O}_7$  substitution series, respectively. Further details on specific models can be found in a short review by Ventura and Gusmão (2001).

### 3.3. $\text{CrO}_2$

$\text{CrO}_2$  is the simplest of the half-metallic ferromagnets. Within an ionic model,  $\text{Cr}^{4+}$  ( $3d^2$ ) ions are ferromagnetically ordered, yielding a magnetic moment of  $2\mu_B$  per formula unit in agreement with magnetization measurements. The temperature dependence of the resistivity is similar to that of  $\text{SrRuO}_3$  and the basic transport mechanisms in both compounds might be very similar. Band-structure calculations using the local spin-density approximation (LSDA) (Lewis *et al* 1997) and LSDA+U (Korotin *et al* 1998) indicate half-metallic behaviour with a finite density of states at the Fermi level for the majority carriers and a gap of about 1.5 eV in the minority density of states. The bands crossing the Fermi energy are predominantly of O( $2p$ ) character; thus, these can be viewed as charge reservoirs leading to a non-integral occupation of the  $d$ -bands, a mechanism called “self-doping” by Korotin *et al* (1998). An almost dispersionless majority spin-band is located about 1 eV below the Fermi energy and is an almost pure  $d$ -band in character. Korotin *et al* (1998) therefore suggested that the charge carriers in the extended hybridized  $p-d$  states move through localized  $d$ -levels near the ion cores and are polarized by the localized moments through Hund’s rule coupling. This scenario is very similar to the double-exchange mechanism proposed by Zener (1951); thus,  $\text{CrO}_2$  might be regarded as a self-doped double-exchange ferromagnet. According to the half-metallic band structure, the local moment is  $2\mu_B$  in agreement with experiment.

The measured resistivity of  $\text{CrO}_2$  is indeed metallic above and below the Curie temperature, see figure 6, which shows the resistivity of a  $\text{CrO}_2$  film grown on  $\text{ZrO}_2$  (Suzuki and Tedrow 1998). A change in the slope of the resistivity is discernible near the Curie temperature of 390 K. Models for the temperature dependence of the resistivity have been proposed, but remain controversial. Lewis *et al* (1997) fitted Bloch-Grüneisen functions to the resistivity data of  $\text{CrO}_2$  single crystals and found good agreement at temperatures below about 200 K with a reasonable choice of parameters. Suzuki and Tedrow (1998) reported a quadratic temperature dependence in polycrystalline  $\text{CrO}_2$  films below about 240 K. Motivated by the band-structure calculations of Lewis *et al* (1997), they fitted their data with a model of parallel conduction of metallic and

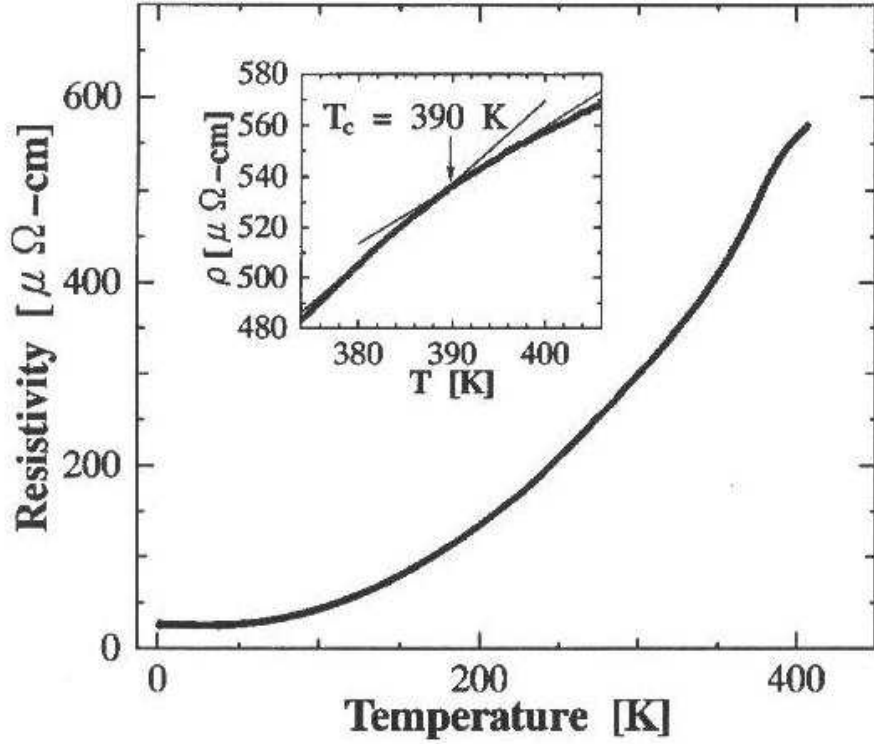


**Figure 6.** Temperature dependence of the resistivity of a  $\text{CrO}_2$  film grown on  $\text{ZrO}_2$ . The inset shows the change in slope of the resistivity near the Curie temperature of 390 K. Reproduced from Suzuki and Tedrow (1998).

semiconducting channels. Barry *et al* (1998) reported a dependence

$$\rho(T) = \rho_0 + \alpha T^2 \exp(-\Delta/kT) \quad (9)$$

indicating a gap  $\Delta$  of the order of 7 meV in the excitation spectrum. This gap was tentatively related to magnon scattering in a half-metallic ferromagnet; since electron-magnon scattering is a spin-flip process, it is impeded by the gap in the minority density of states.

Early spin-resolved photoemission experiments on a polycrystalline  $\text{CrO}_2$  film by Kämper *et al* (1987) showed no spectral weight at the Fermi energy, in contrast to the metallic behaviour of the resistivity. In these experiments nearly 100% spin-polarization was found 2 eV below the Fermi energy. More recent optical data on  $\text{CrO}_2$  bulk polycrystals by Tsujioka *et al* (1997) show a small but finite density of states at the Fermi level. Ultraviolet photoemission and X-ray inverse photoemission measurements show large peaks above and below the Fermi energy that are attributed to Cr  $d$ -bands (Tsujioka *et al* 1997); the  $3d$  band splitting is about 4.5 eV. The position of the main Cr peaks is in good agreement with the LSDA+U calculation, whereas the LSDA calculation yields a peak separation that is clearly too small. This indicates the important influence of the strong  $d-d$  Coulomb interaction on the Cr  $d$ -bands. The finite density of states at the Fermi level, however, indicates that the Cr  $t_{2g}$   $3d$ -bands, being strongly hybridized with the O( $2p$ ) bands, are scarcely influenced by the Coulomb repulsion; these bands

cross the Fermi level and cause the metallic transport properties. Infrared spectroscopy shows an interband transition at 3.35 eV that was attributed to excitations across the minority spin gap and is in agreement with the idea of a half-metallic metal (Singley *et al* 1999). Yamamoto *et al* (2000) report temperature dependent features in the absorption spectra of CrO<sub>2</sub> films near photon energies of 0.5, 1.0 and 1.5 eV. The spectral weight transfer was found to scale with  $(M/M_S)^2$  thus indicating a relation of these features with the spin-polarization. The estimated minority spin gap is 1.5 eV in agreement with band-structure calculations.

The transport and optical properties of CrO<sub>2</sub> were critically discussed by Mazin *et al* (1999). These authors suggest that correlation effects are small and doubt the superiority of LSDA+U calculations over the LSDA method. Mazin *et al* (1999) indeed showed that the separation of the Cr *d*-states depends on the particular method used for band-structure calculations. The density of states strongly varies near the Fermi level, thus yielding the calculated carrier density at the Fermi level somewhat uncertain. A comparison of the specific heat data of Tsujioka *et al* (1997) and the calculated density of states yielded comparatively small effective-mass enhancements in the range 1.1 to 2.5. Mazin *et al* (1999) suggested that the strong temperature dependence of the resistivity is not due to electron-magnon scattering, but caused by the strong band-structure changes due to the coupling to the magnetism, thus leading to enhanced electron scattering by spin fluctuations. A detailed Fermi surface calculation was also reported by Brener *et al* (2000).

### 3.4. La<sub>0.7</sub>A<sub>0.3</sub>MnO<sub>3</sub>

*3.4.1. Resistivity and phase diagram.* CMR manganites are oxides of the type RE<sub>1-x</sub>A<sub>x</sub>MnO<sub>3</sub>, where RE denotes a rare earth and A a divalent, often alkaline earth element; some studies with alkali element dopings, A = Na, K, ... , however, have been made. These oxides were first investigated in the early fifties in ceramic form (Jonker and van Santen 1950, Volger 1954, Wollan and Koehler 1955) and at the end of the sixties in single crystal form (Morrish *et al* 1969, Leung *et al* 1969, Searle and Wang 1969, Oretzki and Gaunt 1970, Searle and Wang 1970). An account of early work can be found in a review article by Goodenough and Longo. Research started to focus again on these oxides in the early nineties after the discovery of a large room temperature magnetoresistance in thin films (von Helmolt *et al* 1993).

Typical resistivity versus temperature curves for La<sub>0.7</sub>(Ca<sub>1-y</sub>Sr<sub>y</sub>)<sub>0.3</sub>MnO<sub>3</sub> single crystals are shown in figure 7. At low temperatures the resistivity is metallic, rising sharply while going through the ferromagnetic transition and showing semiconducting behaviour in the paramagnetic phase in the case of Ca doping, whereas the resistivity in the case of Sr doping remains metallic above the Curie temperature. Accordingly, the ferromagnetic transition in this compound is accompanied by a metal-insulator transition as evidenced by the resistivity rise and the negative temperature coefficient of the resistivity in most compounds above  $T_C$ . The residual resistivity is rather high



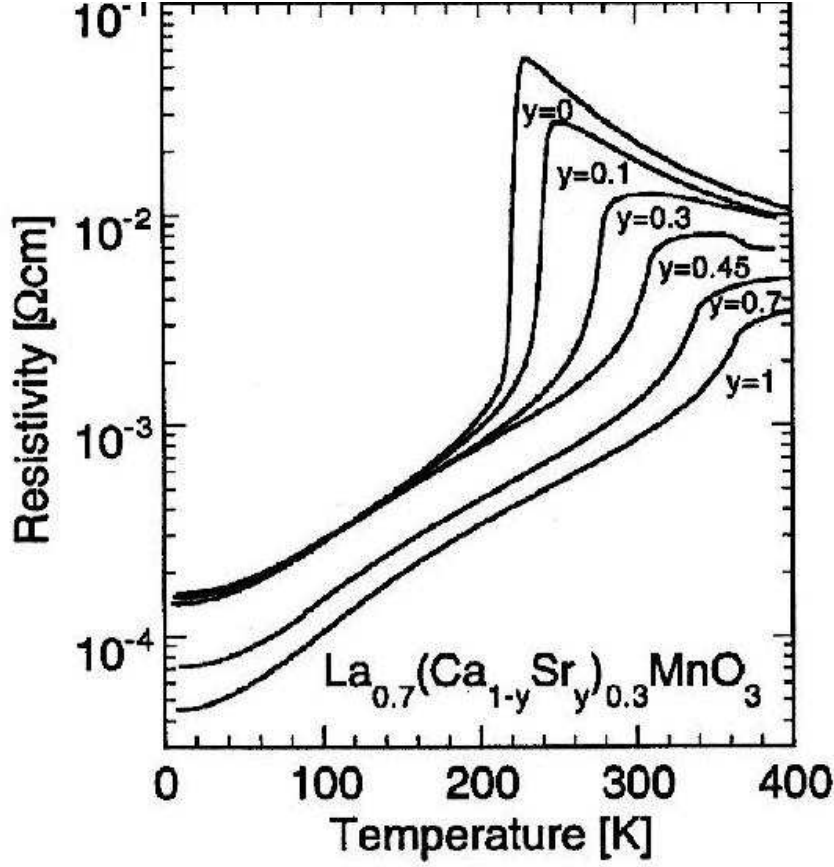


**Figure 7.** Typical resistivity versus temperature curves of  $\text{La}_{0.7}(\text{Ca}_{1-y}\text{Sr}_y)_{0.3}\text{MnO}_3$  single crystals. The anomaly at a temperature of 370 K for the  $y = 0.45$  doping is due to a structural transition from a low temperature orthorhombic to a high temperature rhombohedral phase. After Tomioka *et al* (2001).

with values between 40 and 200  $\mu\Omega\text{cm}$ .

The CMR manganites crystallize in the perovskite structure as shown in figure 1(a). In the ideal perovskite structure the bond lengths between the A and Mn cations and the O anions have the ratio  $\langle \text{A} - \text{O} \rangle / \langle \text{Mn} - \text{O} \rangle = \sqrt{2}$ , see figure 1(a). In an ionic model the bond lengths are mainly determined by the ionic radii. As a measure of deviation from the ideal perovskite structure it is customary to define a tolerance factor by

$$\text{tol} = \frac{\langle \text{A} - \text{O} \rangle}{\sqrt{2} \langle \text{Mn} - \text{O} \rangle}. \quad (10)$$

Note that the tolerance factor depends on both temperature  $T$  and hydrostatic pressure  $p$ ; usually  $d(\text{tol})/dT > 0$  and  $d(\text{tol})/dp < 0$  (Goodenough 1999). A tolerance factor  $\text{tol} < 1$  as found in the CMR manganites of interest in this review, places the Mn–O bonds under compression and the A–O bonds under tension. The arising stresses are alleviated by a cooperative rotation of the  $\text{MnO}_6$  octahedra (Goodenough 1997). This leads to a bending of the Mn–O–Mn bond with a decrease of the bond angle from  $180^\circ$  to  $(180^\circ - \phi)$ . The cubic structure is distorted to orthorhombic symmetry by cooperative

rotations around [110] and to rhombohedral by rotations around [111] (Goodenough and Longo).

Much interest has been devoted to the CMR manganites, since these display a diversified phase diagram. The phase diagram obtained from magnetization and resistivity measurements on polycrystalline  $\text{La}_{0.7}\text{Ca}_{0.3}\text{MnO}_3$  samples by Schiffer *et al* (1995) is shown in figure 8(a). This phase diagram was obtained at constant tolerance factor. On doping with Ca the A-type antiferromagnetic, insulating parent compound  $\text{LaMnO}_3$  becomes a ferromagnetic insulator for  $x < 0.15$  and a ferromagnetic metal for  $0.2 < x < 0.5$ , before entering a G-type antiferromagnetic, insulating phase for  $x > 0.5$ . Colossal magnetoresistance appears in the doping range  $0.2 < x < 0.5$  close to the ferromagnetic transition. The Curie temperature is maximal near  $x = 0.3$ . More detailed phase diagrams showing structural transitions, charge-ordered phases etc. can be found e.g. in Yamada *et al* (1995) and Goodenough (1999). Here the phase diagram will not be further discussed in detail, since the materials of interest for extrinsic magnetoresistance effects are found near a doping of  $x = 0.3$ .

In figure 8(b) the phase diagram at constant doping  $x = 0.3$  is shown as a function of tolerance factor. In the range of tolerance factors  $0.91 \leq \text{tol} \leq 0.93$  a dramatic increase of the Curie temperature was found followed by a slow decrease in the range  $0.93 \leq \text{tol} \leq 0.95$  (Hwang *et al* 1995, Fontcuberta *et al* 1996). This has been attributed to a band narrowing on decrease of the tolerance factor. This band narrowing weakens the ferromagnetic double exchange interaction and, in turn, the antiferromagnetic super-exchange interaction might gain in importance. This issue will be further discussed below. In addition to the dependence on the tolerance factor, the Curie temperature of  $(\text{RE}_{0.7}\text{A}_{0.3})\text{MnO}_3$  perovskites at constant tolerance factor shows a strong linear dependence upon the variance of the A site cation radius distribution  $\sigma^2 = \langle r_A^2 \rangle - \langle r_A \rangle^2$  (Rodriguez-Martinez and Attfield 1996). This might lend some support to localization models, see below.

The saturation magnetic moment at a doping  $x = 0.3$  is near  $3.7\mu_B$  (Jonker and van Santen 1950); within an ionic picture this corresponds to the spin-only moments of ferromagnetically aligned 70%  $\text{Mn}^{3+}$  and 30%  $\text{Mn}^{4+}$  ions.

### 3.4.2. Theoretical models.

*Band-structure.* A fundamental problem arising in the study of the transport mechanism is about the nature of the carriers. These are most often assumed to be of Mn 3d character and the underlying transport mechanism is double exchange; there are, however, some suggestions that the CMR manganites are doped charge-transfer insulators. Although this matter has not been fully resolved, agreement emerges that double exchange is a basic ingredient for any model. Here I will mainly focus on these double-exchange models and modifications due to polaronic effects.

In this context it is informative to look at band-structure calculations. Within the local spin density approximation (LSDA) the electronic structure of the parent

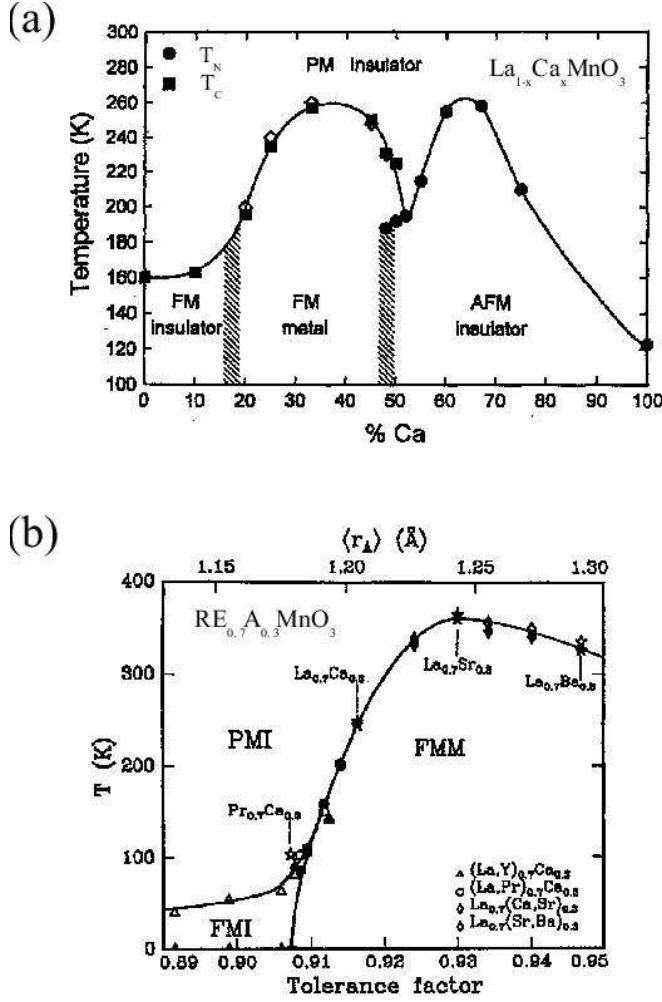


**Figure 8.** (a) Phase diagram as a function of doping at constant tolerance factor  $tol \simeq 0.918$  obtained from magnetization and resistivity measurements on polycrystalline  $\text{La}_{1-x}\text{Ca}_x\text{MnO}_3$  samples. This phase diagram gives an overview over some of the main features found in the CMR manganites. At low temperature, the system evolves on doping from an A-type antiferromagnet over insulating and metallic ferromagnetic phases into an insulating G-type antiferromagnet.  $T_N$  denotes the Néel,  $T_C$  the Curie temperature of the antiferromagnetic and ferromagnetic phases, respectively. After Schiffer *et al* (1995). (b) Phase diagram at constant doping  $x = 0.3$  als a function of tolerance factor. At a critical tolerance factor of about 0.907 the manganites become metallic at low temperature. After Hwang *et al* (1995).

compound  $\text{LaMnO}_3$  was found to be an antiferromagnetic insulator in the orthorhombic phase (Sarma *et al* 1995, Satpathy *et al* 1996). The states near the top of the valence band are of Mn 3d character; accordingly  $\text{LaMnO}_3$  appears as a Mott-Hubbard insulator. On hole doping, band-structure calculations using LSDA (Pickett and Singh 1996, de Boer *et al* 1997, Livesay *et al* 1999) indicated a half-metallic character with a gap of about 2 eV in the minority spin-band. Two Fermi-surface sheets were found in the majority band, namely an electron-like sphere at the  $\Gamma$  point and hole-like cuboids at the

$R$  point derived from the Mn  $3d$  states. This Fermi-surface topology was corroborated by 2D-ACAR measurements (Livesay *et al* 1999), see section 2. On the other hand, LSDA+U (Satpathy *et al* 1996) as well as Hartree-Fock (Su *et al* 2000) calculations also yield an antiferromagnetic insulating ground state for  $\text{LaMnO}_3$ , but this time the states near the top of the valence band are of  $\text{O}(2p)$  character indicating a charge-transfer insulator. It seems most probable that the  $\text{Mn}(3d)\text{--O}(2p)$  hybridization in the majority spin band is quite strong, but that the  $3d$  nature of the carriers is dominant such that a double-exchange picture applies.

*Classical double exchange.* The transport behaviour, especially the simultaneous ferromagnetic and metal-insulator transition, can be understood within the double-exchange model proposed by Zener (1951) and further developed by Anderson and Hasegawa (1955), de Gennes (1960), Searle and Wang (1970) and Kubo and Ohata (1972).

In the perovskite structure the Mn ions are located on a simple cubic lattice, whereas oxygen ions occupy the centers of the cube edges and the rare earth ion or divalent dopant are located at the cube center. Thus, the Mn ions are in an octahedral oxygen coordination and, in the ideal structure with  $\text{tol} = 1$ , the Mn–O–Mn bond angle is  $180^\circ$ . This leads to a crystal-field splitting of the  $\text{Mn}(3d)$  orbitals into low-lying  $t_{2g}$  and energetically higher  $e_g$  levels. Within the double-exchange model it is assumed that charge transport occurs on the Mn–O sublattice, whereas the rare earth and earth alkaline ions act only as a charge reservoir. In the parent compound  $\text{LaMnO}_3$ , the manganese ion is in a trivalent oxidation state  $\text{Mn}^{3+}$  with electronic structure  $3d^4$ . According to Hund’s rules three electrons occupy the  $t_{2g}$  levels and are coupled into a core spin  $S = 3/2$  by the strong intra-atomic Hund’s rule coupling. The fourth electron occupies one of the energetically degenerate  $e_g$  orbitals.  $\text{Mn}^{3+}$  is known to be a strong Jahn-Teller ion and an orthorhombic distortion of the cubic perovskite lattice is indeed found in  $\text{LaMnO}_3$ .

On doping with a divalent ion on the rare earth site, i.e.  $\text{RE}_{1-x}\text{A}_x\text{MnO}_3$ , the manganese ions become mixed valent with manganese fractions  $x$  in the tetravalent state  $\text{Mn}^{4+}$  ( $3d^3$ ) and  $(1-x)$  in the trivalent state  $\text{Mn}^{3+}$  ( $3d^4$ ). Zener (1951) considered a cluster formed from an oxygen and two Mn ions, one in the trivalent and one in the tetravalent state. The basic idea of double exchange is that the configurations  $\text{Mn}^{3+}\text{--O--Mn}^{4+}$  and  $\text{Mn}^{4+}\text{--O--Mn}^{3+}$  are degenerate leading to a delocalization of the hole on the  $\text{Mn}^{4+}$  site:

$$t_{2g}^3 e_g^1 - \text{O} - t_{2g}^3 e_g^0 \leftrightarrow t_{2g}^3 e_g^0 - \text{O} - t_{2g}^3 e_g^1. \quad (11)$$

The transfer of a hole occurs simultaneously from  $\text{Mn}^{4+}$  to O and from O to  $\text{Mn}^{3+}$ ; this process is a real charge transfer process and involves overlap integrals between Mn and O orbitals. Due to the strong Hund’s rule coupling energy  $J_H$ , Zener (1951) suggested that the hole transfer is only possible for parallel orientation of the core spins. This yields the observed simultaneous occurrence of metallic conductivity and ferromagnetism. Zener

(1951) made a rough estimation of the conductivity based on Einstein's relation and the diffusion constant of a hole located at a  $\text{Mn}^{4+}$  site.

Anderson and Hasegawa (1955) considered this three ion cluster in more detail and calculated the transfer matrices and energy levels. They showed that the effective hopping matrix element is given by  $t \cos(\Theta/2)$  within a classical treatment of the core spins, where  $\Theta$  denotes the angle between the core spins and  $t$  is the transfer integral.

De Gennes (1960) was the first to formulate the double exchange problem for a lattice and to derive a band model for the motion of holes. An antiferromagnetic super-exchange interaction competes with the ferromagnetic double-exchange interaction; de Gennes (1960) predicted that this can lead to spin canting at low doping levels  $x$ . Some evidence, however, suggests that phase separation into ferro- and antiferromagnetic regions occurs at low dopings and the canted state is not observed; this is further discussed below. It was shown that antiferromagnetic interactions lower the Curie temperature and may lead to discontinuous transitions (Alonso *et al* 2001) as was observed experimentally in the series  $\text{La}_{0.7}\text{A}_{0.3}\text{MnO}_3$  with  $\text{A} = \text{Sr}, \text{Ba}, \text{Ca}$  by Mira *et al* (1999) and Ziese (2001a); see also the discussion on phase separation. De Gennes (1960) further considered localized and self-trapped carriers and showed that these give rise to a local distortion of the spin system. This is the situation of spin-polarons to be discussed below.

The resistivity as a function of temperature was calculated within the double-exchange model by Kubo and Ohata (1972), Calderon *et al* (1999a) and Ishizaka and Ishihara (1999). These calculations yield a metallic state above and below the Curie temperature. This is in contrast to the experimental results on various manganite systems, since semiconducting behaviour of the resistivity is found in all systems except for  $\text{La}_{0.7}\text{Sr}_{0.3}\text{MnO}_3$ . Since the band-structure assumed in the double exchange model is half-metallic, first order electron-magnon scattering is strictly forbidden. Kubo and Ohata (1972) calculated the low temperature resistivity due to second order electron-magnon processes and found a contribution proportional to  $T^{9/2}$ . An analysis of resistivity data in terms of power law contributions yields an acceptable description with the resistivity given by

$$\rho = \rho_0 + \rho_{9/2}T^{9/2} + \rho_2T^2 \quad (12)$$

up to about half the Curie temperature (Schiffer *et al* 1995, Snyder *et al* 1996). In addition to the second order electron-magnon scattering term  $\rho_{9/2}T^{9/2}$ , a second term  $\rho_2T^2$  appears that might be attributed to electron-electron scattering. Jaime *et al* (1998) argued that the coefficient  $\rho_2$  is much too large as to arise from electron-electron scattering; it is more likely to be due to first order electron-magnon scattering that becomes allowed at finite temperature due to a thermally populated minority band.

Furukawa (2000) proposed an unconventional one-magnon scattering process in half-metals that goes beyond the rigid band approximation and takes into account spin fluctuations; this leads to a  $T^3$  power law of the low temperature resistivity. Calderón and Brey (2001) considered this process in more detail and identified a  $T^{3/2}$  power law

dominating the  $T^3$  response at low temperatures. For a further discussion of the low temperature resistivity see the paragraphs on localization and bi-polaron models.

*Including electron-phonon coupling.* Most researchers agree that double exchange is the basic mechanism underlying the transport properties of the manganites; it seems, however, not to be sufficient to explain the experimental results, especially the colossal magnetoresistance discussed in the following section. Millis *et al* (1995) were among the first to promote the idea that “double exchange alone does not explain the resistivity of  $\text{La}_{1-x}\text{Sr}_x\text{MnO}_3$ ”. Their argument hinges mainly on an estimate of the Curie temperature in a pure double exchange model; this turns out to be an order of magnitude too large. Moreover, Millis *et al* (1995) calculated the resistivity within the double exchange model including spin fluctuations and found a resistivity decrease below  $T_C$  and a positive magnetoresistance above  $T_C$ , both features in contradiction to the experimental results. It has to be noted, however, that this calculation does not agree with the results of Kubo and Ohata (1972), Calderón *et al* (1999a) as well as Ishizaka and Ishihara (1999). Millis *et al* (1995, 1996a, 1996b, 1996c) proposed that the electron-phonon coupling due to the dynamic Jahn-Teller distortion has to be included. This leads to the localization of conduction band electrons as small polarons (Holstein polarons, see Holstein 1959) above the Curie temperature. The basic idea is that transport in the manganites is determined by a competition between “self-trapping” of small polarons and delocalization due to the ferromagnetic ordering. If  $E_p$  denotes the polaron binding energy and  $t_{eff}$  the effective hopping matrix element, then a dimensionless measure of the electron-phonon coupling can be introduced as

$$\lambda = E_p/t_{eff}. \quad (13)$$

If  $\lambda$  is larger than a critical value, the electrons are “self-trapped” as small polarons. On cooling through the Curie temperature, the hopping matrix element  $t_{eff}$  is enhanced by the double exchange interaction and a polaron unbinding transition is induced.

Strong experimental evidence for small polaron formation comes from resistivity (Snyder *et al* 1996, Ziese and Srinithiwarawong 1998), thermopower (Jaime *et al* 1996, Palstra *et al* 1997), Hall effect (Jaime *et al* 1997), optical conductivity (Quijada *et al* 1998), mobility (Wang *et al* 1999), neutron scattering (Adams *et al* 2000, Dai *et al* 2000, Zhang *et al* 2001), volume thermal expansion (de Teresa *et al* 1997), nuclear magnetic resonance (Allodi *et al* 1998, Kapusta *et al* 1999), a large isotope effect (Shengelaya *et al* 1996, Zhao *et al* 1997, Babushkina *et al* 1998, Franck *et al* 1998, Zhou and Goodenough 1998), X-ray absorption fine structure spectroscopy (Booth *et al* 1998, Lanzara *et al* 1998) as well as Raman scattering (Yoon *et al* 1998, Björnsson *et al* 2000).

Calculations of the Curie temperature within a model including both double exchange and electron-phonon interactions (Millis *et al* 1996a, 1996c) yielded results in agreement with experimental findings. The calculated Curie temperature decreases significantly with the electron-phonon coupling. The resistivity as a function of temperature displayed a metal-insulator transition at the Curie temperature for strong

electron-phonon coupling. This transition is accompanied by a large magnetoresistance.  $\rho(T)$  in the paramagnetic phase can be tuned from semiconducting to metallic behaviour with decreasing electron-phonon coupling strength. The optical conductivity shows a Drude peak in the ferromagnetic phase, whereas  $\sigma(\omega) \rightarrow 0$  at low frequencies in the paramagnetic region. Moreover, above the Curie temperature a broad maximum in  $\sigma(\omega)$  appears due to transitions between the Jahn-Teller split  $e_g$  levels. The agreement with experiment is quite encouraging and indicates that this model contains the essential physics.

Narimanov and Varma (2001) determined the properties of the double exchange model coupled to phonons as a function of the electron-lattice coupling. Here also a competition between the itinerancy of electrons and localization due to polaron formation is found. If the electron-lattice coupling is larger than the bandwidth, the ferromagnetic transition is first order; in this case the lattice distortions present in the paramagnetic phase abruptly vanish below the Curie temperature. In the opposite limit of a small electron-phonon coupling, the transition is second order and lattice distortions in the paramagnetic phase are very small. This is consistent with observations of a diffuse component in neutron scattering experiments (Lynn *et al* 1996). Furthermore, within this model a strong dependence of the Curie temperature on the ion mass is found in agreement with the isotope effect.

*Spin polarons.* Röder *et al* (1996), see also Zang *et al* (1996), investigated a similar model of double exchange with a coupling of the charge carriers to longitudinal optical phonons due to the Jahn-Teller effect. Since both the static and dynamic Jahn-Teller effect split the  $e_g$  degeneracy, the model was solved using mean-field theory in a single orbital approximation valid for dopings  $x < 0.5$ . The Curie temperature was found to be considerably reduced by the electron-phonon coupling in agreement with the results of Millis *et al* (1996a). The effective kinetic energy  $K_{eff}$  shows an abrupt decrease as a function of the electron-phonon coupling constant due to “self-trapping” of charge carriers into a small polaronic state. The small polaron has spin character as evidenced by the temperature dependence of the numerically calculated spin-distribution. Strictly speaking, “self-trapping” is impossible in a model with translational invariance and there should always be polaronic band conductivity (Friedman 1964); however, small polarons might be localized by charge fluctuations if the polaronic bandwidth is narrow. Within this model, the metal-insulator transition is due to an abrupt unbinding of “self-trapped” spin-polarons as the effective kinetic energy is increased by the onset of ferromagnetic order. This transition is promoted by an applied magnetic field in qualitative agreement with experimental data.

The model of Röder *et al* (1996) is a discrete version of a continuum model for the thermally induced abrupt shrinking of a donor state in a ferromagnetic semiconductor as proposed by Emin and coworkers (Emin *et al* 1987, Hillery *et al* 1988, Emin and Holstein 1976). These models were developed in order to understand the sharp metal-insulator transition observed in ferromagnetic semiconductors such as non-stoichiometric EuO. In

these an impurity band forms and consequently the charge-carrier density is low. Main ingredients of the model are an intra-atomic exchange interaction as well as a short-range electron-phonon coupling. The strength of the electron-phonon interaction is assumed to be close to the critical value for “self-trapping” such that some additional mechanism like spin fluctuations might tip the balance and lead to the localization of small polarons in the paramagnetic phase. On cooling through  $T_C$  the onset of ferromagnetic ordering triggers an abrupt expansion of the small polaronic state. This model is in agreement with data on EuO (Oliver *et al* 1970, Penney *et al* 1972) and might have some relevance for CMR (Ziese and Sritiwarawong 1998).

*Vibronic states.* The strong increase in the Curie temperature with tolerance factor above a critical value  $tol_c$ , see figure 8(b), and with doping above  $x > x_c \sim 1/8$ , see figure 8(a) was addressed by Goodenough and co-workers within a vibronic state model. The basic idea is best illustrated for data as function of tolerance factor and is as follows (Goodenough 1997, 1999): below a critical tolerance factor  $tol_c$  the perovskite structure is distorted by static Jahn-Teller displacements of the O ions into an O'-orthorhombic symmetry ( $c < a\sqrt{2}$ ). The  $e_g$  orbitals show long range order and the manganites are antiferromagnetic or weakly ferromagnetic insulators in this regime (Zhou and Goodenough 1998). The decisive role of cooperative Jahn-Teller deformations in stabilizing orbital ordering and the A-type antiferromagnetic structure was confirmed in a theoretical study (Capone *et al* 2000). Above  $tol_c$  the structure changes to O-orthorhombic ( $c > a\sqrt{2}$ ) and the Curie temperature increases drastically by over 200 K. Goodenough argues that in this region the cooperative oxygen displacements are dynamic. In this regime the transport properties change from insulating to metallic. In view of the strong electron-lattice coupling, this transition might be understood if the coupling between orbitals and vibrational modes, both of  $e_g$  symmetry, is studied in more detail. Double exchange within a  $Mn^{4+}$ -O- $Mn^{3+}$  cluster, see equation (11), occurs with a hole transfer time  $\tau_h$ . If there are dynamic cooperative oxygen displacements with accompanying orbital reorientations, the holes will not be delocalized over the whole crystal, since the transitions are only possible along bridges with occupied  $e_g$  orbitals parallel to the  $Mn^{4+}$ -O- $Mn^{3+}$  bond. If the vibration period is long,  $\omega_0^{-1} \gg \tau_h$ , a hole is only delocalized on a Mn pair; this is called a Zener polaron. It will be itinerant as soon as the molecular orbital reorientation time  $\tau_r$  is of the order of the vibration period. With the estimate  $\tau_r \simeq (\Delta_{JT}/W)\omega_0^{-1}$ , where  $W$  is the electronic bandwidth and  $\Delta_{JT}$  the Jahn-Teller-stabilization energy, one obtains the following conditions for itinerancy (Goodenough 1999, Goodenough *et al* 1961):

$$\Delta_{JT} \ll \hbar\omega_0 \ll W. \quad (14)$$

For a  $(180^\circ - \phi)$  Mn-O-Mn bond angle the bandwidth is obtained within a tight-binding model as (Goodenough 1999)

$$W \propto \cos(\phi) \cos(\Theta/2), \quad (15)$$



where  $\Theta$  is the angle between adjacent core spins. Moreover, the phonon frequency  $\omega_0$  will also depend on  $\phi$ . Thus, within this vibronic state model, the strong increase of the Curie temperature and the electron delocalization might be attributed to both an increase in the bandwidth or a decrease in  $\omega_0$ . The isotope effect puts a more vital role on changes in  $\omega_0$ . A larger oxygen mass  $M_O$  softens the breathing mode  $\omega_0 \propto M_O^{-1/2}$  and drives the system towards static oxygen displacements and the O'-orthorhombic structure.

Since the transport properties change from insulating to metallic in this crossover regime, one might use the virial theorem to obtain a clue towards the interplay between lattice and electronic properties (Goodenough 1992, Archibald *et al* 1996). For spherically symmetric potentials decaying algebraically as  $V(r) \propto r^{-n}$  the virial theorem relates the mean kinetic energy  $\langle T \rangle$  to the mean potential energy  $\langle V \rangle$ :

$$2\langle T \rangle + n\langle V \rangle = 0. \quad (16)$$

If the kinetic energy is diminished by electron delocalization, the absolute value of the potential energy  $|\langle V \rangle|$  has to decrease accordingly. Since the relevant electrons occupy antibonding  $e_g$  states, a shortening of the  $\langle \text{Mn} - \text{O} \rangle$  bond produces such a decrease in  $|\langle V \rangle|$ . If the electronic system undergoes a discontinuous metal-insulator transition, the volume change must be discontinuous and the  $\langle \text{Mn} - \text{O} \rangle$  bond distribution shows a double well potential. Therefore, such a system is likely to undergo phase separation into hole-rich and hole-depleted regions. Rivadulla *et al* (2001) studied the evolution of magnetization and Jahn-Teller vibrational anisotropy as a function of Mn-O-Mn bond angle. At a critical bond angle ( $\sim 159^\circ$ ) the vibrational anisotropy changes between two degenerate Jahn-Teller modes and the saturation moment changes drastically. Phase separation might arise from a spatial variation of the vibrational anisotropy over the sample.

Evidence for this model, especially for dynamic Jahn-Teller distortions comes from measurements of the pressure dependent resistivity and thermopower of  $\text{La}_{1-x}\text{Sr}_x\text{MnO}_3$  ( $x = 0.12, 0.15$ ) single crystals (Zhou *et al* 1997) and  $^{16}\text{O}/^{18}\text{O}$  oxygen isotope exchanged  $(\text{La}_{1-x}\text{Nd}_x)_{0.7}\text{Ca}_{0.3}\text{MnO}_3$  samples (Zhou and Goodenough 1998) as well as from thermal conductivity measurements on  $\text{La}_{1-x}\text{Sr}_x\text{MnO}_3$  crystals (Zhou and Goodenough 2001). A discontinuous change in the Curie temperature of a  $\text{La}_{0.86}\text{Sr}_{0.14}\text{MnO}_3$  crystal as a function of pressure at  $p = 3$  kbar was interpreted as a transition from vibronic to metallic ferromagnetism (Zhou and Goodenough 2000). Further evidence comes from resistivity and thermopower measurements on a  $\text{LaMnO}_3$  single crystal above the orbital ordering temperature  $T_{JT} = 750$  K (Zhou and Goodenough 1999) and from a comprehensive study of the phase diagram of  $\text{La}_{1-x}\text{Sr}_x\text{MnO}_3$ ,  $0 \leq x \leq 0.35$  melt grown samples (Liu *et al* 2001). The vibronic model was originally proposed to explain the magnetic properties of  $\text{LaMn}_{1-x}\text{Ga}_x\text{O}_3$  (Goodenough *et al* 1961) and was verified by thermal conductivity, magnetization and ac-susceptibility measurements on this system under pressure (Zhou *et al* 2001).

*Localization.* The models discussed so far stress the importance of polaronic effects due to the strong electron-lattice coupling. In another class of models proposed by Kogan and Auslender (1988, 1998), Kogan *et al* (1999), Coey *et al* (1995), Varma (1996), Viret *et al* (1997b) and Wagner *et al* (1998), Anderson localization of the charge carriers due to spin fluctuations above  $T_C$  (and charge fluctuations due to the doping disorder) is supposed to cause the semiconducting behaviour in the paramagnetic regime as well as the metal-insulator transition at the Curie temperature. Kogan and Auslender (1988, 1998) showed that spin fluctuations localize charge carriers leading to a shift in the mobility edge as a function of the fluctuation strength. Accordingly, the metal-insulator transition occurs, when the mobility edge crosses the Fermi level. Kogan and Auslender (1988) found for the resistivity the expression

$$\rho = \rho_0 \exp \left[ \frac{1 - \langle \vec{S}_0 \cdot \vec{S}_1 \rangle / S^2}{1 + \langle S_z \rangle / S} \frac{W}{4kT} \right], \quad (17)$$

where  $\rho_0$  is a constant,  $\langle \vec{S}_0 \cdot \vec{S}_1 \rangle$  the spin-correlator for spins of magnitude  $S$ ,  $\langle S_z \rangle$  the mean spin-component along the magnetic field direction and  $W$  the bandwidth. This model is in quantitative agreement with data on the ferromagnetic semiconductor  $\text{Cd}_{0.99}\text{In}_{0.01}\text{Cr}_2\text{Se}_4$  (Kogan and Auslender 1988). Kogan and Auslender (1998) and Li *et al* (1997a), however, pointed out that such models are likely to apply only to low density materials. Indeed, it can be shown that electronic states near the band center of a double exchange ferromagnet are delocalized irrespective of the disorder strength. Since the manganites have a metallic carrier density of about one hole per unit cell (Jakob *et al* 1998, Matl *et al* 1998, Asamitsu and Tokura 1998, Ziese and Srinithiwarawong 1999), localization models might not explain the magnetotransport properties of these compounds. Wang and Zhang (1999) calculated the temperature dependent resistivity of a nearly half-metallic ferromagnet with Anderson localized minority carriers. These authors found a temperature dependence

$$\rho = \rho_0 + \rho_{5/2} T^{5/2} \quad (18)$$

above some cross-over temperature that was estimated to about 60 K. Below this temperature the resistivity follows a  $T^{3/2}$ -law. Equation (18) is also in good agreement with experimental data below about  $T_C/2$  (Ziese 2000b).

*Bi-polaron models* Alexandrov and Bratkovsky (1999a, 1999b, 1999c, 1999d) proposed a model based on the bi-polaron unbinding transition in order to explain the magnetotransport properties of the manganites. Based on results of electron-energy-loss spectroscopy (EELS) measurements on  $\text{La}_{1-x}\text{Sr}_x\text{MnO}_3$  films showing a significant  $\text{O}(2p)$  hole density (Ju *et al* 1997), Alexandrov and Bratkovsky (1999a, 1999b) concluded that the manganites are charge-transfer-type doped insulators with  $\text{O}(2p)$  holes. The holes in the  $\text{O}(2p)$  band are supposed to form bi-polarons immobilized by the strong electron-phonon interaction. If a pair of holes is localized on a single O ion, a singlet state forms; the exchange interaction with local  $\text{Mn}(3d^4)$  moments leads to a pair-breaking of

these singlets. Accordingly, the polaron density decreases in the paramagnetic phase on cooling due to a gradual condensation into bi-polarons. At the Curie temperature the instability of the bi-polarons caused by the exchange interaction leads to a sharp polaron density increase. Numerical calculations show a large effect of an applied magnetic field on the polaron density consistent with a large magnetoresistance. The competing energy scales driving the metal-insulator transition in this model are the bi-polaron binding energy and the exchange interaction. In contrast to the preceding models which predicted a large mobility increase when entering the ferromagnetic state, this model predicts a carrier-density collapse at the Curie temperature. Hall-effect measurements usually show small carrier-density variations near the ferromagnetic transition (Matl *et al* 1998, Jakob *et al* 1998, Ziese and Srinitiwawong 1999) and large mobility variations in contradiction to the model. Moreover, the EELS measurements are very sensitive to surface contamination and have to be treated with some care, since significant oxygen condensation can occur even at quite low pressures. Zhao *et al* (2000a, 2000b) analyzed the temperature dependence of the resistivity and found evidence for small polaron transport in the ferromagnetic phase and bi-polaron formation above  $T_C$ . The low temperature resistivity can be excellently modelled by band transport of small polarons with

$$\rho(T) = (\hbar^2/ne^2at) (A\omega_0)/\sinh^2(\hbar\omega_0/2k_B T). \quad (19)$$

Here  $a$  denotes the lattice constant,  $n$  the carrier density,  $t$  the hopping integral,  $\omega_0$  an optical phonon frequency and  $A$  is a constant. It has to be noted, however, that this expression also holds true for small polarons derived from Mn(3d) states. In further work, Alexandrov *et al* (2001) presented evidence for a polaronic Fermi liquid in optimally doped manganites from studies of the resistivity and thermopower of oxygen isotope-exchanged thin films. Here the effective carrier mass  $m^*$  is renormalized due to the strong electron-phonon interaction and depends on the ion mass according to  $m^* = m \exp(A/\omega)$ , where  $m$  denotes the bare band mass. From an experimental point of view, the polaronic liquid scenario yields a much better description of the low temperature resistivity behaviour than any of the power laws found within double exchange or localization models (Zhao *et al* 2000a, Ziese unpublished).

*Phase separation and percolation.* In studies of CMR manganites the issue of phase separation has emerged, especially in the regime of low dopings  $x$  or small tolerance factor. Phase separation in manganites is discussed in detail in a review by Dagotto *et al* (2001); here the presentation will be restricted to some general ideas.

The issue of phase separation in manganites is not new. Already the first extensive neutron study of  $\text{La}_{1-x}\text{Ca}_x\text{MnO}_3$  by Wollan and Koehler (1955) reported the co-existence of ferromagnetic and A-type antiferromagnetic reflections in non-stoichiometric  $\text{LaMnO}_3$  (14, 18 and 20%  $\text{Mn}^{4+}$ ) and in  $\text{La}_{0.89}\text{Ca}_{0.11}\text{MnO}_3$ . The authors concluded: “The fact that the magnetic measurements show the (200) and (220) ferromagnetic reflections to be field sensitive and the superstructure reflections (100)

and (210) to be unaffected by the field is strong evidence in favour of accounting for the overall magnetic structure of samples in this composition range as consisting of an incoherent mixture of ferro- and antiferromagnetic regions or domains.” Astonishingly enough, this major experimental work was published five years before the theoretical work of de Gennes (1960) who interpreted the spin structure at low dopings as a canted antiferromagnet. Within de Gennes’ model the spontaneous magnetization at low doping is proportional to the doping (de Gennes 1960). Khomskii (2000) pointed out that the electron energy in this approximation is given by  $E = E_0 - t^2/J_H x^2$  such that  $\partial^2 E/\partial x^2 < 0$  and accordingly the compressibility is negative. This indicates the instability of the canted state and a tendency to phase separation; for more detailed arguments see Kagan *et al* (1999) and Arovas and Guinea (1998). This discussion is far from being settled, see e.g. the magnetization data by Geck *et al* (2001) that support evidence for a canted antiferromagnetic state in  $\text{La}_{0.94}\text{Sr}_{0.06}\text{MnO}_3$  single crystals.

Intimately related to the concept of phase separation is the idea of percolation of insulating and metallic regions. A percolation mechanism for the metal-insulator transition was proposed by Bastiaansen and Knops (1998). Starting from a half-metallic band-structure, where electrons can propagate only in magnetic domains with the magnetization parallel to the electron spin, the metal-insulator transition temperature corresponds to the percolation threshold for magnetic domains. Above  $T_C$  both majority and minority carriers percolate leading to a resistivity decrease. Monte-Carlo simulations of resistor networks within the Ising model including nearest neighbour and next-nearest neighbour bonds yielded qualitative agreement with experimental data concerning both the temperature variation of the resistivity and the influence of a magnetic field (Bastiaansen and Knops 1998). Since this model does not take into account the gradual spin precession in the rather thick domain walls, it is unlikely to capture the essential physics of the manganites. However, in the light of recent results on phase separation (Moreo *et al* 1999), percolation of metallic and semiconducting regions might occur near  $T_C$ , especially in compounds with a low Curie temperature. The manganites have a tendency to segregate into hole-rich ferromagnetic metallic and undoped antiferromagnetic insulating regions. These might coexist near the metal-insulator transition, such that the resistivity below  $T_C$  is determined by percolating metallic regions. Scanning-tunnelling microscopy studies of LCMO single crystals and films revealed the coexistence of metallic and semiconducting regions on length scales of several 10 nm (Fäth *et al* 1999). The application of a magnetic field leads to the reversible growth of metallic regions. The origin of this phase separation is not fully understood, since a separation into differently charged regions is energetically unfavourable due to the long range Coulomb interaction. Therefore, the experimental findings might be related to structural disorder like twinning, variation of the oxygen content or cation disorder (Fäth *et al* 1999). Uehara *et al* (1999) reported a percolation transition in  $\text{La}_{5/8-y}\text{Pr}_y\text{Ca}_{3/8}\text{MnO}_3$  as evidenced by electron microscopy. In this system phase separation into metallic ferromagnetic and charge-ordered insulating domains occurs on a sub-micrometer scale. This phase separation is not of a charge-segregation

type, but is one between the optimally doped ferromagnetic and  $x = 1/2$  charge-ordered states. This explains the large length scale of about  $0.5 \mu\text{m}$  observed for the domains.

Mayr *et al* (2001) modelled the resistivity of manganites by a random resistor network, based on the idea of phase separation between metallic and insulating regions. Near percolation small magnetic fields induce large changes in the resistivity in agreement with experiment. Weiße *et al* (2001) propose a two-phase scenario of competing ferromagnetic metallic and insulating polaronic phases; the balance between these two phases can be tuned by the variation of various parameters. The magnetization exhibits a first order transition which is consistent with the neutron scattering data of Lynn *et al* (1996) and the magnetization data of Mira *et al* (1999) and Ziese (2001a). Dzero *et al* (2000) apply percolation theory to study the phase diagram at low dopings  $x$ . Modelling the metallic phase as a two-band Fermi liquid and the insulating phase as a band insulator, they arrive at a transition from the antiferromagnetic insulating to the metallic ferromagnetic state at  $x \simeq 0.16$ .

*Magnetoimpurity theory.* The magnetoimpurity theory developed by E. L. Nagaev (see Nagaev 2001 and references therein) treats the manganites as specific examples within the more general class of ferromagnetic semiconductors. According to this model the mechanism underlying the resistivity maximum at the Curie temperature and CMR should be essentially the same in the manganites as in other ferromagnetic semiconductors such as EuO and  $\text{NdCr}_2\text{S}_4$ . Within this approach the manganites are considered as degenerate semiconductors; holes might move in a band derived from Mn states, but are more likely to move in an O band (Nagaev 1996). The transport properties are modelled within a *sd*-model, where the d states refer to the Mn  $t_{2g}$  states and the “s-states” to the Mn  $e_g$  states. The theory explicitly takes random fluctuations of the acceptor states into account: this leads to Anderson localization in the band tails enhancing the carrier density close to charged impurities. At finite temperature the carrier density fluctuations lead to spatial fluctuations of the magnetization, where regions close to impurities acquire an excess magnetic moment. This scatters charge carriers and leads to the temperature dependence of the resistivity, especially the resistivity maximum. Nagaev (1999) argues that polaron formation is unimportant, since the *sd*-exchange energy is much larger than the lattice polarization energy. Furthermore, since this mechanism is supposed to describe the magnetotransport phenomena in all ferromagnetic semiconductors, with many systems showing no Jahn-Teller distortions, Nagaev argues that the Jahn-Teller effect is unimportant for CMR. This model seems to contradict the isotope effect found in many manganites. This was reconciled by Nagaev (1998) by relating the isotope effect to the fact that the thermodynamic equilibrium densities of oxygen vacancies or excess oxygen atoms depend on the oxygen mass. Data on the oxygen isotope effect in  $\text{La}_{0.8}\text{Ca}_{0.2}\text{MnO}_3$  partially support this scenario (Franck *et al* 1998).

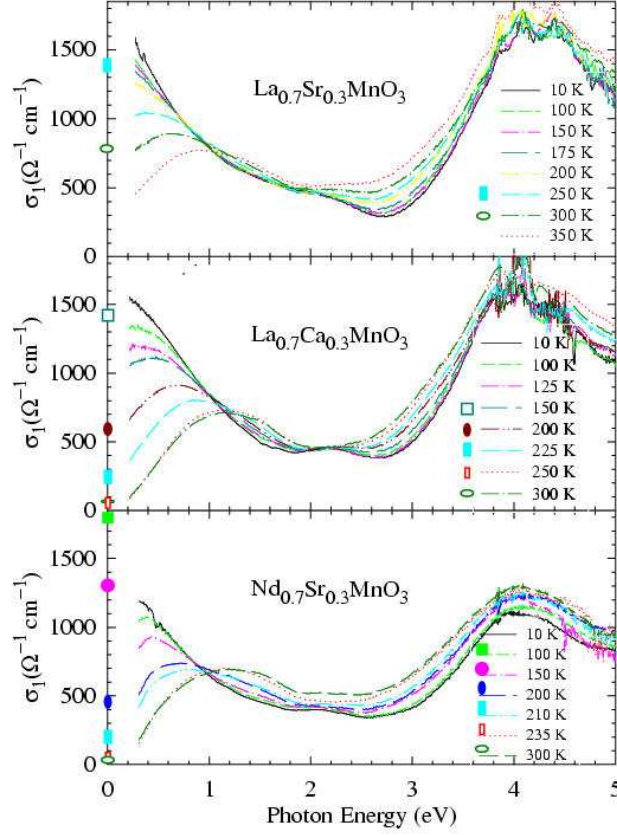


**Figure 9.** Frequency dependence of the real part of the optical conductivity  $\sigma_1$  of epitaxial manganite films at different temperatures. Reproduced from Quijada *et al* (1998).

*3.4.3. Optical properties.* The optical properties of the manganites are still highly controversial. Here only a very brief overview of recent developments is given. Okimoto *et al* (1997) measured the reflectivity of  $\text{La}_{1-x}\text{Sr}_x\text{MnO}_3$  single crystals with dopings  $x = 0.0, 0.1, 0.175$  and  $0.3$  in a wide range of temperatures for frequencies from the infrared to the ultraviolet. At high photon energies three major, doping and temperature independent peaks are observed; these were assigned to one intra-atomic transition from  $\text{La}(5p) \rightarrow \text{La}(5d)$  at 25 eV and interband transitions from  $\text{O}(2s) \rightarrow \text{Mn}(3d)$  at 17 eV and  $\text{O}(2p) \rightarrow \text{La}(5d)$  at 8 eV, respectively. Below about 3 eV the optical conductivity is strongly temperature and frequency dependent. For dopings 0.1, 0.175 and 0.3 a strong transfer of optical weight to lower frequencies is observed on decrease of temperature. Above  $T_C$  an optical gap is seen for all dopings that disappears on cooling through the ferromagnetic transition for  $x = 0.175$  and  $0.3$  in agreement with the metallic ground state of these compounds. Quijada *et al* (1998) measured the optical conductivity of high quality epitaxial  $\text{La}_{0.7}\text{Sr}_{0.3}\text{MnO}_3$ ,  $\text{La}_{0.7}\text{Ca}_{0.3}\text{MnO}_3$  and  $\text{Nd}_{0.7}\text{Sr}_{0.3}\text{MnO}_3$  films for photon energies up to 5 eV. The three samples show a similar optical conductivity that is in agreement with the data of Okimoto *et al* (1997) for  $x = 0.3$ . Below

photon energies of 5 eV there are three major features, see figure 9: (i) a strong, temperature independent peak centered at 4 eV, (ii) a shallow, strongly temperature dependent minimum developing at low temperatures and (iii) above  $T_C$  a small peak near 1 eV that shifts to lower energy on decrease of temperature and develops into a Drude peak. The assignment of the features is controversial. Okimoto *et al* (1997) interpreted the maximum near 1 eV as an interband transition  $O(2p) \rightarrow Mn(3d) (e_g)$ . These authors estimated Hund's rule coupling energy from the peak position of the interband transitions and found about 0.9 eV for  $x = 0.3$ . Quijada *et al* (1998), on the other hand, assigned the temperature independent peak at 4 eV to the interband transition  $O(2p) \rightarrow Mn(3d) (e_g)$ , since this transition involves electrons of both spin directions on the oxygen and is not believed to be strongly temperature dependent. The features at 1 eV and 3 eV were interpreted as arising from  $e_g \rightarrow e_g$  interband transitions with the same and parallel spins, respectively. This yields an estimate of the Hund's rule coupling energy of about 1.5 eV. The interpretation of Quijada *et al* (1998) was later criticized by Chattopadhyay *et al* (2000). Chattopadhyay *et al* (2000) derived the optical conductivity and the Curie temperature within a double exchange only model; these authors found that the Curie temperature depends linearly on the change of the kinetic energy between zero temperature and  $T_C$ . The kinetic energy does not depend on details of the band structure; it can be derived from the optical conductivity and compared with the measured transition temperature. On the basis of this model, Chattopadhyay *et al* (2000) argued that the strongly temperature dependent feature in the optical conductivity at 3 eV does not correspond to transitions into the minority  $e_g$  band, since the derived value of the Hund's rule coupling energy is too small to reproduce the measured Curie temperature. The  $e_g \rightarrow e_g$  transition is expected to be at a higher photon energy above 4 eV. The analysis of the spectral weight transfer as a function of temperature in terms of a kinetic energy change leads to the conclusion that electron-phonon coupling and correlation effects are vital to explain the physics of the manganites.

### 3.5. $Sr_2FeMoO_6$

$Sr_2FeMoO_6$  belongs to the class of ordered double perovskites  $AA'BB'O_6$ . These are known to be ferromagnetic for  $B' = Cr, Fe$ ,  $B = Mo, Re$  and  $A = A'$  an alkaline earth element (Longo and Ward 1961, Sleight *et al* 1962, Patterson *et al* 1963, Sleight and Weiher 1972). For the ordered double perovskites a rock-salt structure is observed. There is a rapidly increasing bulk of research work on double perovskites; recent research focused mainly on  $Sr_2FeMoO_6$  with a Curie temperature of about 420 K (Kobayashi *et al* 1998). Ca and Ba substitution was found to decrease the Curie temperature to 345 K ( $Ca_2FeMoO_6$ ) and 367 K ( $Ba_2FeMoO_6$ ) (Borges *et al* 1999). The highest Curie temperature was reported for  $Ca_2FeReO_6$  with  $T_C \sim 538$  K (Longo and Ward 1961).

Band-structure calculations for  $Sr_2FeMoO_6$  and  $Sr_2FeReO_6$  using the full potential augmented plane-wave (FLAPW) method based on the generalized gradient

approximation (GGA) yielded a half-metallic band structure (Kobayashi *et al* 1998, Kobayashi *et al* 1999). In the majority band an energy gap of about 1 eV was seen at the Fermi level between the occupied Fe  $e_g$  and the unoccupied Re or Mo  $t_{2g}$  levels. The minority density of states is finite at the Fermi level with carriers of hybridized Fe(3d) and Mo(4d) or Re(5d) character, respectively.

Within an ionic model,  $A_2\text{MoFeO}_6$  is a ferrimagnet with Fe and Mo sublattices. Recent neutron-powder diffraction, Mössbauer spectroscopy and X-ray diffraction studies yield the following consistent picture regarding crystal and magnetic structure. At room temperature and below the compound is cubic, tetragonal or monoclinic for Ba, Sr, and Ca substitution, respectively (Borges *et al* 1999, Greneche *et al* 2001, Chmaissem *et al* 2000, Ritter *et al* 2000).  $\text{Sr}_2\text{FeMoO}_6$  shows a crystallographic transition from cubic to tetragonal on cooling through the Curie temperature (Chmaissem *et al* 2000, Ritter *et al* 2000). First Mössbauer-investigations on  $\text{Ca}_2\text{MoFeO}_6$  showed a formal  $\text{Fe}^{3+}/\text{Mo}^{5+}$  charge configuration (Pinsard-Gaudart *et al* 2000). The  $\text{Fe}^{3+}$  ( $3d^5$ ) ion is in a high spin state with  $\mu_{\text{Fe}} = 5\mu_B$  and the  $\text{Mo}^{5+}$  ( $4d^1$ ) ion has a magnetic moment  $\mu_{\text{Mo}} = \mu_B$ , such that a net moment of  $4\mu_B$  results. Neutron diffraction data, however, indicate reduced magnetic moments between  $0..0.5\mu_B$  on the Mo site coupled antiferromagnetically to Fe moments of magnitude  $\mu_{\text{Fe}} = 3.7..4.3\mu_B$  (Chmaissem *et al* 2000, Ritter *et al* 2000, García-Landa *et al* 1999). X-ray absorption spectroscopy (Ray *et al* 2001b) indicates a Mo moment smaller than  $0.25\mu_B$ . The measured isomer shift is rather large and indicates a mixed valence state of the Fe-ion (Greneche *et al* 2001, Balcells *et al* 2001, Lindén *et al* 2000). This is in agreement with the reduced magnetic moment on the Mo site. The low temperature magnetic moment as determined from global magnetization is often found to be considerably reduced from the ideal value of  $4\mu_B$  to about  $3-3.5\mu_B$  (García-Landa *et al* 1999, Borges *et al* 1999, Manako *et al* 1999, Tomioka *et al* 2000, Balcells *et al* 2001). This is attributed to cation disorder on the Fe/Mo sites (Ogale *et al* 1999). Balcells *et al* (2001) observed a decrease of the saturation magnetization proportional to the antisite concentration. The magnetization is reduced by  $8\mu_B$  per antisite in agreement with a simple ionic model. This is also consistent with the data of Tomioka *et al* (2000). From the analysis of Mössbauer spectra Greneche *et al* (2001) concluded that antisite defects predominate in comparison to anphase boundaries. Martínez *et al* (2000) determined the effective magnetic moment  $\mu_{\text{eff}} \simeq 3.4\mu_B$  from the high temperature susceptibility. This value indicates a  $\text{Fe}(3d^6)\text{Mo}(4d^0)$  state. The Re-compounds  $A_2\text{FeReO}_6$  are less well studied; measurements of isomer shifts, however, also indicate the mixed valence nature of Fe in these materials; the mixed valent character was observed to decrease from Ba to Ca substitution (Gopalakrishnan *et al* 2000). In conclusion, these data indicate that the double perovskites are itinerant ferromagnets with a mixed valence of the Fe-ions; the itinerant carriers are mainly of Mo(4d) and Re(5d) character.

The resistivity depends sensitively on the preparation conditions, presumably due to cation disorder, grain-boundary scattering and oxygen content. In  $\text{Sr}_2\text{FeMoO}_6$  both semiconducting and metallic behaviour has been observed (Tomioka *et al* 2000, Westerburg *et al* 2000, Asano *et al* 1999, Manako *et al* 1999, Chmaissem *et al* 2000).



Judging from measurements on a single crystal grown by the floating zone method, the stoichiometric compound has a metallic resistivity below and above the Curie temperature (Tomioka *et al* 2000). However, Niebieskikwiat *et al* (2000) presented evidence for a strong influence of environmental conditions on the resistivity. Careful measurements under vacuum show a metal-insulator transition at the Curie temperature (Niebieskikwiat *et al* 2000). The residual resistivity is quite high with  $200 - 300 \mu\Omega\text{cm}$  (Tomioka *et al* 2000, Westerburg *et al* 2000) presumably due to cation disorder scattering. The nature of carriers is electron-like with a density of about  $1.1 \times 10^{28} \text{ m}^{-3}$  corresponding to one electron per Fe/Mo pair (Tomioka *et al* 2000). The optical conductivity in the ferromagnetic phase shows a Drude component and two excitation maxima at 0.5 eV and 4 eV, respectively. These have been interpreted as charge-transfer transitions from the up spin  $\text{Fe}(e_{g\uparrow})$  to the  $\text{Mo}(t_{2g})$  band (0.5 eV) and the  $\text{O}(2p)$  to  $\text{Mo/Fe}(t_{2g\downarrow})$  down spin band (4 eV), respectively (Tomioka *et al* 2000). In the Re-compounds there is some evidence that  $\text{Ba}_2\text{FeReO}_6$  is metallic, whereas  $\text{Ca}_2\text{FeReO}_6$  is insulating (Gopalakrishnan *et al* 2000, Prellier *et al* 2000); this correlates to the decreasing mixed valence character of the Fe ion.

A considerable low field magnetoresistance often appears in magnetotransport measurements that is likely to be of extrinsic origin arising from grain-boundary or cation-disorder scattering. At the Curie temperature a small magnetoresistance maximum of about -5% in 8 T was observed (Westerburg *et al* 2000). Alonso *et al* (2000) report a magnetoresistance increasing with temperature in  $\text{Ca}_2\text{FeMoO}_6$ . The data on the intrinsic magnetoresistance are too scarce to allow a further discussion.

The origin of the itinerant ferrimagnetism in FeMo and FeRe double perovskites seems to be intimately linked to a specific band structure, namely the strong overlap between the Fe  $t_{2g\downarrow}$  and the Mo(4d) or Re(5d) levels, respectively. It is striking indeed that  $\text{Sr}_2\text{MMoO}_6$  with  $\text{M} = \text{Cr}, \text{Mn}, \text{Co}$  (Moritomo *et al* 2000) and  $\text{Sr}_2\text{FeWO}_6$  (Kobayashi *et al* 2000, Dass and Goodenough 2001, Ray *et al* 2001a) are insulating, especially since W and Mo are iso-electronic. Moreover, Mo is known to have a small exchange integral and a magnetic moment on the Mo site is rare. Theoretical models stress the hybridization between the Fe  $t_{2g\downarrow}$  and Mo(4d) bands at the Fermi level that induces spin-polarization on the Mo site. Sarma *et al* (2000) find a large enhancement of the effective exchange integral that leads to a negative effective Coulomb interaction strength  $U$ . This is consistent with Mo core level spectroscopy (Sarma *et al* 2000). Fang *et al* (2001) point out that the strong hybridization leads to both a gain in kinetic energy and an induced spin-polarization on Mo/Re, both stabilizing ferrimagnetism. The W(5d) bands are slightly too high in energy to allow for sufficient hybridization with the Fe(3d) states; consequently,  $\text{Sr}_2\text{FeWO}_6$  is an antiferromagnetic insulator dominated by super-exchange. These models obviously have to be further developed; they are, however, in agreement with the percolative nature of charge transport in  $\text{Sr}_2\text{FeMo}_x\text{W}_{1-x}\text{O}_6$  alloys (Kobayashi *et al* 2000, Dass and Goodenough 2001, Ray *et al* 2001a).

Electron doping in the series  $\text{Sr}_{2-x}\text{La}_x\text{FeMoO}_6$  raises the Curie temperature from 420 K to 490 K (Navarro *et al* 2001).

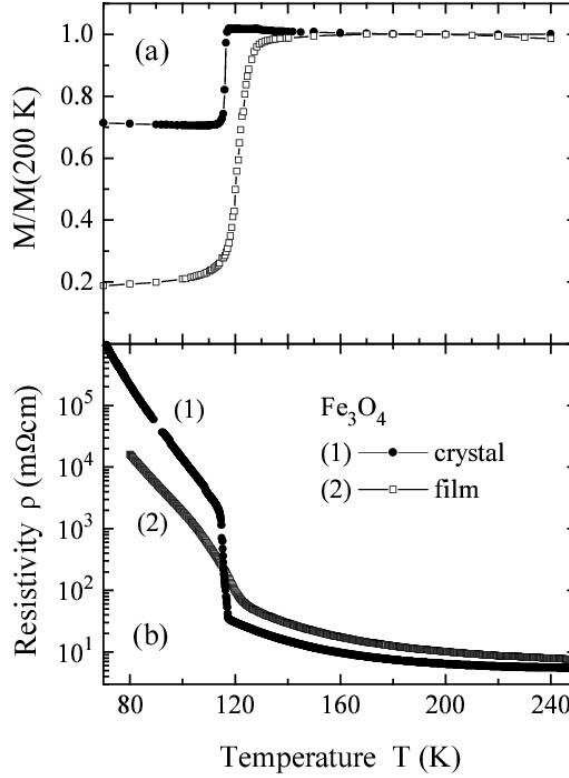


**Figure 10.** (a) Magnetization and (b) resistivity of a magnetite single crystal and a 200 nm thick magnetite film as a function of temperature. The magnetization was measured in applied fields of 5 mT along [110] in the case of the crystal and in 10 mT along [100] in the case of the film. After Ziese and Blythe (2000).

### 3.6. $\text{Fe}_3\text{O}_4$

Magnetite is a well-studied ferrimagnet and for many details the reader is referred to the extensive reviews of Brabers, Brabers and Whall as well as Krupička and Novák; here only some magnetotransport properties will be discussed. Magnetite shows semiconducting behaviour between the Verwey transition temperature  $T_V$  (Verwey 1939) and 320 K, crossing over to metallic behaviour at higher temperatures (Todo *et al* 1995). At the Verwey transition a jump in the resistivity is observed; the magnitude of this jump depends on the stoichiometry and reaches up to a factor of 100. The temperature dependent resistivity of a single crystal and a 200 nm thick film are shown in figure 10(b). The single crystal shows a sharp resistivity jump of nearly two orders of magnitude at the Verwey temperature,  $T_V = 116.5$  K; the film has a higher Verwey temperature  $T_V = 119$  K, but the resistivity transition is much more gradual. Stoichiometric magnetite has a Verwey temperature  $T_V \simeq 123$  K; this indicates that the two samples shown in figure 10 are somewhat iron deficient. The magnetization measured in small magnetic fields shows a sharp increase when going through the Verwey temperature.

Magnetite crystallizes in the inverse spinel structure. At room temperature, in

this structure large O ions are located on a close-packed face-centered cubic lattice, whereas the Fe ions occupy interstitial sites. There are two kinds of cation sites, namely the tetrahedrally coordinated A site occupied only by  $\text{Fe}^{3+}$  ions and the octahedrally coordinated B site occupied by both  $\text{Fe}^{2+}$  and  $\text{Fe}^{3+}$  ions. The A- and B-site sublattices are ferrimagnetically aligned such that the net moment is equal to the magnetic moment  $\mu = 4\mu_B$  of the  $\text{Fe}^{2+}$  ( $3d^6$ ) ion.

The Verwey transition is associated with a order-disorder transition from a charge ordered state of the Fe ions on the B sites at low temperatures to a statistical distribution at higher temperatures (Verwey 1939). The conductivity of magnetite at room temperature which is exceptionally high among the ferrites is due to electron transfer between  $\text{Fe}^{2+}$  and  $\text{Fe}^{3+}$  ions on the B sites – or, to put it in other words, due to the mixed valence nature of the Fe ions on the B sites. Below the Verwey transition, in the charge ordered state, carrier transport occurs via electron hopping and it is intuitively clear that the resistivity shows semiconducting/insulating behaviour. Band-structure calculations (de Groot and Buschow 1986, Pénicaud *et al* 1992, Yanase and Siratori 1984, Yanase and Hamada 1999) indicate a half-metallic nature with a gap in the majority density of states. However, this is not in agreement with the experimentally observed semiconducting resistivity up to about 320 K. Here the strong electron-phonon interaction is important leading to the formation of small polarons. In the charge ordered phase, the strong intersite Coulomb interaction leads to a band-splitting and semiconducting behaviour. Ihle and Lorenz (1985, 1986) showed that short-range polaronic order and band-splitting due to the strong intersite Coulomb interaction persist above the Verwey transition up to high temperatures. However, above  $T_V$  a narrow band is formed at the Fermi level and gradually populated at higher temperatures. This leads to thermally activated polaronic band motion above the Verwey transition. In parallel to the polaronic band conductivity, polaronic hopping conductivity becomes important at higher temperatures. If both conduction processes are taken into account, good agreement between the calculated and measured conductivity is found, and especially the conductivity maximum near room temperature is reproduced (Ihle and Lorenz 1986). The band-splitting is confirmed in LSDA+U band-structure calculations performed by Anisimov *et al* (1996).

Photoemission measurements of the band structure of  $\text{Fe}_3\text{O}_4$  single crystals (Chainanai *et al* 1995) and thin films grown on Pt (111) (Cai *et al* 1998) indicate a finite density of states at the Fermi level and corroborate the predicted metallic nature in the cubic phase. This is in agreement with the analysis of optical conductivity data by Degiorgi *et al* (1987) and Park *et al* (1998). Park *et al* (1998) observe a clear opening of an optical gap below the Verwey transition. Above the transition a significant spectral weight transfer in the  $\text{Fe}(3d)$  intersite transition region occurs in qualitative agreement with considerable short-range order as assumed in the model of Ihle and Lorenz (1985, 1986). A careful analysis of the optical conductivity by Degiorgi *et al* (1987) revealed a small Drude contribution at 300 K and 130 K in agreement with polaronic band transport above  $T_V$ . A broad conductivity maximum near 0.2 eV was

attributed to small polaron hopping (Degiorgi *et al* 1987). On the other hand, Park *et al* (1997) conclude from their photoemission and inverse photoemission data on a magnetite single crystal that there is no spectral weight at the Fermi level. On heating through the transition the single particle gap does not collapse, but is merely reduced by about 50 meV from  $150 \pm 30$  meV to  $100 \pm 30$  meV. This is consistent with the conductivity jump by a factor of a hundred, if semiconducting transport is assumed above and below  $T_V$ . In conclusion, a unified picture of transport in magnetite has not yet been found. The model of Ihle and Lorenz (1985, 1986), however, is supported by a bulk of dc conductivity, optical conductivity and photoemission spectroscopy data. For further discussions on the transport properties of magnetite the reader is referred to the review of Brabers (1995) and to a recent review on metal-insulator transitions by Imada *et al* (1998).

#### 4. Intrinsic magnetoresistance

In this section a brief overview on the intrinsic magnetoresistance of  $\text{SrRuO}_3$ ,  $\text{Tl}_2\text{Mn}_2\text{O}_7$ ,  $\text{CrO}_2$ , the manganites and magnetite is given in order to facilitate comparison with the extrinsic magnetoresistance that will be discussed in later sections.

##### 4.1. $\text{SrRuO}_3$

The magnetoresistance of  $\text{SrRuO}_3$  films grown on  $2^\circ$  miscut  $\text{SrTiO}_3$  substrates was measured by Kacedon *et al* (1997) and Klein *et al* (1998). The magnetoresistance depends sensitively on either the current and the magnetic field direction as usually found in single crystals (Campbell and Fert 1982). Near the Curie temperature a maximum in the magnetoresistance ratio was found that does not saturate in magnetic fields up to 8 T. The value of the maximal magnetoresistance depends on the current and field direction with values between  $-2\%$  and  $-11\%$ . Klein *et al* (1998) interpreted this magnetoresistance peak as arising from an increase of the magnetization and a corresponding reduction of spin-disorder scattering. At lower temperatures anisotropic magnetoresistance is found and the resistance change is mainly due to a change in the magnetization direction. Again, the magnetoresistance values reported by both groups do not agree; Klein *et al* (1998) found about  $-18\%$  in a field of 6 T for currents along  $[001]$  at low temperatures, whereas Kacedon *et al* (1997) reported only about  $-3\%$  in a field of 8 T and for the same current direction. It is not clear, to what extent the magnetoresistance values are influenced by sample inhomogeneities and extrinsic effects.

##### 4.2. $\text{Tl}_2\text{Mn}_2\text{O}_7$

The pyrochlore  $\text{Tl}_2\text{Mn}_2\text{O}_7$  shows a large magnetoresistance near the Curie temperature that is actually larger than the magnetoresistance observed in  $\text{La}_{0.7}\text{Ca}_{0.3}\text{MnO}_3$  (Ramirez and Subramanian 1997). As already indicated in the previous section, the model of Majumdar and Littlewood (1998a, 1998b) describing the dynamics of a low density

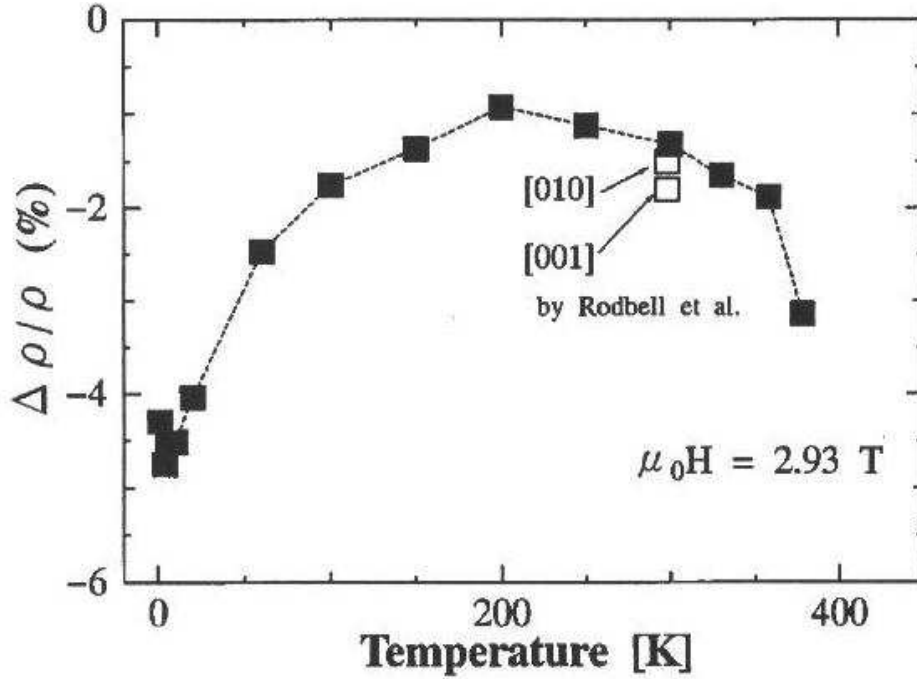


**Figure 11.** Longitudinal magnetoresistance ratio at 2.93 T of a textured  $\text{CrO}_2$  film on  $\text{ZrO}_2$  as a function of temperature. For comparison, data by Rodbell *et al* (1966) are shown. Reproduced from Suzuki and Tedrow (1998).

electron gas coupled to spin fluctuations seems to capture the relevant physics of the magnetotransport phenomena in  $\text{Tl}_2\text{Mn}_2\text{O}_7$ . Within this model the large magnetoresistance near the Curie temperature arises from two mechanisms: in the metallic phase spin-disorder scattering is anomalously large due to the low carrier density; above  $T_C$  spin-polarons form in an intermediate temperature range that display a strong field dependence of the binding energy. In both cases the application of a magnetic field leads to a large decrease of the resistivity.

#### 4.3. $\text{CrO}_2$

The magnetoresistance of textured  $\text{CrO}_2$  films was studied by Suzuki and Tedrow (1998, 1999). The longitudinal magnetoresistance ratio in a magnetic field of 2.93 T is shown in figure 11 as a function of temperature. The magnetoresistance shows a maximum at low temperatures and an increase at high temperatures above about 300 K. The Curie temperature of this film was 390 K; thus, one cannot decide if  $\text{CrO}_2$  displays a magnetoresistance maximum at  $T_C$  as expected from the interpretation as a self-doped double-exchange ferromagnet (Korotin *et al* 1998). Above about 200 K the longitudinal magnetoresistance is linear in the applied field, whereas a concave non-linear behaviour is seen below this temperature. The non-linear field dependence was attributed to cyclotron orbital motion of the conduction electrons (Suzuki and Tedrow 1998).

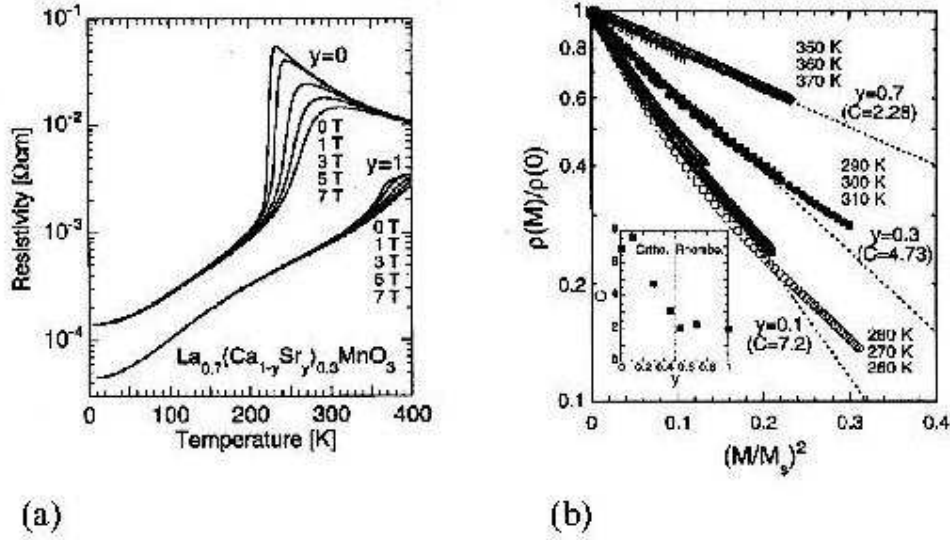


**Figure 12.** (a) Resistivity versus temperature for  $\text{La}_{0.7}(\text{Ca}_{1-y}\text{Sr}_y)_{0.3}\text{MnO}_3$  ( $y = 0$ ,  $y = 1$ ) single crystals in various applied fields. The magnetoresistance is maximal near the metal-insulator transition. (b) Magnetoresistance as a function of the normalized magnetization  $M/M_S$  for samples with  $y = 0.1$ ,  $0.3$  and  $0.7$ . A scaling  $\rho/\rho_0$  with  $(M/M_S)^2$  is observed. After Tomioka *et al* (2001).

#### 4.4. $\text{La}_{0.7}\text{A}_{0.3}\text{MnO}_3$

**4.4.1. Colossal magnetoresistance.** The manganites have received intense research interest, since these compounds display a new kind of magnetoresistance called colossal magnetoresistance. This magnetoresistance appears as a sharp magnetoresistance peak at the Curie temperature. In figure 12(a) typical resistivity data of  $\text{La}_{0.7}(\text{Ca}_{1-y}\text{Sr}_y)_{0.3}\text{MnO}_3$  single crystals in various magnetic fields are shown. The magnetoresistance is maximal near the metal-insulator transition leading to a peak in the magnetoresistance ratio

$$\frac{\Delta\rho}{\rho_0} = \frac{\rho(H) - \rho_0}{\rho_0}. \quad (20)$$

The height of this magnetoresistance peak is seen to decrease with increasing Curie temperature. This is a general trend in the manganites and magnetoresistance values of nearly 100% can be found in compounds with low Curie temperatures (McCormack *et al* 1994, Jin *et al* 1995a, 1995b, Coey *et al* 1999). Figure 12(b) shows that the magnetoresistance depends on temperature and field through the magnetization. Often a scaling  $\Delta\rho/\rho_0 = -C(M/M_S)^2$  is found for small values of the reduced magnetization (Tokura *et al* 1994, Urushibara *et al* 1995, Fontcuberta *et al* 1996, O'Donnell *et al* 1996). The scaling constant  $C$  lies in the range  $1 \leq C \leq 4$  and depends on doping (Urushibara *et al* 1995). This can be understood within the Kondo lattice model in the classical spin limit (Furukawa 1994, 1995a, 1995b, Inoue and Maekawa 1995).  $C$  depends on the value of the Hund's rule coupling with  $C = 1$  in the weak coupling limit  $J_H \ll 1$ ; in the strong coupling limit  $C$  depends on doping and is of the order  $C \sim 5$  in qualitative agreement with experiment (Furukawa 1994). It has to be pointed out,

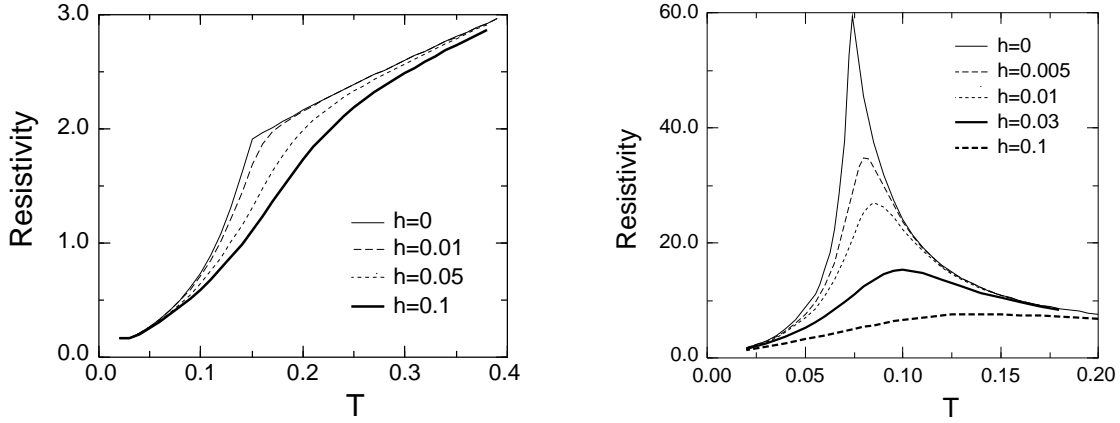


**Figure 13.** Temperature dependence of the resistivity at different values of the normalized magnetic field  $h$  for two values of the electron-phonon coupling,  $\lambda = 0.7$  (left panel) and  $\lambda = 1.12$  (right panel). The parameter  $h$  is related to the physical field  $H$  by  $h = g\mu_B S H/t$ . Using a gyromagnetic ratio  $g = 2$ , a hopping integral  $t = 0.6$  eV and the core spin  $S = 3/2$  means that  $h = 0.01$  corresponds to  $H = 15$  T. The reduced electron-lattice coupling strength is given by  $\lambda = G^2/kt$ , where  $G$  denotes the electron-phonon coupling constant and  $k$  the phonon spring-constant. The temperature  $T$  is given in units of  $t$ . Reproduced from Millis *et al* (1996c).

however, that a quadratic dependence of the resistivity on the magnetization is also present in conventional ferromagnets such as Ni (Gerlach and Schneiderhan 1930).

Colossal magnetoresistance can be qualitatively understood within the double-exchange model. An applied magnetic field leads to a better alignment of the core spins and, therefore, to a decrease in conductivity. This effect is strongest near the Curie temperature, where both spin disorder and the susceptibility are large. Accordingly, a maximum in the magnetoresistance appears near  $T_C$ . This argument applies to spin-disorder scattering in ferromagnets in general and does not explain the extraordinary magnitude of the magnetoresistance in the manganites. As already discussed in the previous section, many groups have suggested that double exchange alone is not sufficient in order to explain the colossal magnetoresistance. The models proposed evoke a competition between double exchange and another mechanism – such as polaron formation due to the strong electron-phonon coupling or localization by spin fluctuations; this competition is supposed to drive the metal-insulator transition. The balance between the two competing mechanisms is very sensitive to an applied magnetic field that suppresses spin fluctuations and enhances the ferromagnetic order. The debate on the essential transport mechanism in the manganites has not yet been decided. However, as indicated in the previous section there is strong evidence for polaron formation and there seems to be consensus that the electron-phonon coupling is large. Here theoretical results by Millis *et al* (1996c) are reproduced, see figure 13(a) and (b). The resistivity was obtained from a dynamical mean field calculation including double exchange and a coupling of carriers to phonons. The calculations show that the resistivity above  $T_C$  can be tuned from semiconducting to metallic on decrease of the

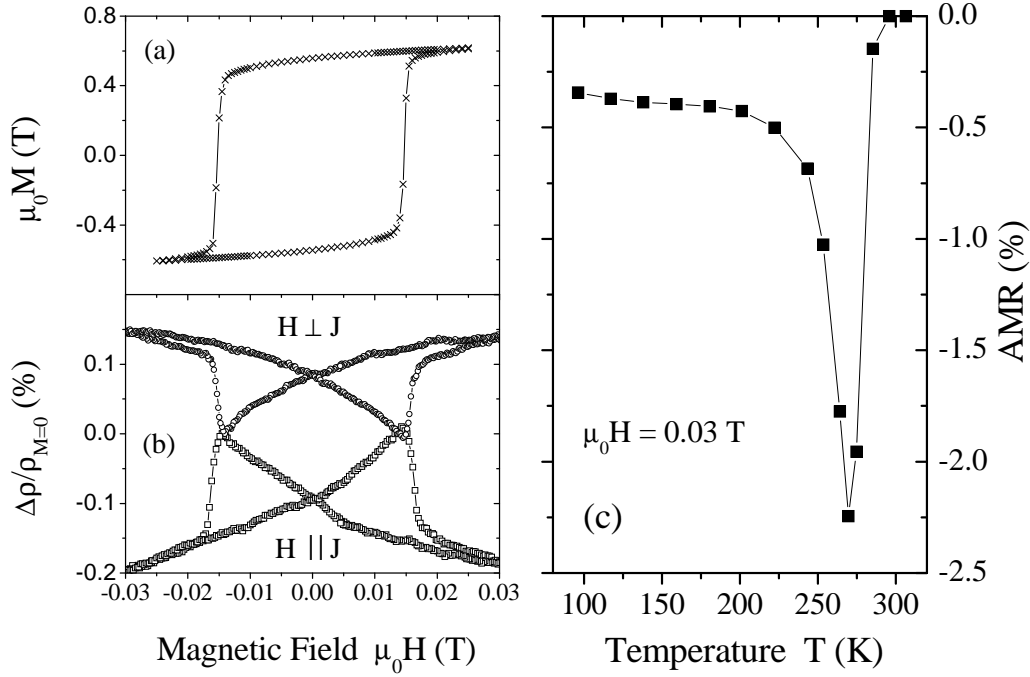


**Figure 14.** (a) Magnetization hysteresis loop of a high quality epitaxial  $\text{La}_{0.7}\text{Ca}_{0.3}\text{MnO}_3$  film at 96 K. (b) Magnetoresistance ratio of the same film as a function of the applied field at 96 K. The magnetic field was applied parallel and perpendicular to the current. The maxima (minima) in the longitudinal (transverse) magnetoresistance appear at the coercive field. (c) Anisotropic magnetoresistance  $AMR$  at 0.03 T as a function of temperature. After Ziese and Sena (1998).

electron-phonon coupling strength. This is in qualitative agreement with measurements on  $\text{La}_{0.7}\text{Ca}_{0.3}\text{MnO}_3$  and  $\text{La}_{0.7}\text{Sr}_{0.3}\text{MnO}_3$  single crystals, see figure 12(a). An applied magnetic field leads to a strong resistivity decrease in agreement with the observation of colossal magnetoresistance. Furthermore, the calculated magnetoresistance increases with decreasing Curie temperature as observed in experiments. The field scale for CMR, however, appears to be too large.

*4.4.2. Anisotropic magnetoresistance.* Anisotropic magnetoresistance (AMR) is present in all ferromagnets and is defined as the resistivity change as a function of angle between the current  $J$  and the magnetization  $M$ . If  $\rho_{\parallel}$  and  $\rho_{\perp}$  denote the resistivity in the longitudinal ( $J \parallel M$ ) and transverse ( $J \perp M$ ) geometries, respectively, then the anisotropic magnetoresistance is defined by

$$AMR = \frac{\rho_{\parallel} - \rho_{\perp}}{\frac{1}{3}\rho_{\parallel} + \frac{2}{3}\rho_{\perp}}. \quad (21)$$

Anisotropic magnetoresistance in elemental ferromagnets was reviewed by Campbell and Fert (1982).

The anisotropic magnetoresistance in the manganites was found to be much smaller than the colossal magnetoresistance (Eckstein *et al* 1996, O'Donnell *et al* 1997a,



1997b, Li *et al* 1997b, Ziese and Sena 1998, Lourenço *et al* 1999, O'Donnell *et al* 2000, Ziese 2000b). Therefore, only a few studies have been published on anisotropic magnetoresistance in the manganites. It is a low field effect and is discussed here for later comparison with extrinsic magnetoresistance effects.

Low field magnetoresistance data of a high quality  $\text{La}_{0.7}\text{Ca}_{0.3}\text{MnO}_3$  epitaxial film are shown in figure 14(a). At saturation, the transverse resistivity is larger than the longitudinal resistivity leading to a negative anisotropic magnetoresistance. The longitudinal (transverse) resistivity has maxima (minima) at the coercive field as can be seen from the comparison with the magnetization-hysteresis loop taken at the same temperature. Thus, the magnetic field dependence of the resistivity reflects the magnetic domain structure in the sample.  $AMR$  values determined at 0.03 T are shown in figure 14(b) as a function of temperature. Whereas the  $AMR$  is temperature independent with a value of about  $-0.4\%$  at low temperatures, a maximum is seen near the Curie temperature. The temperature dependent  $AMR$  can be decomposed into a normal component  $\propto M_S^2$  and an anomalous component  $\propto \rho^2 M_S^2$  that scales with the anomalous Hall resistivity (Ziese 2001b). Since the low field magnetoresistance in the manganites depends sensitively on the microstructure, such a clear anisotropic magnetoresistance can only be found in high quality epitaxial films.

Anisotropic magnetoresistance is due to the mixing of majority and minority states by the spin-orbit interaction (Campbell and Fert 1982). Ziese and Sena (1998) derived an expression for the anisotropic magnetoresistance within a simple atomic state model following the work of Campbell *et al* (1970) and Malozemoff (1985); this describes the normal  $AMR$  component. A Hamiltonian containing only the crystal field splitting  $\Delta_{CF}$ , the exchange splitting  $E_{ex}$  and the spin orbit coupling  $A[L_z S_z + (L_+ S_- + L_- S_+)/2]$  was considered. Treating the spin-orbit interaction as a small perturbation, the eigenfunctions derived from the  $3d$  wave functions were calculated to second order in this interaction. Assuming scattering by spherically symmetric impurities, the anisotropic magnetoresistance can be derived by the analysis of the symmetry of the scattering matrix elements. This yields

$$\frac{\rho_{\parallel} - \rho_{\perp}}{\frac{1}{3}\rho_{\parallel} + \frac{2}{3}\rho_{\perp}} = -\frac{3}{2} \left[ \frac{A^2}{(E_{ex} - \Delta_{CF})^2} - \frac{A^2}{\Delta_{CF}^2} \right]. \quad (22)$$

This expression contains only the local parameters  $\Delta_{CF}$ ,  $E_{ex}$  and  $A$ . With  $\Delta_{CF} \simeq 1.5$  eV,  $E_{ex} \simeq 2.0$  eV and  $A \simeq 0.04$  eV a value of  $AMR = -0.85\%$  is found. Considering the simplicity of the model, this is in good agreement with the experimental value at low temperatures.

#### 4.5. $\text{Fe}_3\text{O}_4$

The magnetoresistance of magnetite single crystals (Domenicali 1950, Kostopoulos 1972, Kostopoulos and Alexopoulos 1976, Shiozaki *et al* 1981, Belov *et al* 1982, 1983, Gridin *et al* 1996, Ziese and Blythe 2000) and films (Feng *et al* 1975, Gong *et al* 1997, Li *et al* 1998a, Ogale *et al* 1998, Ziese and Blythe 2000) was studied by several authors. The

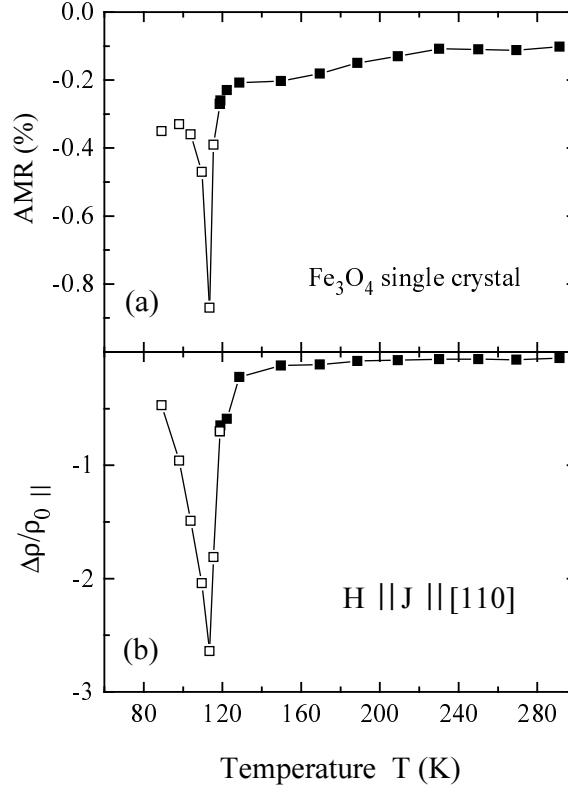


**Figure 15.** (a) Anisotropic magnetoresistance of a magnetite single crystal for current along  $[110]$ . (b) Longitudinal magnetoresistance for current and applied magnetic field along  $[110]$ . The open (solid) symbols show the magnetoresistance in the monoclinic (cubic) phase below and above the Verwey transition, respectively. After Ziese and Blythe (2000).

magnitude of the magnetoresistance in a constant applied field varies greatly among the studies. Coey *et al* (1998a) pointed out that this is related to the microstructure of the samples; extended defects like grain boundaries lead to a significant magnetoresistance increase, especially an unsaturated high field magnetoresistance. There are two recent studies on the magnetoresistance of  $\text{Fe}_3\text{O}_4$  single crystals by Gridin *et al* (1996) and Ziese and Blythe (2000). Both groups report a maximum of a few percent in the magnetoresistance at the Verwey transition temperature, presumably due to a magnetic field dependent shift of this charge-order transition. Typical magnetoresistance data in an applied field of 1 T are shown in figure 15(a) and (b). The current flow was along  $[110]$ . The longitudinal magnetoresistance has a minimum at  $T_V$  of -3%. The anisotropic magnetoresistance was derived from measurements with the applied field along and transverse to  $[110]$ . Apart from the magnetoresistance maximum at the Verwey transition the  $\text{Fe}_3\text{O}_4$  single crystal shows only anisotropic magnetoresistance with values between -0.2% and -0.1% above the transition (Ziese and Blythe 2000).

## Extrinsic magnetotransport phenomena

### 5. Domain-wall scattering

In 1934 Heaps reported on a resistance discontinuity associated with the Barkhausen effect. A Ni wire under bending stress showed a large Barkhausen jump and a sudden resistance decrease of relative magnitude  $\Delta R/R = 6.35 \times 10^{-5}$  at about the same applied field. Although Heaps (1934) interpreted this observation in terms of magnetization rotations, a contemporary interpretation might as well associate the resistance jump with domain-wall resistance. The concept of domain-wall scattering emerged in the sixties and has been studied since, see the experimental work on Fe whiskers by Taylor *et al* (1968) and the theoretical work by Cabrera and Falicov (1974a, 1974b) and Berger (1978, 1991). More recent work was stimulated by studies into quantum tunnelling of domain walls using magnetoresistance as a probe (Hong and Giordano 1998), the analogy between domain-walls and metallic multilayer systems showing giant magnetoresistance (Gregg *et al* 1996), the prospect of using a domain-wall switch in spin-electronic devices as well as the speculation of large domain-wall scattering in the manganites due to the large spin-polarization (Zhang and Yang 1996).

Domain-wall resistance and anisotropic magnetoresistance (AMR) depend sensitively on the domain configuration; furthermore, both are believed to be of the same order of magnitude. Great care has therefore to be devoted to the study of the micromagnetic state of ferromagnetic samples to distinguish between these two magnetoresistance mechanisms. At present, a consensus on the observability of domain-wall scattering has not been reached. Experiments yield a range of values and agreement has not even been reached on the sign of the effect. In the following two sections we discuss the state in elemental ferromagnets and manganites, respectively.

#### 5.1. Elemental ferromagnets

Early experiments on iron whiskers showed large magnetoresistive effects partially attributed to domain-wall scattering (Taylor *et al* 1968). The interpretation relied on an assumed domain structure. The results were interpreted within models by Cabrera and Falicov (1974a, 1974b) and Berger (1978). Interest into domain-wall scattering revived during the nineties. Gregg *et al* (1996) prepared a pattern of stripe domains in a Co film with perpendicular anisotropy and measured the magnetoresistance in a perpendicular field with an electric current perpendicular to the domain walls. They argued that the magnetoresistance must arise from domain-wall scattering, since the magnetization and current are always perpendicular. This assertion was later contested by Rüdiger *et al* (1999a) on the grounds of magnetic force microscopy (MFM) studies and micromagnetic modelling of Co wires. Viret *et al* (1996) tried to extract the domain-wall resistance in Co and Ni films by adding the longitudinal and transverse magnetoresistance and identifying the non-vanishing contributions with domain-wall contributions. This method relies on the fact that the anisotropic magnetoresistance

depends on the square of the cosine of the angle between magnetization and current, such that the AMR adds to a constant when measured before and after a field or current rotation by  $90^\circ$ . However, this argument relies on the assumption of perfect cubic crystal anisotropy and the absence of misalignments between current, field and crystal axes. Since the observed effects are very small, these assumptions are doubtful. Both Gregg *et al* (1996) and Viret *et al* (1996) found a positive domain-wall resistivity. Hong and Giordano (1998) measured the magnetoresistance of 30 nm thin Ni wires and found a negative contribution to the resistivity in the presence of domain walls. However, this result also relies on an assumed domain structure and has to be treated with care. Wegrowe *et al* (1999) compared experimental magnetoresistance data of Ni and Co wires with a model for the magnetization reversal and found discrepancies in the case of Co wires presumably due to domain-wall nucleation. It has to be clear that any interpretation of magnetoresistance data has to be based on the actual domain structure of the sample. Such comprehensive investigations have been conducted by Kent *et al* (Kent *et al* 1999, Rüdiger *et al* 1998a, 1998b, 1999a, 1999b). Therefore their results are reviewed here in more detail.

Kent *et al* studied the magnetoresistance of Fe and Co wires of width in the range 0.65 to 20  $\mu\text{m}$  and thickness in the range 25 to 200 nm. The domain structures in these wires were characterized using MFM and micromagnetic modelling. The Co wires have a perpendicular anisotropy such that the magnetization within a domain is oriented along the surface normal. MFM and micromagnetic modelling, however, show that flux-closure domains exist; the fraction of the flux-closure caps depends on the film thickness varying between 35% and 17% for thicknesses between 50 and 200 nm. The existence of these flux-closure domains was neglected by Gregg *et al* (1996). The magnetoresistance in these wires is due to normal state (Lorentz) magnetoresistance, anisotropic magnetoresistance as well as a domain-wall contribution. The anisotropic magnetoresistance in Fe and Co is positive, i.e.  $\rho_{\parallel} > \rho_{\perp}$ . In contrast, the Lorentz magnetoresistance shows the opposite behaviour, i.e. the transverse MR is larger than the longitudinal MR. Since the Lorentz magnetoresistance depends on the local induction, a considerable normal state magnetoresistance due to the large saturation magnetization in Fe ( $\mu_0 M_S = 2.2$  T) and Co ( $\mu_0 M_S = 1.8$  T) is present even at zero applied field. This leads to the existence of a compensation temperature with equal resistivities of magnetic domains oriented perpendicular or parallel to the current. These resistivities are obtained by extrapolation of the normal state resistivity above saturation. The compensation temperatures are about 65 K for Fe and 85 K for Co, respectively. In the absence of domain wall effects, at the compensation temperature the resistivity measured in zero field should agree with that determined by extrapolation. The experiment, however, shows a negative resistivity contribution in Fe films for thicknesses below 100 nm due to domain walls, see figure 16. This negative contribution increases with domain-wall density and decreases with film thickness. At other temperatures, the domain-wall resistivity can be estimated by the difference in the measured resistivity and the resistivity estimated from the high field extrapolation

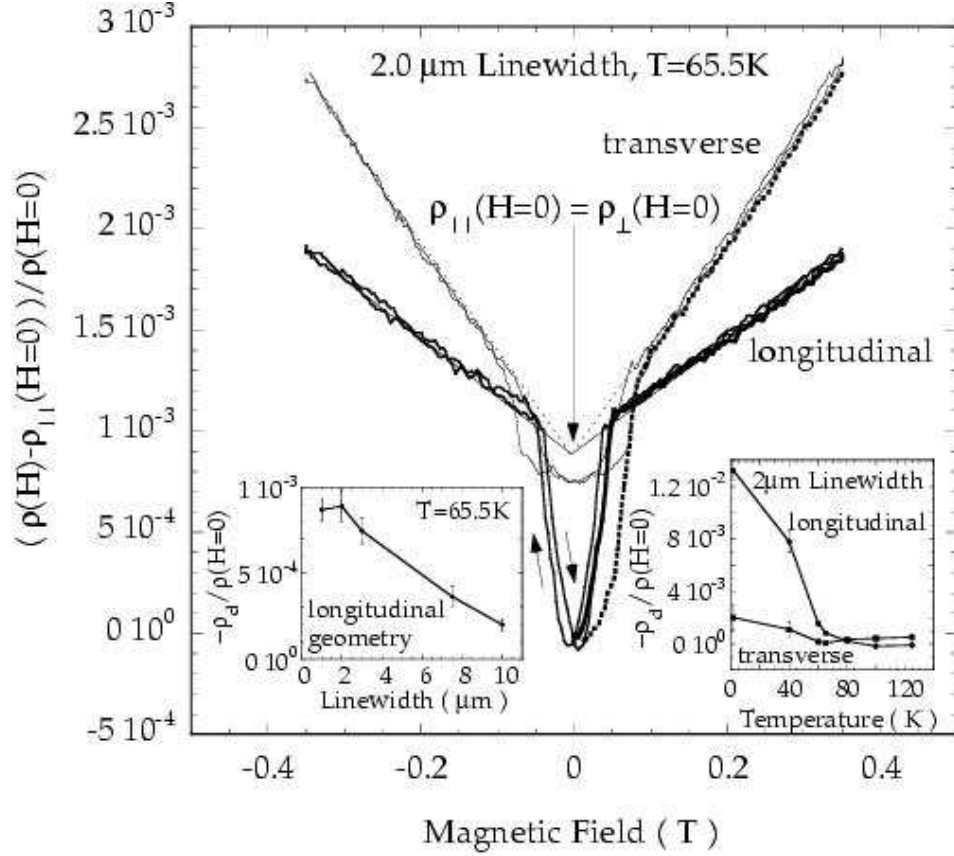


**Figure 16.** Magnetoresistance of a 2  $\mu\text{m}$  Fe wire at 65.5 K. The extrapolation of the high field MR data in transverse (dotted line) and longitudinal (solid line) geometry shows that  $\rho_{\perp}(H=0) = \rho_{\parallel}(H=0)$ . The resistivity with walls present,  $\rho(H=0)$ , is smaller than this extrapolation and indicates that domain walls lower the wire resistivity. The left-hand inset shows this negative domain-wall contribution as a function of Fe wire linewidth at this compensation temperature in the longitudinal geometry. The right-hand inset shows the domain-wall contribution as a function of temperature deduced using the model described in the text. Reproduced from Rüdiger *et al* (1998a).

combined with the measured domain configuration. This yields a negative domain-wall resistivity in Fe wires persisting up to temperatures of about 80 K. In Co the situation is different. The measured resistivities are always very close to the effective resistivities calculated from the extrapolation values and the measured domain configuration. However, at the compensation temperature of about 85 K a small positive contribution to the magnetoresistance ratio of  $9 \times 10^{-4}$  is found. This is consistent with an additional contribution due to domain-wall scattering.

A report on domain-wall resistance in Co zig-zag wires found a negative domain-wall contribution of  $-6 \times 10^{-4}$  at 5 K (Taniyama *et al* 1999). This persists up to 200 K. An investigation by Ebels *et al* (2000) on 35 nm thin Co wires identified a steplike resistance increase of about  $1 \times 10^{-3}$ - $3 \times 10^{-3}$ . In these thin wires the c-axis grows parallel to the wire axis and both shape and crystal anisotropy lead to magnetic

domains being oriented along the wire. During a hysteresis loop in a parallel magnetic field head-to-head domain walls can be induced that supposedly lead to the resistance increase.

This discussion shows that the experimental situation is controversial; the status of theoretical studies is also far from being clearcut. The analogy between a domain wall and a metallic multilayer system intuitively leads to the idea of a positive resistivity contribution of the domain wall. This idea was advanced by Gregg *et al* (1996) and later confirmed by Levy and Zhang (1997) by a more rigorous calculation. These treatments visualize an itinerant electron traversing the domain wall and adiabatically tracking the rotating exchange field. Majority and minority carriers in the bulk conduct in parallel with different resistivities  $\rho^\uparrow, \rho^\downarrow$ . Levy and Zhang (1997) showed that the carrier wave functions in the domain wall contain contributions of both spin orientations, thus facilitating a spin mixing that leads to an additional resistivity due to the different resistivities for majority and minority carriers. The domain-wall resistivity was found to be anisotropic with respect to the current direction relative to the domain wall. This anisotropy was investigated by Viret *et al* (2000) in FePd films and was found to be consistent with the predictions. Levy and Zhang (1997) obtained a domain-wall resistivity proportional to  $\delta^{-2}$ , where  $\delta$  denotes the domain-wall width. van Hoof *et al* (1999) and Brataas *et al* (1999b) calculated the domain-wall resistivity in Ni, Fe and Co due to spin-flip scattering both within a two-band model and using a realistic band-structure. Within the two-band model these authors recovered Levy and Zhang's (1997) result of a domain-wall resistivity proportional to  $\delta^{-2}$ . The first-principles calculation including a realistic bandstructure, however, yielded a considerably larger domain-wall magnetoresistance inversely proportional to  $\delta$  in contrast to the two-band result.

On the other hand, Tatara and Fukuyama (1997) and Lyanda-Geller *et al* (1998) pointed out that domain walls might contribute to the de-coherence of electrons, thus leading to a resistivity decrease due to the suppression of weak localization effects. Although this is in qualitative agreement with the results of Kent *et al* (1999) and Taniyama *et al* (1999), Kent *et al* (1999) pointed out that the negative MR contribution persists to much higher temperatures than expected for quantum interference effects. Indeed, Rüdiger *et al* (1998a) estimated the maximum temperature for the observation of weak localization effects by equating the wall de-coherence time to the inelastic scattering time and found a value of 7 K being an order of magnitude lower than observed. Finally, based on the observation that the negative domain-wall contribution vanishes for large film thicknesses, Rüdiger *et al* (1999b) argued that surface scattering might be important; in their model the negative magnetoresistance arises from the deflection of charge carriers away from the surface that is being mediated by the presence of domain walls. A recent calculation by van Gorkom *et al* (1999a) showed that a negative domain-wall resistance can also arise from the reduced magnetization in a domain wall, if the ratio of the spin-dependent relaxation times is appropriate. This can be seen as follows. The Drude resistivity of a single domain ferromagnet is given

within the two-band Stoner model by (van Gorkom *et al* 1999a)

$$\rho = \frac{m}{e^2} \frac{1}{n_{\uparrow}\tau_{\uparrow} + n_{\downarrow}\tau_{\downarrow}}, \quad (23)$$

where  $n_{\uparrow}$  ( $n_{\downarrow}$ ) denote the majority (minority) density of states and  $\tau_{\uparrow}$  ( $\tau_{\downarrow}$ ) the relaxation time for majority (minority) electrons. A redistribution of the electrons in a domain wall with  $n_{\uparrow(\downarrow)} = n_{0\uparrow(\downarrow)} + \delta n_{\uparrow(\downarrow)}$ ,  $\delta n_{\uparrow} = -\delta n_{\downarrow}$  modifies the resistivity according to

$$\delta\rho = -\rho^2 \frac{e^2}{m} \delta n_{\uparrow} (\tau_{\uparrow} - \tau_{\downarrow}). \quad (24)$$

Depending on the ratio of the spin-dependent relaxation times, this resistivity change can be positive or negative. van Gorkom *et al* (1999a) calculated  $\delta n_{\uparrow}$  and  $\delta\rho$  self-consistently for a semiclassical domain-wall model and indeed found a negative domain-wall resistance for  $\tau_{\uparrow} > \tau_{\downarrow}$ . Since the relaxation times depend on the type of impurity (Campbell and Fert 1982), this model can be experimentally checked by measuring the domain-wall resistivities of a series of alloys.

Despite the experimental and theoretical debate on the relation between domain-wall magnetoresistance and domain-wall width, it is generally accepted that a significant magnetoresistance will only arise in the case of a narrow wall. It is therefore promising to investigate nanocontacts with geometrically constrained domain walls. Indeed, Bruno (1999) showed that the domain-wall width of such a geometrically constrained wall is of the order of the width of the constriction. García *et al* (1999) investigated the magnetoresistance of Ni nanocontacts and found values of up to 75% (with respect to the zero field value) at room temperature for contacts with a conductance of only a few conductance units  $2e^2/h$ . This was explained by Tatara *et al* (1999) by scattering at a narrow domain wall located at the nanocontact. The agreement between theory and experimental values, however, is only qualitative (Tatara *et al* 1999); the theory shows that the magnetoresistance is enhanced at small contact sizes corresponding to conductances of only a few conductance units. A similar experiment was performed by Wegrowe *et al* (2000). These authors investigated the magnetoresistance of Co nanowires exchange biased by a GdCo<sub>1.6</sub> layer. In this configuration, a domain wall is expected to form at the interface and to be compressed by an applied magnetic field. Wegrowe *et al* (2000) observed a strong decrease of the domain-wall resistance as a function of the domain-wall width in the range 5 nm to 10 nm. The limited range of domain-wall thicknesses accessible in this experiment did not allow to distinguish between the various predictions for the domain-wall width dependence. The resistance contribution of partial domain walls located on either side of permalloy/permalloy, Co/permalloy, Co/Co, Ni/Ni and Co/Cu point contacts was found to be negative (van Gorkom *et al* 1999b, Theeuwens *et al* 2001). Following the theoretical results of van Gorkom *et al* (1999a) this could be interpreted as arising from boundary scattering in combination with an appropriate ratio of the spin dependent relaxation times.

## 5.2. Magnetic oxides

Within the double-exchange model, the transfer integral  $t \cos(\Theta/2)$  for the  $e_g$  electrons depends sensitively on the angle  $\Theta$  between the core spins of the adjacent  $\text{Mn}^{3+}$  and  $\text{Mn}^{4+}$  sites. Therefore, it is expected that a narrow domain wall has a considerable influence on the conductance of the manganites. The scattering by domain walls in double-exchange ferromagnets was treated by Zhang and Yang (1996), Yamanaka and Nagaosa (1996), Gehring (1997) and Brey (1999). Whereas Zhang and Yang (1996) calculated the temperature and field dependence of the resistivity due to the temperature and field dependence of the average domain size, Yamanaka and Nagaosa (1996), as well as Gehring (1997), calculated the conductance of a single domain wall as a function of the domain-wall width  $\delta$ . Both assumed a  $180^\circ$  Néel wall with a constant spin-rotation angle in the wall,  $\Theta = \pi a/\delta$ , where  $a$  denotes the lattice parameter. Within a tight binding model the dispersion relation is given by

$$\epsilon = 2t \cos(\Theta) [1 - \cos(ka)] , \quad (25)$$

where  $k$  denotes the wave vector perpendicular to the wall. Since  $\Theta = 0$  outside the wall and  $\Theta = \pi a/\delta$  inside the domain wall, the band width in the wall is reduced. Thus, depending on the wave vector of the electrons incident under an angle  $\phi$  with respect to the wall normal,

- (i) the electrons will be scattered regardless of incoming angle  $\phi$ , if  $k_f a < \Theta/2$ ,
- (ii) for  $\Theta/2 < k_f a < \pi - \Theta/2$  only the electrons propagating at an angle  $\phi$  such that  $k_f a \cos(\phi) < \Theta/2$  will be scattered,
- (iii) for  $k_f a > \pi - \Theta/2$  electrons satisfying  $k_f a \cos(\phi) < \Theta/2$  and  $k_f a \cos(\phi) > \pi - \Theta/2$  will be scattered.

Gehring (1997) estimated  $k_f \sim 0.7\pi/a$  such that case (ii) is likely to apply. Thus, electrons incident under an angle  $\phi_0 < \phi < \pi/2$  with  $\cos(\phi_0) = \Theta/(2k_f a)$ , will be scattered through an angle  $\pi - 2\phi$  giving a contribution to the resistivity proportional to  $k_f [1 - \cos(\pi - 2\phi)] = 2k_f \cos^2(\phi)$ , whereas electrons incident at smaller angles pass the wall nearly undisturbed. The magnetoconductivity of a single wall is then given by

$$\frac{\Delta G_{wall}}{G_0} = \frac{\int_{\phi_0}^{\pi/2} d\phi \sin \phi [1 - \cos(\pi - 2\phi)]}{\int_0^{\pi/2} d\phi \sin \phi} = \frac{2}{3} \left( \frac{\pi}{2k_f \delta} \right)^3 , \quad (26)$$

and decays very strongly with the domain-wall thickness. Surprisingly, according to this calculation, the domain-wall resistance in the manganites decays much more strongly with wall thickness than in elemental ferromagnets.

Yamanaka and Nagaosa (1996) numerically calculated the conductivity as a function of the energy  $\epsilon$  of the incident electron using Landauer's formula. In the case of a thick wall, a one-dimensional continuum model can be applied. An effective potential

$$V(x) = \begin{cases} V = 2t [1 - \cos(\frac{\pi a}{2\delta})] & : \text{ in the wall} \\ 0 & : \text{ elsewhere} \end{cases} \quad (27)$$



was used in the one-dimensional Schrödinger equation leading to a transmission coefficient

$$G_s(\epsilon) = \frac{1}{1 + \frac{V^2}{4\epsilon(V-\epsilon)} \sinh^2 \left( \frac{\delta}{a} \sqrt{\frac{V-\epsilon}{t}} \right)} \quad (28)$$

with  $\epsilon = 2t[1 - \cos(ka)]$ . For large domain-wall thicknesses this can be approximated by

$$G_s \sim \begin{cases} \left[ \frac{\delta}{a} \right]^2 \frac{\epsilon}{t} & : \quad \epsilon < t \left[ \frac{a}{\delta} \right]^2 \\ 1 & : \quad \epsilon > t \left[ \frac{a}{\delta} \right]^2 \end{cases} \quad (29)$$

Integrating over all wave vectors up to  $k_f$  yields

$$\frac{\Delta G_{wall}}{G_0} = \frac{2}{5} \left( \frac{1}{k_f \delta} \right)^3, \quad (30)$$

which, apart from a numerical factor, agrees with Gehring's result.

Brey (1999) calculated the magnetoresistance of a domain wall in the manganites numerically as a function of domain-wall thickness taking into account the modulation of the hopping amplitude due to the spin canting inside the domain wall as well as the shift of the chemical potential of the Mn ion levels. He obtained a decreasing magnetoresistance with increasing wall thickness; for a wall thickness  $\delta = 10a$  he found a value  $\Delta G/G = 0.01$ .

Experimentally the issue of domain-wall scattering in the manganites was addressed by Wolfman *et al* (1998), Wang and Li (1998), Mathur *et al* (1999), Wu *et al* (1999), Ziese *et al* (1999b) and Suzuki *et al* (2000). Mathur *et al* (1999) measured the resistivity of a patterned LCMO track. This track had narrow constrictions separating regions with wider linewidth (“bellies”); small permanent magnets were placed near every second belly. After magnetizing to saturation in an in-plane field, the magnetic field was slowly reversed; the unbiased “belly” regions are believed to reverse the magnetization at small negative fields, thus creating domain walls near the constrictions. Mathur *et al* (1999) report a step-like behaviour of the resistivity hysteresis below about 130 K. This was attributed to the switching of individual “belly” regions and, accordingly, to the creation of single domain walls. The areal resistivity was found to be large about  $8 \times 10^{-14} \Omega \text{m}^2$  at 77 K. Mathur *et al* (1999) estimated an areal domain-wall resistivity of  $1.6 \times 10^{-18} \Omega \text{m}^2$  within a Born approximation. Using  $\rho \delta (\Delta G/G)$  with  $\rho = 100 \mu\Omega \text{cm}$ , a domain-wall width  $\delta = 30 \text{ nm}$  and  $\Delta G/G$  according to equation (30) yields an even smaller value of about  $7.6 \times 10^{-20} \Omega \text{m}^2$ . This discrepancy might indicate some internal structure of the domain walls (Mathur *et al* 1999).

Wu *et al* (1999) and Suzuki *et al* (2000) investigated the magnetoresistance of compressively strained LSMO films on  $\text{LaAlO}_3$ . These films have a perpendicular magnetic anisotropy leading to the formation of perpendicular magnetic domains on a scale of about 200 nm. If the magnetoresistance is measured after sweeping an in-plane or an out-of-plane field perpendicular to the current, the resistivity should return to the same value in zero field apart from domain-wall scattering effects due to the different

domain configurations. The measurement on a 80 nm LSMO film at 300 K yielded a deviation of about 0.1% in the two field configurations. This corresponds to a domain-wall areal resistivity of  $10^{-15} \Omega\text{m}^2$ . This value is significantly smaller than the value obtained by Mathur *et al* (1999), possibly due to the higher measurement temperature. The calculation of Brey (1999) yielded an areal resistivity of  $3 \times 10^{-16} \Omega\text{m}^2$  smaller than the value observed by Mathur *et al* (1999), but close to the value found by Wu *et al* (1999). This shows that the precision of the experimental values is not sufficient at the moment in order to test different theories.

Ziese *et al* (1999b) determined the domain-wall width in various LCMO films, i.e. a polycrystalline film on Si (200 nm), an as-deposited film on  $\text{LaAlO}_3$  (120 nm) and an annealed film on  $\text{LaAlO}_3$  (9 nm) using magnetic viscosity measurements. The magnetic viscosity  $S = dM/d\ln(t)$  is related to the average activation volume  $v$  by

$$S = \frac{kT}{vM_S} \chi_{irr}, \quad (31)$$

where  $M_S$  denotes the saturation magnetization and  $\chi_{irr}$  the irreversible susceptibility. From measurements of  $S$ ,  $M_S$  and  $\chi_{irr}$  the average activation volume can be determined. This is related to the domain-wall thickness  $\delta$  via  $v = \delta^3$ . Ziese *et al* (1999b) found that the domain-wall thickness did not significantly depend on the microstructure, see figure 17. This is surprising, since it was believed that domain walls located near grain boundaries were relatively narrow due to the weakened double-exchange coupling near the defect. Gehring (1997) speculated that the large low field magnetoresistance observed in polycrystalline materials is due to electron scattering by narrow domain walls near the grain boundaries. Experimentally, this idea could not be confirmed, since the magnetoresistance of the epitaxial and polycrystalline films investigated by Ziese *et al* (1999b) varied by one order of magnitude, whereas the measured domain-wall thickness was identical. Furthermore, the observed domain-wall thickness is very large compared to the lattice parameter being in agreement with the calculated Bloch-wall thickness using typical values for the magnetocrystalline anisotropy and Curie temperature. The domain-wall energy, also shown in figure 17, can be calculated from the measured magnetic viscosity, the coercive and fluctuation fields.

The magnetoresistance of  $\text{Pr}_{0.67}\text{Sr}_{0.33}\text{MnO}_3$  films grown under compressive strain on  $\text{LaAlO}_3$  substrates was investigated by Wang and Li (1998) and Wolfman *et al* (1998). In these samples a large magnetoresistance arises when the magnetic field is applied perpendicular to the film. It is known from magnetic anisotropy investigations that manganite films under compressive strain exhibit a perpendicular anisotropy (O'Donnell *et al* 1998). Since the observed magnetoresistance is not correlated to specific crystallographic defects, the authors suggested that it arises from domain-wall scattering at domain walls separating out-of-plane domains.

Domain-wall scattering was also reported in  $\text{SrRuO}_3$  films at low temperature (Klein *et al* 1998).  $\text{SrRuO}_3$  grows on  $\text{SrTiO}_3$  with the c-axis in-plane and the a- and b-axes at  $45^\circ$  with respect to the substrate normal. Lorentz microscopy imaging at low temperatures revealed a stripe domain pattern with domain walls along  $[1\bar{1}0]$ .

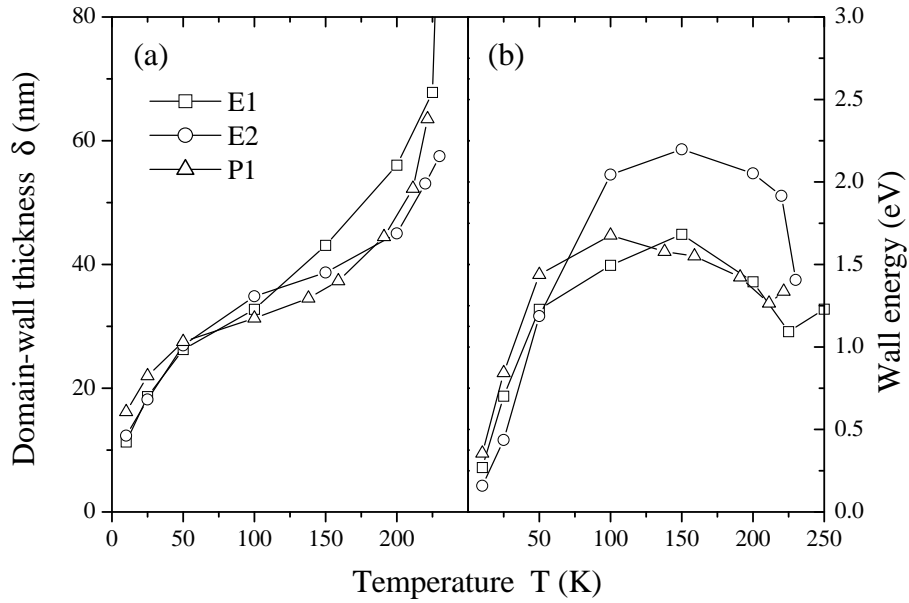


**Figure 17.** (a) Domain-wall thickness  $\delta$  and (b) domain-wall energy as determined from magnetic viscosity measurements on a 9 nm thick annealed LCMO film on LaAlO<sub>3</sub> (E1), a 120 nm thick as-deposited LCMO film on LaAlO<sub>3</sub> (E2) and a 200 nm thick polycrystalline LCMO film on Si (P1). After Ziese *et al* (1999b).

Resistance measurements at 5 K after zero-field cooling with the current along [001] and the magnetic field along  $[1\bar{1}0]$  showed a large irreversible drop in magnetic field below about 0.3 T. This effect was not observed with the current along  $[1\bar{1}0]$ . In 0.3 T the magnetization of the film was technically saturated and the stripe domains had been driven out of the film; the stripe domain pattern was not recovered after removal of the magnetic field, implying that the irreversible resistivity drop was related to this particular domain structure. Klein *et al* (1998) interpreted these results as evidence for domain-wall scattering. The magnitude of the areal domain-wall resistivity was found to be large of the order of  $2 \times 10^{-15} \Omega\text{m}^2$ . As already noted in the beginning of this section, this result has to be treated with care, since the domain structure during the complete hysteresis cycle is unknown and AMR effects cannot be completely ruled out.

Versluijs *et al* (2001) studied the magnetoresistance of Fe<sub>3</sub>O<sub>4</sub> nanocontacts in an experimental arrangement similar to that of García *et al* (1999). For conductances smaller than the conductance quantum a large magnetoresistance up to 90% at 7 mT was determined; this was found to decay strongly with increasing conductance similar to the results of García *et al* (1999) for Ni nanocontacts. The contacts have non-linear I–V characteristics with  $I = GV + cV^3$ ,  $c = G^{0.3 \pm 0.1}$ . The authors favour an interpretation of the data within a model of spin scattering at a constricted domain-wall. The “magnetic balloon effect”, i.e. a displacement of the domain wall from the constriction due to the spin pressure exerted by the electron flow qualitatively accounts for the non-linear I–V curves as well as the decrease of the magnetoresistance with applied voltage.

## 6. Surface and interface properties

Since the main application of half-metallic magnets will be in integrated devices, interfacial properties are of crucial importance. The investigation of interfacial properties is in its early stages and few quantitative results have yet been established. Here we report on first investigations of oxide-vacuum, oxide-metal and oxide-superconductor interfaces.

### 6.1. Oxide-vacuum interface

The magnetic properties near the surface of a  $\text{La}_{0.7}\text{Sr}_{0.3}\text{MnO}_3$  film were investigated by Park *et al* (1998a, 1998b) using SQUID magnetometry, magnetic circular dichroism (MCD) at the Mn L-edge and spin-resolved photoemission spectroscopy (SPES). These techniques probe the magnetization in the bulk and in surface layers of thickness  $\sim 5$  nm (MCD) and  $\sim 0.5$  nm (SPES), respectively. The film investigated was cleaned in an UHV-chamber by a sequence of annealing processes that resulted in a large surface roughness of  $\sim 2$  nm. The main result is reproduced in figure 18, showing the normalized magnetization measured on different length scales. The spin-polarization near the surface is strongly reduced and recovers on a length scale of more than 5 nm. Since numerous applications depend on the interfacial spin-polarization, this result might have serious implications for possible applications at room temperature. However, since the roughness was considerably larger than the penetration depth for SPES measurements, the intrinsic nature of this result is not obvious.

Alvarado (1979) compared the surfacial magnetization of a  $\text{Fe}_3\text{O}_4$  crystal as determined by SPES to the bulk magnetization and found a significant reduction of the former. Data were collected between 4 K and 500 K and in this temperature range the surfacial magnetization decreases approximately linearly with temperature. This behaviour can be successfully modelled taking into account the reduction of nearest neighbour magnetic ions and the surface reconstruction (Srinitiwara Wong and Gehring 2001).

Wei *et al* (1997, 1998) investigated the surface electronic properties of  $\text{La}_{0.7}\text{Ca}_{0.3}\text{MnO}_3$  and  $\text{Fe}_3\text{O}_4$  using scanning tunnelling microscopy. At 77 K both compounds show a density of states compatible with a half-metallic state.

Choi *et al* (1999a, 1999b) investigated the surfaces of crystalline  $\text{La}_{1-x}\text{Ca}_x\text{MnO}_3$  films with dopings  $x = 0.1$  and  $x = 0.35$  using angle-resolved core-level photoemission. From the ratio of the Mn, La and Ca core-level intensities it was concluded that  $\text{La}_{0.65}\text{Ca}_{0.35}\text{MnO}_3$  films are terminated by a Mn–O layer, whereas  $\text{La}_{0.9}\text{Ca}_{0.1}\text{MnO}_3$  films have a La/Ca–O terminal layer. Moreover, a significant surface segregation was found with the Ca content being strongly enhanced near the surface; this was also found to depend on doping with a surface Ca fraction of 0.9 for  $x = 0.1$  and 0.6 for  $x = 0.35$ . The authors conclude that the surface could be fundamentally different from the bulk and that any measurement of bulk properties using surface sensitive techniques such as angle-resolved photoemission has to be treated with care. These investigations

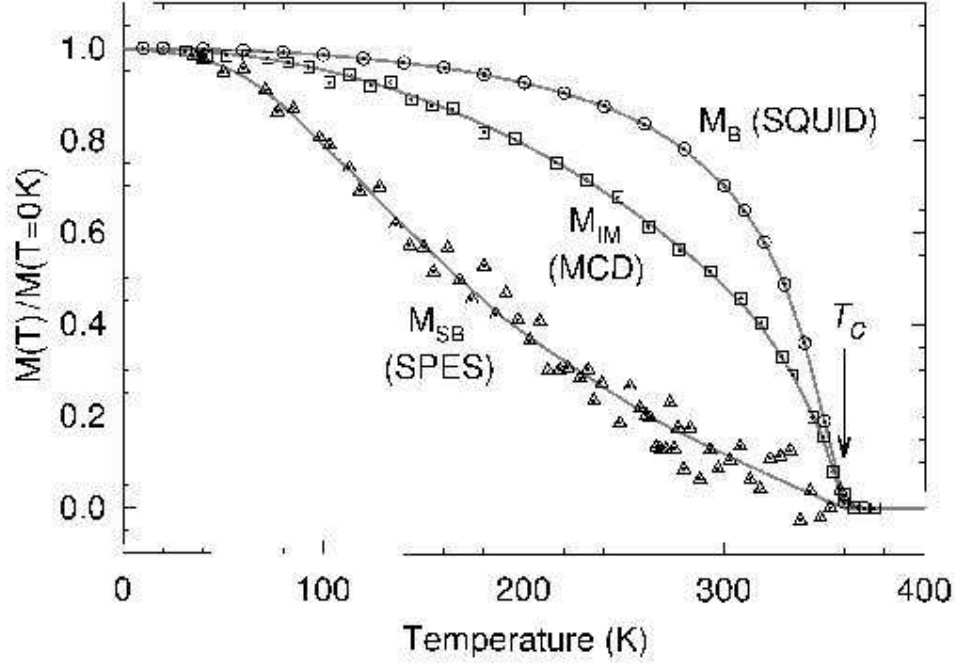


**Figure 18.** Temperature dependence of the magnetization measured on different length scales.  $M_B$ ,  $M_{IM}$  and  $M_{SB}$  denote the bulk, the intermediate length scale ( $\sim 5$  nm) and the surface boundary ( $\sim 0.5$  nm) magnetization, respectively. Reproduced from Park *et al* (1998a).

were extended with two studies by Dulli *et al* (2000a, 2000b) on crystalline films with composition  $\text{La}_{0.65}\text{Sr}_{0.35}\text{MnO}_3$ . In line with the results on the Ca-doped compound an appreciable amount of Sr segregation near the surface was detected and the formation of a Ruddlesden-Popper phase  $(\text{La,Sr})_2\text{MnO}_4$  was suggested (Dulli *et al* 2000b). The same authors argue that a surface electronic phase transition occurs at 240 K that is different from the bulk ferromagnetic transition at 370 K. Measurements of the O(1s) core level binding energy and the density of states as a function of temperature show that the surface becomes insulating below 240 K (Dulli *et al* 2000a). This result is consistent with transport measurements on ultrathin films described in the next paragraph.

An indirect approach to investigate the interface properties of manganite films was suggested by Sun *et al* (1999) and Ziese *et al* (1999c), measuring the thickness dependence of the conductance of  $\text{La}_{0.67}\text{Sr}_{0.33}\text{MnO}_3$  films on  $\text{LaAlO}_3$  and  $\text{NdGaO}_3$  and  $\text{La}_{0.7}\text{Ca}_{0.3}\text{MnO}_3$  films on  $\text{LaAlO}_3$ ,  $(\text{LaAlO}_3)_{0.3}(\text{Sr}_2\text{AlTaO}_6)_{0.7}$  (LSAT) and  $\text{SrTiO}_3$ , respectively. The conductance was found to depend linearly on film thickness, see figure 19; the extrapolation to zero conductance yielded finite values that were interpreted as electrically dead layers (Sun *et al* 1999). The dead layer thickness depends on the substrate with  $d_{\text{dead}} = 3$  nm (LSMO on  $\text{NdGaO}_3$ , 14 K), 5 nm (LSMO on  $\text{LaAlO}_3$ , 14 K), 1 nm (LCMO on  $\text{LaAlO}_3$  and LSAT, 77 K) and 11 nm (LCMO on  $\text{SrTiO}_3$ , 77 K), respectively. However, in the case of thin films surface scattering has to be taken into account and deviations from a linear dependence of the conductance on the thickness

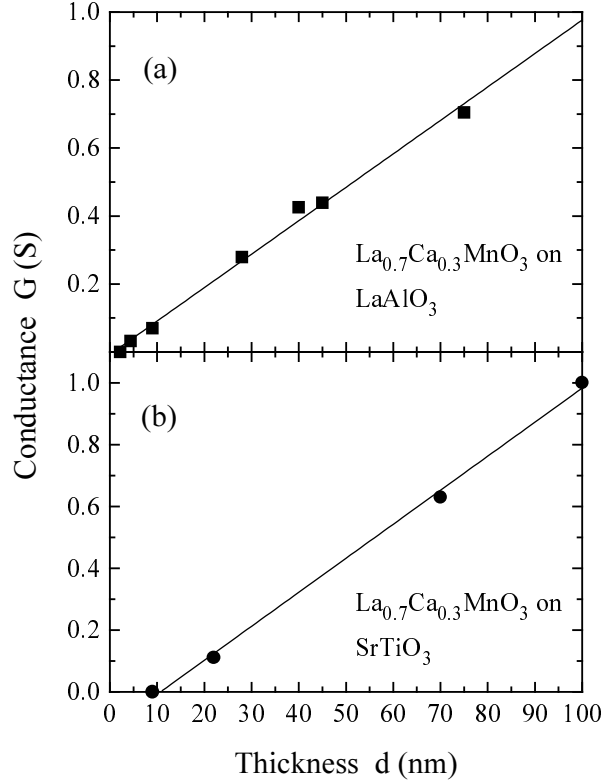


**Figure 19.** Conductance measured at 77 K in zero field for annealed LCMO films grown on (a)  $\text{LaAlO}_3$  and (b)  $\text{SrTiO}_3$ . The lines were calculated according to equation (33). Reproduced from Ziese *et al* (1999c).

are to be expected for very thin films. The conductance of a film is given by (MacDonald 1956)

$$G = \sigma_b d \left[ 1 - 3\ell_b/8d + (3\ell_b/2d) \int_1^\infty (x^{-3} - x^{-5}) \exp(-dx/\ell_b) dx \right], \quad (32)$$

where  $\sigma_b$  denotes the bulk conductivity and  $\ell_b$  the mean free path in the bulk. In the limits of thick and thin films this reduces to (MacDonald 1956)

$$G = \sigma_b(d - 3\ell_b/8) \quad \ell_b \ll d \quad (33)$$

$$G = \sigma_b(3d^2/4\ell_b) \ln(\ell_b/d) \quad \ell_b \gg d. \quad (34)$$

The bulk mean free path at 77 K can be estimated from the resistivity of thick films using the Drude formula with a carrier density (Ziese and Srinitiwara Wong 1999)  $n = 5.2 \times 10^{-27} \text{ m}^{-3}$ ; this yields a value  $\ell_b = 1.7 \text{ nm}$ . Accordingly, the majority of the films investigated satisfy the condition  $d \gg \ell_b$  and Eq. (33) may be used. This predicts a linear dependence of the conductance on film thickness with a finite abscissa as found experimentally, see figure 19. The value of the dead layer of about 1 nm found for LCMO films on  $\text{LaAlO}_3$  and LSAT is of the same magnitude as the bulk mean free path. Thus, annealed films on  $\text{LaAlO}_3$  and LSAT do not show a dead layer. The situation for annealed films on  $\text{SrTiO}_3$  is different, since here an insulating layer of about

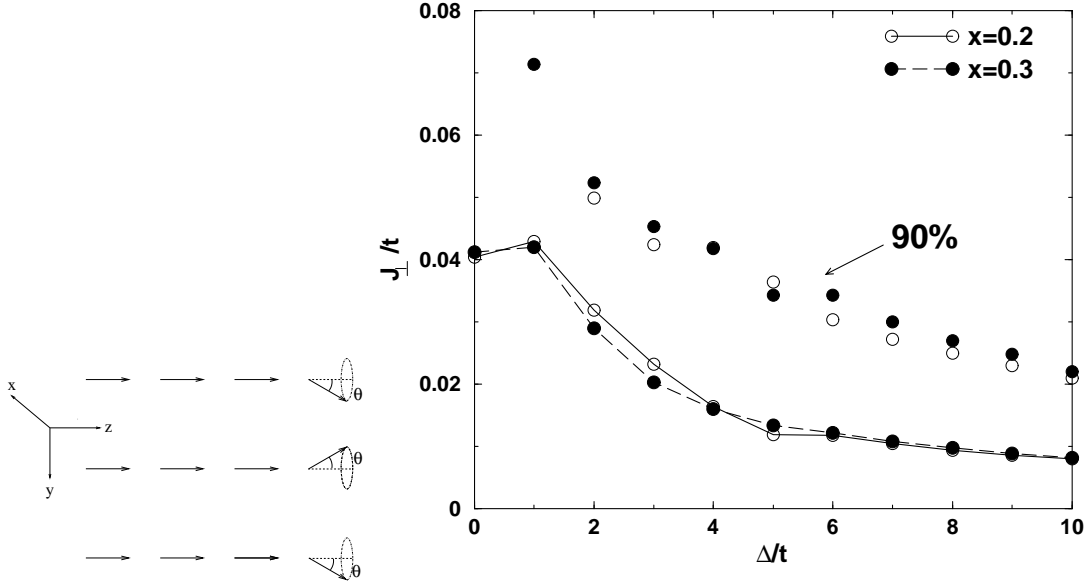


**Figure 20.** Left panel: Magnetic structure with canting angle  $\Theta$  considered in the theoretical calculation. Right panel: Surface magnetic phase diagram of a doped manganite. The lines separate the fully ferromagnetic and the canted regions. The symbols indicate that the order is 90% antiferromagnetic, i.e.  $\Theta = 81^\circ$ . Solid and open dots are the results for hole concentrations  $x = 0.3$  and  $x = 0.2$ , respectively.  $\Delta$  denotes the surface  $e_g$  level energy splitting,  $t$  the hopping integral and  $J_\perp$  the antiferromagnetic coupling constant. Reproduced from Calderon *et al* (1999b).

10 nm is found. This might be related to coherent film growth of LCMO on  $\text{SrTiO}_3$  resulting in large strains at small film thickness. Indeed, high resolution microscopy (HREM) studies of thin (6 nm - 12 nm)  $\text{La}_{0.73}\text{Ca}_{0.27}\text{MnO}_3$  films grown on  $\text{SrTiO}_3$  showed a change in structure in those films as compared to the bulk due to the in-plane tensile strain (Zandbergen *et al* 1999). An elongation of the in-plane oxygen square was found which is a Jahn-Teller-like distortion induced by the substrate. The resulting misfit energy is relaxed via twin boundaries; the twin-boundary density was found to increase strongly with decreasing film thickness. This Jahn-Teller-like distortion is supposed to lead to a ferromagnetic insulating state of these thin films. It was predicted that the Curie temperature is very sensitive to bi-axial strain (Millis *et al* 1998) in qualitative agreement with the experimental observation. In ultrathin films, however, the structural change seems to stabilize the Curie temperature at a rather high value.

## 6.2. Theoretical results

Two models for the description of the manganite-vacuum surface have been proposed by Calderon *et al* (1999b) and Filippetti and Pickett (1999, 2000), respectively. These models arrive at seemingly opposite conclusions and the main results are summarized below.

The (001) surface electronic structure and surface magnetization of manganites

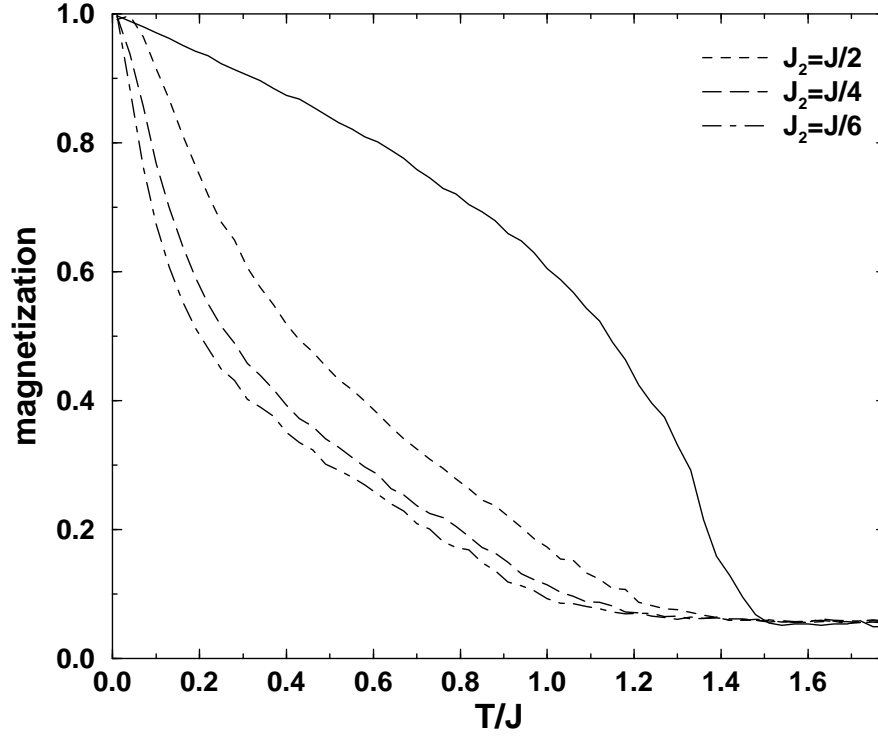


**Figure 21.** Normalized magnetization of the surface layer as a function of temperature for various ferromagnetic coupling constants  $J_2$  between the surface spins and the spins of the first innermost layer. The solid line is the result for the bulk magnetization.  $J$  denotes the bulk ferromagnetic coupling constant. Reproduced from Calderon *et al* (1999b).

were theoretically investigated by Calderon *et al* (1999b). At the surface, the oxygen octahedra surrounding each manganese ion are incomplete resulting in a tetragonal distortion and a splitting of the  $e_g$  levels by an amount  $\Delta$ . Since the  $d_{3z^2-r^2}$  orbitals point towards the surface, these are shifted to lower energy levels than the  $d_{x^2-y^2}$  orbitals. The calculation shows that for energy splittings  $\Delta > t$ , where  $t$  is the hopping matrix element, the  $d_{3z^2-r^2}$  levels at the surface are fully occupied, whereas the  $d_{x^2-y^2}$  levels are empty. This results in a suppression of the double-exchange coupling at the surface; the surface-spin structure is therefore determined by the antiferromagnetic super-exchange coupling between Mn ions with coupling constant  $J_\perp$ . Calderon *et al* (1999b) considered the case of a simple spin-canting by an angle  $\Theta$  in the surface layer, see figure 20(a). The canting angle  $\Theta$  was then calculated as a function of the  $e_g$  level surface splitting  $\Delta$  and the antiferromagnetic exchange constant  $J_\perp$ . The resulting magnetic phase diagram is shown in figure 20(b). For realistic values of the antiferromagnetic coupling constant,  $J_\perp \sim 0.02t$  (Perring *et al* 1997), and values  $t \sim 0.1 - 0.3$  eV as well as  $\Delta \sim 0.5 - 1.5$  eV, the surface spin-structure is nearly antiferromagnetic. The magnetization of the surface layer was calculated within an effective Heisenberg model with bulk ferromagnetic coupling  $J$ , surface antiferromagnetic coupling  $J_1 \sim -J/100$  and ferromagnetic coupling  $J_2 \sim J/6 - J/2$  between the surface layer and the first



innermost layer. The surface magnetization for various couplings  $J_2$  is compared to the bulk magnetization in figure 21. The surface magnetization decays much more strongly with temperature than the bulk magnetization due to a reduced spin stiffness at the surface. The theoretical results are in qualitative agreement with the measured spin-polarization, see figure 18.

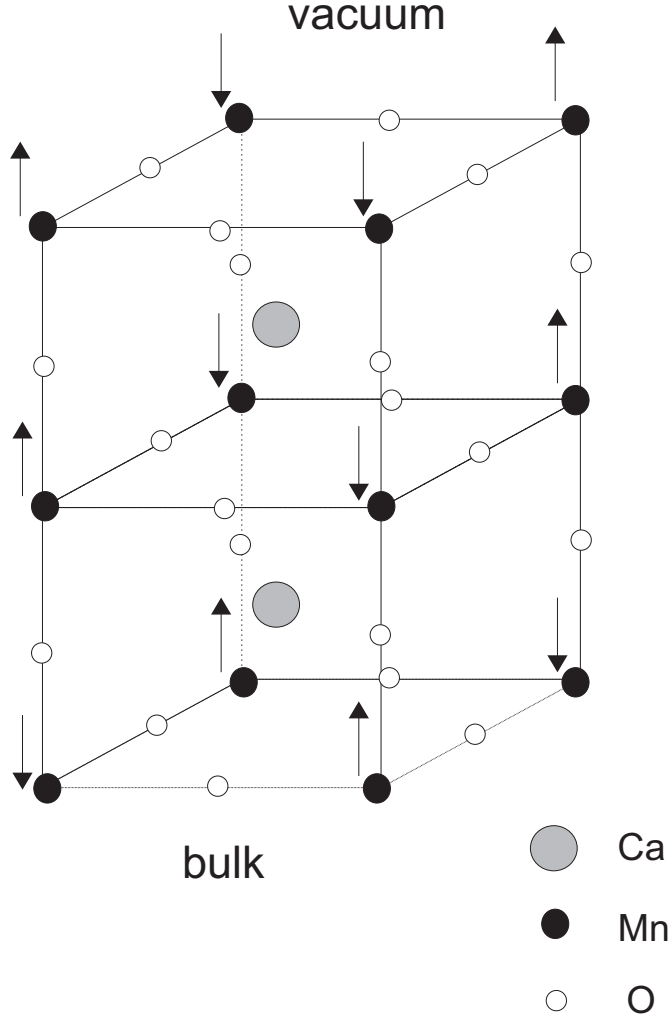


**Figure 22.** Structure of cubic  $\text{CaMnO}_3$ . The arrows near the Mn-ions indicate the core spins. These have a G-type antiferromagnetic order in the bulk. The surface layer, however, is found to be ferromagnetically coupled to the sub-surface layer while retaining the antiferromagnetic in-plane order. After Filippetti and Pickett (2000).

Filippetti and Pickett performed first principles calculations using local spin-density functional theory in order to investigate magnetic reconstructions at the (001) surface of  $\text{CaMnO}_3$  (Filippetti and Pickett 1999) and of  $\text{La}_{0.5}\text{Ca}_{0.5}\text{MnO}_3$  (Filippetti and Pickett 2000). At these dopings a bulk antiferromagnetic structure prevails with G-type and A-type antiferromagnetic ordering for  $\text{CaMnO}_3$  and  $\text{La}_{0.5}\text{Ca}_{0.5}\text{MnO}_3$ , respectively. The striking result of these studies is a ferromagnetic coupling of the surface spins to the sub-surface layer while retaining the antiferromagnetic in-plane structure. This result

**Table 2.** Interface resistance  $RA$  of various manganite-metal contacts.

Manganite	Metal	$T$ (K)	$RA$ ( $\Omega\text{cm}^2$ )	Ref.
LSMO	Pd	4.2	$< 2 \times 10^{-8}$	Mieville (1998)
LSMO	Au	4.2	$(0.64 - 1) \times 10^{-6}$	Mieville (1998)
LSMO	Nb	4.2	$4 \times 10^{-4}$	Mieville (1998)
LSMO	Al	4.2	$10 - 20$	Mieville (1998)
LCMO	Ti	77	0.5	Ziese (1999)
LCMO	Cr	10	3.0	Ziese (1999)
LCMO	Cr	77	3.3	Ziese (1999)

does not depend on the Ca-doping and is thought to apply also in the ferromagnetic phase. The resulting spin structure is sketched in Fig. 22 for  $\text{CaMnO}_3$ . This spin-flip process is driven by the formation of a deep surface state with  $d_{z^2}$  orbital character at the Fermi level. This state promotes a double-exchange like coupling between the spins in the surface and sub-surface layer, a scenario in stark contrast to the assumption of weakened double exchange at the surface made by Calderon *et al* (1999b).

The experimental data collected to date do not allow for a distinction between these two models.

### 6.3. Oxide-metal interface

The resistance of oxide/metal interfaces was systematically investigated by Mieville *et al* (1998) for  $\text{La}_{0.67}\text{Sr}_{0.33}\text{MnO}_3$ ,  $\text{SrRuO}_3$  and  $\text{La}_{0.5}\text{Sr}_{0.5}\text{CoO}_3$  as conducting ferromagnetic oxides and the metals Au, Pd, Nb and Al. It was found that the interface resistance increased with the oxygen affinity of the metal, presumably due to both the formation of an oxygen depleted layer in the ferromagnetic oxide as well as an oxide layer in the metal. Pd yielded a particularly low interface resistance. RF Ar ion plasma cleaning was found to increase the interface resistance. Values for the areal resistivity  $RA$  are given in table 2. Ziese (1999) investigated LCMO/Cr and LCMO/Ti contacts and also found the formation of an interfacial layer with a high resistance. Values are listed in table 2. On the other hand,  $\text{SrRuO}_3$  showed a remarkable compositional stability evidenced by very low interface resistivities with all metals investigated: Au, Pd, Al, Nb. The high corrosion resistance was also shown by lifting a  $\text{SrRuO}_3$  film from its  $\text{SrTiO}_3$  substrate by selective wet chemical etching with an acid (50% HF: 70%  $\text{HNO}_3$ :  $\text{H}_2\text{O} = 1:1:1$ ) (Gan *et al* 1998). Magnetic and electrical measurements on the free-standing film in comparison to strained films on  $\text{SrTiO}_3$  substrates showed an enhancement of the magnetocrystalline anisotropy due to strain and reductions of the Curie temperature and the resistivity in the strained state.

Coombes and Gehring (1998) theoretically investigated the perturbation produced on manganites by a metallic interface. These authors considered a nickel-LCMO interface modelled as a perfect epitaxy within a tight binding approximation. The magnetic moment on a Mn lattice site was calculated as a function of the distance from

the interface assuming a full spin-polarization of the nickel ion at the interface. The perturbation of the Mn spin was found to decay to the bulk values within about five lattice sites from the interface. Below  $T_C$  a drop in the magnetic moment of the first Mn ions was observed, whereas above  $T_C$  a magnetization is induced on the Mn site. Ziese *et al* (1998a) and Gibbs *et al* (1998) investigated LCMO/Ni heterostructures in out-of-plane geometry in order to investigate the induced magnetization. However, the transport properties of those heterostructures turned out to be dominated by a large interface resistance due to oxidation.

#### 6.4. Ferromagnet-superconductor hybrids

Since the manganites have the perovskite structure and a similar lattice constant as high temperature superconductors, attempts have been made to grow hetero-epitaxial ferromagnetic/superconducting structures to investigate magnetotransport properties of such devices. These investigations fall into three classes: the growth and investigation of multilayers, the investigation of spin-injection devices and the direct study of interface properties, especially Andreev reflection. These studies are briefly reviewed in the following.

Jakob *et al* (1995) and Przyslupski *et al* (1997) investigated  $\text{La}_{0.7}\text{Ba}_{0.3}\text{MnO}_3$ /- $\text{YBa}_2\text{Cu}_3\text{O}_7$  and  $\text{Nd}_{0.67}\text{Sr}_{0.33}\text{MnO}_3$ / $\text{YBa}_2\text{Cu}_3\text{O}_7$  multilayers, respectively. Jakob *et al* (1995) reported hetero-epitaxial growth of multilayers with a Curie temperature of about 220 K and a reduced superconducting temperature of about 50 K. The multilayers show the coexistence of superconductivity and ferromagnetism, especially a colossal magnetoresistance effect. The YBCO layers are decoupled by the LBMO layers and show quasi-two-dimensional behaviour as derived from the scaling of the resistance with the magnetic field component perpendicular to the layers. Przyslupski *et al* (1997) also reported hetero-epitaxial multilayer growth, a Curie temperature of about 150 K and a critical temperature of about 75 K. Superconductivity and ferromagnetism also coexist in these NSMO/YBCO-multilayers.

Considerable work has been devoted to the study of spin-injection devices based on ferromagnetic manganites and high temperature superconductors, see Dong *et al* (1997, 1998), Yeh *et al* (1999) and Vas'ko *et al* (1997). Various geometries were used to study spin-polarized carrier injection; the set-up used by Dong *et al* (1997) is sketched in figure 23. The critical current of a YBCO layer was measured with current injection through a NSMO or a  $\text{LaNiO}_3$  layer. The critical current was found to decrease much stronger with injection of spin-polarized quasi-particles from the NSMO layer than with injection of unpolarized quasi-particles from the  $\text{LaNiO}_3$  layer, see figure 24. However, since the YBCO film grown on  $\text{LaNiO}_3$  shows degraded properties, especially a lower critical temperature, pinning effects from the changed microstructure have to be taken into account. The comparison between the two results for spin-polarized and unpolarized carrier injection seems to rule out heating effects being responsible for the decrease of the critical current. Dong *et al* (1997) interpreted their results within a semi-

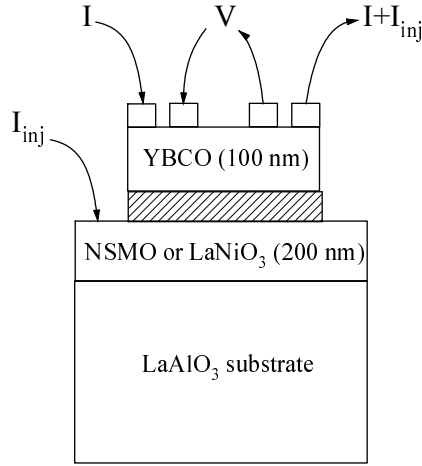


**Figure 23.** Schematic drawing of a spin-injection device as used by Dong *et al* (1997).

quantitative non-equilibrium thermodynamic model of quasi-particle injection at high energies. Yeh *et al* (1999) investigated spin-injection in LCMO/YSZ/YBa<sub>2</sub>Cu<sub>3</sub>O<sub>7</sub> and LSMO/SrTiO<sub>3</sub>/YBa<sub>2</sub>Cu<sub>3</sub>O<sub>7</sub> heterostructures with two thicknesses (2 nm and 10 nm) of the SrTiO<sub>3</sub> barrier. YSZ denotes yttrium-stabilized zirconia. A large difference in the critical current densities determined from continuous and pulsed current measurements was observed. This indicates significant Joule heating in the dc measurements. For 2 nm thick SrTiO<sub>3</sub> and 1.3 nm thick YSZ barriers a strong decrease of the critical current with the injected spin-polarized current was found. Surprisingly, for the 10 nm thick SrTiO<sub>3</sub> barrier, a variation of the critical current with the injected spin-polarized current could not be detected. A LaNiO<sub>3</sub>/SrTiO<sub>3</sub>/YBa<sub>2</sub>Cu<sub>3</sub>O<sub>7</sub> control sample also did not show any suppression of the critical current on quasiparticle injection. Yeh *et al* (1999) argued that the suppression of the critical current density in the heterostructures with thin barriers is due to the pair-breaking effect of spin-polarized quasiparticles. The thicker SrTiO<sub>3</sub> barrier is supposed to provide a larger hypothetical interface impedance, thereby suppressing spin-polarized quasiparticle injection.

In a related study Mikheenko *et al* (2001) investigated the effect of spin-injection on the relaxation from the Bean critical state established in a YBa<sub>2</sub>Cu<sub>3</sub>O<sub>7</sub> film; a large change of the magnetic moment was detected. In view of the experimental data obtained so far the large variation of device parameters seems to preclude the observation of any reliable trend. Therefore, in order to decide on the mechanism of spin-injection and pair-breaking more experimental data are clearly necessary.

A detailed study of the transport properties of La<sub>0.67</sub>Ba<sub>0.33</sub>MnO<sub>3</sub>/DyBa<sub>2</sub>Cu<sub>3</sub>O<sub>7</sub>-interfaces was performed by Vas'ko *et al* (1998). The Curie temperature was 305 K and the critical temperature 90 K. The differential conductance of the ferromagnetic/superconducting interface was measured as a function of temperature, bias voltage and magnetic field. The main finding was a dip in the differential conductance near zero bias at temperatures below about 60 K, see figure 25. At

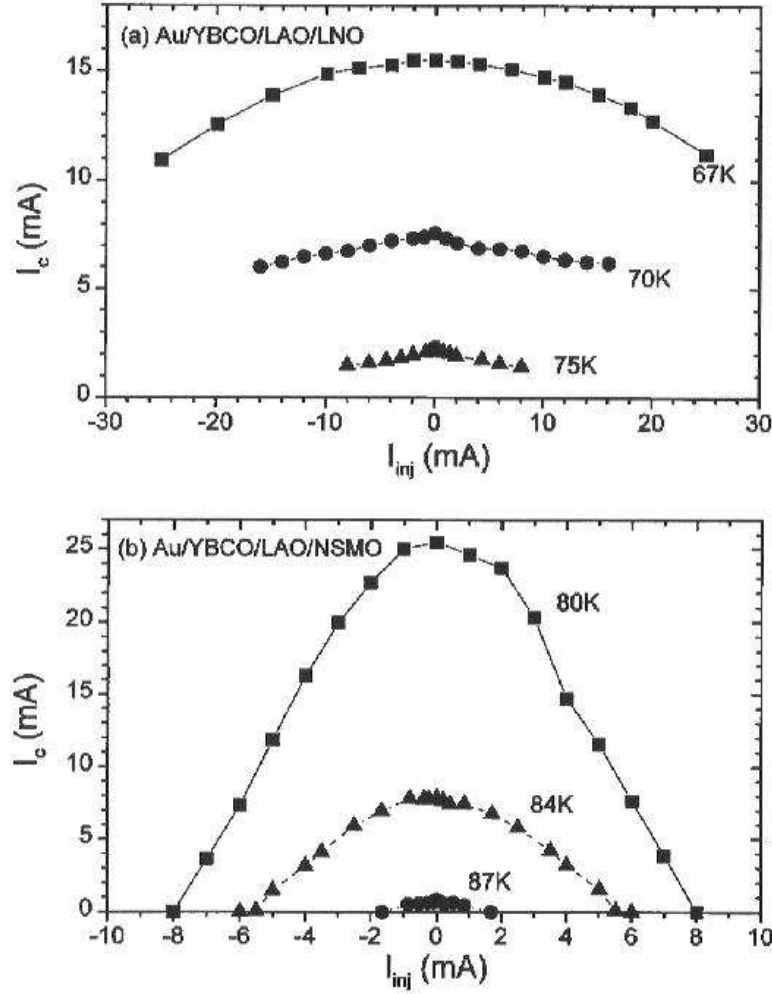


**Figure 24.** Critical current of the YBCO layer shown in figure 23 as a function of the current injected from (a) a  $\text{LaNiO}_3$  and (b) a  $\text{Nd}_{0.7}\text{Sr}_{0.3}\text{MnO}_3$  layer. The injection of a spin-polarized current apparently leads to a much stronger decay of the critical current. Reproduced from Dong *et al* (1997).

high temperatures the conductance decreases at large bias voltages, presumably due to heating effects. The voltage dependence of the differential conductance at low temperatures does not depend on the applied magnetic field for fields up to 12 T. The conductance dip was interpreted as being due to Andreev reflection at a clean ferromagnetic/superconducting interface. Since LBMO has a high spin-polarization, Andreev reflection is suppressed. The disappearance of the conductance dip at about 60 K might indicate that the superconductor is in the orthorhombic II phase near the interface. This study shows that the fabrication of fairly clean superconductor/ferromagnet interfaces is feasible using manganites and high temperature superconductors. The measurement of Andreev reflection at these interfaces might prove to be a powerful tool for the investigation of symmetries of the superconducting order parameter. Calculations of conductance spectra for s- and

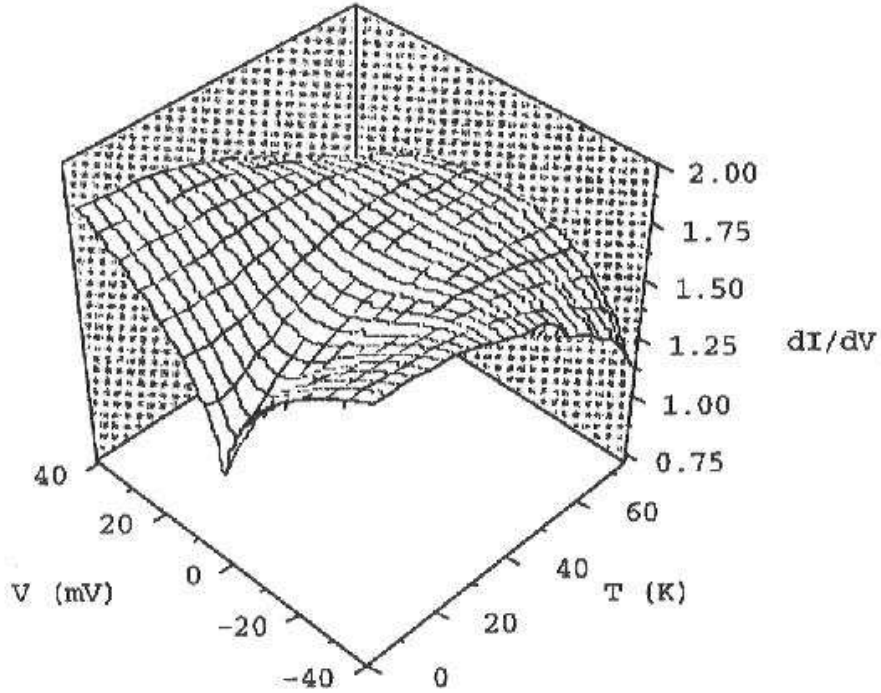


**Figure 25.** Temperature and voltage-bias dependence of the differential conductance of the interface between the ferromagnet  $\text{La}_{0.67}\text{Ba}_{0.33}\text{MnO}_3$  and the superconductor  $\text{YBa}_2\text{Cu}_3\text{O}_7$ . Reproduced from Vas'ko *et al* (1998).

d-wave superconductors have already been performed (Zhu *et al* 1999, Merrill and Si 1999, Bhattacharjee and Sardar 2000).

The electronic structure and magnetism of a LSMO interface buried under  $\text{YBa}_2\text{Cu}_3\text{O}_7$  capping layers of various thicknesses  $\leq 8$  nm was investigated by Stadler *et al* (1999, 2000) using x-ray magnetic circular dichroism (XMCD) and x-ray absorption spectroscopy (XAS) at the Mn  $L_{2,3}$  edge. From a comparison of the data with spectra measured on a  $\text{La}_{1-x}\text{Sr}_x\text{MnO}_3$  series it was concluded that the cation stoichiometry at the interface is changed. La ions are presumably replaced by Ba ions from the  $\text{YBa}_2\text{Cu}_3\text{O}_7$  layer leading to a decreased La concentration near the interface. The XMCD signal is consistent with a progressive replacement of the ferromagnetic order by an antiferromagnetic structure. A comparison with Al capped LSMO films shows that the spectral changes are not due to de-oxygenation. The antiferromagnetic structure at the interface is likely to decrease the spin-polarization.

### 6.5. Exchange biasing, multilayers and GMR

In view of possible applications of the magnetic oxides in tunnelling junctions that generally have a pinned magnetic electrode, the study of exchange biasing of the magnetic layer by an antiferromagnet is important. Exchange biasing of magnetite layers by antiferromagnetic layers such as NiO (Berry *et al* 1993, Lind *et al* 1995, Ball *et al* 1996, van der Heijden *et al* 1999) and CoO (Ijiri *et al* 1998a, 1998b,

Kleint *et al* 1998) has been achieved. In this case, the coupling mechanism seems to be similar to exchange coupling in elemental ferromagnets. In the manganites the situation might be different, since the double-exchange mechanism that provides the magnetic coupling is short-ranged and very sensitive to structural disorder. So far, only two groups reported studies on the exchange-biasing of manganite layers: Niarchos and coworkers (Panagiotopoulos *et al* 1999a, 1999b, Moutis *et al* 2001) and Nikolaev *et al* (2000a) studied exchange coupling in  $\text{La}_{2/3}\text{Ca}_{1/3}\text{MnO}_3/\text{La}_{1/3}\text{Ca}_{2/3}\text{MnO}_3$  multilayers. Panagiotopoulos *et al* (1999a, 1999b) grew multilayers with various bilayer thicknesses between 2 and 32 nm using pulsed laser deposition. The magnetization hysteresis loops were found to be shifted after field cooling in a field of 1 T with respect to the hysteresis loops obtained after zero field cooling. The exchange biasing field measured at 10 K displays a marked dependence on the bilayer thickness with a maximum exchange field at a bilayer thickness of 10 nm. The temperature dependence of the magnetization, however, indicates superparamagnetic behaviour of the multilayers with a blocking temperature of about 70 K. The exchange-biasing field vanishes at the blocking temperature. The superparamagnetic behaviour indicates an unfavourable structural morphology of the samples and possibly very rough interfaces. Nikolaev *et al* (2000) fabricated  $\text{La}_{1/3}\text{Ca}_{2/3}\text{MnO}_3/\text{La}_{2/3}\text{Ca}_{1/3}\text{MnO}_3/\text{La}_{1/3}\text{Ca}_{2/3}\text{MnO}_3$  trilayers using ozone-assisted molecular beam epitaxy. Even very thin (2.3 nm – 4.6 nm) manganite films showed metallic conductivity and ferromagnetism below comparatively high Curie temperatures of 200 K. The exchange field was found to be about 800 G at 5 K. Shifted hysteresis loops were also observed in NSMO ceramics (Baszyński *et al* 1999) and  $\text{La}_{0.5}\text{Ca}_{0.5}\text{MnO}_3$  films (Roy *et al* 1999).

There is substantial work on the properties of magnetite multilayers that will not be reviewed here. It is more interesting to look at the studies of manganite multilayers, since it is clear from the theoretical work discussed above that these samples might exhibit interesting physical properties. First studies of multilayers formed from thin ferromagnetic manganite layers sandwiched in between insulating layers report an enhancement of the magnetoresistance (Kwon *et al* 1997, Venimadhav *et al* 2000, Pietambaram *et al* 2001); the mechanism leading to this enhancement is unclear but might simply be due to structural and chemical inhomogeneity. Studies on high quality samples reveal antiferromagnetic interlayer coupling and giant magnetoresistance (Nikolaev *et al* 1999, Nikolaev *et al* 2000b, Krivorotov *et al* 2001). Nikolaev *et al* (1999, 2000b) showed that ferromagnetic  $\text{La}_{0.67}\text{Ba}_{0.33}\text{MnO}_3$  layers coupled via  $\text{LaNiO}_3$  spacers showed oscillatory exchange coupling as a function of the spacer thickness. At antiferromagnetic coupling a small positive magnetoresistance was seen. This is in contrast to the usual giant magnetoresistance in metallic multilayers which is negative. The result, however, is in agreement with the observations on  $\text{Fe}_3\text{O}_4/\text{TiN}$  multilayers also showing positive magnetoresistance (Orozco *et al* 1999). The explanation of this phenomenon is still qualitative: the positive magnetoresistance is attributed to quantum confinement enhanced by the half-metallic nature of the ferro- and ferrimagnetic constituent layers.

## 6.6. Oxide-semiconductor interfaces

To the best of the author's knowledge, no data are available on ferromagnetic oxide/semiconductor interfaces. It is possible to grow manganite films directly on Si or GaAs substrates resulting in polycrystalline films due to the large thermal expansion coefficient of the semiconductor substrate and strong inter-diffusion. Several groups reported the heteroepitaxial growth of manganite films on YSZ buffered Si substrates (Trajanovic *et al* 1996, Fontcuberta *et al* 1999, Gillman *et al* 1998). However, the film quality seems to be worse than for films grown on lattice matched substrates. Due to the presence of the thick insulating buffer layer, spin-injection from the ferromagnetic oxide into the semiconductor cannot be facilitated.

## 7. Ferromagnetic tunnelling junctions

### 7.1. Basic theory

The magneto-conductance of a ferromagnet-insulator-ferromagnet tunnelling junction was first derived by Julliere (1975). A schematic drawing of a ferromagnetic tunnelling junction is shown in figure 26: two ferromagnetic electrodes are separated by a thin insulating layer. The parallel and anti-parallel orientation of the ferromagnetic electrodes leads to different conductances in these two states. A schematic density of states for the tunnelling junction is indicated in the figure assuming identical, half-metallic ferromagnets. If the spin of the carrier is conserved in the tunnelling process, tunnelling is only possible for parallel electrode orientation. A simple expression for the tunnelling magnetoconductance can be derived as follows (Julliere 1975). Let  $P$  and  $P'$  denote the spin-polarization of the ferromagnetic electrodes. If the carrier spin is conserved during tunnelling, the conductance is proportional to the sum of the products of the spin-polarized densities of states. One obtains in the parallel ( $\uparrow\uparrow$ ) and antiparallel ( $\uparrow\downarrow$ ) states:

$$G_{\uparrow\uparrow} \propto (1 + P)(1 + P') + (1 - P)(1 - P') \propto 1 + PP' \quad (35)$$

$$G_{\uparrow\downarrow} \propto (1 + P)(1 - P') + (1 - P)(1 + P') \propto 1 - PP'. \quad (36)$$

This yields for the magnetoconductance and magnetoresistance (TMR), respectively

$$\frac{\Delta G}{G} \equiv \frac{G_{\uparrow\uparrow} - G_{\uparrow\downarrow}}{G_{\uparrow\uparrow}} = \frac{2PP'}{1 + PP'} \quad (37)$$

$$\frac{\Delta R}{R} \equiv \frac{R_{\uparrow\downarrow} - R_{\uparrow\uparrow}}{R_{\uparrow\uparrow}} = \frac{2PP'}{1 - PP'}. \quad (38)$$

In the case of two identical ferromagnets, the magnetoresistance is always negative; it diverges for two half-metallic electrodes. In the general case, the magnetoresistance can be both positive and negative.

Slonczewski (1989) calculated the tunnelling conductance within a free electron model using the Landauer-Büttiker formula (Landauer 1957, Büttiker 1988). The exchange fields in the ferromagnetic electrodes were assumed to span an angle  $\Theta$ . The



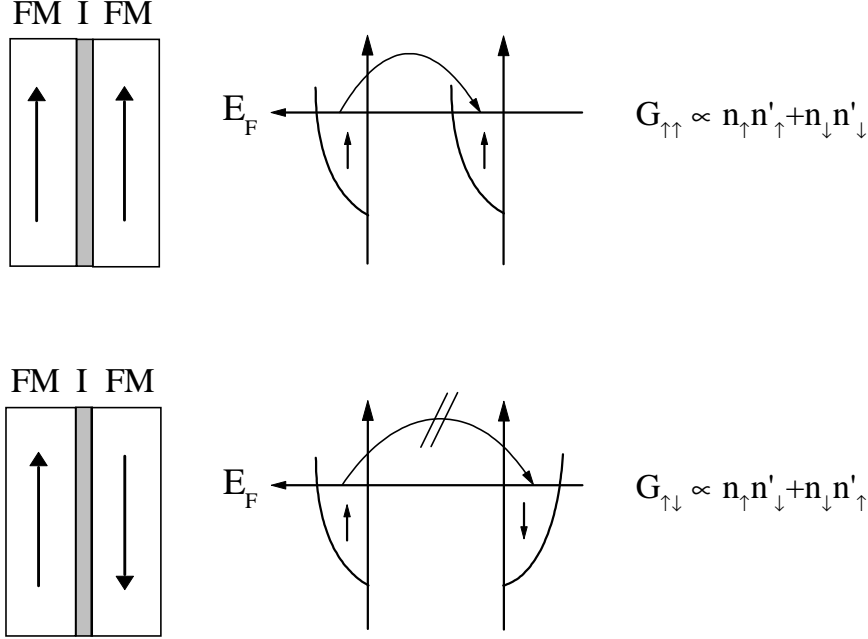


**Figure 26.** Schematic drawing of a ferromagnetic tunnelling junction and of the corresponding density of states. FM indicates the ferromagnetic electrodes and I the insulating barrier. For simplicity the density of states of a half-metallic ferromagnet are shown. The conductivities in the parallel and antiparallel state,  $G_{\uparrow\uparrow}$  and  $G_{\uparrow\downarrow}$  are proportional to the densities of states at the Fermi level,  $n_{\uparrow}$ ,  $n_{\downarrow}$  (left electrode) and  $n'_{\uparrow}$ ,  $n'_{\downarrow}$  (right electrode), if spin-flip processes in the barrier can be neglected.

transmission coefficient  $T(k_{\parallel})$  of an incoming electron of defined spin is calculated.  $k_{\parallel}$  denotes the wave vector component parallel to the barrier. Assuming the absence of diffuse scattering in the barrier, the tunnelling conductance is given by

$$G = \frac{e^2}{(2\pi)^2 \hbar} \int d^2 k_{\parallel} T(k_{\parallel}). \quad (39)$$

Slonczewski evaluated equation (39) by integrating over  $k_{\parallel}$  and keeping only the leading term in  $1/d$ . The conductance is found to be of the form

$$G \propto [1 + P_{fb}^2 \cos(\Theta)] \quad (40)$$

with an effective polarization  $P_{fb}$  depending on the band splitting. In the one-band case  $P_{fb} = 1$  resulting in a complete spin-valve effect, in the two-band case

$$P_{fb} = \frac{(k_{\uparrow} - k_{\downarrow})}{(k_{\uparrow} + k_{\downarrow})} \frac{(\kappa^2 - k_{\uparrow}k_{\downarrow})}{(\kappa^2 + k_{\uparrow}k_{\downarrow})} \equiv P A_{fb} \quad (41)$$

with the wave-vectors  $k_{\uparrow}$ ,  $k_{\downarrow}$  of the  $\uparrow$  and  $\downarrow$  electrons and the inverse of the decay length in the barrier  $\kappa = \sqrt{2(U_0 - E_F)}$ .  $U_0$  denotes the barrier height and  $E_F$  the Fermi energy. For free electrons, the first factor in equation (41) simply reduces to the standard definition of the spin-polarization  $P = (n_{\uparrow} - n_{\downarrow})/(n_{\uparrow} + n_{\downarrow})$ . The second factor  $A_{fb}$ , however, is related to interface properties and has the range  $-1 < A_{fb} < 1$ . It

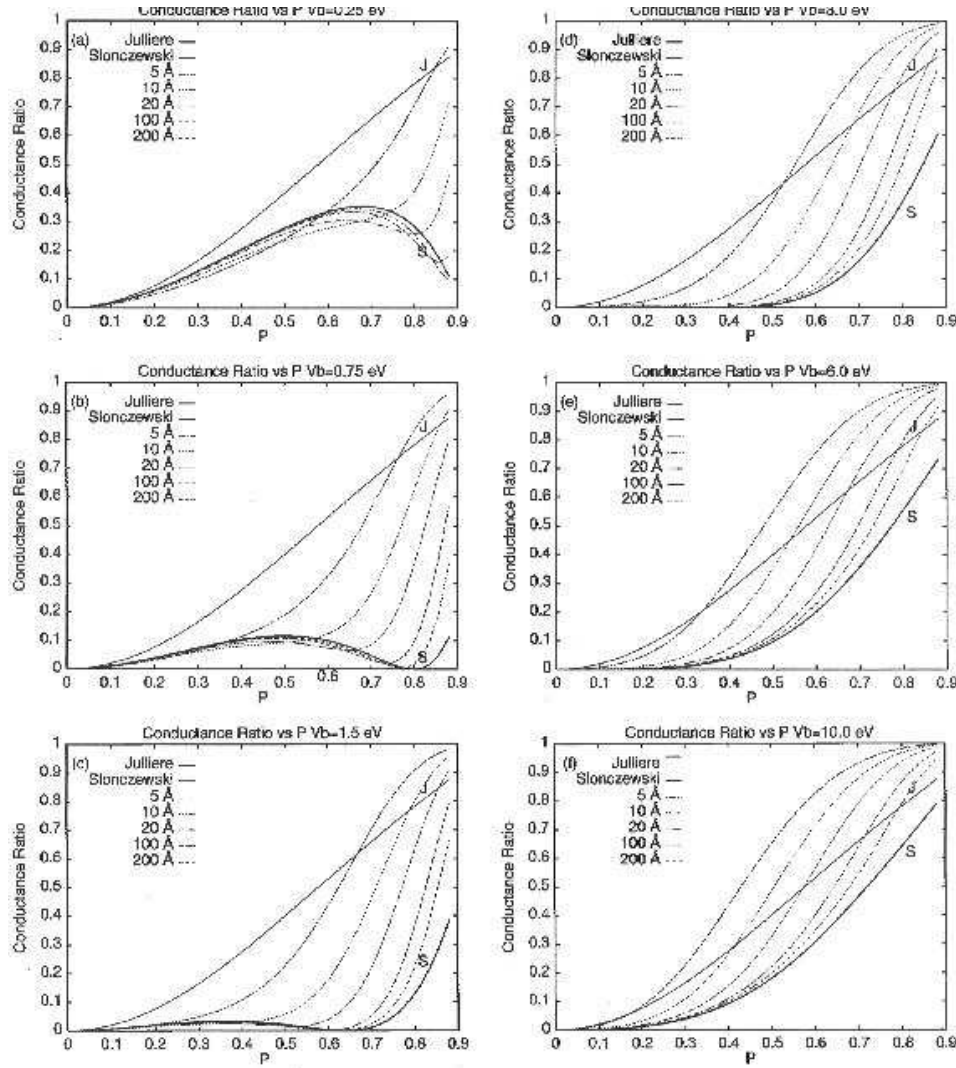


**Figure 27.** Conductance ratio  $\Delta G/G$  for free electron spin-dependent tunnelling for various barrier heights (a) 0.25 eV, (b) 0.75 eV, (c) 1.5 eV, (d) 3.0 eV, (e) 6.0 eV and (f) 10.0 eV. In each panel, barrier widths of 0.5, 1, 2, 10 and 20 nm are shown along with the Julliere and Slonczewski results labelled by (J) and (S), respectively. Reproduced from Maclaren *et al* (1997).

changes sign as a function of barrier height, indicating that the sign of the apparent spin-polarization can be modified by the appropriate choice of the barrier material.

The tunnelling conductance in the free-electron model was numerically calculated by MacLaren *et al* (1997) in order to investigate the validity of Slonczewski's and Julliere's results. In figure 27 the conductance ratio  $\Delta G/G$  calculated by numerically integrating Eq. (39) is shown as a function of the polarization  $P$  for various barrier heights and thicknesses. For comparison, Julliere's expression  $\Delta G/G = 2P^2/(1 + P^2)$  and Slonczewski's approximation are also shown. Slonczewski's expression for  $\Delta G/G$  is a good approximation for large barrier thicknesses and small barrier heights, whereas Julliere's expression fails to reproduce any dependence on barrier height and thickness.

MacLaren *et al* (1997) further calculated the tunnelling conductance taking into account the band-structure of the iron electrodes. These results also confirmed a considerable dependence of the tunnelling magnetoconductance on the barrier height and a small variation with barrier thickness. Therefore, it has to be concluded that Julliere's model fails to incorporate the relevant physics of spin-polarized tunnelling. As will be seen later, however, this model yields TMR values in surprisingly good agreement with experiment, if the spin-polarization is defined in an appropriate way.

The bias-dependence of the tunnelling conductance is generally quite complicated. Since the carriers tunnel directly between the electrodes, a quadratic voltage dependence is expected at low bias according to the Simmons' model for free electron tunnelling (Simmons 1963). Guinea (1998) investigated the bias dependence due to the excitation of bulk and interface magnons. He found that, for a barrier of thickness  $d$ , bulk magnons with wavelengths larger than  $d$  can be created with roughly equal probability. At zero temperature magnons are created at finite voltage bias yielding a conductance

$$G(V) \propto \begin{cases} (V/J)^{3/2} & : V \ll J (a^2/d^2) \\ (a/d)^3 & : V \gg J (a^2/d^2) \end{cases} \quad (42)$$

$a$  denotes the lattice parameter and  $J$  the exchange constant.

The contribution to the bias dependence by interface antiferromagnons was found to be

$$G(V) \propto \begin{cases} (V/J_{AF})^2 & : V \ll J_{AF} (a/d) \\ (a/d)^2 & : V \gg J_{AF} (a/d) \end{cases} \quad (43)$$

$J_{AF}$  denotes the interface exchange constant.

## 7.2. Model systems

In this section some tunnelling systems using the elemental ferromagnets Fe, Co, Ni and their alloys  $\text{Ni}_{80}\text{Fe}_{20}$  and  $\text{Fe}_{50}\text{Co}_{50}$  will be discussed in order to give a brief overview of the current status of magnetic tunnelling junctions before turning to oxide tunnelling junctions. Various barrier materials such as Ge, GeO, NiO,  $\text{Al}_2\text{O}_3$ , AlN, MgO and  $\text{HfO}_2$  have been used;  $\text{Al}_2\text{O}_3$  is the most popular one.

Experimental work on ferromagnetic tunnelling junctions was initiated by Julliere as early as 1975. However, interest in these devices was small, since the tunnelling magnetoresistance at room temperature was only a fraction of a percent. This situation changed after magnetoresistance values in excess of 10% were reported by Moodera *et al* in 1995. Meanwhile it is possible to fabricate ferromagnetic tunnelling junctions reproducibly with a magnetoresistance of more than 20% at room temperature. Moodera *et al* (1998) reported TMR values for a  $\text{Co}/\text{Al}_2\text{O}_3/\text{Ni}_{80}\text{Fe}_{20}$  junction of 20.2%, 27.1% and 27.3% at 295 K, 77 K and 4.2 K, respectively. As already described in section 2, the spin-polarization of the conduction electrons can be measured using a superconducting counter-electrode as a spin detector. This yields  $P_{\text{Co}} = 35\%$  and  $P_{\text{NiFe}} = 45\%$ . Within Julliere's model, a tunnelling magnetoresistance of 27.2% is found, being in perfect

agreement with the measured value. Thus, Julliere's model apparently yields a good description of the tunnelling magnetoresistance. The spin-polarization has to be defined via measurements of ferromagnet/insulator/superconductor tunnelling using the same barrier material.

In order to achieve a large tunnelling magnetoresistance it is necessary to (i) grow smooth and clean FM/I-interfaces, (ii) have defect free barriers of large height and (c) have well defined and separated coercive fields to fully realize the antiferromagnetic state in the field range  $H_{c1} < H < H_{c2}$ .

An exciting development in the field of tunnelling junctions is the recent investigation of spin-polarized tunnelling in double tunnelling junctions (Schelp *et al* 1997, Brückl *et al* 1998, Montaigne *et al* 1998, Takahashi and Maekawa 1998, Barnás and Fert 1998, Brataas *et al* 1999a). A double tunnelling junction consists of two ferromagnetic electrodes separated by a small ferromagnetic island. If the electrode dimensions are very small such that the island capacitance  $C$  is also very small, the junction enters the Coulomb blockade regime for temperatures smaller than the Coulomb energy  $E_c = e^2/2C$ . Brückl *et al* (1998) observed an anomalous increase of the magnetoresistance in permalloy/ $\text{Al}_2\text{O}_3$ /Co/ $\text{Al}_2\text{O}_3$ /permalloy tunnelling junctions at temperatures below 5 K. The lateral dimensions of the junctions were of order  $100 \times 200 \text{ nm}^2$ . This was interpreted as arising from spin-polarized tunnelling in the Coulomb-blockade regime. Takahashi and Maekawa (1998) calculated the tunnelling magnetoresistance of a double tunnelling junction in the Coulomb blockade regime. At low temperatures charging of the intermediate island is unfavourable and tunnelling proceeds via a co-tunnelling process, namely by the simultaneous tunnelling of a charge carrier from one electrode to the island and from the island to the other electrode. Since this is a second order process, the magnetoresistance is found to be

$$\frac{\Delta R}{R_{\uparrow\uparrow}} = \left[ \frac{1 + P^2}{1 - P^2} \right]^2 - 1, \quad (44)$$

being larger than for a single tunnelling junction. Barnás and Fert (1998) analyzed double tunnelling junctions using a different approach and found oscillations in the magnetoresistance as a function of the applied voltage. These are due to discrete charging effects. A quantitative experimental verification of these predictions in microfabricated tunnelling junctions has not yet been carried out. This is due to the challenging microfabrication requirements to achieve small structures with small capacitances. However, higher-order tunnelling processes have been successfully studied in insulating Co-Al-O films (Mitani *et al* 1998a, 1998b). These films show a striking enhancement of the magnetoresistance in the Coulomb blockade-regime. Surprisingly, the magnetoresistance in this regime is independent of the bias voltage, although the resistivity is a strong function of the applied voltage bias. These results can be understood quantitatively within a model of spin-polarized tunnelling between large grains via several small grains (Mitani *et al* 1998a), see discussion in the following section.

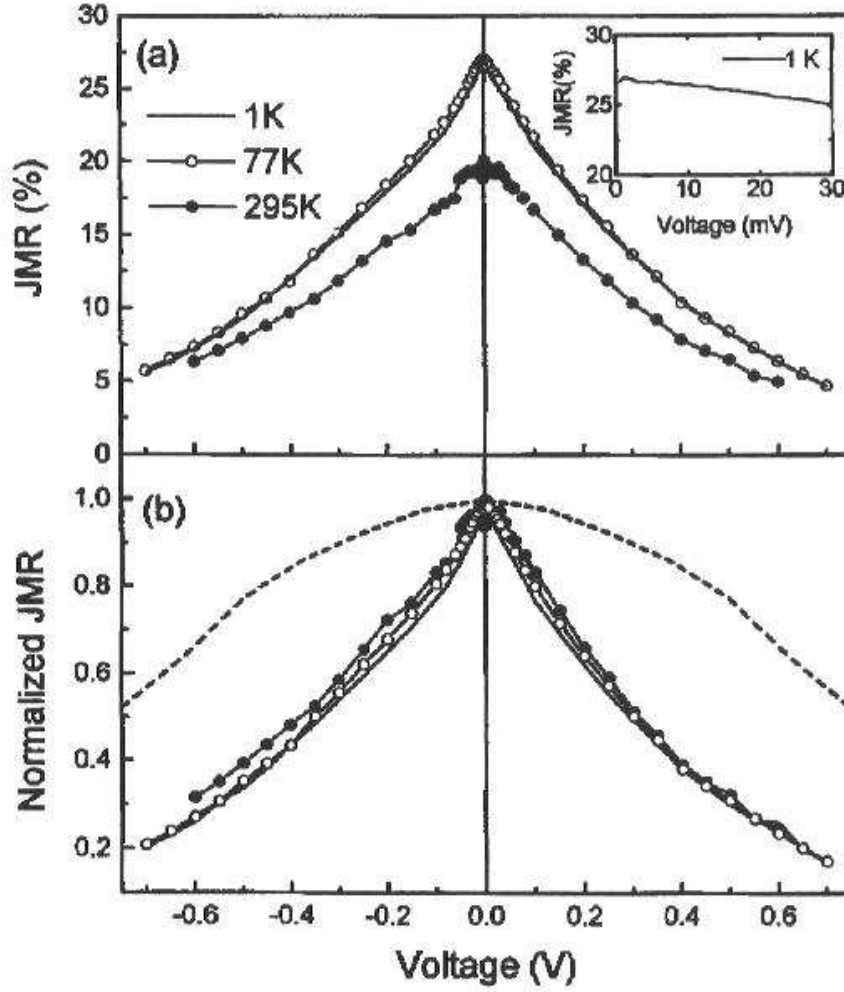


**Figure 28.** TMR versus bias voltage at three temperatures for a Co/Al<sub>2</sub>O<sub>3</sub>/Ni<sub>80</sub>Fe<sub>20</sub> junction. Data shown are (a) the actual percentages and (b) normalized at zero bias. The inset shows the TMR in the low bias region displaying near constancy of TMR. The dashed line in (b) is the theoretically expected variation for a Fe-Al<sub>2</sub>O<sub>3</sub>-Fe junction with a 3 eV barrier height (from Fig. 1 of Bratkovsky (1997)). Reproduced from Moodera *et al* (1998).

### 7.3. Temperature and voltage dependence

It is generally observed that the tunnelling magnetoresistance decreases with temperature as well as with bias voltage. A number of studies were devoted to the voltage dependence and we briefly review this field of research at the end of this section. First we discuss the temperature dependence that was studied in great detail by Shang *et al* (1998).

Shang *et al* (1998) based their investigation of the temperature dependent conductance and magnetoconductance on Julliere's model, since this reproduces the correct magnitude of the TMR at low temperatures. The total conductance is written as

$$G(\Theta) = G_T [1 + P_1 P_2 \cos(\Theta)] + G_{SI}, \quad (45)$$

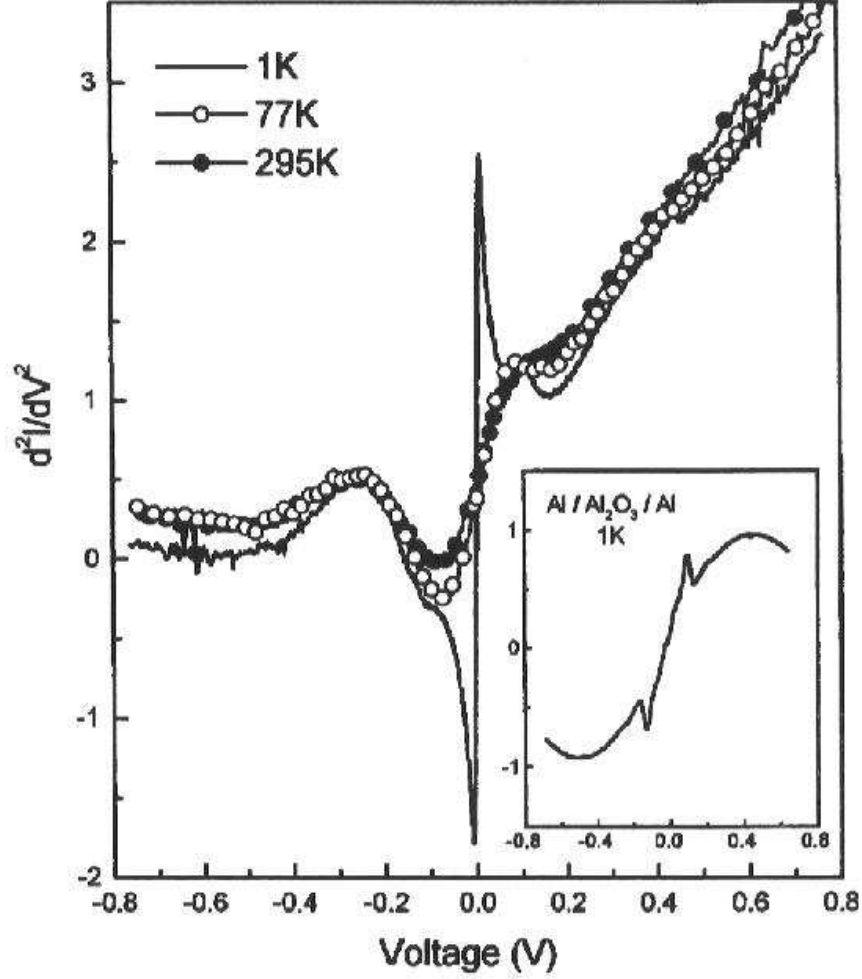


**Figure 29.** Inelastic tunnelling spectroscopy spectra at three temperatures for the same junction as in Fig. 28, measured at  $B = 0$ . Similar spectra are seen for junctions where one electrode is a ferromagnet and the other electrode is Al. The inset shows an inelastic tunnelling spectrum of an Al/Al<sub>2</sub>O<sub>3</sub>/Al reference junction for comparison. The dip near 100 mV was interpreted as arising from the excitation of an Al–O stretching mode, compare with the inset that shows the same feature in a non-magnetic Al/Al<sub>2</sub>O<sub>3</sub>/Al junction, whereas the sharp features near 17 mV were assigned to magnon excitation. Reproduced from Moodera *et al* (1998).

where the first term on the right hand side is the usual spin-polarized tunnelling conductance and the second term  $G_{SI}$  is an inelastic contribution independent of the magnetization. This inelastic contribution might arise from inelastic tunnelling via localized states in the barrier or from conduction through pin-holes. The temperature dependent pre-factor is given by

$$G_T = G_0 \frac{CT}{\sin(CT)}, \quad (46)$$

where  $G_0$  is a constant and  $C = 1.387 \times 10^{-3} d / \sqrt{\Phi}$  with the barrier width  $d$  in nm and the barrier height  $\Phi$  in eV. For typical parameters,  $G_T$  at room temperature is only a

few percent higher than at 4.2 K. The spin-polarization is thought to be proportional to the surface magnetization. The magnetization far below the Curie temperature is reduced by the excitation of spin waves producing a term proportional to  $T^{3/2}$ . This temperature dependence was confirmed in bulk samples, thin films and for the surface magnetization. The surface spin waves, however, showed a largely reduced spin stiffness. Therefore, for the spin-polarization at low temperatures one can write

$$P(T) = P_0 (1 - \alpha T^{3/2}) \quad (47)$$

with the zero temperature spin-polarization  $P_0$  and a material dependent parameter  $\alpha$ .

Shang *et al* (1998) analyzed the measured tunnelling resistance and TMR of  $\text{Co}/\text{Al}_2\text{O}_3/\text{Ni}_{80}\text{Fe}_{20}$ ,  $\text{Co}/\text{Al}_2\text{O}_3/\text{Ni}_{80}\text{Fe}_{20}/\text{NiO}$  and  $\text{Co}/\text{Al}_2\text{O}_3/\text{Co}/\text{NiO}$  tunnelling junctions. They found good agreement between theory and experimental data in the temperature range  $77 \text{ K} \leq T \leq 400 \text{ K}$  using the parameters  $\alpha_{\text{Co}} = 1 - 6 \times 10^{-6} T^{-3/2}$  and  $\alpha_{\text{NiFe}} = 3 - 5 \times 10^{-5} K^{-3/2}$  as well as an inelastic conductance  $G_{SI} \propto T^{1.35 \pm 0.15}$ . The  $\alpha$  values obtained are comparable to values extracted from magnetization measurements; these show a rough scaling with the Curie temperature ( $T_C = 1360 \text{ K}$  for Co and  $850 \text{ K}$  for  $\text{Ni}_{80}\text{Fe}_{20}$ ). The temperature dependence of  $G_{SI}$  is in good agreement with theoretical predictions of inelastic tunnelling through an amorphous barrier via pairs of localized states that yields a temperature dependence  $\propto T^{4/3}$  (Glazman and Matveev 1988). This indicates the existence of defect states in the barrier. Although this analysis was performed on the basis of the simple Julliere model, it indicates that the magnetoresistance in high quality tunnelling junctions is reduced by both the excitation of interface spin waves as well as inelastic processes via defect states in the barrier material.

The tunnelling resistances in the parallel and antiparallel states show different bias voltage dependences leading to a bias voltage dependence of the tunnelling magnetoconductance. The TMR is found to be voltage independent at very low voltages,  $V < 10 \text{ mV}$  and is then seen to decrease strongly on a voltage scale of about  $500 \text{ mV}$ , see figure 28. The junction resistance as a function of bias voltage usually shows a cusp at zero voltage and at low temperatures. This cusp was termed “zero bias anomaly”. Slonczewski’s model contains a bias voltage dependence through the parameter  $\kappa$  being related to the effective barrier height. This voltage dependence, however, is much too small to explain the experimental data. Zhang *et al* (1997a) and Bratkovsky (1997) calculated the TMR at high electron energies and found a quenching of the TMR by hot electrons. The tunnelling conductance was found to be linear in bias voltage at low voltages  $< 200 \text{ mV}$  in qualitative agreement with theory. Moodera *et al* (1998), however, observed in high quality junctions a stronger voltage dependence than predicted by theory, see figure 28, and interpreted this result as arising from magnon scattering. Indeed, inelastic tunnelling spectroscopy spectra of a  $\text{Co}/\text{Al}_2\text{O}_3/\text{Ni}_{80}\text{Fe}_{20}$  junction showed features at about  $\pm 100 \text{ mV}$  as well as  $17 \text{ mV}$ , see figure 29. Although the feature near  $100 \text{ mV}$  has been identified as being due to an Al–O stretching mode, it is believed to also have some magnon contribution; the sharp feature emerging at  $1 \text{ K}$

at 17 mV is also attributed to a magnon excitation. According to the results of Guinea (1998) magnon scattering should lead to a voltage dependence  $\propto V^{3/2}$ , see equation (42), in qualitative agreement with experiment.

Zhang and White (1998) suggested that extrinsic factors might cause the considerable voltage dependence of the magnetoresistance. This idea was based on a correlation between the maximal magnetoresistance value and the non-linear  $I$ - $V$ -curves of permalloy/ $\text{Al}_2\text{O}_3$ /Co (CoFe) junctions showing that a small magnetoresistance ratio is related with a strong non-linearity. The junctions with unfavourable characteristics are likely to have numerous defect states in the barrier leading to inelastic tunnelling processes that are spin-independent. Zhang and White (1998) proposed a phenomenological model taking into account the inelastic tunnelling current  $I_i$  and derived the magnetoresistance ratio in this case:

$$\frac{\Delta G}{G} = \frac{(\Delta G/G)_{\text{Julliere}}}{1 + I_i/I_{\uparrow\downarrow}}, \quad (48)$$

where  $I_{\uparrow\downarrow}$  denotes the direct tunnelling current in the case of antiparallel electrode magnetization. Assuming a spatially and energetically uniform distribution of the defect states, the calculated  $I$ - $V$ -curves agree qualitatively with the measured characteristics of high and low quality junctions, lending support to this model.

#### 7.4. Oxide tunnelling junctions

Ferromagnetic oxide tunnelling junctions based on manganite electrodes were fabricated and investigated by the IBM group (Sun *et al* 1996, Lu *et al* 1996, Li *et al* 1997c, Sun *et al* 1997, 1998, Sun 1998), the Orsay group (Viret *et al* 1997a), the Cambridge group (Moon-Ho Jo *et al* 2000a, 2000b) and further by Obata *et al* (1999), Yin *et al* (2000) and Noh *et al* (2001). Kwon *et al* (1998) investigated LSMO ramp-edge junctions. Heteroepitaxial magnetite tunnelling junctions were investigated by the IBM group (Li *et al* 1998b) and the Eindhoven group (van der Zaag *et al* 2000). A “mixed” junction based on a LSMO and a magnetite electrode was studied by Ghosh *et al* (1998). This research was motivated by the large spin-polarization of the manganites and of magnetite. Indeed, TMR values in excess of 100% at 4.2 K have been reported by Sun *et al* (1998), Viret *et al* (1997a) and Obata *et al* (1999). In this section the fabrication technique is reviewed, typical results for resistance, magnetoresistance and non-linear conductance are discussed and an analysis of limiting factors and future trends is given.

LSMO/ $\text{SrTiO}_3$ /LSMO trilayer structures are usually grown by pulsed laser deposition on  $\text{LaAlO}_3$  or  $\text{SrTiO}_3$  substrates. Whereas Sun *et al* (1998) report a peak-to-peak roughness of a single  $\text{La}_{0.7}\text{Sr}_{0.3}\text{MnO}_3$  layer of 1.5 nm, Obata *et al* (1999) achieved the growth of atomically flat  $\text{La}_{0.8}\text{Sr}_{0.2}\text{MnO}_3$  films. Noh *et al* (2001) report on the fabrication of LSMO/ $\text{SrTiO}_3$ /LSMO trilayer structures by 90° off-axis sputtering and found improved junction uniformity compared to junctions made by pulsed laser deposition.  $\text{SrTiO}_3$  (STO) layers with thicknesses between 1.6 nm and 5 nm have been used as tunnelling barriers. High resolution transmission electron micrographs of cross-



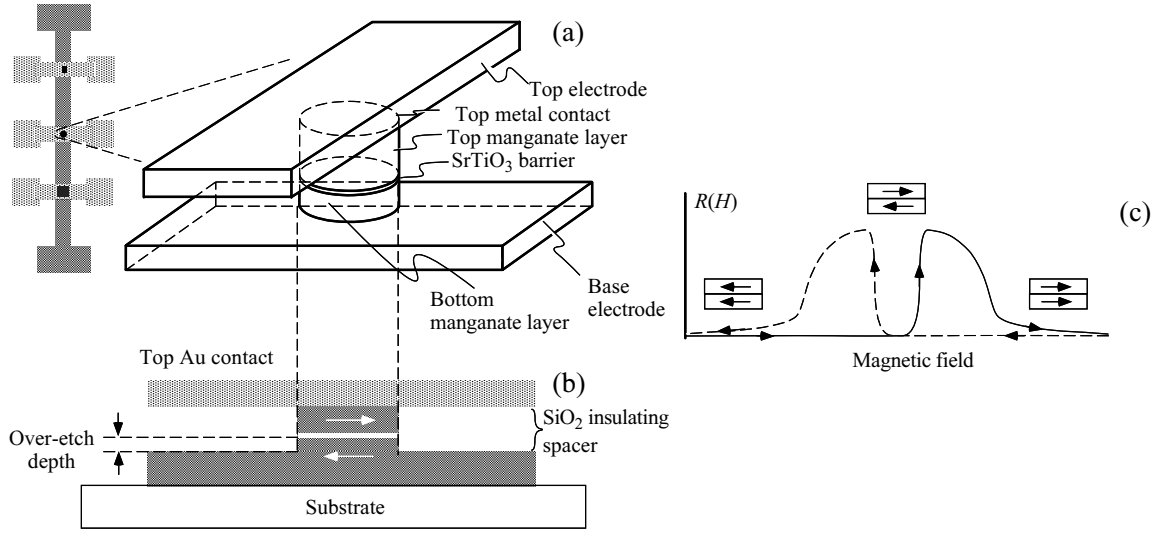


**Figure 30.** A schematic view of a LSMO/STO/LSMO trilayer thin film junction structure. (a) Left: top-view of the device; right: 3-dimensional illustration of the current-perpendicular pillar structure. (b): Side view of the structure, showing the over-etch steps which add additional magnetic coupling between the top and bottom ferromagnetic electrodes. (c) Schematic junction resistance as a function of sweeping magnetic field, showing the transitions from parallel to anti-parallel to parallel state of the magnetic moment alignments of the electrodes. Reproduced from Sun (1998).

sectional images obtained from LSMO/STO/LSMO trilayers indicate heteroepitaxial growth (Lu *et al* 1996). Typically, a self-aligned photolithographic process is employed to define the junctions. The trilayer structure is patterned using ion-beam milling to define the base electrode. After applying photoresist and developing, the top electrode is defined by ion-beam milling the top manganite layer; the ion milling is timed to stop at the bottom electrode. Next the junctions are coated with a SiO<sub>2</sub> film by sputtering. The photoresist left after the second ion-milling step is used as the lift-off stencil to open self-aligned contact holes to the top electrodes. Finally a Au or Cu metallization layer is deposited and patterned to make electrical contacts to the bottom and top electrodes.

A schematic view of a LSMO/STO/LSMO trilayer thin film junction structure is shown in figure 30. These structures show non-linear conductance curves; the non-linear conductance is often found to be quadratic in the bias voltage at low voltages which is taken as an indication of tunnelling as the main transport mechanism. However, more complex bias voltage dependences of the conductance have been reported that are not understood at present, see Sun (1998). Figure 31 shows (a) the magnetization hysteresis of a single LSMO layer indicating the coercive field and (b), (c) the resistance hysteresis at 4.2 K of two LSMO/STO/LSMO tunnelling junctions. Both junctions show typical TMR behaviour: a resistance maximum for antiparallel alignment of the electrode magnetizations and a nearly field independent resistance for parallel

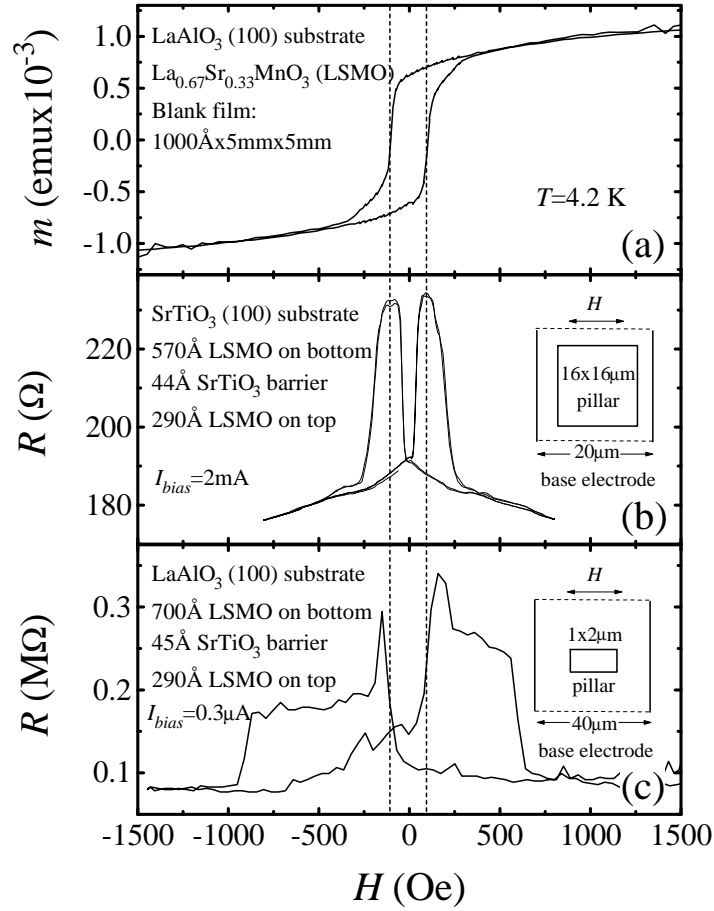


**Figure 31.** Comparing the  $R(H)$  curves of devices to magnetic hysteresis from a blank film. (a) Magnetic hysteresis loop of a blank film. (b)  $R(H)$  loop of a low resistance junction showing similar switching field as the blank film's coercive field  $H_c$ . (c) High resistance junction. The lower switching field corresponds well to the blank film's  $H_c$ , whereas the upper switching field is well above  $H_c$ , indicating an additional magnetic interaction present for magnetic states within the pillar. The insets in (b) and (c) show the geometry of the electrodes for the particular junctions and the relative field orientation in each case. Reproduced from Sun (1998).

alignment. The resistance hysteresis of the larger tunnelling junction in figure 31b is very similar to corresponding curves of conventional ferromagnetic tunnelling junctions. The smaller junction in figure 31c shows large noise, presumably due to complicated domain patterns in the ferromagnetic electrodes. The magnetoresistance of the junction in (c) reaches about 200%, whereas the larger junction in (b) has a magnetoresistance of only 20%. Very large values of 870% (Sun *et al* 1998) and 450% (Viret *et al* 1997a) have been reported at low temperatures. However, the junction characteristics are not reproducible.

Several groups have investigated the TMR ratio as a function of temperature. Lu *et al* (1996) reported a strong decrease of the magnetoresistance with temperature in LSMO/STO/LSMO junctions; the TMR ratio is found to vanish above about 200 K,

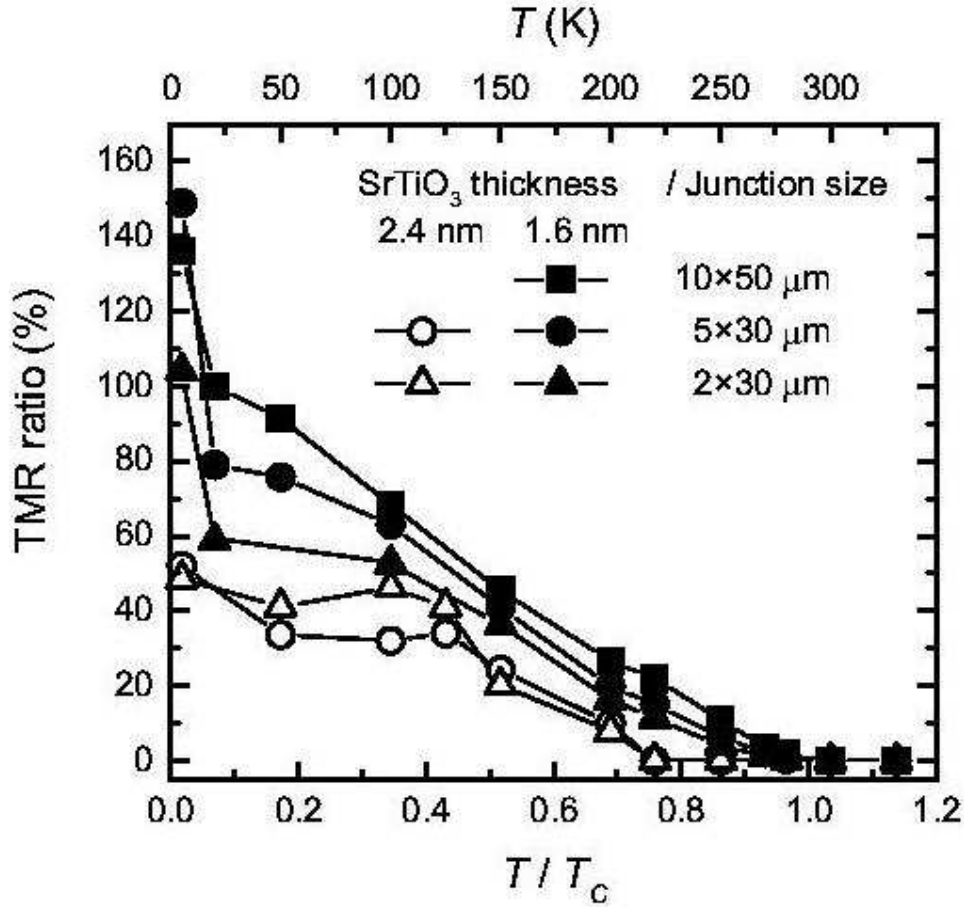


**Figure 32.** Temperature dependence of maximum TMR ratios for  $\text{La}_{0.8}\text{Sr}_{0.2}\text{MnO}_3/\text{SrTiO}_3/\text{La}_{0.8}\text{Sr}_{0.2}\text{MnO}_3$  junctions with different areas and  $\text{SrTiO}_3$  thicknesses. Reproduced from Obata *et al* (1999).

whereas the Curie temperature of the electrodes is much higher with  $T_C = 347$  K. Obata *et al* (1999) report TMR values extending up to the Curie temperature in LSMO/STO/LSMO junctions with very smooth interfaces and thin STO barriers with thickness of 1.6 nm, see figure 32. Yin *et al* (2000) obtained a similar result in LSMO/ $\text{La}_{0.85}\text{Sr}_{0.15}\text{MnO}_3$ /LSMO junctions. However, even in this case the TMR ratio decreases much faster with temperature than the bulk magnetization. This behaviour might not be surprising, since the spin-polarization is controlled by the interfacial magnetization that shows a much stronger decay with temperature than the bulk magnetization. Indeed, as discussed in section 6, measurements of the surface spin-polarization by Park *et al* (1998a) indicate that the surface spin-polarization is strongly reduced in comparison to the bulk magnetization in qualitative agreement with the tunnelling magnetoresistance. The strong temperature dependence, however, might to some extent still be of extrinsic origin related to non-stoichiometry of the interface region and interface roughness. Viret *et al* (1997a) observed a maximum in the tunnelling resistance for parallel magnetization at about 200 K. In view of the dependence of the Curie temperature on oxygen content, this might be interpreted as due to an oxygen

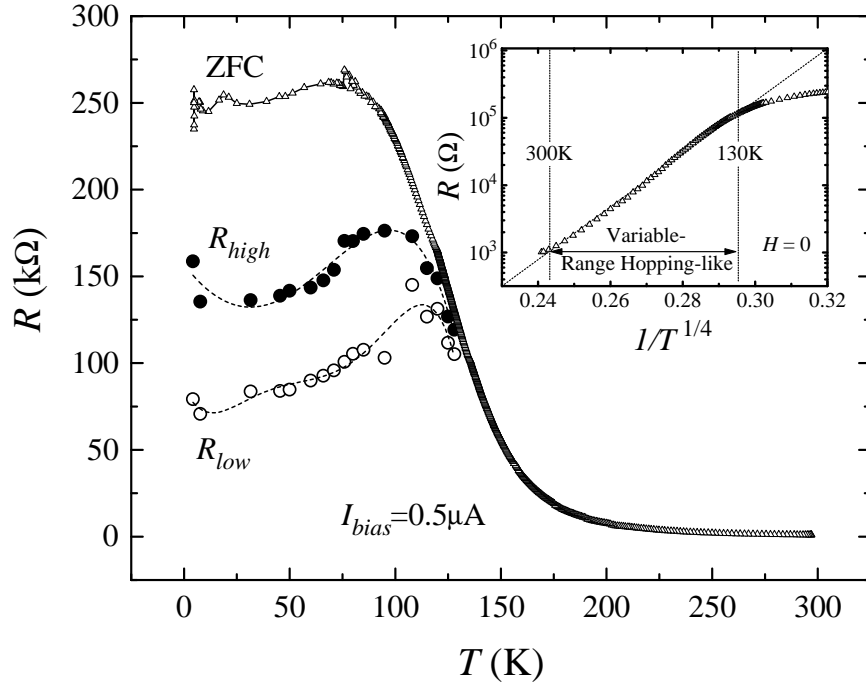


**Figure 33.** Temperature dependence of a LSMO/STO/LSMO junction. The initial zero-field-cooled trace of this junction gives a higher resistance value at low temperatures than observed in subsequent measurement cycles. Solid and open circles: Resistive-high and -low states as measured from individual  $R(H)$  loops. Inset: junction resistance plotted versus  $T^{-1/4}$  in order to show the variable range hopping in the high temperature region between 130 K and room temperature. Reproduced from Sun (1998).

deficient LSMO layer near the interface. This is corroborated by the results of Gilabert *et al* (2001) who observed a strong photoconductivity in a  $\text{La}_{0.81}\text{MnO}_3/\text{Al}_2\text{O}_3/\text{Nb}$  junction below 95 K. This finding was interpreted as arising from photoinduced charge-carrier generation in an oxygen-depleted region near the interface, thus effectively reducing the tunnelling barrier thickness. Sun *et al* (1997) found indications of variable range hopping in the junction resistance above about 130 K, where the TMR vanishes, see figure 33. This was interpreted as indicating a high defect density in the  $\text{SrTiO}_3$  barrier leading to defect-state mediated tunnelling through the barrier at higher temperatures. Fits of the Simmons model to the non-linear conductance yield small tunnelling barriers with values 0.5-0.7 eV (Sun *et al* 1997) and 0.1-0.2 eV (Obata *et al* 1999). These are much smaller than the  $\text{SrTiO}_3$  band gap of about 3 eV and also indicate the presence of defect states. Sun *et al* (1998) reported a zero bias dip in the conductance for temperatures below 130 K and bias voltages below 200 meV. Since this zero bias dip was also present in LSMO/ $\text{Al}_2\text{O}_3$ /permalloy junctions, it was related to the properties of the LSMO bottom electrode. Sun *et al* (1998) suggested this feature to arise from a Coulomb gap effect due to metallic inclusions of approximate size 1.5 nm at the interface. The nature of the metallic inclusions is unknown; it was speculated that these are related to the

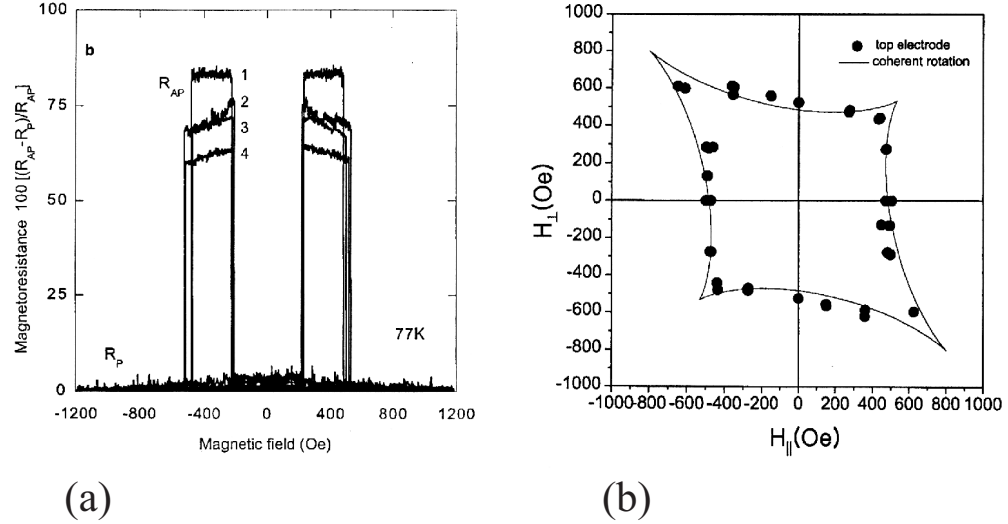


**Figure 34.** (a) Resistance of LCMO/NdGaO<sub>3</sub>/LCMO trilayer junctions at 77 K. Here the magnetoresistance is defined with respect to  $R_{\uparrow\downarrow}$ . The junctions show coherent sharp switching at well defined switching fields and a rather high magnetoresistance. This corresponds to a spin-polarization of 86%. Adapted from Moon-Ho Jo *et al* (2000a). (b) Switching field of a junction as shown in (a) plotted in the  $(H_{\parallel}, H_{\perp})$  plane.  $H_{\parallel}$  and  $H_{\perp}$  are the field components defined with respect to the magnetic easy axis. The solid lines show the result of a calculation within a single domain model with an anisotropy consisting of a twofold and a fourfold term; this is consistent with the observed angular dependence of the switching field. The agreement between calculation and measured values strongly suggests a coherent rotation mechanism. Adapted from Moon-Ho Jo *et al* (2000b).

localization length of the spin-polarized carriers. Moreover, the different switching fields of the electrodes are only induced by shape anisotropy. This might not be sufficient to guarantee the full development of the antiferromagnetic state at intermediate fields and might lead to a strong reduction of the magnetoresistance.

Moon-Ho Jo *et al* (2000a, 2000b) reported the fabrication of trilayer tunnelling junctions made from LCMO with NdGaO<sub>3</sub> as a tunnelling barrier. Due to the small lattice mismatch between LCMO and NdGaO<sub>3</sub> strain effects are minimized and these junctions show excellent reproducibility and very sharp resistance switching between bistable resistance states. Magnetoresistance curves are shown in figure 34(a). The magnetization reversal mechanism in the bottom and top electrodes was investigated by angular dependent magnetotransport measurements (Moon-Ho Jo *et al* 2000b). The bottom electrode shows a twofold symmetry consistent with magnetocrystalline anisotropy; the top electrode shows an additional fourfold contribution. The analysis of the reversal mechanism within Stoner-Wohlfarth single domain theory strongly indicates coherent magnetization reversal in the top electrode. This is illustrated in figure 34(b) showing the observed switching fields in the  $(H_{\parallel}, H_{\perp})$  plane compared to the calculation for coherent rotation. The agreement is remarkable. Thus one might assume that extrinsic effects such as incomplete magnetization reversal do not influence

the magnetotunnelling values obtained for these junctions. Indeed, Moon-Ho Jo *et al* observe a spin-polarization of 86% at 77 K (2000a) that is higher than the value measured directly by Andreev reflection (Soulen *et al* 1998). However, the effective spin-polarization in these junctions does also strongly decrease with temperature and was seen to vanish above 150 K. As in the data of Sun *et al* (1997) the junction resistivity indicates an activated non-tunnelling conductance. Moon-Ho Jo *et al* (2000a), however, argue that this is insufficient to explain the drastic decrease in tunnelling magnetoresistance above 120 K. They propose a model based on percolative phase separation at the interface: within this model the decrease of the spin-polarization is caused by the growth of paramagnetic regions nucleated near interface defects at the expense of ferromagnetic regions. This model is consistent with the mesoscopic results of Fäth *et al* (1999), see section 3.

Direct evidence for phase separation near  $\text{La}_{0.67}\text{Ca}_{0.33}\text{MnO}_3/\text{SrTiO}_3$  interfaces has been obtained from a NMR study as a function of thickness,  $6 \text{ nm} \leq t \leq 108 \text{ nm}$  of the manganite layer (Bibes *et al* 2001).  $^{55}\text{Mn}$  NMR spectra show the occurrence of two lines: a dominant line of mixed-valent character and a small contribution from  $\text{Mn}^{4+}$ . The NMR enhancement factors of both lines are large, thus indicating ferromagnetic states. These NMR signals are related to ferromagnetic metallic and ferromagnetic insulating regions. Since the  $\text{Mn}^{4+}$  line becomes more pronounced at small film thickness, the ferromagnetic insulating region is located near the interface. The total spectrum intensity normalized to the layer thickness decreases with decreasing film thickness; this indicates that some fraction of the sample is non-ferromagnetic and presumably insulating.

From this discussion it becomes clear that an understanding of manganite tunnelling junctions is far from complete. Calculations of the tunnelling conductance using the full manganite band structure might be of help. Experimentally the interface quality, the barrier material as well as the oxygenation state have to be improved. It might prove helpful to investigate junctions of mixed type with a well defined  $\text{Al}_2\text{O}_3$  barrier and a conventional ferromagnetic electrode of known properties.

Li *et al* (1998b) fabricated tunnelling junctions from heteroepitaxially grown  $\text{Fe}_3\text{O}_4/\text{MgO}/\text{Fe}_3\text{O}_4$  trilayers using a similar process as for the fabrication of manganite junctions. Since magnetite is believed to be a half-metallic ferrimagnet with a high Curie temperature, the junctions have potential to be used at room temperature. Different coercive fields were achieved by growing on a  $\text{CoCr}_2\text{O}_4$  buffer layer that yields a magnetically softer bottom electrode. At room temperature, however, the difference between the two coercivities becomes quite small. The tunnelling magnetoresistance is disappointingly small, see figure 35. At room temperature a magnetoresistance of about 0.5% increasing to 1.5% at 150 K was found. This is in agreement with results by van der Zaag (2000). Although a strong decay of the surface magnetization with temperature was found by Alvarado (1979) in magnetite crystals, this effect should not place a severe limit on the spin-polarization at 150 K or 300 K due to the high Curie temperature. At present, this small magnetoresistance in magnetite tunnelling junctions

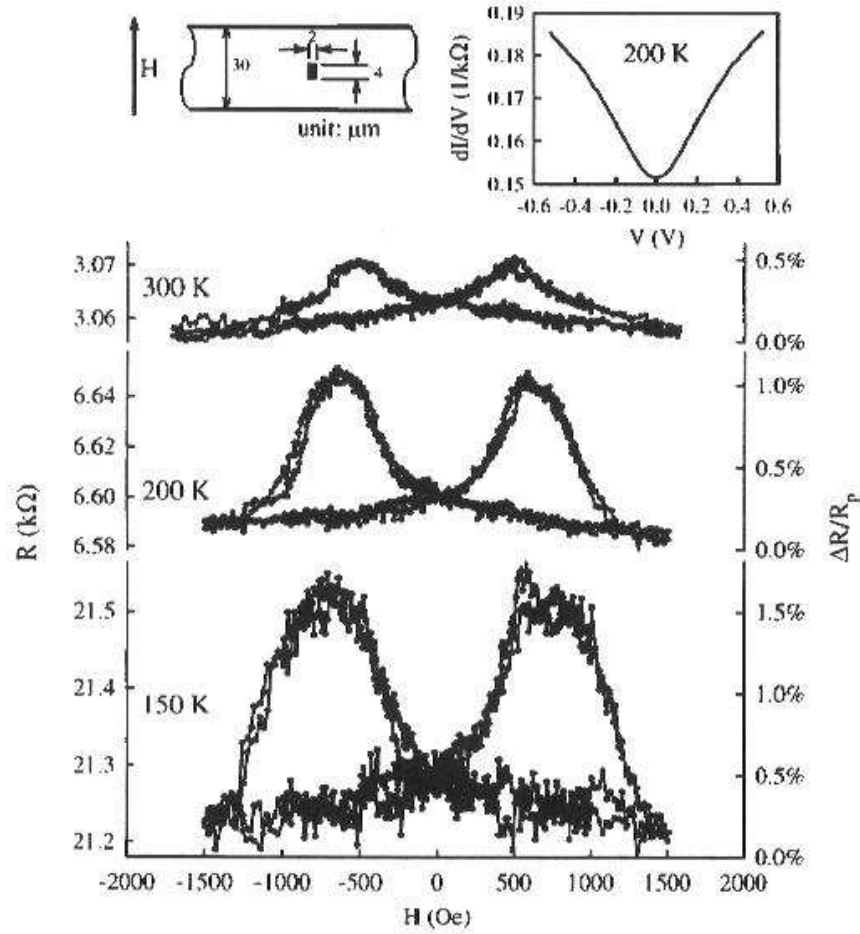


**Figure 35.** Resistance and magnetoresistance versus magnetic field at various temperatures for a  $\text{Fe}_3\text{O}_4/\text{MgO}/\text{Fe}_3\text{O}_4$  tunnelling junction with a rectangular  $2 \times 4 \mu\text{m}^2$  top electrode. The insets show the junction geometry and the dynamic conductance as function of bias voltage at 200 K. Reproduced from Li *et al* (1998b).

is not understood.

Barry *et al* (2001) studied a tunnelling junction fabricated from a  $\text{CrO}_2$  bottom electrode, a native oxide layer, probably composed of antiferromagnetic  $\text{Cr}_2\text{O}_3$ , and a Co top electrode. The current-voltage characteristics are non-linear and an analysis within Simmons' model yields a barrier thickness of about 2 nm and a barrier height of 0.76 eV. The tunnelling magnetoresistance is 1% at 77 K.

Ghosh *et al* (1998) investigated LSMO/STO/ $\text{Fe}_3\text{O}_4$  tunnelling junctions. A positive magnetoresistance was observed in large applied fields consistent with the opposite spin-polarization in the manganites and magnetite. However, the junction resistance did not show any apparent correlation with magnetic properties, especially the coercive fields. Therefore, the results on these junctions are at present not very well understood.

### 7.5. Barriers and band-structure

In the foregoing sections, it has been shown that Julliere's model provides a consistent description of spin-polarized tunnelling, if the spin-polarization as determined from ferromagnet-insulator-superconductor tunnelling is used. The meaning of these spin-polarization values, however, is somewhat unclear, since these contradict basic ideas on the band-structure of ferromagnetic metals. Indeed, the spin-polarization of Ni, Co and LSMO determined from tunnelling measurements into Al is *positive*, see table 1. For LSMO this result is expected, since in the simplest band picture only the majority  $e_g$  band lies at the Fermi level and the spin-polarization should be  $P = +1$ . In the case of the elemental ferromagnets, however, physical intuition leads one to expect a negative spin-polarization, since the minority density of states significantly exceeds the majority one. Gadzuk (1969) studied band-structure effects on the tunnelling electron distribution for non-magnetic metals. The band-structure was modelled as consisting of a wide, free-electron-like  $s$ -band with parabolic dispersion and a narrow tight-binding  $d$ -band with a linear  $k$ -dependence. Gadzuk (1969) found that the tunnelling probability of  $d$  electrons is drastically reduced compared to that of  $s$  electrons, i.e. "tight-binding electrons are not only tightly bound with respect to conduction processes but also with respect to tunneling." Similar methods were used to treat the spin-polarization of ferromagnetic metals observed in tunnelling (Hertz and Aoi 1973, Stearns 1977) and in field emission (Politzer and Cutler 1972, Chazalviel and Yafet 1977). Main conclusion from this theoretical work is that electrons from bands of low-effective mass contribute most to tunnelling. The spin-polarization of these  $s$  electrons is induced by the exchange splitting of the  $d$  bands through  $s - d$  hybridization and generally is of the opposite sign as the spin-polarization derived from band structure. Within a rigid Stoner band-model Stearns (1977) obtained a relationship between the spin-polarization and the magnetic moment of the conduction electrons  $\mu_c$ :

$$P = \mu_c f(\Delta/E_F), \quad (49)$$

where  $f(\Delta/E_F)$  denotes a slowly varying function of the ratio of band splitting  $\Delta$  and Fermi energy  $E_F$  with  $f(0) = 1/3$ . This expression is in agreement with the results of Paraskevopoulos *et al* (1977) and Meservey *et al* (1980). A second solution to explain the experimentally observed spin-polarizations was proposed by Fulde *et al* (1973). These authors studied the electronic structure of a Ni surface and found a spin-dependent surface resonance state in the ferromagnetic region. A majority spin resonance significantly changes the local surface density of states and might lead to a spin-polarization drastically different from the bulk value. The classical data of Meservey and Tedrow did not settle the controversy on the physical mechanisms underlying spin-polarized tunnelling, see discussion in Meservey *et al* (1980). Here recent work will be reviewed in more detail, since it makes essential contributions to the understanding of this problem.

When comparing data on ferromagnet-insulator-ferromagnet and ferromagnet-insulator-superconductor tunnelling, it is immediately clear that the choice of barrier is



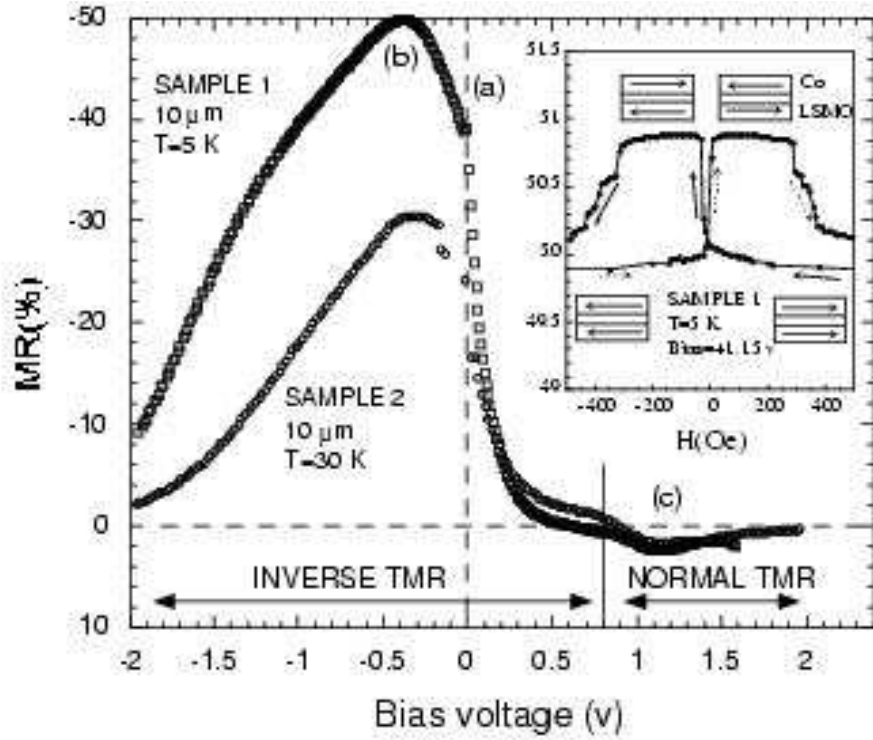


**Figure 36.** TMR ratio as a function of the applied dc bias for 10  $\mu\text{m}$  Co/SrTiO<sub>3</sub>/LSMO junctions. The inverse TMR is maximum at about  $-0.4$  V, and reaches  $-50\%$  and  $-30\%$  for samples 1 and 2, respectively. At positive bias the TMR decreases rapidly and a normal TMR of, respectively,  $1.5\%$  and  $1\%$  is measured at  $+1.15$  V for samples 1 and 2. The inset shows the normal TMR measured at 5 K on sample 1 for a positive bias of  $+1.15$  V. The different TMR values of the two samples are likely to be related to the LSMO/SrTiO<sub>3</sub> interface quality. Reproduced from de Teresa *et al* (1999a).

quite limited. Actually most of the experiments involving elemental ferromagnets have been performed with the use of Al<sub>2</sub>O<sub>3</sub> as a barrier, although some experiments with AlN (Plaskett *et al* 1997), GdO<sub>x</sub> (Nowak and Rauluszkiewicz 1992), NiO (Nowak and Rauluszkiewicz 1992), MgO (Platt *et al* 1997) and HfO<sub>2</sub> (Platt *et al* 1997) barriers have been reported. Among these Al<sub>2</sub>O<sub>3</sub> has proven to be the most successful barrier for spin-polarized tunnelling junctions. This might be attributed to the excellent wetting properties of Al and its ability to oxidize readily. The barrier material of choice when working with manganites is SrTiO<sub>3</sub>, although experiments with PrBa<sub>2</sub>Cu<sub>2.8</sub>Ga<sub>0.2</sub>O<sub>7</sub> and CeO<sub>2</sub> barriers have been reported (Viret *et al* 1999). Since a positive spin-polarization of LSMO in conjunction with a SrTiO<sub>3</sub> barrier is found in tunnelling experiments with an Al counterelectrode (Worledge and Geballe 2000) and is expected from band-structure, LSMO might be used as a spin-analyzer.

A convincing experiment demonstrating the influence of both barrier and band-structure on spin-polarized tunnelling was performed by de Teresa *et al* (1999a, 1999b). This group fabricated LSMO/SrTiO<sub>3</sub>/Co tunnelling junctions using a combined pulsed laser ablation/sputtering process and conventional UV lithography. The junctions

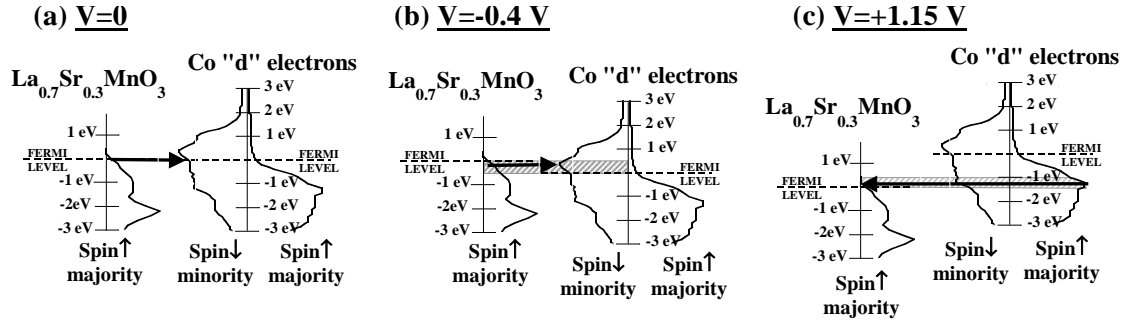


**Figure 37.** Relative positions of the  $d$ -band DOS in Co and LSMO for (a) a bias around zero, (b) a negative bias of  $-0.4$  V, and (c) a positive bias of  $+1.15$  V. In each case, arrows indicate the route of the higher tunnelling rate which occurs between majority states of LSMO and minority states of Co in the antiparallel configuration [(a),(b)] or between majority states of LSMO and majority states of Co in the parallel configuration (c). Reproduced from de Teresa *et al* (1999a).

showed a clear magnetotunnelling effect and, depending on the bias voltage, an inverse tunnelling magnetoresistance with the resistance lower in the antiparallel state was observed. Since LSMO has a positive spin-polarization, this clearly indicates a *negative* spin-polarization of the Co electrode in agreement with the band-structure. The bias dependence of the tunnelling magnetoresistance of this LSMO/SrTiO<sub>3</sub>/Co structure is shown in figure 36. For bias voltages between  $-2$  V and  $0.8$  V an inverse tunnelling magnetoresistance is seen with a broad maximum near  $-0.4$  V; above  $0.8$  V the magnetoresistance becomes normal. This behaviour can be understood considering the schematic density of states shown in figure 37. At zero bias, majority-spin electrons can tunnel from the LSMO electrode into the minority  $d$ -states of the Co electrode, when the magnetizations are antiparallel; this leads to an inverse tunnelling magnetoresistance. At a bias voltage of  $-0.4$  V tunnelling into the minority DOS peak of the Co electrode is possible and the TMR is maximum. On the other hand, at positive bias voltages the majority density of states in the Co electrode becomes slightly larger than the minority DOS and a small, but normal TMR is found. In this way, spin-polarized tunnelling provides a direct map of the spin-integrated band-structure of Co.

This experiment shows that Co has a negative spin-polarization when adjacent to a SrTiO<sub>3</sub> barrier, whereas the spin-polarization is positive when adjacent to a Al<sub>2</sub>O<sub>3</sub> barrier. In a related experiment, Sharma *et al* (1999) showed that permalloy (Ni<sub>80</sub>Fe<sub>20</sub>) has a positive spin-polarization when adjacent to Al<sub>2</sub>O<sub>3</sub> but a negative one when adjacent to Ta<sub>2</sub>O<sub>5</sub>. In this experiment tunnelling junctions were grown with two permalloy electrodes and a mixed Al<sub>2</sub>O<sub>3</sub>/Ta<sub>2</sub>O<sub>5</sub> barrier. If a positive bias was applied with respect to the Al<sub>2</sub>O<sub>3</sub> side of the barrier, a positive tunnelling magnetoresistance was observed, whereas an inverse TMR appeared when a negative bias was applied. This clearly shows that the apparent spin-polarization of permalloy depends on the barrier material.

An influence of the barrier was already predicted by Slonczewski within the free electron model, see equation (41). A more detailed model by Tsymbal and Pettifor (1997) considers the character of the metal-insulator bonding. Tsymbal and Pettifor (1997) calculate the tunnelling conductance within the ballistic regime using the Kubo formula and taking into account a realistic band-structure for the ferromagnetic electrodes (Co and Fe). In order to investigate the influence of the metal-insulator bonding, three models were investigated. In the first case only  $ss\sigma$  bonding was taken into account, whereas  $sp\sigma$  and  $sd\sigma$  bonding was considered in the second and third calculations. The  $ss\sigma$ ,  $sp\sigma$  and  $sd\sigma$  hopping integrals were chosen to be the same as for the bulk ferromagnet.

In the case of Co, the total density of states near the interface is asymmetric giving a much larger weight to the minority states, as expected. The conductance taking only  $ss\sigma$  bonding into account, however, is larger in the majority channel and leads to a positive spin-polarization of 34% in excellent agreement with measurements on Co/Al<sub>2</sub>O<sub>3</sub>. If  $sp\sigma$  coupling is switched on, the result remains unchanged. This change of sign in the spin-polarization is due to the fact that only  $s$ -electrons from the ferromagnet are coupled into the insulator such that the conductance is dominated by the  $s$ -electron partial DOS. The  $s$ -electron partial DOS, however, is reduced in the minority channel as compared to the majority channel as a consequence of the strong  $s$ - $d$  hybridization; the conductance is therefore quite similar to the  $s$ -electron partial DOS. When  $sd\sigma$  bonding is switched on,  $d$  electrons participate strongly in the tunnelling process and the spin-polarization is found to be negative,  $-11\%$ , as expected. In the case of Fe electrodes a similar picture is found with a spin-polarization of 45% in the case of  $ss\sigma$  bonding and of 8% in the case of combined  $ss\sigma$ ,  $sp\sigma$  and  $sd\sigma$  bonding. Again the calculated spin-polarization of 45% is in good agreement with measurements on Fe/Al<sub>2</sub>O<sub>3</sub>.

These calculations indicate that there is strong bonding between the Co  $d$ -orbitals and the Al  $sp$ -orbitals at a Co/Al<sub>2</sub>O<sub>3</sub> interface leading to a positive spin-polarization due to propagating  $s$ -electrons. In the case of a Co/SrTiO<sub>3</sub> interface, the bonding seems to be mainly of  $d$ - $d$  character between Co and Sr/Ti. Although these ideas give a qualitative explanation of the trends seen in the experiments, microscopic understanding can only be achieved through detailed calculations in comparison to investigations of the respective interfaces. The dependence of spin-polarized tunnelling on the barrier material presents an additional degree of freedom to the physicist and requires numerical techniques for a controlled engineering.

Seneor *et al* (1999) reported magnetotunneling measurements on Co/Al<sub>2</sub>O<sub>3</sub>/Fe<sub>3</sub>O<sub>4</sub> junctions at 4.2 K. Here a sharp gap in the magnetoresistance was seen below a bias voltage of 10 meV. This might be related to a gap in the magnetite band-structure due to correlation effects in the charge-ordered state. The spin-polarization observed in this experiment and in the Fe<sub>3</sub>O<sub>4</sub>/MgO/Fe<sub>3</sub>O<sub>4</sub> tunnelling junctions of Li *et al* (1998b) was much smaller than the predicted full spin-polarization. Srinitiwara Wong and Gehring (2001) suggested that this might be a feature of the more than half-filled band structure. Since the dwell time of an electron on a Fe<sup>2+</sup> ion is comparatively

long, the wave function relaxes to an atomic state wave function. An electron tunnelling from such an ion is described by the angular momentum coupling relation  $|2; 2\rangle = \sqrt{5/6}|5/2; 5/2 \downarrow\rangle - \sqrt{1/6}|5/2; 3/2 \uparrow\rangle$ ; it follows that the spin-polarization of this slow process is  $P = (\sqrt{5/6})^2 - (\sqrt{1/6})^2 = 2/3$ . Srinitiwara Wong and Gehring (2001) further calculated the tunnelling probabilities between  $\text{Fe}^{2+}$  and  $\text{Fe}^{3+}$  ions as a function of the magnetic quantum number.

### 7.6. Current-induced switching of the magnetization

Recent interest has focused on switching of magnetic nanoparticles or thin magnetic layers by a spin-polarized current. This concept was originally proposed by Slonczewski (1996). Although the theoretical description is not settled yet (Bazaliy *et al* 1998, Sun 2000, Heide *et al* 2001), convincing evidence of current-driven magnetization switching has been presented for the switching of thin Co layers in Co/Cu/Co-pillars (Katine *et al* 2000, Albert *et al* 2000, Grollier *et al* 2001). Here the work of Sun (1999) on the switching of magnetic nanoparticles in manganite trilayer junctions is reviewed, which was the first report on the occurrence of current-induced magnetic switching and is the only report of this phenomenon in oxide magnets. The interpretation of the data follows the model of Slonczewski (1996).

Figure 38(a) shows the principal design of such a switching experiment. A ferromagnetic nanoparticle, here approximated by a cubic Stoner-Wohlfarth particle of side length  $a$ , has a magnetization  $\vec{M}$ ,  $|\vec{M}| = M_S$ , making an angle  $\theta$  with the z-axis. A spin-polarized electric current  $\vec{J}$  flows through the nanoparticle; the spin-current density  $\vec{S}$  makes an angle  $\phi$  with the z-axis. For a spin-polarization  $P$  the spin-current density is given by  $S = (\hbar/2e)PJ$ . Within a spin-diffusion length  $\lambda_s$  the direction of the spin-current relaxes towards  $\vec{M}$ . The angular momentum is transferred to the particle's magnetization which induces a torque density on the magnetization of magnitude (Sun 1999)

$$\vec{\tau}_s = \vec{M} \times (\vec{S} \times \vec{M}) / \lambda_s M_S^2. \quad (50)$$

If for simplicity one assumes uniaxial anisotropy with an anisotropy constant  $K_u$  and an easy axis along  $\hat{z}$  and if a magnetic field  $\vec{H}$  is applied along  $\hat{z}$ , one obtains a second torque density

$$\vec{\tau}_a = \mu_0(H_A \cos(\theta) + H)\vec{M} \times \hat{z}, \quad (51)$$

with the anisotropy field  $H_A = 2K_u/M$ . The dynamic evolution of the magnetization is governed by the Landau-Lifshitz-Gilbert equation:

$$\frac{d\vec{M}}{dt} = \gamma(\vec{\tau}_1 + \vec{\tau}_2) - (\alpha/M_S)\vec{M} \times \frac{d\vec{M}}{dt} \quad (52)$$

with gyromagnetic ratio  $\gamma$  and damping parameter  $\alpha$ .

If the spin-current density exceeds a critical value, the magnetization might be flipped. The critical current is given by (Sun 1999)

$$I_c = \frac{2e\alpha}{P\hbar} \frac{a^2 \lambda_s M H_A}{|\cos(\phi)|} \left[ 1 + \frac{H}{H_A} \right]. \quad (53)$$

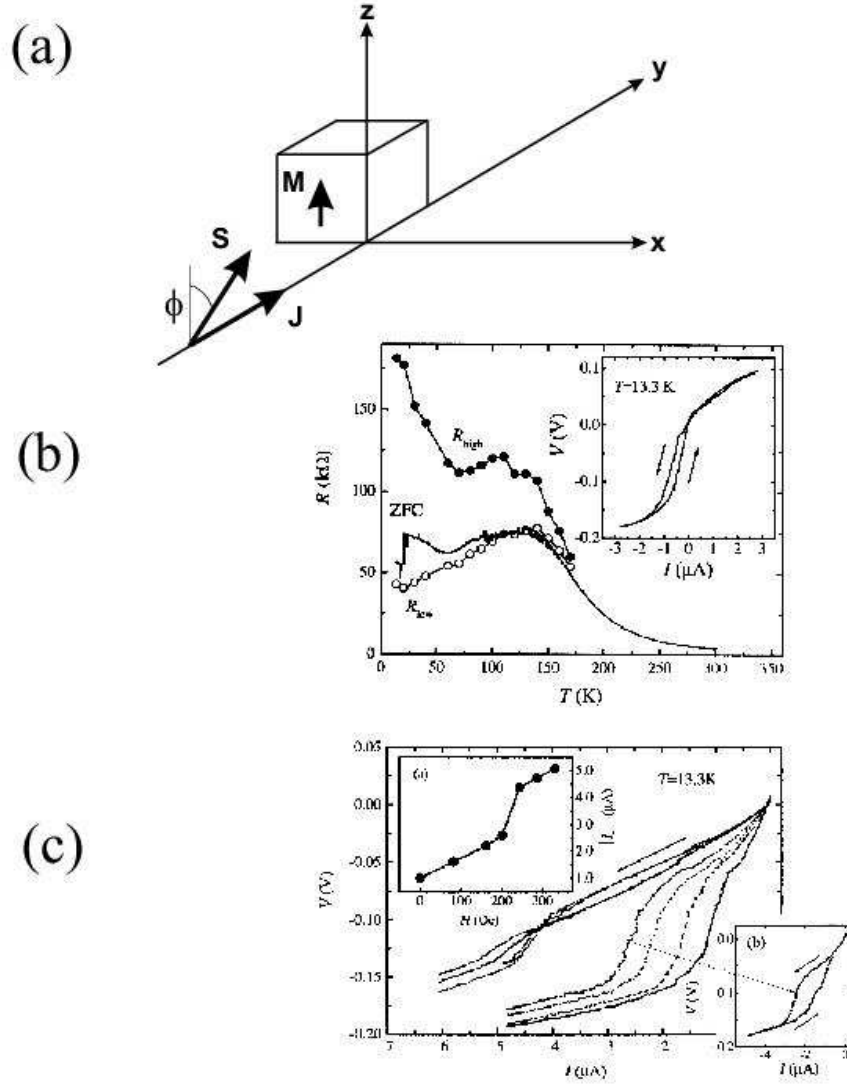


**Figure 38.** (a) Schematic setup of a current-driven switching experiment. An electric current  $\vec{J}$  is injected into a ferromagnetic nanoparticle, here modelled as a cubic Stoner-Wohlfarth particle with magnetization  $\vec{M}$ . The injected spin-current density  $\vec{S}$  is oriented under an angle  $\phi$  with respect to the z-axis. (b) Temperature dependence of a manganite trilayer junction in the zero field cooled (ZFC), resistance low (parallel electrode magnetization) and resistance high state. The inset shows a current-voltage characteristic measured at 13.3 K in zero field. A hysteretic jump near  $I_c \sim -1 \mu\text{A}$  is clearly visible. (c) Current-voltage characteristics taken on the same sample at 13.3 K in various applied fields. As shown in the right inset these characteristics are hysteretic; for clarity only curves taken for one sweep direction are shown in the main panel. The left inset shows the critical current as a function of the applied field. At about 200 K one of the electrodes switches and induces a step in the  $I_c(H)$  curve. (b) and (c) after Sun (1999).

Assuming the nanoparticle to be superparamagnetic, the anisotropy energy can be related to the blocking temperature  $T_B$  via  $a^2 \lambda_s M H_A \simeq 40 T_B$ . Thus the theory yields two predictions: (1) the magnitude of the critical current is determined by the blocking temperature and (2) the critical current is proportional to the applied field.

The experiment uses manganite trilayer junctions as already discussed in section 7.4. Since these junctions were grown by laser ablation, there is a certain number of particulates distributed between the electrodes. Typical areal densities are  $10^6 \text{ cm}^{-2}$  for particles larger than 100 nm and  $10^8 - 10^9 \text{ cm}^{-2}$  for small particles in the range 10–50 nm. These particles form grain boundaries of low conductivity and weak magnetic coupling, see next section, with the electrodes. Accordingly, bottom and top electrode will be connected by some particles; the local current density at these shunts is likely to be high.

Detailed magnetotransport measurements of trilayer junctions revealed three distinctive features shown in figures 38(b) and (c): (1) the resistance after zero field cooling as well as in the high resistance state shows a minimum around 60 K. This is identified with the blocking temperature  $T_B$  of the particulates in the film. (2) Current-voltage characteristics are asymmetric and show a hysteretic step-like feature. This is related to switching of a magnetic nanoparticle in the barrier. The critical current is defined at the location of the step. (3) If a magnetic field is applied parallel to the trilayer junction, this critical current increases linearly with field below  $H < 200 \text{ Oe}$ . Above this field one of the electrodes switches influencing the magnetic coupling between the nanoparticle and the electrodes and yielding a step in the  $I_c(H)$  curve. From the blocking temperature a typical particle dimension of 17 nm was estimated which is reasonable. The anisotropy field  $H_A \simeq 120 \text{ Oe}$  was determined from the field dependence of the critical current. With  $P = 1$ , the damping coefficient can be estimated to  $\alpha \simeq 0.01$  in agreement with measurements (Lofland *et al* 1995).

### 7.7. Intrinsic tunnelling in layered manganites

The resistivity and magnetoresistance of  $\text{La}_{2-2x}\text{Sr}_{1+2x}\text{Mn}_2\text{O}_7$  single crystals for the dopings  $x = 0.3$  and  $x = 0.4$  were found to differ significantly (Moritomo *et al* 1996, Kimura *et al* 1996). Whereas crystals for both dopings showed a large resistivity anisotropy, the magnetoresistance in the ordered phase was found to be isotropic for  $x = 0.4$ , but strongly anisotropic for  $x = 0.3$ . The ordering temperatures are 90 K ( $x = 0.3$ ) and 121 K ( $x = 0.3$ ), respectively. The resistivity along the c-axis displays insulating behaviour above the magnetic ordering temperature. Perring *et al* (1998) performed a neutron scattering study on single crystals with dopings  $x = 0.3, 0.4$  in order to determine the magnetic structure. Whereas the  $x = 0.4$  compound appears to be ferromagnetically ordered below 121 K, the  $x = 0.3$  compound was found to order ferromagnetically in the ab-planes with these ferromagnetic sheets stacked antiferromagnetically along the c-axis. A magnetic field of 1.5 T applied parallel to the ab-planes was found to switch the magnetic order from antiferromagnetic to ferromagnetic. Simultaneous measurements of the antiferromagnetic superstructure peaks and the c-axis magnetoresistance revealed a similar field dependence; the magnetoresistance saturates, when the antiferromagnetic order is destroyed, see figure 39. Perring *et al* (1998) argued that the semiconducting behaviour of the c-

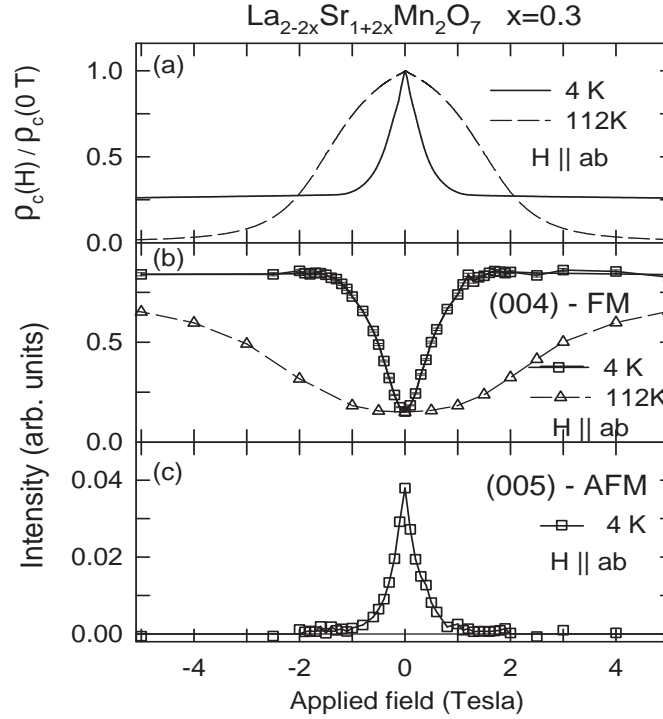


**Figure 39.** (a) Field-dependent switching of the resistivity, (b) ferromagnetic, and (c) antiferromagnetic Bragg intensities in the tunnelling ( $T = 4$  K) and colossal ( $T = 112$  K) magnetoresistance regimes. The simultaneous disappearance of the antiferromagnetic superstructure peaks (see (c)) and the saturation of the magnetoresistance (see (a)) was interpreted as arising from intrinsic spin-polarized tunnelling between ferromagnetically ordered sheets. Reproduced from Perring *et al* (1998).

axis resistivity above the magnetic ordering temperature indicates the insulating nature of the  $(\text{La}, \text{Sr})_2\text{O}_2$  spacing layers. The  $\text{MnO}$  layers are metallic ferromagnets due to the double-exchange interaction. Accordingly, the layered manganites can be viewed as an intrinsic stack of tunnelling junctions such as  $\text{Bi}_2\text{Sr}_2\text{CaCu}_2\text{O}_8$  single crystals are stacks of intrinsic Joesphson junctions. At 4 K a magnetoresistance  $\Delta R/R = 300\%$  is measured, see figure 39. Neglecting shunting currents, the spin-polarization can be calculated from the magnetoresistance ratio within Julliere's model, equation (38), yielding  $P = 0.77$ .

## 8. Grain-boundary junctions

As already discussed in section 3, the double exchange mechanism is extraordinarily sensitive to distortions of the  $\text{Mn-O-Mn}$  bond. This leads to the formation of insulating regions in the strain fields of extended defects such as grain boundaries. Therefore, polycrystalline manganite samples do actually behave as granular metals, although the variation in stoichiometry across grain boundaries is likely to be negligible. An unexpectedly large low field magnetoresistance was discovered in polycrystalline manganite bulk and thin film samples (Hwang *et al* 1996, Gupta *et al* 1996). This

finding initiated numerous studies on extrinsic magnetoresistance effects in magnetic oxides; investigations were extended to other systems such as  $\text{CrO}_2$ ,  $\text{Tl}_2\text{Mn}_2\text{O}_7$ , the double perovskite  $\text{Sr}_2\text{MoFeO}_6$  as well as  $\text{SrRuO}_3$ . The characteristics of the extrinsic magnetoresistance in these materials will be compared at the end of this section. The bulk of the experimental data, however, is related to the manganites.

### 8.1. Basic theory: granular metals

With few exceptions, models for grain-boundary magnetoresistance are based on spin-polarized tunnelling.<sup>§</sup> This implies that the grain boundary strongly hinders charge transport leading to the formation of an insulating region; simultaneously the adjacent grains are only weakly magnetically coupled across this interfacial region. Thus, polycrystalline manganite samples are similar to granular ferromagnetic metals; at this point a brief review of the properties of granular metals seems appropriate.

A typical granular metal consists of small grains surrounded by insulating material. Usually the values of both grain diameter  $d$  as well as grain separation  $s$  follow a broad distribution. Carrier transport involves charging of grains that costs a charging energy  $E_c = e^2/(4\pi\epsilon_0 d)F(s/d)$ , where  $\epsilon_0$  denotes the vacuum permittivity and the function  $F(s/d)$  depends on grain shape. The conductivity is proportional to the tunnelling matrix element  $\exp[-2\chi s]$  with  $\chi = (2m\Phi/\hbar^2)^{1/2}$  (Simmons 1963) and the population of a single grain  $\exp[-E_c/2k_B T]$ ; these terms determine the essential temperature dependence of the conductivity.

$$\sigma \propto \exp[-2\chi s - E_c/(2k_B T)] \quad (54)$$

$\Phi$  denotes the barrier height and  $m$  the effective mass. In order to obtain the conductivity, this expression has to be averaged over the distributions for grain diameter and separation.

Granular metals are often fabricated by a co-deposition process of a metal and a dielectric, e.g. the co-sputtering of Ni, Co, Fe and  $\text{SiO}_2$  (Gittleman *et al* 1972, Barzilai *et al* 1981, Honda *et al* 1997). In this case the metal grains are formed by diffusion of metal atoms or clusters and, for a given composition, there exists a definite relationship between grain diameter  $d$  and grain separation  $s$  such that  $s/d$  is constant (Sheng *et al* 1973). Therefore,  $sE_c$  is a constant:  $s\chi E_c = C$ . Under this constraint the averaging of the conductivity can be easily carried out. Tunnelling occurs mainly between grains with an optimum charging energy  $E_c^0 = 2(C/k_B T)^{1/2}$  such that the conductivity in equation (54) is maximized (Sheng *et al* 1973). This results in a typical temperature dependence of the conductivity given by

$$\sigma \propto \exp[-2(C/k_B T)^{1/2}] \quad (55)$$

<sup>§</sup> A notable exception is the model of Evetts *et al* (1998) that relates the grain-boundary magnetoresistance to a magnetization enhancement in the grain-boundary region induced by the alignment of the adjacent, magnetically soft grains.



Whereas this model for the temperature dependence of the conductivity is broadly accepted, the theoretical situation for the magnetotransport properties of granular metals is less clear. In a pioneering work Helman and Abeles (1976) proposed a model for the magnetoconductivity. They assumed the existence of a magnetic energy term  $E_M$  such that the hopping probability of a charge carrier from a grain is reduced (enhanced) if its spin is parallel (antiparallel) to the grain magnetization:

$$\sigma \propto \exp(-2\chi s) \left\{ \frac{1}{2}(1 + P) \exp[-(E_c + E_M)/(2k_B T)] + \frac{1}{2}(1 - P) \exp[-(E_c - E_M)/(2k_B T)] \right\} \quad (56)$$

The magnetic energy term is expressed in terms of the spin correlation function of neighbouring grains:  $E_M = J[1 - \langle \vec{S}_1 \cdot \vec{S}_2 \rangle / S^2] / 2$ ;  $J$  denotes the exchange coupling constant. In a linear approximation the magnetoresistance is given by

$$\Delta\rho/\rho_0 = -\frac{JP}{4k_B T} \frac{[M^2(H) - M^2(0)]}{M_S^2} \quad (57)$$

with the magnetization  $M(H)$  and the saturation magnetization  $M_S$ . This expression yields semiquantitative agreement with experimental data on Co-SiO<sub>2</sub> and Ni-SiO<sub>2</sub> granular metals at temperatures above 50 K; especially the ferromagnetic to superparamagnetic transition can be successfully modelled (Helman and Abeles 1976, Barzilai *et al* 1981). It is surprising, however, that the spin polarization  $P$  appears linearly in the expression for the magnetoresistance. Thus, the magnetoresistance should be positive for Fe and negative for Ni grains which is not seen experimentally. There seems to be some inconsistency in the work of Helman and Abeles (1976) in that it relates the spin dependence of the hopping probability to one grain, whereas the magnetic energy is an intergrain property. This issue is somehow resolved by Wagner *et al* (1998) within a different context, namely hopping between spin polarons in single crystalline material. If the existence of a magnetic energy term  $E_M = (J/2)[1 - \vec{S}_1 \cdot \vec{S}_2 / S^2]$  is accepted, the conductivity is given by  $\sigma \propto \exp[-2\chi s - (E_c + E_M)/(k_B T)]$  and the magnetoresistance by  $\Delta\rho/\rho_0 = -[1 - \exp[-J(M/M_S)^2/2k_B T]]$ . It is reasonable that two mechanisms contribute to the conductivity, namely tunnelling through the barrier and thermal hopping over the barrier; these lead to two contributions to the magnetoresistance, a temperature independent one due to tunnelling and a temperature dependent one due to hopping. A systematic investigation of these effects, however, has not yet been carried out.

Data on the magnetoresistance of granular metals, see e.g. Mitani *et al* (1997), Honda *et al* (1997), show that the magnetoresistance in granular metals is often independent of or weakly dependent on temperature. This lead Inoue and Maekawa (1996) to contest equation (57) and propose another mechanism for the magnetoresistance in granular materials. Since the tunnelling probability depends on the relative directions of the grain magnetizations, see equation (40), the field dependence of the conductivity arises mainly from the pre-exponential factor,  $\sigma \propto (1 +$

$P^2 \cos(\Theta)) \exp(-2\chi s)$ . Averaging over  $\Theta$  and the grain separation  $s$  yields a temperature dependence of the conductivity as in equation (55) and a magnetoconductivity

$$\left\langle \frac{\Delta G}{G} \right\rangle = \left\langle 1 - \frac{G(\Theta)}{G_{\uparrow\uparrow}} \right\rangle = \frac{m^2 P^2}{1 + m^2 P^2} \quad (58)$$

with  $m = M(H)/M_S$ .  $\langle \dots \rangle$  denotes the angular average. At saturation this is just half of the magnetoconductivity of a single ferromagnetic tunnelling junction. Coey *et al* (1998b) suggested to replace the factor  $(1 - P^2)/(1 + P^2)$  by  $2S/(2S + 1)^2$  where  $S$  denotes the core spin.

The model of Inoue and Maekawa was refined by Mitani *et al* (1998a) by taking into account co-tunnelling processes between large and small grains. These authors consider the simultaneous tunnelling of charge carriers from a large grain with charging energy  $E_c/n$  via  $n$  small grains with charging energy  $E_c$  to another large grain. In this case the conductivity is given as a sum over all these higher order processes:

$$\sigma \propto \sum_{n=1}^{\infty} \exp \left[ -\frac{E_c}{2n k_B T} \right] [(1 + P^2 m^2) \exp[-2\chi s]]^n f(n) \quad (59)$$

The function  $f(n)$  includes the influence of a distribution of conduction paths as well as temperature. The exponential in the sum is strongly peaked as a function of the order number  $n$ . Following an analysis similar to that above, the conductivity is found to be of a form

$$\sigma \propto (1 + P^2 m^2)^{n^*+1} \exp \left[ -2\sqrt{\frac{2\chi s E_c}{k_B T}} \right] \quad (60)$$

with  $n^* = (E_c/8\chi s k_B T)^{1/2}$ . The magnetoresistance is found to be

$$\frac{\Delta \rho}{\rho_0} = (1 + P^2 m^2)^{-(n^*+1)} - 1 \simeq -P^2 m^2 \left[ 1 + \sqrt{\frac{E_c}{8\chi s k_B T}} \right], \quad (61)$$

where the last approximation is valid for  $P^2 \ll 1$ . In conclusion, higher order tunnelling processes become important at low temperatures and lead to a gradual increase of the magnetoresistance. This is in agreement with experiments on granular CoAlO films (Mitani *et al* 1998a).

Equation (58) was derived under the assumption that the grains within a specific percolation path are connected in parallel. In reality a granular material is a complicated conduction network. In the case of a narrow distribution of grain separations as it might occur in polycrystalline films with tunnelling barriers defined by grain boundaries, a multitude of conduction paths contribute to the global resistance. This can be approximated by a resistor network. As an illustration the magnetoresistance of a one-dimensional array of resistors connected in series is calculated here. Assuming a random distribution of grain magnetization at zero field and a resistance  $R = 1/(G_0(1 + P^2 \cos(\Theta)))$  the following magnetoresistance is obtained:

$$\left\langle \frac{\Delta R}{R_0} \right\rangle = \left\langle \frac{R(\Theta) - R_{\uparrow\uparrow}}{R(\Theta)} \right\rangle = 1 - \frac{P^2}{(1 + P^2) \operatorname{atanh}(P^2)}. \quad (62)$$

For spin-polarizations  $P > 0.5$  this result differs significantly from equation (58) and demonstrates the influence of the conduction network. Therefore, care has to be taken, whenever spin polarization values are derived from measurements on granular samples.

The dynamic conductance has already been discussed in section 7.1. The mechanisms listed there, most importantly bulk and interface magnon scattering, also contribute to the tunnelling processes in grain-boundary junctions. However, it has been experimentally found that often inelastic tunnelling processes are observed in grain-boundary junctions. Inelastic tunnelling through a barrier with a constant density of states was investigated by Glazman and Matveev (1988). They calculated the contributions to the conductance from tunnelling via  $n$  impurities; these are generally bias dependent and proportional to  $V^{n-2/(n+1)}$ .

## 8.2. Experimental data on grain-boundary junctions

Various grain-boundary systems such as polycrystalline samples, pressed powders, bi-crystal junctions, step-edge junctions and laser-patterned junctions have been investigated. The main experimental data are summarized in this section.

*8.2.1. Are polycrystalline manganite samples classical granular metals?* Typical polycrystalline manganite samples have grain sizes in the range 100 nm...10  $\mu$ m being too large for charging effects to dominate. Therefore, the temperature dependence of the resistivity does not follow equation (55), but is rather determined by the specific transport mechanisms in the barrier. Moreover, the grains are coupled ferromagnetically.

A systematic study of the magnetotransport and magnetic properties of  $\text{La}_{2/3}\text{Sr}_{1/3}\text{MnO}_3$  ceramics was reported by Balcells *et al* (2000). At small grain sizes below about 40 nm charging effects become significant. The charging energy was found to be reciprocal to the grain diameter as expected. This regime can be understood using the theory of granular metals as outlined above. The intergranular magnetoresistance to be discussed in the following sections involves effects beyond this classical model; within the discussion a theoretical description will evolve.

*8.2.2. Polycrystalline materials.* The effects of grain boundaries on the resistivity and magnetoresistance of polycrystalline manganite compounds were reported very early (Volger 1953, van den Brom and Volger 1967). The recent research was initiated by the work of Hwang *et al* (1996) and Gupta *et al* (1996). These authors compared the magnetoresistance and magnetization of  $\text{La}_{0.67}\text{Sr}_{0.33}\text{MnO}_3$  single crystals and polycrystalline ceramics (Hwang *et al* 1996) and  $\text{La}_{0.67}\text{Ca}_{0.33}\text{MnO}_3$  and  $\text{La}_{0.67}\text{Sr}_{0.33}\text{MnO}_3$  epitaxial and polycrystalline films (Gupta *et al* 1996), respectively. Both investigations found that the resistivity and magnetoresistance depended sensitively on the microstructure, whereas the magnetization was hardly affected by it.

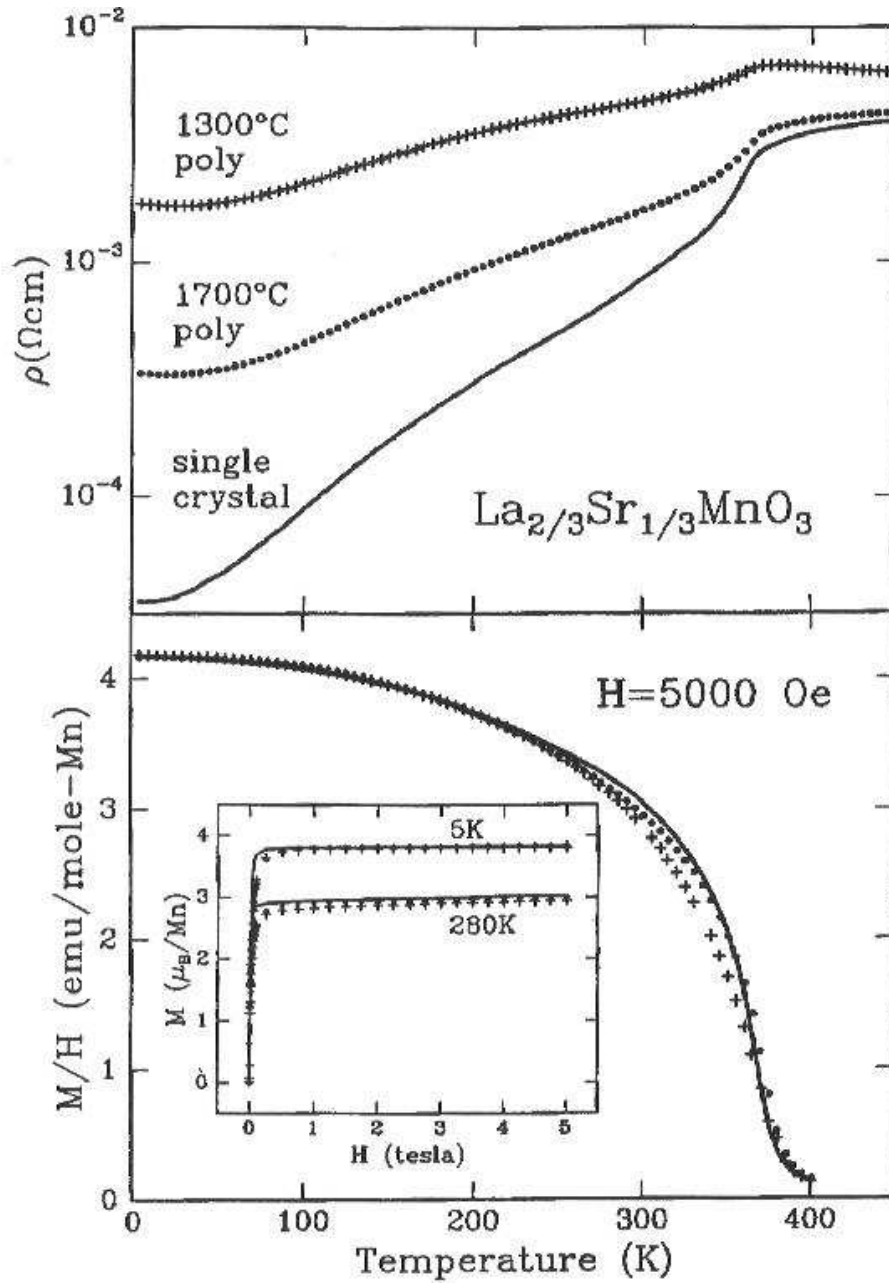


**Figure 40.** Top panel: zero field resistivity of  $\text{La}_{0.67}\text{Sr}_{0.33}\text{MnO}_3$  single crystal and polycrystals as a function of temperature. Bottom panel: magnetization of the samples as a function of temperature measured at  $B = 0.5$  T. The inset shows the field dependent magnetization at 5 K and 280 K. Reproduced from Hwang *et al* (1996).

Hwang *et al* (1996) investigated a LSMO single crystal and two LSMO ceramic samples sintered at 1300°C and 1700°C, respectively. The sample sintered at the higher temperature had the larger grain size. The data of Hwang *et al* (1996) are reproduced in figures 40 and 41. Figure 40 shows the zero field resistivity and the magnetization of the samples as a function of temperature. Whereas the low temperature resistivity depends strongly on the microstructure, the magnetization of the three samples is virtually

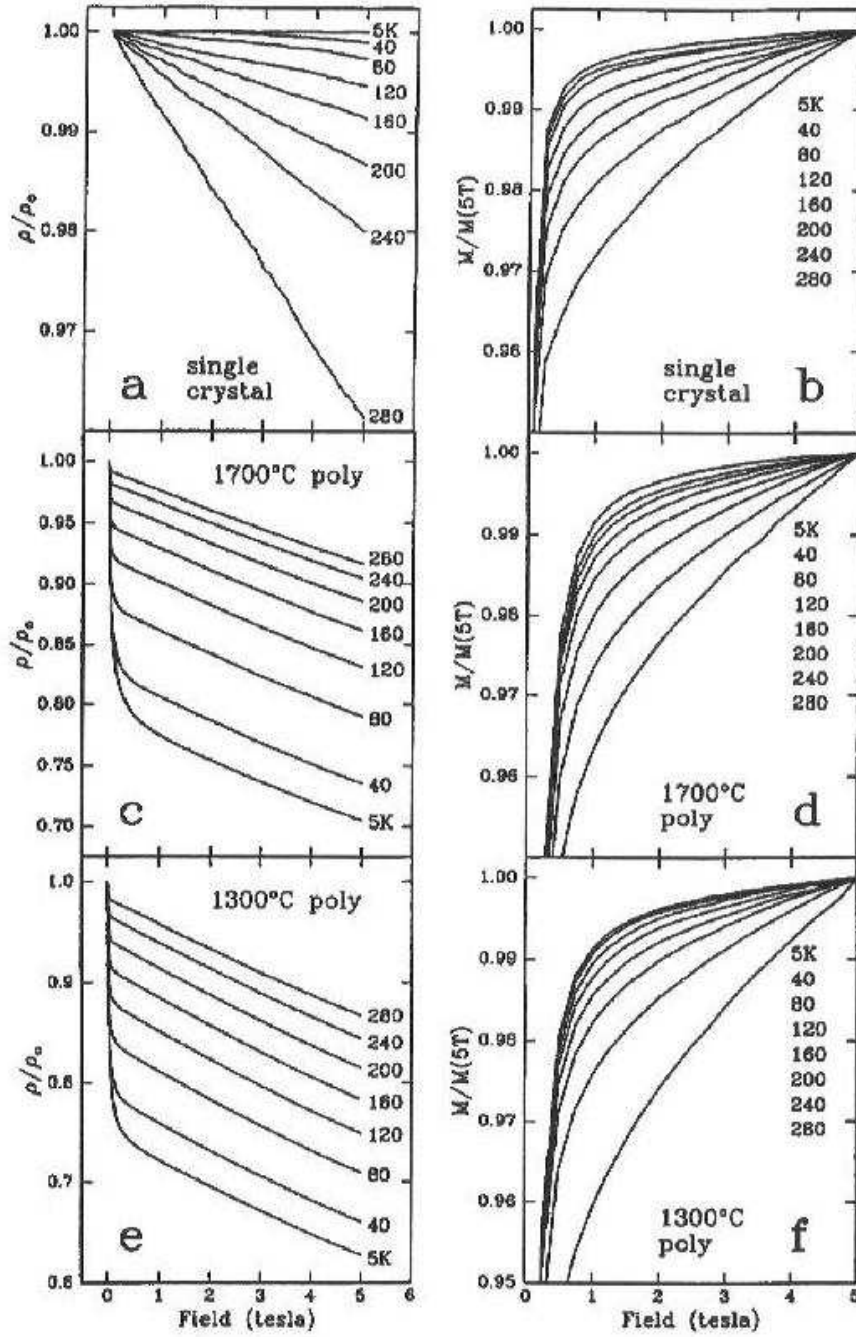


**Figure 41.** Magnetoresistance data of the samples of figure 40. Panels a, c and e: normalized resistivity  $\rho/\rho_0$  as a function of magnetic field.  $\rho_0$  denotes the zero field resistivity. Panels b, d and f: magnetic field dependence of the normalized magnetization. Reproduced from Hwang *et al* 1996.

identical. The effect of the grain boundaries on the magnetoresistance is even more dramatic. Figure 41 shows the field dependent resistivity and magnetization of the samples investigated. Whereas the single crystal shows a magnetoresistance linear in magnetic field, the polycrystalline samples show a sharp drop at low magnetic fields followed by a linear dependence at higher fields. Again the field dependence of the

magnetization is virtually identical for the three samples. The magnitude of the low field magnetoresistance increases with decreasing temperature in contrast to the intrinsic magnetoresistance that has a maximum near the Curie temperature and decreases with decreasing temperature.

These results cannot be explained by the intrinsic magnetoresistance alone, since the intrinsic magnetoresistance is only a function of the magnetization. Hwang *et al* (1996) suggested that the low field magnetoresistance in polycrystalline samples is due to spin-polarized tunnelling between misaligned grains. It was shown by Wang *et al* (1998) that, phenomenologically, one has to distinguish weak and strong links between the grains. Only weak links give rise to a considerable low field magnetoresistance. Whereas the microstructural characteristics of the two types of links are not clear, the formation of weak or strong links can be controlled by the fabrication conditions.

The results of Gupta *et al* (1996) on epitaxial and polycrystalline films are in full agreement with the work on polycrystalline ceramics. However, by growing manganite films on polycrystalline  $\text{SrTiO}_3$  substrates with controlled grain size, Gupta *et al* (1996) were able to determine the grain-size dependence. If the polycrystalline films are idealized to consist of low resistivity grains ( $\rho_g$ ) of size  $l_g$  and thin ( $l_{gb} \ll l_g$ ) high resistivity grain boundaries ( $\rho_{gb}$ ), then the resistivity is expected to follow  $\rho = \rho_g + (l_{gb}/l_g)\rho_{gb}$ . A linear dependence of the resistivity measured at 10 K on the inverse grain diameter was indeed observed and the interface resistivity was derived as  $l_{gb}\rho_{gb} \sim 6 \times 10^{-5} \text{ } \Omega\text{cm}^2$ . Versluijs *et al* (1999) used a scanning tunnelling microscope in order to simultaneously image the surface topography and map the potential distribution of  $\text{La}_{0.7}\text{Sr}_{0.3}\text{MnO}_3$  films deposited on single crystal and polycrystalline MgO. Near the crystallite boundaries potential steps were found. At room temperature grain-boundary areal resistivities were found to be in the range  $3 \times 10^{-7}$ – $3 \times 10^{-5} \text{ } \Omega\text{cm}^2$  with a typical value of  $6 \times 10^{-6} \text{ } \Omega\text{cm}^2$ . This is one order of magnitude smaller than the value deduced by Gupta *et al* (1996) and might be related to the higher measurement temperature. Scanning tunnelling potentiometry measurements performed by Grévin *et al* (2000) on epitaxial LSMO films on MgO revealed occasional potential steps; these have low areal resistivities in the range  $0.3 \dots 0.8 \times 10^{-7} \text{ } \Omega\text{cm}^2$  possibly related to the good crystallinity of the film.

The resistivity and magnetoresistance of manganite, magnetite and  $\text{CrO}_2$  powder compacts was investigated by Coey (1998c, 1999), Coey *et al* (1998a, 1998b) and Manoharan *et al* (1998). Coey *et al* (1998b) investigated a  $\text{CrO}_2$  and a diluted 25%  $\text{CrO}_2$ /75%  $\text{Cr}_2\text{O}_3$  powder compact. Both samples show an increasing low field magnetoresistance with decreasing temperature; the diluted powder compact has a low temperature magnetoresistance of roughly 50%. Using equation (58) and a spin-polarization of 100% one obtains  $\langle \Delta G/G \rangle = 50\%$ , in agreement with the experimentally observed value. This is a rare example of a system that attains the theoretically expected magnetoresistance ratio at low temperature; it is more often observed that the measured magnetoresistance is considerably smaller than expected from Julliere's model. Coey *et al* (1998b) report dynamic conductance data at low temperatures that were attributed

to Coulomb-gap effects.

The dependence of the intergranular magnetoresistance of LSMO and LCMO ceramics on the grain size was investigated by Balcells *et al* (1998b) and Hueso *et al* (1999), respectively. The intergranular magnetoresistance was found to increase with decreasing grain size. Balcells *et al* (1998b) reported a saturation of the low field magnetoresistance at about 30%. The logarithm of the resistivity at constant temperature varied inversely proportional to the grain size indicating that the tunnelling barrier thickness increased with decreasing grain size. For submicronic grains an intergranular Coulomb gap with a charging energy  $E_C < 50$  K was found. Walter *et al* (1999) also reported a saturation of the low field magnetoresistance of LSMO films with various degrees of texture at about 34%.

Balcells *et al* (1999) and Petrov *et al* (1999) reported the magnetoresistance of granular LSMO/CeO<sub>2</sub> and LCMO/SrTiO<sub>3</sub> composites as a function of the manganite fraction. An enhanced low field magnetoresistance was found near the percolation threshold. The low field magnetoresistance was also found to be enhanced in LSMO/glass composites (Gupta *et al* 2001) and LSMO/Pr<sub>0.5</sub>Sr<sub>0.5</sub>MnO<sub>3</sub> composites (Liu *et al* 2001).

*8.2.3. Bi-crystal junctions.* Bi-crystal junctions have been investigated by Steenbeck *et al* (1997, 1998), Mathur *et al* (1997, 1999), Isaac *et al* (1998), Evetts *et al* (1998), Klein *et al* (1999), Westerburg *et al* (1999), Miller *et al* (2000), Philipp *et al* (2000) and Mathieu *et al* (2001a, 2001b). Generally these junctions are fabricated as follows. Manganite thin films are deposited on a bi-crystal substrate with a misalignment between the crystallographic directions of 24°, 36.8° or 45°. After deposition the manganite films are patterned into a meander-like track crossing the grain-boundary several times. Thus the investigation of a single grain boundary is possible. 45° grain boundaries were also fabricated on SrTiO<sub>3</sub> substrates using MgO and CeO<sub>2</sub> buffer layers in a chess board pattern (Mathieu *et al* 2000); these junctions yielded results similar to bi-crystal junctions.

The characteristics of resistivity and magnetoresistance seen in the bi-crystal junctions are similar to polycrystalline samples, see figure 42a. The resistivity shows a maximum far below the Curie temperature; a sharp decrease is found in the resistivity for small applied magnetic fields. This low field magnetoresistance increases with decreasing temperature with values up to nearly 100% at low temperatures. Steenbeck *et al* (1998), Westerburg *et al* (1999) and Philipp *et al* (2000) report field dependencies of the magnetoresistance similar to tunnel junctions for magnetic fields applied parallel to the junction, i.e. a large two-level magnetoresistance effect. The areal resistivity of the grain boundary increases with tilt angle (Isaac *et al* 1998). However, the various groups report a range of values, see table 3.

*8.2.4. Step-edge junctions.* Ziese *et al* (1999a) investigated step-edge junctions made from LCMO films. LaAlO<sub>3</sub> substrates were patterned prior to film deposition by

(a) bi-crystal

(b) step-edge

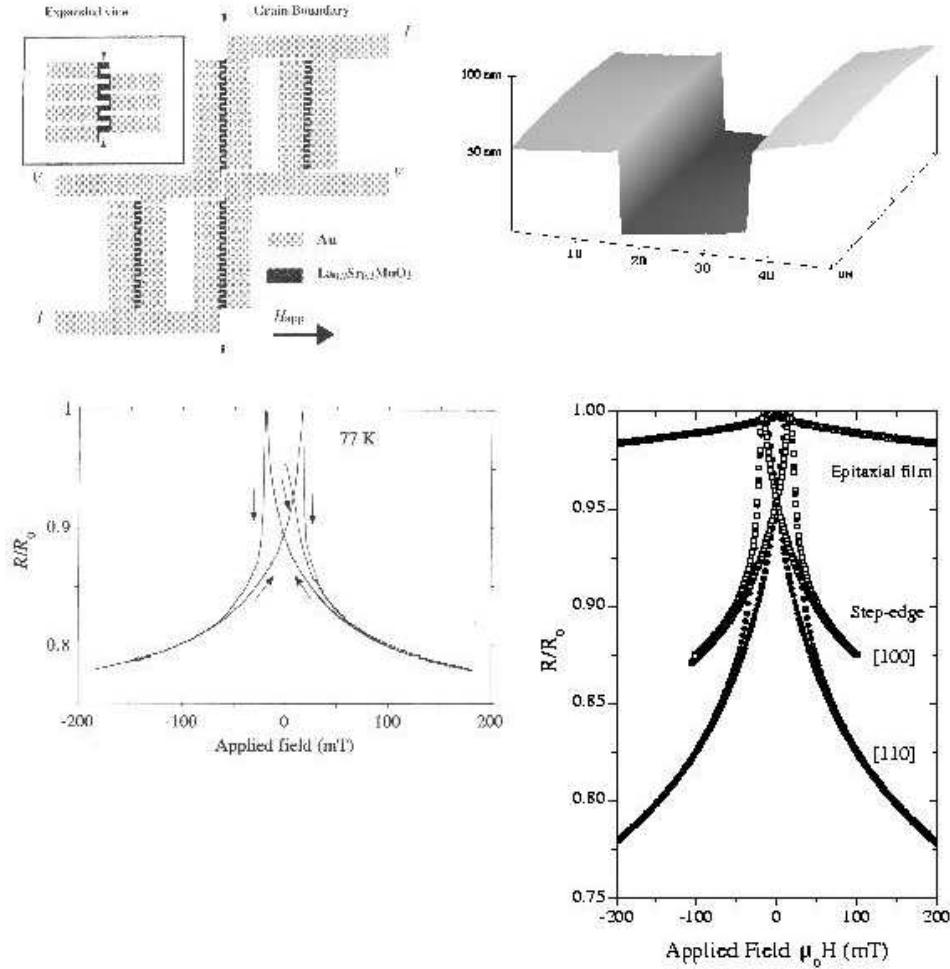


**Figure 42.** (a) General layout and magnetoresistance response of a bi-crystal junction. Adapted from Mathur *et al* (1997). (b) Atomic force microscopy picture of a step-edge junction. Magnetoresistance ratio at 100 K of an epitaxial film and step-edge arrays along [100] and [110], respectively. For the step-edge arrays the electrical current flows across the steps. After Ziese *et al* (1999a).

chemically assisted ion-beam etching such that an array of steps along [100] or [110] was formed. The steps were 100 nm to 200 nm high and 20  $\mu\text{m}$  apart; the substrates contained 150 [100] or 200 [110] steps, respectively. 25 nm thick LCMO films were deposited on the patterned substrates using pulsed laser deposition. These films show a large resistance anisotropy, the resistance showing intrinsic behaviour for electric currents flowing along the steps and typical grain-boundary behaviour for currents across the steps. This resistance anisotropy can be related to disordered regions near the step edges. In comparison to epitaxial films, the magnetoresistance is strongly enhanced, see figure 42b. The magnetoresistance value at fixed field and temperature seems to be determined by the local defect structure and varies between different samples.



**Table 3.** Interface resistance  $RA$  of various bi-crystal junctions. For comparison, the interface resistance measured in polycrystalline films is also shown.

Temperature $T$ (K)	Tilt angle	Material	$RA$ ( $\Omega\text{cm}^2$ )	Ref.
32	36.8°	LSMO	$4.1 \times 10^{-6}$	Steenbeck (1997)
32	36.8°	LSMO	$16 \times 10^{-6}$	Steenbeck (1998)
77	4°	LCMO	$0.2 \times 10^{-8}$	Isaac (1998)
77	24°	LCMO	$20 \times 10^{-8}$	Isaac (1998)
77	36.8°	LCMO	$10 \times 10^{-8}$	Isaac (1998)
77	45°	LCMO	$25 \times 10^{-8}$	Isaac (1998)
10	24°	LCMO	$10^{-2} - 1$	Klein (1999)
4.2	45°	LCMO	$170 \times 10^{-6}$	Westerburg (1999)
10	poly	LCMO	$6 \times 10^{-5}$	Gupta (1996)
300	poly	LSMO	$6 \times 10^{-6}$	Versluijs (1999)
300	epitaxial	LSMO	$5 \times 10^{-8}$	Grévin (2000)

After annealing the film deposited on [100] step edges at 950°C for 2 h in flowing oxygen, the resistance and magnetoresistance resumed the typical behaviour of epitaxial films. Similar results were obtained on “scratch” junctions by Srinitiwara Wong and Ziese (1998).

*8.2.5. Laser-patterned junctions.* Bibes *et al* (1999a, 1999b) reported on the temperature and magnetic field dependence of the magnetotransport properties of laser-patterned planar junctions. A 248 nm KrF Excimer laser with a fluence of about 2.5 J/m<sup>2</sup> was used to define tracks of 10  $\mu\text{m}$  and 40  $\mu\text{m}$  width on SrTiO<sub>3</sub> substrates. These tracks consisted of overlapping disks of molten material, about 0.1-0.2  $\mu\text{m}$  deep. Microcrack formation was observed within these disk regions. LSMO films were deposited by pulsed laser deposition on these patterned substrates. A strongly enhanced resistance was only found for the 40  $\mu\text{m}$  wide tracks. However, both 10  $\mu\text{m}$  and 40  $\mu\text{m}$  tracks lead to a significantly enhanced low field magnetoresistance with the characteristic magnetic field and temperature dependence.

### 8.3. General characteristics and models

Since considerable research efforts have been focused on the investigation of grain-boundary junctions, a lot of systems have been studied and certain general features have emerged. In this section the general characteristics will be summarized and the current status of models for grain-boundary transport will be reviewed.

When discussing magnetoresistance of ferromagnets, it is useful to distinguish the low field magnetoresistance from the high field behaviour. The magnetic field scale of the low field magnetoresistance is the coercive field. Grain-boundary junctions generally show a large low field magnetoresistance crossing over to a much more gradual decrease of the resistance, see figure 41. There is consensus that the low field magnetoresistance is due to spin-polarized tunnelling between grains with different orientations. These

grains are aligned in magnetic fields of the order of the coercive field, thus explaining the steep decrease in resistance at low fields. This is consistent with noise measurements (Mathieu *et al* 2001a) that prove the importance of magnetic domain fluctuations in this field regime. The observed magnetoresistance, however, is always considerably smaller than the value derived from equation (62). Furthermore, Julliere's model predicts no magnetoresistance for parallel orientation of the grain magnetization, in contradiction with the ubiquitous high field magnetoresistance slope. These deviations from the basic theory will be discussed in the following. Only few exceptions have been found to this general picture, see e.g. the large two-level magnetoresistance in a bi-crystal junction reported by Philipp *et al* (2000). In this case the tunnelling barrier is apparently of high quality and, correspondingly, the high field magnetoresistance is absent and the spin polarization derived from the resistance switching is high. These exceptions, however, enforce the general conclusions.

Some non-linear conductance measurements have been performed to assess the transport mechanism. Whereas measurements on polycrystalline ceramics are usually performed at low voltages in the linear region, the non-linear conductance of bi-crystal junctions (Steenbeck *et al* 1998, Mathur *et al* 1999, Klein *et al* 1999, Westerburg *et al* 1999, Höfener *et al* 2000), step-edges junctions (Ziese *et al* 1999a, Ziese 1999) and mechanically induced grain boundaries (Srinitiwara Wong and Ziese 1998, Ziese 1999) has been measured. Whereas the non-linear conductance depends somewhat on the microstructure, measurements on several systems indicate an inelastic tunnelling process. Steenbeck *et al* (1998) reported a quadratic voltage dependence of the conductance in annealed bi-crystal junctions, whereas Klein *et al* (1999), Westerburg *et al* (1999) and Höfener *et al* (2000) observe clear deviations from a quadratic dependence. Klein *et al* (1999), Ziese (1999) and Höfener *et al* (2000) measured the non-linear conductance at various temperatures and studied the evolution of the non-linearity with temperature. These investigations found clear evidence for inelastic tunnelling via localized states. Ziese (1999) analyzed the voltage dependence of the conductance using the general form

$$G = \frac{dI}{dV} = G_0(1 + g_x V^x), \quad (63)$$

where  $G_0$  denotes the zero bias conductance and  $g_x$  the non-linear conductance. This ansatz was motivated by the results of Glazman and Matveev (1988) on inelastic tunnelling via  $n$  localized states; in this case  $x = n - 2/(n + 1)$ . Moreover, the analysis of the junction resistivity of conventional ferromagnetic tunnelling junctions by Shang *et al* (1998), see previous section, indicated the presence of inelastic tunnelling processes via two localized states in the barrier. The conductance exponent  $x$  of a step-edge array, a polycrystalline LCMO film on MgO and a Cr-LCMO contact (see section 6) are shown in figure 43 as a function of temperature. The conductance exponent shows a crossover from a value  $x \sim 1.2 - 1.4$  below the Curie temperature to  $x \simeq 2$  above  $T_C$ . Accordingly, the non-linear conductance  $g_x$  decreases sharply at the Curie temperature indicating that inelastic tunnelling processes are only present below  $T_C$ , whereas a small

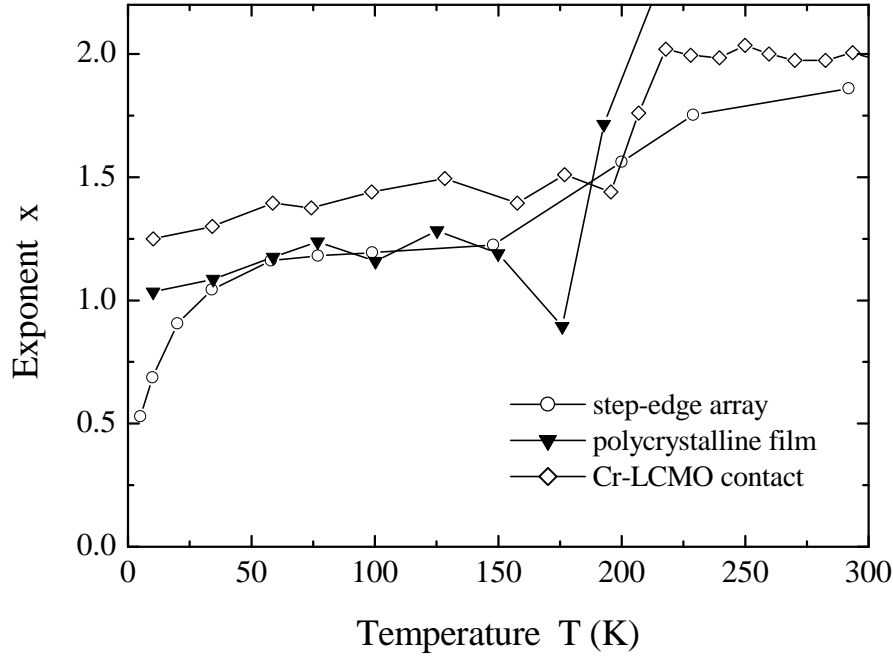


**Figure 43.** Conductance exponent  $x$  as a function of temperature for a step-edge array, a polycrystalline LCMO film on MgO and a Cr-LCMO contact. Reproduced from Ziese (1999).

elastic tunnelling component persists in the paramagnetic phase. These results are in agreement with the investigation on bi-crystal junctions by Klein *et al* (1999) and Höfener *et al* (2000). From these non-linear conductance measurements it might be concluded that tunnelling between ferromagnetic grains occurs mainly via one or two localized states. This qualitatively explains the experimentally observed reduction of the magnetoresistance in comparison to Julliere's model, since a spin-polarization loss results during the inelastic tunnelling process. This idea was further developed by Höfener *et al* (2000): the bi-crystal magnetoresistance was observed to decrease drastically with increasing voltage bias, since the junction is shunted by inelastic tunnelling processes that do not conserve the spin. Höfener *et al* (2000) proposed an extension of Julliere's model to a three-current model by taking inelastic tunnelling into account; this is the same approach used by Zhang and White (1998). This leads to a voltage dependent magnetoresistance

$$\frac{\Delta R}{R}(V, T) = \frac{I_{\uparrow\downarrow}}{I_{\uparrow\downarrow} + I_i}(V, T) \left( \frac{\Delta R}{R} \right)_{\text{Julliere}}. \quad (64)$$

Here  $I_i$  denotes the current due to inelastic tunnelling and  $I_{\uparrow\downarrow}$  the current through the junction in the antiparallel magnetization state due to direct tunnelling. Independent measurements of the voltage dependent magnetoresistance and the elastic to inelastic current ratio showed significant correlation, thus corroborating the importance of inelastic tunnelling processes. Lee *et al* (1999) argued that spin-polarized tunnelling

in manganite ceramics proceeds mainly via one localized state. Within this model these authors derived a “universal” magnetoresistance value of  $\Delta R/R \simeq m^2/3$ .  $m$  denotes the magnetization of the grains normalized by the saturation magnetization. At low temperatures a value of 1/3 is found in rough agreement with experiment (Lee *et al* 1999). However, the assumption of tunnelling via one localized state as well as the derived temperature dependence proportional to the square of the magnetization are in contradiction to experimental results. Coey *et al* (1998b) observed a non-linear conductance in  $\text{CrO}_2$  pressed powders at low temperature and interpreted this within a Coulomb-blockade model. Versluijs *et al* (2000) obtained non-linear  $I$ - $V$ -curves in nanocontacts between LSMO single crystals that might also arise from inelastic tunnelling.

The high field magnetoresistance slope has been consistently interpreted as arising from the barrier material (Guinea 1998, Evetts *et al* 1998, Ziese 1999, Lee *et al* 1999). In a limited field range, the magnetoresistance, as well as the magnetoconductance, are linear at high fields. However, Lee *et al* (1999) showed that the magnetoconductance of manganite polycrystals is linear in magnetic field to a very good approximation. It is generally argued that the high field slope  $d(\sigma/\sigma_0)/dB$  is proportional to the grain-boundary susceptibility  $\chi_{\text{GB}}$  (Guinea 1998, Evetts *et al* 1998, Ziese 1999, Lee *et al* 1999). Here  $\sigma$  denotes the conductivity and  $\sigma_0$  the zero field conductivity. Such a relationship was derived by Guinea (1998) within a model including tunnelling via paramagnetic impurities which leads to a high field slope being proportional to the Curie susceptibility. However, the temperature dependence of  $\chi_{\text{GB}}$ , see figure 44 for data on various manganite samples, indicates some magnetic ordering of the grain-boundary region. Moreover, the high field magnetoresistance slope extends to very high fields  $> 8$  T, whereas a paramagnetic grain-boundary region containing  $\text{Mn}^{4+}$ -ions is expected to saturate at about 1 T at 4.2 K. Some evidence for the magnetic state of the grain-boundary region comes from the work of Fontcuberta (Fontcuberta *et al* 1998, Balcells *et al* 1998a, 1998b, Martínez *et al* 1998), Ziese (Ziese *et al* 1998b, Ziese *et al* 1999a, Ziese 1999), Zhang *et al* (1997) and Zhu (Zhu *et al* 2001). Fontcuberta *et al* studied LSMO ceramics with various grain sizes and observed an increase of the thickness of the tunnelling barrier as well as a reduction of the saturation magnetization with decreasing grain size. This indicates that the surface layer of the grains is in a magnetically disordered state. This magnetically frustrated interface region is presumably insulating and serves as the tunnelling barrier between the ferromagnetic grains. This interpretation is corroborated by studies of various rare-earth substitutions on the magnetotransport properties (Fontcuberta *et al* 1998, Zhou *et al* 1999). There seem to be ideal cation substitutions maximizing the low field magnetoresistance. This might be related to enhanced spin disorder induced by the competition of double exchange and super-exchange interactions. Zhang *et al* (1997) related the tunnelling barrier to the energy difference between the bulk and surface double-exchange systems. Within this approach resistivity versus temperature curves could be successfully modelled. Zhu *et al* (2001) directly observed a spin-

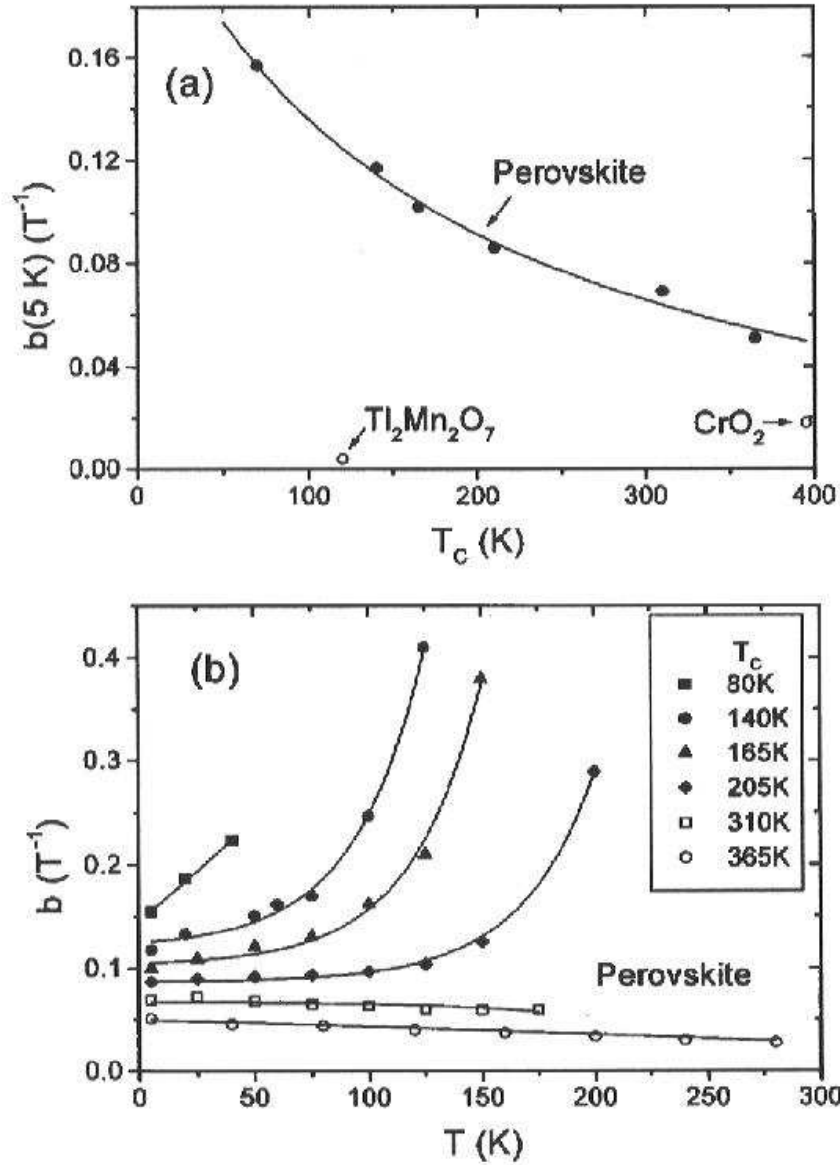


**Figure 44.** Top panel: slope  $b$  of the high field magnetoconductance as a function of the Curie temperature for various manganites. Bottom panel: high field magnetoconductivity slope as a function of temperature.  $b$  is proportional to the grain-boundary susceptibility  $\chi_{\text{GB}}$ . Reproduced from Lee *et al* (1999).

freezing transition in LSMO nanoparticles with a mean grain size below 50 nm: at temperatures below 45 K the field cooled magnetization suddenly increases. This transition indicates the alignment of the surface magnetic moments with the moments in the nanoparticle core. Ziese *et al* investigated the grain-boundary magnetoresistance as a function of angle between the applied field and the current and found typical anisotropic magnetoresistance (see also Coey 1999) of the same order of magnitude as in epitaxial films (Ziese *et al* 1999a, Ziese 1999). This was interpreted by Ziese (1999) to indicate tunnelling via manganese ions in the barrier, since the anisotropic magnetoresistance is mainly determined by the local environment of the magnetic ion,

see section 4. It is therefore likely that electrons tunnel between different grains via magnetically coupled, frustrated manganese ions in the grain-boundary region. Since this region has a negligible volume compared to the rest of the film, a direct magnetic investigation has not been possible so far. However, indirect information on the magnetic state of the grain boundary stems from resistance relaxation experiments (Ziese *et al* 1998b). In these experiments the resistance relaxation of various manganite samples was measured after a field step from 1 T to the remanence field of the magnet of about 7 mT. The relaxation was found to be logarithmic in time, see figure 45a. The relaxation rate

$$S_R = \frac{1}{R_0} \frac{dR}{d \ln t} \quad (65)$$

scales with the low field magnetoresistance, see figure 45b proving that the relaxation is due to magnetization processes in the grain-boundary region. This was corroborated by measurements of the magnetic viscosity of a polycrystalline LCMO film on Si (Ziese *et al* 1999b). The resistance relaxation expected from magnetic viscosity of the grains is one order of magnitude smaller than the resistance relaxation due to the barrier spins. The logarithmic time decay indicates a frustrated magnetic state of the barrier spins.

Calculations of the surface structure of double-exchange ferromagnets indicate an antiferromagnetic ordering (Calderon *et al* 1999b). Assuming an antiferromagnetically ordered interface between two ferromagnetic grains, Calderon *et al* (1999b) calculated the high field magnetoresistance and found a linear resistivity decrease in agreement with experiment. However, it might be argued that the linear high field magnetoresistance is a signature of any frustrated spin structure in the barrier, since it arises from the action of the applied field against the exchange field.

The magnetic properties of the grain boundary play a central role in the understanding of the magnetotransport properties in polycrystalline manganites. Local magnetic information has been obtained by magneto-optical imaging (Miller *et al* 2000) and magnetic force microscopy (MFM) (Soh *et al* 2000, 2001) of bi-crystal junctions. Miller *et al* (2000) detected a reorientation of the grain-boundary magnetization pointing out-of-plane, whereas the grain magnetization lies in plane. This magnetization rotation might contribute to the low field magnetoresistance. More astonishing are the results of MFM studies on the temperature dependence of the grain-boundary magnetization: this was found to have a higher Curie temperature than bulk material (Soh *et al* 2000, 2001)! Figure 46 shows MFM-scans near a grain boundary grown on a bi-crystal substrate at temperatures between 300 K and 365 K. At 300 K a domain-wall located at the grain boundary is seen. Above the bulk Curie temperature of 300 K the grain magnetization vanishes; a clear magnetic signal is recorded, however, at 355 K, localized near the grain boundary. This magnetic state is also found near natural defects. It vanishes above 370 K. From these studies it follows that the grain-boundary region is magnetically ordered; moreover, the size of this mesoscale magnetic region varies with temperature and the nature of the underlying defect. This provides additional evidence for the mechanism of tunnelling through a magnetic barrier.

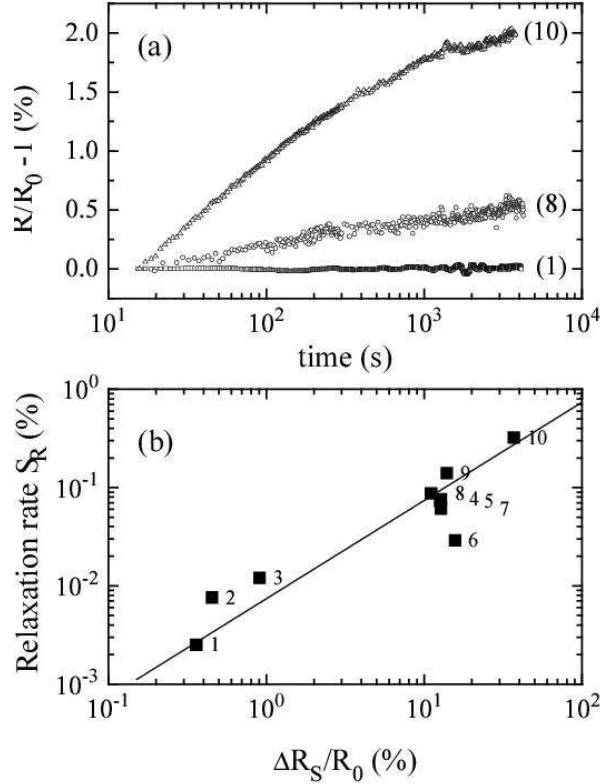


**Figure 45.** (a) Resistance relaxation after a sudden field change from 1 T to 7 mT of (1) an annealed LCMO film on  $(\text{LaAlO}_3)_{0.3}(\text{Sr}_2\text{AlTaO}_6)_{0.7}$  (LSAT), (8) a mechanically induced grain boundary, and (10) a Ti/Ni/LCMO/Ti heterostructure. (b) Resistance relaxation  $S_R$  versus low-field magnetoresistance  $\Delta R_S/R_0$  for various LCMO structures: (1) 250 nm thin annealed film on LSAT, (2) 120 nm thin as-deposited film on  $\text{LaAlO}_3$ , (3) 20 nm thin as-deposited film on  $\text{LaAlO}_3$ , (4) annealed film on Si, (5) as-deposited film on Si, (6) as-deposited film on MgO, (7) step-edge array, (8) mechanically induced grain boundary, (9) Ti/LCMO/Ti heterostructure, (10) Ti/Ni/LCMO/Ti heterostructure. The solid line is a fit of a linear law  $S \propto \Delta R_S/R_0$  to the data. Reproduced from Ziese *et al* (1998b).

The temperature dependence of the grain-boundary resistance is not very well understood. In all samples a broad resistance maximum is seen well below the Curie temperature. At low temperatures  $< 20$  K, a resistance upturn is observed. Phenomenologically, such a temperature dependence can be reproduced by considering a model of parallel conduction channels (de Andr s *et al* 1999). Since the resistivity is dominated by the least resistive paths, parallel conduction through well linked grains and intergranular regions can be considered. In such a model, the intergranular regions are assumed to be semiconducting, whereas the grains are metallic. Introducing effective cross sections for both channels, a satisfactory fit to the data can be made (de Andr s *et al* 1999). This model, however, is not fully satisfying, since it does not provide information on the microscopic transport mechanism. Ziese and Srinitiwawong (1998) showed that the resistivity of polycrystalline LCMO and LBMO films above

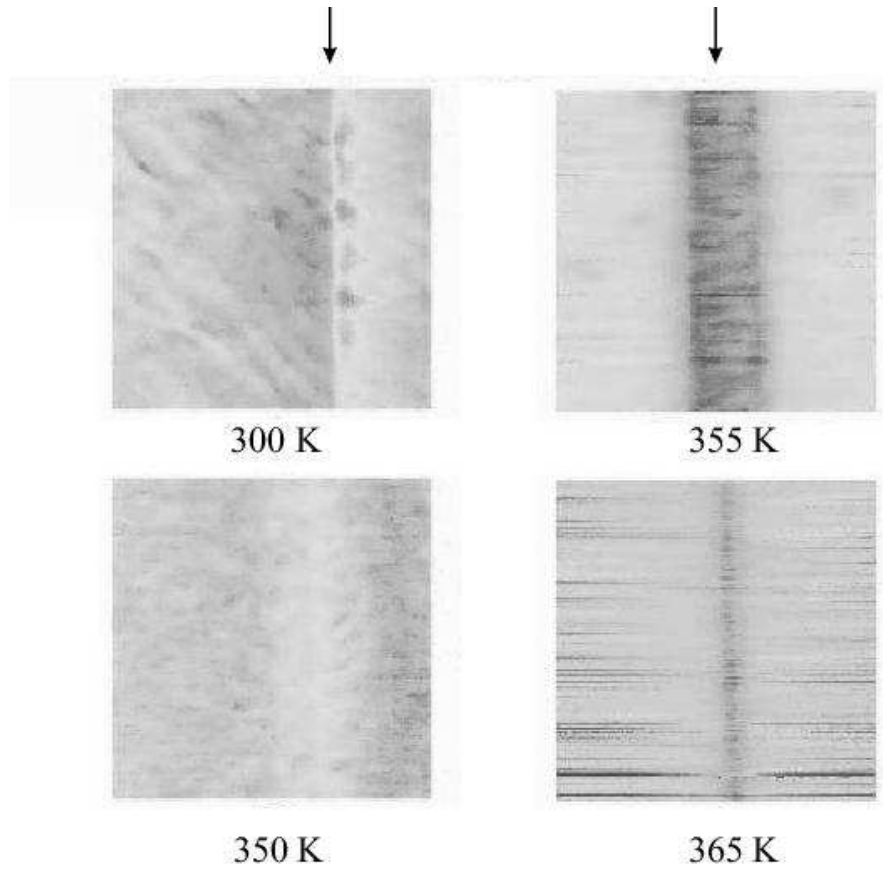


**Figure 46.** MFM-images showing the evolution of the magnetic structure near a grain boundary in a  $\text{La}_{0.7}\text{Sr}_{0.3}\text{MnO}_3$  film grown on a  $\text{SrTiO}_3$  bi-crystal; the location of the grain boundary is marked by arrows. At 300 K a domain wall located at the grain boundary is observed. Above 350 K the grain magnetization vanishes; at 355 K, however, a clear magnetic signal is obtained in the vicinity of the grain boundary. The grain boundary magnetization vanishes above 370 K. Adapted from Soh *et al* (2001).

the Curie temperature followed a variable range hopping law  $\rho \propto \exp[-(T_0/T)^{1/4}]$ , whereas epitaxial films are better described by polaron transport in the adiabatic limit,  $\rho \propto T \exp[-U/kT]$ . This result is consistent with the idea of intergranular transport via impurities. Balcells *et al* (1998b) found a  $\rho \propto \exp[(E_C/T)^{1/2}]$  variation of the resistivity of ceramic LSMO samples at low temperature and interpreted this behaviour as arising from a Coulomb gap. In contrast to this result, Raychaudhuri *et al* (1999) observed variable range hopping at low temperatures in polycrystalline LSMO. The broad resistance maximum at intermediate temperatures might be an indication of a mainly antiferromagnetic spin structure at the interface. The ubiquitous resistance minimum at low temperatures was interpreted by Rozenberg *et al* (2000) as due to the thermal disordering of a mainly antiferromagnetically aligned spin structure.

In conclusion, a consensus seems to emerge on the nature of spin-polarized transport in polycrystalline magnetic oxides. It was realized that charge-carrier transport occurs via inelastic tunnelling processes. This implies that the magnetotransport depends



strongly on the barrier characteristics. The grain-boundary region shows magnetic order, presumably a frustrated magnetic state or a mainly antiferromagnetic state with some frustration, causing an approximately linear high field magnetoresistance extending to very large fields. The inelastic tunnelling process is detrimental to the low field magnetoresistance, since the spin-polarization is reduced during the transit through the magnetically disordered barrier. This is confirmed by calculations of the apparent spin-polarization of ferromagnetic tunnelling junctions with a disordered barrier (Tsymbal and Pettifor 1998). The great future challenge is to produce grain-boundary junctions with non-magnetic or magnetically ordered tunnelling barriers in order to improve the effective spin-polarization. Annealed bi-crystal junctions seem to be promising candidates for such a development (Steenbeck *et al* 1998).

#### 8.4. Other ferromagnetic oxides

*8.4.1. Polycrystalline material.* Apart from the low field magnetoresistance studies of manganite ceramics discussed above, the extrinsic magnetoresistance of polycrystalline material of  $\text{CrO}_2$  (Hwang and Cheong 1997a, Coey *et al* 1998a, Manoharan *et al* 1998, Dai *et al* 2000, Dai and Tang 2000a, 2000b),  $\text{Tl}_2\text{Mn}_2\text{O}_7$  (Hwang and Cheong 1997b),  $\text{Sr}_2\text{MoFeO}_6$  (Kim *et al* 1999, Yuan *et al* 1999) and  $\text{La}_{1.2}\text{Sr}_{1.8}\text{Mn}_2\text{O}_7$  (Dörr *et al* 1999) was studied. These investigations usually show a large low field magnetoresistance between about 20% and 60% at low temperature. This is consistent with spin-polarized tunnelling between (nearly) half-metallic ferromagnets. The magnetoresistance of magnetite was found to be small of only a few percent. Typical data of a  $\text{Sr}_2\text{MoFeO}_6$  polycrystal are shown in figure 47a. The temperature dependence of the tunnelling magnetoresistance, however, varies strongly among these compounds. This is illustrated in figure 47b comparing the normalized low field magnetoresistance as a function of the reduced temperature,  $T/T_C$ , for  $\text{CrO}_2$ ,  $\text{La}_{2/3}\text{Sr}_{1/3}\text{MnO}_3$ ,  $\text{Tl}_2\text{Mn}_2\text{O}_7$  and  $\text{Sr}_2\text{MoFeO}_6$ . A clear trend emerges: the decay of the tunnelling magnetoresistance with temperature becomes smaller along this series. This was corroborated by Lee *et al* (1999). For  $\text{Sr}_2\text{MoFeO}_6$  the magnetoresistance is proportional to  $M^2$  as expected for spin-polarized tunnelling. The interpretation of these data is not fully clear. The different temperature dependences seem to be related to both the interfacial magnetism and the tunnelling barrier properties. One might speculate that  $\text{Sr}_2\text{MoFeO}_6$  has the most robust interfacial magnetization of the four compounds compared. At the same time the tunnelling barrier might contain less magnetically active localized states. On a microscopic scale the distinction between grains and barrier might not be suitable, since the transition between those is supposed to be gradual. The spin structure of the itinerant and super-exchange ferromagnets  $\text{Sr}_2\text{MoFeO}_6$  and  $\text{Tl}_2\text{Mn}_2\text{O}_7$  might be less sensitive to structural disorder than in the double exchange systems  $\text{La}_{2/3}\text{Sr}_{1/3}\text{MnO}_3$  and  $\text{CrO}_2$ , since the latter show a competition between ferromagnetic double exchange and antiferromagnetic super-exchange. The double exchange mechanism is supposed to be weakened near an interface due to the reduced carrier mobility. Scanning tunnelling microscopic

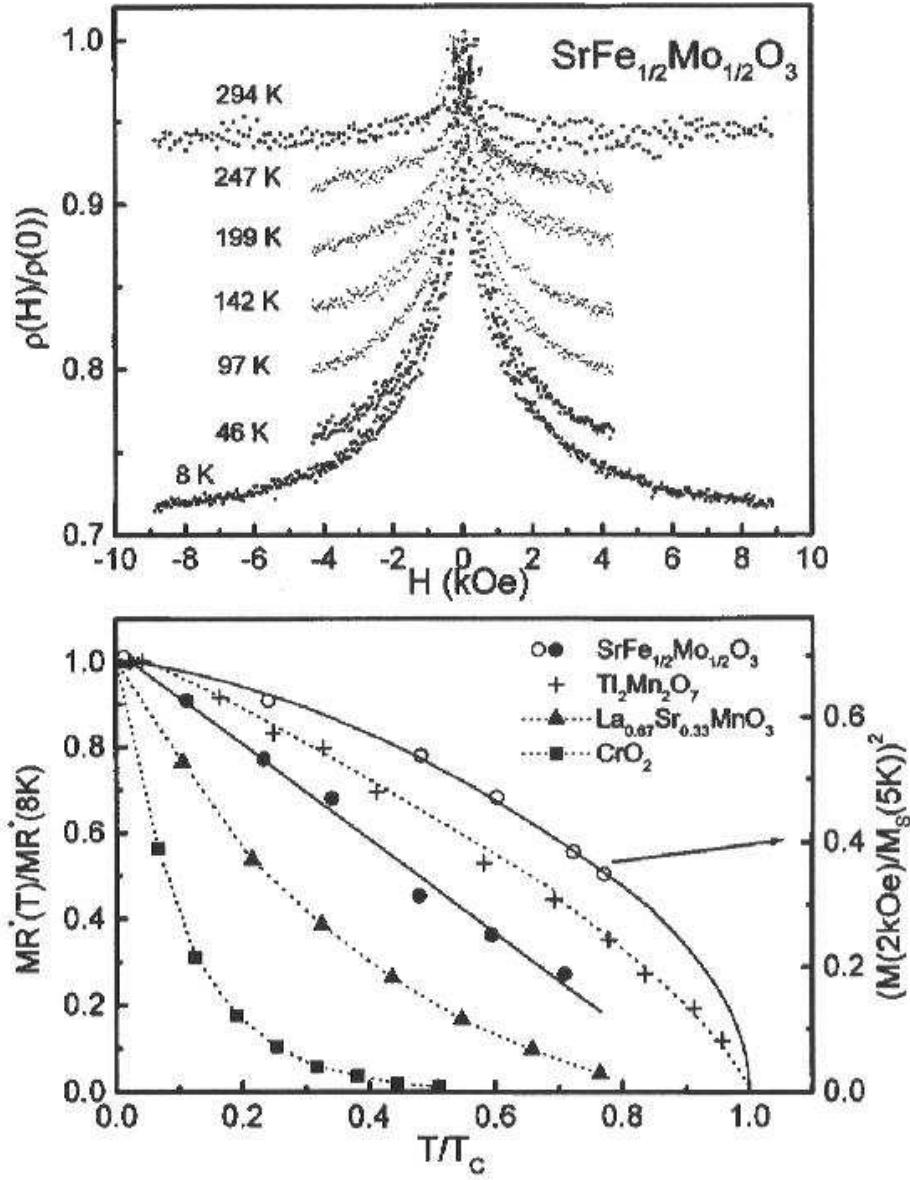


**Figure 47.** Top panel: the magnetic field dependence of the normalized resistance of  $\text{Sr}_2\text{FeMoO}_6$  at various temperatures. Bottom panel: the normalized low field magnetoresistance of  $\text{Sr}_2\text{FeMoO}_6$ , defined as  $MR^* = [\rho(0) - \rho(2\text{kOe})]/\rho(0)$ , plotted as a function of the reduced temperature  $T/T_C$  with those of  $\text{Tl}_2\text{Mn}_2\text{O}_3$ ,  $\text{CrO}_2$  and  $\text{La}_{0.67}\text{Sr}_{0.33}\text{MnO}_3$ . Reproduced from Kim *et al* (1999).

and spectroscopic investigations on manganite polycrystals indicated a semiconducting nature of the intergranular layers with a band gap of 0.3-0.45 eV; there might also be some band bending in the adjacent grains (Kar *et al* 1998). These microscopic investigations, however, are in the early stages and further studies on well characterized systems are clearly desirable.

A promising candidate for room temperature applications is  $\text{Fe}_3\text{O}_4$  with a Curie temperature of 858 K and the predicted half-metallic character. It has, however, been notoriously difficult to obtain a significant extrinsic magnetoresistance even at

low temperatures, see the studies by Coey *et al* (1998a), Ziese *et al* (1998b), Li *et al* (1998a), Nishimura *et al* (2000), Kitamoto *et al* (2000), Chen and Du (2000), Uotani *et al* (2000) and Taniyama *et al* (2001). Two recent studies along different routes report the successful observation of giant room temperature magnetoresistance in magnetite. Versluijs *et al* (2001) used nanocontacts between magnetite crystals, see section 5. The authors interpreted their results within a model of domain-wall scattering at a nano-constricted wall. The non-linear  $I$ - $V$  curves, however, are also in agreement with a tunnelling mechanism. Chen *et al* (2001) investigated the magnetoresistance of Zn-doped magnetite polycrystals and observed a spectacular room temperature magnetoresistance of more than 50% at a doping concentration of 40%. At this doping level insulating  $\alpha$ -Fe<sub>2</sub>O<sub>3</sub> precipitates form between grains; these appear to be good tunnelling barriers minimizing spin-polarization loss near the grain-boundary as well as inelastic tunnelling effects. The spin-polarization vanishes sharply at the Curie temperature of 318 K. If the interpretation of the large magnetoresistance due to spin-polarized tunnelling is correct, this work opens the way to efficiently engineer room temperature devices based on magnetite.

*8.4.2. Controlled defect structures.* Some investigations focused on the controlled fabrication of grain boundaries in other ferro- and ferrimagnetic oxides. This research was driven by the realization that the strong magnetoresistance decay as a function of temperature observed in the manganites and in CrO<sub>2</sub> precluded room temperature applications. Possible remedies are magnetic oxides with a high Curie temperature or with a robust interfacial spin structure as indicated by the encouraging results on polycrystalline material. Grain-boundary junctions introduced in SrRuO<sub>3</sub> films (Bibes *et al* 1999b), Sr<sub>2</sub>MoFeO<sub>6</sub> films (Yin *et al* 1999) and Fe<sub>3</sub>O<sub>4</sub> films (Ziese *et al* 1998b) were investigated. All these experiments showed only a small extrinsic magnetoresistance. 24° bi-crystal junctions had no effect on the magnetoresistance of SrRuO<sub>3</sub> films, whereas laser-patterned junctions enhanced the high field magnetoresistance, but did not induce a low field magnetoresistance characteristic of spin-polarized tunnelling (Bibes *et al* 1999b). 24° bi-crystal junctions in Sr<sub>2</sub>MoFeO<sub>6</sub> films showed a small magnetoresistance of about 2% at 2 kG and 20 K, twice the value of the magnetoresistance of a virgin film (Yin *et al* 1999). Ziese *et al* (1998b) did not observe any significant enhancement of the magnetoresistance of Fe<sub>3</sub>O<sub>4</sub> “scratch” junctions compared to epitaxial films. This is consistent with the small extrinsic magnetoresistance in Fe<sub>3</sub>O<sub>4</sub> polycrystalline films and pressed powders (Coey *et al* 1998a). It has to be noted, however, that magnetite films show a high field extrinsic magnetoresistance due to antiphase boundaries (Ziese and Blythe 2000) that might mask any contribution from artificially introduced defects.

In conclusion, these results indicate that the large low field magnetoresistance observed in manganite bi-crystal junctions might be specific to this double-exchange system. It seems that it is much more difficult to introduce insulating regions in the itinerant ferromagnets SrRuO<sub>3</sub>, Sr<sub>2</sub>MoFeO<sub>6</sub> and the ferrimagnet Fe<sub>3</sub>O<sub>4</sub> and thus to decouple the magnetic electrodes. This, apart from the lower spin-polarization in

SrRuO<sub>3</sub>, seems to be the limiting factor in the device performance of those junctions. One might state this conclusion in another way: the instability of the interfacial spin structure of the manganites toward antiferromagnetic ordering or magnetic frustration is a pre-requisite to readily fabricate grain-boundary junctions. The large low field magnetoresistance observed in polycrystalline samples does not contradict this conclusion, since strong magnetic disorder is often induced in small particles. Disordered magnetism at grain boundaries was also reported for pure nanocrystalline iron (Bonetti *et al* 1999).

## 9. Summary, Conclusions and Outlook

In this work extrinsic magnetoresistance phenomena in magnetic oxides were reviewed. Besides domain-wall scattering, the most important effects are spin-polarized tunnelling in ferromagnetic junctions and grain-boundary magnetoresistance. One indicator for the potential of a magnetic material in tunnelling structures is the degree of spin-polarization. Here the magnetic oxides are almost unique in having spin-polarizations approaching 100%. Great progress has been made in recent years in both the fabrication of tunnelling junctions and the understanding of the transport mechanisms in grain-boundary junctions. A huge magnetoresistance was seen in La<sub>0.7</sub>Sr<sub>0.3</sub>MnO<sub>3</sub>/insulator/La<sub>0.7</sub>Sr<sub>0.3</sub>MnO<sub>3</sub> tunnelling junctions at 4.2 K in agreement with the large spin-polarization. The magnetoresistance ratio, however, decays strongly with increasing temperature rendering these junctions useless for room-temperature applications. This strong decay appears to be related to a reduced interfacial spin-polarization. At present, it is not clear whether this is mainly an intrinsic effect related to surface reconstruction or is more a problem of producing high quality atomically flat interfaces. A similar problem was found in grain-boundary junctions. Here, insulating connections between different crystallites in polycrystalline material are formed leading to spin-polarized tunnelling between ferromagnetic grains. This process is very similar to the tunnelling process in ferromagnetic tunnelling junctions. The insulating layer between the grains, however, has many defect states leading to inelastic tunnelling processes and an apparent spin-polarization decrease.

There are some indications that domain-wall scattering might be important in magnetic oxides. A rigorous experimental proof including a precise measurement of its magnitude, however, has not yet been given. The use of nano-constricted domain walls certainly opens the most promising perspectives for further research.

In summary, the physics of spin-polarized transport in both ferromagnetic tunnel junctions and grain-boundary junctions has led to great challenges to both theoretical as well as experimental physics and many interesting discoveries have been made. The initial aim of fabricating magnetic field sensors operating at room temperature, however, has not yet been achieved. This is in part due to the sensitive surface chemistry of the materials and furthermore due to the relatively low Curie temperatures. Here, the investigation of Sr<sub>2</sub>FeMoO<sub>6</sub> that has a  $T_C$  above 400 K and a seemingly robust interfacial

magnetization might lead to a breakthrough. Magnetite has a high Curie temperature, but has not been successfully used as electrode material for tunnelling junctions.

An issue that has not been addressed in this review but that is of particular importance for applications is the noise level in magnetic oxides. In the oxides studied so far – mixed-valence manganites,  $\text{CrO}_2$  and  $\text{Fe}_3\text{O}_4$  (see Alers *et al* 1996, Rajeswari *et al* 1996, Hardner *et al* 1997 and Raquet *et al* 1999) – a large  $1/f$  noise exceeding the noise level in elemental metals by three to four orders of magnitude was found. The  $1/f$  dependence can be understood within the Dutta-Dimon-Horn model as arising from a very broad distribution of thermally activated fluctuators coupling to the resistivity (Dutta *et al* 1979). This, however, is a very formal treatment analogous to the analysis of magnetic after-effects by a distribution of thermally activated processes or the modelling of the low temperature properties of glasses with a distribution of two-level systems. The physical nature of the processes is usually difficult to reveal. Two candidates causing the large noise level in magnetic oxides are thermally activated motion of oxygen defects as well as electronic excitations of reversed spin in a nearly half-metallic band-structure. Further work is clearly necessary in order to understand the noise properties of magnetic oxides and to limit their negative influence on device performance.

The investigation of spin-polarized tunnelling in ferromagnetic oxides constitutes a research area within the emerging field of spin-electronics (also called magneto-electronics, Prinz 1998). Spin-electronics denotes a novel field of solid-state electronics that strives to realize electronic devices based on the differential manipulation of currents with well-defined spin direction. The simplest device is a magnetic field sensor and such devices have been realized on the basis of oxides working at low temperatures (ferromagnetic tunnelling junctions) and utilizing colossal magnetoresistance at room temperature (thick film sensors, Balcells *et al* 1996) or at 360 K (bridge sensors, Steinbeiß and Steenbeck 1998). There are three-terminal devices, so-called spin transistors, made from elemental ferromagnets (Johnson 1993a, 1993b) or semiconductor/ferromagnet hybrids (Monsma *et al* 1995), but such devices have not yet been realized using ferromagnetic oxides. However, since magnetic oxides are almost unique in having a half-metallic band structure, research in this direction will certainly have a huge potential.

Many challenging problems, e.g. the intrinsic transport mechanism in mixed-valence manganites, the realization and investigation of double tunnelling junctions, the relation between tunnelling current and band-structure, the study of surface and interface magnetism, the investigation of bonding effects between ferromagnets and insulating barriers as well as a microscopic description of grain-boundary transport, remain and will certainly lead to the discovery of much more interesting physics.

## Acknowledgments

This work was supported by the European Union TMR “OXSEN” network and by the DFG under DFG ES 86/7-1 within the Forschergruppe “Oxidische Grenzflächen”.

I thank Prof. Gillian Gehring, University of Sheffield, for valuable discussions and a critical reading of the manuscript.

## References

- Abe M, Nakagawa T and Nomura S 1973 *J. Phys. Soc. Japan* **35** 1360.
- Adams C P, Lynn J W, Mukovskii Y M, Arsenov A A and Shulyatev D A 2000 *Phys. Rev. Lett.* **85** 3954.
- Ahn K, Felser C, Seshadri R, Kremer R K and Simon A 2000 *J. Alloys Compounds* **303-304** 252.
- Albert F J, Katine J A, Buhrmann R A and Ralph D C 2000 *Appl. Phys. Lett.* **77** 3809.
- Alers G B, Ramirez A P and Jin S 1996 *Appl. Phys. Lett.* **68** 3644.
- Alexandrov A S and Bratkowsky A M 1999a *Phys. Rev. Lett.* **82** 141.
- Alexandrov A S and Bratkowsky A M 1999b *J. Phys.: Condens. Matter* **11** 1989.
- Alexandrov A S and Bratkowsky A M 1999c *Phys. Rev. B* **60** 6215.
- Alexandrov A S and Bratkowsky A M 1999d *J. Phys.: Condens. Matter* **11** L531.
- Alexandrov A S, Zhao G-M, Keller H, Lorenz B, Wang Y S and Chu C W 2001 *Phys. Rev. B* **64** 140404(R).
- Allen P B, Berger H, Chauvet O, Forro L, Jarlborg T, Junod A, Revaz B and Santi G 1996 *Phys. Rev. B* **53** 4393.
- Allodi G, De Renzi R and Guidi G 1998 *Phys. Rev. B* **57** 1024.
- Alonso J A, Martínez-Lope M J, Casais M T and Fernández-Díaz M T 1999 *Phys. Rev. Lett.* **82** 189.
- Alonso J A, Casais M T, Martínez-Lope M J, Martínez J L, Velasco P, Muñoz A and Fernández-Díaz M T 2000 *Chem. Mater.* **12** 161.
- Alonso J L, Fernández L A, Guinea F, Laliena V and Martín-Mayor V 2001 *Phys. Rev. B* **63** 064416.
- Alvarado S F, Eib W, Meier F, Pierce D T, Sattler K, Siegmann H C and Remeika J P 1975 *Phys. Rev. Lett.* **34** 319.
- Alvarado S F 1979 *Z. Phys. B* **33** 51.
- Anderson P W and Hasegawa H 1955 *Phys. Rev.* **100** 675.
- Anisimov V I, Elfimov I S, Hamada N and Terakura K 1996 *Phys. Rev. B* **54** 4387.
- Ansermet J-Ph 1998 *J. Phys.: Condens. Matter* **10** 6027.
- Archibald W, Zhou J-S and Goodenough J B 1996 *Phys. Rev. B* **53** 14445.
- Arovas D and Guinea F 1998 *Phys. Rev. B* **58** 9150.
- Asamitsu A and Tokura Y 1998 *Phys. Rev. B* **58** 47.
- Asano H, Ogale S B, Garrison J, Orozco A, Li Y H, Smolyaninova V, Galley C, Downes M, Rajeswari M, Ramesh R and Venkatesan T 1999 *Appl. Phys. Lett.* **74** 3696.
- Babushkina N A, Belova L M, Gorbenko O Yu, Kaul A R, Bosak A A, Ozhogin V I and Kugel K I 1998 *Nature (London)* **391** 159.
- Balcells Ll, Enrich R, Mora J, Calleja A, Fontcuberta J and Obradors X 1996 *Appl. Phys. Lett.* **69** 1486.
- Balcells Ll, Fontcuberta J, Martínez B and Obradors X 1998a *J. Phys.: Condens. Matter* **10** 1883.
- Balcells Ll, Fontcuberta J, Marínez B and Obradors X 1998b *Phys. Rev. B* **58** R14697.
- Balcells Ll, Carrillo A E, Martínez B and Fontcuberta J 1999 *Appl. Phys. Lett.* **74** 4014.
- Balcells Ll, Martínez B, Sandiumenge F and Fontcuberta J 2000 *J. Phys.: Condens. Matter* **12** 3013.
- Balcells Ll, Navarro J, Bibes M, Roig A, Martínez B and Fontcuberta J 2001 *Appl. Phys. Lett.* **78** 781.
- Ball A R, Leenaers A J G, van der Zaag P J, Shaw K A, Singer B, Lind D M, Frederikze H and Rekvelde M Th 1996 *Appl. Phys. Lett.* **69** 583.
- Barnás J and Fert A 1998 *Phys. Rev. Lett.* **80** 1058.
- Barry A, Coey J M D and Viret M 2001 *J. Phys.: Condens. Matter* **12** L173.
- Barry A, Coey J M D, Ranno L and Ounadjela K 1998 *J. Appl. Phys.* **83** 7166.
- Barzilai S, Goldstein Y, Balberg I and Helman J S 1981 *Phys. Rev. B* **23** 1809.
- Bastiaansen P J M and Knops H J F 1998 *J. Phys. Chem. Solids* **59** 297.
- Baszyński J, Kovač J and Kowalczyk A 1999 *J. Magn. Magn. Mater.* **195** 93.
- Battle P D, Blundell S J, Green M A, Hayer W, Honold M, Klehe A K, Laskey N S, Millburn J E, Murphy L, Rosseinsky M J, Samarin N A, Singleton J, Sluchanko N E, Sullivan S P and Vente J

- F 1996 *J. Phys.: Condens. Matter* **8** L427.
- Battle P D, Kasmir N, Millburn J E, Rosseinsky M J, Patel R T, Spring L E, Vente J F, Blundell S J, Hayes W, Klehe A K, Mihut A and Singleton J 1998 *J. Appl. Phys.* **83** 6379.
- Bazaliy Ya B, Jones B A and Zhang S-C 1998 *Phys. Rev. B* **57** R3113.
- Belov K P, Goryaga A N, Pronin V N and Skipetrova L A 1982 *Pis'ma Zh. Eksp. Teor. Fiz.* **36** 118 [1982 *JETP Lett.* **36** 146].
- Belov K P, Goryaga A N, Pronin V N and Skipetrova L A 1983 *Pis'ma Zh. Eksp. Teor. Fiz.* **37** 392 [1983 *JETP Lett.* **37** 464].
- Berger L 1978 *J. Appl. Phys.* **49** 2156.
- Berger L 1991 *J. Appl. Phys.* **69** 1550.
- Berry S D, Lind D M, Chern G and Mathias H 1993 *J. Magn. Magn. Mater.* **123** 126.
- Bhattacharjee S and Sardar M 2000 *Phys. Rev. B* **62** R6139.
- Bibes M, Martínez B, Fontcuberta J, Trtik V, Benítez F, Sánchez F and Varela M 1999a *Appl. Phys. Lett.* **75** 2120.
- Bibes M, Martínez B, Fontcuberta J, Trtik V, Benitez F, Ferrater C, Sánchez F and Varela M 1999b *Phys. Rev. B* **60** 9579.
- Bibes M, Balcells Ll, Valencia S, Fontcuberta J, Wojcik M, Jedryka E and Nadolski S 2001 *Phys. Rev. Lett.* **87** 067210.
- Björnsson P, Rübhausen M, Bäckström J, Käll M, Eriksson S, Eriksen J and Börjesson L 2000 *Phys. Rev. B* **61** 1193.
- Bonetti E, Del Bianco L, Fiorani D, Rinaldi D, Caciuffo R and Hernando A 1999 *Phys. Rev. Lett.* **83** 2829.
- Booth C H, Bridges F, Kwei G H, Lawrence J M, Cornelius A L and Neumeier J J 1998 *Phys. Rev. Lett.* **80** 853.
- Borges R P, Thomas R M, Cullinan C, Coey J M D, Suryanarayanan R, Ben-Dor L, Pinsard-Gaudart L and Revcolevschi A 1999 *J. Phys.: Condens. Matter* **11** L445.
- Brabers V A M in *Handbook of Magnetic Materials, Vol. 8* edited by Buschow K H J (North-Holland Publishing Company, Amsterdam) p. 189.
- Brabers V A M and Whall T E in *Landolt-Börnstein New Series III/27d* p. 17.
- Brataas A, Nazarov Yu V, Inoue J and Bauer G E W 1999a *Phys. Rev. B* **59** 93.
- Brataas A, Tataru G and Bauer G E W 1999b *Phys. Rev. B* **60** 3406.
- Bratkovsky A M 1997 *Phys. Rev. B* **56** 2344.
- Brener N E, Tyler J M, Callaway J, Bagayoko D and Zhao G L 2000 *Phys. Rev. B* **61** 16582.
- Brey L 1999 *cond-mat/9905209* preprint.
- Bruno P 1999 *Phys. Rev. Lett.* **83** 2425.
- Brückl H, Reiss G, Vinzelberg H, Bertram M, Mönch I and Schumann J 1998 *Phys. Rev. B* **58** R8893.
- Busch G, Campagna M, Cotti P and Siegmann H Ch 1969 *Phys. Rev. Lett.* **22** 597.
- Büttiker M 1988 *IBM J. Res. Dev.* **32** 317.
- Cabrera G G and Falicov L M 1974a *phys. stat. sol. (b)* **61** 539.
- Cabrera G G and Falicov L M 1974b *phys. stat. sol. (b)* **62** 217.
- Cai Y Q, Ritter M, Weiss W and Bradshaw A M 1998 *Phys. Rev. B* **58** 5043.
- Calderón M J, Vergés J A and Brey L 1999a *Phys. Rev. Lett.* **59** 4170.
- Calderón M J, Brey L and Guinea F 1999b *Phys. Rev. B* **60** 6698.
- Calderón M J and Brey L 2001 *Phys. Rev. B* **64** 140403.
- Callaghan A, Moeller C W and Ward R 1966 *Inorg. Chem.* **5** 1572.
- Campbell I A, Fert A and Jaoul O 1970 *J. Phys. C: Solid State Phys.* **3** S95.
- Campbell I A and Fert A 1982 in *Ferromagnetic Materials, Vol. 3* edited by Wohlfarth E P (North-Holland Publishing Company, Amsterdam) p. 751.
- Cao G, McCall S, Shepard M, Crow J E and Guertin R P 1997 *Phys. Rev. B* **56** 321.
- Capone M, Feinberg D and Grilli M 2000 *Eur. Phys. J. B* **17** 103.
- Chainani A, Yokoya T, Morimoto T, Takahashi T and Todo S 1995 *Phys. Rev. B* **51** 17976.



- Chattopadhyay A, Millis A J and Das Sarma S 2000 *Phys. Rev. B* **61** 10738.
- Chazalviel J-N and Yafet Y 1977 *Phys. Rev. B* **15** 1062.
- Chen P and Du Y W 2000 *J. Magn. Magn. Mater.* **219** 265.
- Chen P, Xing D Y, Du Y W, Zhu J M and Feng D 2001 *Phys. Rev. Lett.* **87** 107202.
- Chikazumi S 1997 *Physics of Ferromagnetism* (Clarendon Press, Oxford) p. 163ff.
- Chmaissem O, Kruk R, Dabrowski B, Brown D E, Xiong X, Kolesnik S, Jorgensen J D and Kimball C W, 2000 *Phys. Rev. B* **62** 14197.
- Choi J, Zhang J, Liou S-H, Dowben P A and Plummer E W 1999a *Phys. Rev. B* **59** 13453.
- Choi J, Dulli H, Liou S-H, Dowben P A and Langell M A 1999b *phys. stat. sol. (b)* **214** 45.
- Chuprakov I S and Dahmen K H 1998 *Appl. Phys. Lett.* **72** 2165.
- Coey J M D, Viret M, Ranno L and Ounadjela K 1995 *Phys. Rev. Lett.* **75** 3910.
- Coey J M D, Berkowitz A E, Balcells Ll, Putris F F and Parker F T 1998a *Appl. Phys. Lett.* **72** 734.
- Coey J M D, Berkowitz A E, Balcells Ll, Putris F F and Barry A 1998b *Phys. Rev. Lett.* **80** 3815.
- Coey J M D 1998 *Phil. Trans. R. Soc. Lond. A* **356** 1519.
- Coey J M D 1999 *J. Appl. Phys.* **85** 5576.
- Coey J M D, Viret M and von Molnár S 1999 *Adv. Phys.* **48** 167.
- Coey J M D “Materials for Spin Electronics”, in *Spin Electronics* edited by Ziese M and Thornton M J (Springer, Heidelberg, 2001).
- Coombes D J and Gehring G A 1998 *J. Magn. Magn. Mater.* **177-181** 862.
- Dagotto E, Hotta T and Moreo A 2001 *Phys. Rep.* **344** 1.
- Dai J, Tang J, Xu H, Spinu L, Wang W, Wang K, Kumbhar A, Li M and Diebold U 2000 *Appl. Phys. Lett.* **77** 2840.
- Dai J and Tang J 2001a *Phys. Rev. B* **63** 054434.
- Dai J and Tang J 2001b *Phys. Rev. B* **63** 064410.
- Dai P, Fernandez-Baca J A, Wakabayashi N, Plummer E W, Tomioka Y and Tokura Y 2000 *Phys. Rev. Lett.* **85** 2553.
- Dass R I and Goodenough J B 2001 *Phys. Rev. B* **63** 064417.
- de Andrés A, García-Hernández M and Martínez J L 1999 *Phys. Rev. B* **60** 7328.
- de Boer P K, van Leuken H, de Groot R A, Rojo T and Barberis G E 1997 *Solid State Commun.* **102** 621.
- Degiori L, Wachter P and Ihle D 1987 *Phys. Rev. B* **35** 9259.
- de Gennes P-G 1960 *Phys. Rev.* **118** 141.
- de Groot R A, Mueller F M, van Engen P G and Buschow K H J 1983 *Phys. Rev. Lett.* **50** 2024.
- de Groot R A and Buschow K H J 1986 *J. Magn. Magn. Mater.* **54-57** 1377.
- de Teresa J M, Ibarra M R, Algarabel P A, Ritter C, Marquina C, Blasco J, García J del Moral A and Arnold Z 1997 *Nature (London)* **387** 256.
- de Teresa J M, Barthélémy A, Fert A, Contour J P, Lyonnet R, Montaigne F, Seneor P and Vaurès A 1999a *Phys. Rev. Lett.* **82** 4288.
- de Teresa J M, Barthélémy A, Fert A, Contour J P, Montaigne F and Seneor P 1999b *Science* **286** 507.
- Dodge J S, Weber C P, Corson J, Orenstein J, Schlesinger Z, Reiner J W and Beasley M R 2000 *Phys. Rev. Lett.* **85** 4932.
- Domenicali C A 1950 *Phys. Rev.* **78** 458.
- Dong Z W, Ramesh R, Venkatesan T, Johnson M, Chen Z Y, Pai S P, Talyansky V, Sharma R P, Shreekala R, Lobb C J and Greene R L 1997 *Appl. Phys. Lett.* **71** 1718.
- Dong Z W, Pai S P, Ramesh R, Venkatesan T, Johnson M, Chen Z Y, Cavanaugh A, Zhao Y G, Jiang X L, Sharma R P, Ogale S and Greene R L 1998 *J. Appl. Phys.* **83** 6780.
- Dörr K, Müller K-H, Ruck K, Krabbes G and Schultz L 1999 *J. Appl. Phys.* **85** 5420.
- Dulli H, Plummer E W, Dowben P A, Choi J and Liou S-H 2000a *Appl. Phys. Lett.* **77** 570.
- Dulli H, Dowben P A, Liou S-H and Plummer E W 2000b *Phys. Rev. B* **62** R14629.
- Dutta P, Dimon P and Horn P M 1979 *Phys. Rev. Lett.* **43** 646.
- Dzero M O, Gor'kov L P and Kresin V Z 2000 *Eur. Phys. J B* **14** 459.

Ebels U, Radulescu A, Henry Y, Piraux L and Ounadjela K 2000 *Phys. Rev. Lett.* **84** 983.

Eckstein J N, Bozovic I, O'Donnell J, Onellion M and Rzechowski M S 1996 *Appl. Phys. Lett.* **69** 1312.

Eib W and Alvarado S F 1976 *Phys. Rev. Lett.* **37** 444.

Emery V J and Kivelson S A 1995 *Phys. Rev. Lett.* **74** 3253.

Emin D and Holstein T 1976 *Phys. Rev. Lett.* **36** 323.

Emin D, Hillery M S and Liu N-L H 1987 *Phys. Rev. B* **35** 641.

Evetts J E, Blamire M G, Mathur N D, Isaac S P, Teo B-S, Cohen L F and MacManus-Driscoll J L 1998 *Phil. Trans. R. Soc. Lond. A* **356** 1593.

Fang Z, Terakura K and Kanamori J 2001 *cond-mat/0103189* preprint.

Fäth M, Freisem S, Menovsky A A, Tomioka Y, Aarts J and Mydosh J A 1999 *Science* **285** 1540.

Feng J S-Y, Pashley R D and Nicolet M-A 1975 *J. Phys. C: Solid State Phys.* **8** 1010.

Fert A and Campbell I A 1968 *Phys. Rev. Lett.* **21** 1190.

Filippetti A and Pickett W E 1999 *Phys. Rev. Lett.* **20** 4184.

Filippetti A and Pickett W E 2000 *Phys. Rev. B* **62** 11571.

Fisk Z and Webb G W 1976 *Phys. Rev. Lett.* **36** 1084.

Fontcuberta J, Martínez B, Seffar A, Piñol S, García-Muñoz J L and Obradors X 1996 *Phys. Rev. Lett.* **76** 1122.

Fontcuberta J, Martínez B, Laukhin V, Balcells LL, Obradors X, Cohenca C H and Jardim R F 1998 *Phil. Trans. R. Soc. Lond. A* **356** 1577.

Fontcuberta J, Bibes M, Martínez B, Trtik V, Ferrater C, Sánchez F and Varela M 1999 *J. Appl. Phys.* **85** 4800.

Fontcuberta J 1999 *Physics World* **12** 33.

Franck J P, Isaac I, Chen W, Chrzanowski J and Irwin J C 1998 *Phys. Rev. B* **58** 5189.

Friedman L 1964 *Phys. Rev.* **135** A233.

Fujioka K, Okamoto J, Mizokawa T, Fujimori A, Hase I, Abbate M, Lin H J, Chen C T, Takeda Y and Takano M 1997 *Phys. Rev. B* **56** 6380.

Fulde P, Luther A and Watson R E 1973 *Phys. Rev. B* **8** 440.

Furukawa N 1994 *J. Phys. Soc. Japan* **63** 3214.

Furukawa N 1995a *J. Phys. Soc. Japan* **64** 2734.

Furukawa N 1995b *J. Phys. Soc. Japan* **64** 3164.

Furukawa N 1998 *cond-mat/9812066* preprint.

Furukawa N 2000 *J. Phys. Soc. Japan* **69** 1954.

Gadzuk J W 1969 *Phys. Rev.* **182** 416.

Gan Q, Rao R A, Eom C B, Garrett J L and Lee M 1998 *Appl. Phys. Lett.* **72** 978.

García N, Muñoz M and Zhao Y-W 1999 *Phys. Rev. Lett.* **82** 2923.

García-Landa B, Ritter C, Ibarra M R, Blasco J, Algarabel P A, Mahendiran R and García J 1999 *Solid State Commun.* **110** 435.

Geck J, Büchner B, Hücker M, Klingeler R, Gross R, Pinsard-Gaudart L and Revcolevschi A 2001 *Phys. Rev. B* **64** 144430.

Gehring G A 1997 *unpublished*.

Gerlach W and Schneiderhan K 1930 *Ann. Physik* **6** 772.

Ghosh K, Ogale S B, Pai S P, Robson M, Li E, Jin I, Dong Z W, Greene R L, Ramesh R and Venkatesan T 1998 *Appl. Phys. Lett.* **73** 689.

Gibbs M R J, Ziese M, Gehring G A, Blythe H J, Coombes D J, Sena S P and Shearwood C 1998 *Phil. Trans. R. Soc. Lond. A* **356** 1681.

Gilabert A, Plecenik A, Fröhlich K, Gaži Š, Pripko M, Mozolová Ž, Machajdík D, Beňačka Š, Medici M G, Grajcar M and Kúš P 2001 *Appl. Phys. Lett.* **78** 1712.

Gillman E S, Li M and Dahmen K-H 1998 *J. Appl. Phys.* **84** 6217.

Gittleman J I, Goldstein Y and Bozowski S 1972 *Phys. Rev. B* **5** 3609.

Glazman L I and Matveev K A 1988 *Zh. Eksp. Teor.* **94** 332 [*Sov. Phys. JETP* **67** 1276].

Gong G Q, Gupta A, Xiao G, Qian W and Dravid V P 1997 *Phys. Rev. B* **56** 5096.

- Goodenough J B and Longo M in *Landolt-Börnstein* III/4, p. 126.
- Goodenough J B 1955 *Phys. Rev.* **100** 564.
- Goodenough J B 1958 *J. Phys. Chem. Solids* **10** 287.
- Goodenough J B, Wold A, Arnott R J and Menyuk N 1961 *Phys. Rev.* **124** 373.
- Goodenough J B 1992 *Ferroelectrics* **130** 77.
- Goodenough J B 1997 *J. Appl. Phys.* **81** 5330.
- Goodenough J B 1999 *Aust. J. Phys.* **52** 155.
- Gopalakrishnan J, Chattopadhyay A, Ogale S B, Venkatesan T, Greene R L, Millis A J, Ramesha K, Hannoyer B and Marest G 2000 *Phys. Rev. B* **61** 9538.
- Gregg J F, Allen W, Ounadjela K, Viret M, Hehn M, Thompson S M and Coey J M D 1996 *Phys. Rev. Lett.* **77** 1580.
- Greneche J M, Venkatesan M, Suryanarayanan R and Coey J M D 2001 *Phys. Rev. B* **63** 174403.
- Grévin B, Maggio-Aprile I, Bentzen A, Ranno L, Llobet A and Fischer Ø 2000 *Phys. Rev. B* **62** 8596.
- Gridin V V, Hearne G R and Honig J M 1996 *Phys. Rev. B* **53** 15518.
- Grollier J, Cros V, Hamzic A, George J M, Jaffrès H, Fert A, Faini G, Ben Youssef J and Legall H 2001 *Appl. Phys. Lett.* **78** 3663.
- Guinea F 1998 *Phys. Rev. B* **58** 9212.
- Gupta A, Gong G Q, Xiao G, Duncombe P R, Lecoeur P, Trouilloud P, Wang Y Y, Dravid V P and Sun J Z 1996 *Phys. Rev. B* **54** R15629.
- Gupta A and Sun J Z 1999 *J. Magn. Magn. Mater.* **200** 24.
- Gupta S, Ranjit R, Mitra C, Raychaudhuri P and Pinto R 2001 *Appl. Phys. Lett.* **78** 362.
- Hardner H T, Weissmann M B, Jaime M, Treece R E, Dorsey P C, Horwitz J S and Chrisey D B 1997 *J. Appl. Phys.* **81** 272.
- Heaps C W 1934 *Phys. Rev.* **45** 320.
- Heide C, Zilberman P E and Elliott R J 2001 *Phys. Rev. B* **63** 064424.
- Helman J S and Abeles B 1976 *Phys. Rev. Lett.* **37** 1429.
- Hertz J A and Aoi K 1973 *Phys. Rev. B* **8** 3252.
- Hillery M S, Emin D and Liu N-L H 1988 *Phys. Rev. B* **38** 9771.
- Höfener C, Philipp J B, Klein J, Alff L, Marx A, Büchner B and Gross R 2000 *Europhys. Lett.* **50** 681.
- Holstein T 1959 *Ann. Phys. (N.Y.)* **8** 325.
- Honda S, Okada T, Nawate M and Tokumoto M 1997 *Phys. Rev. B* **56** 14566.
- Hong K and Giordano N 1998 *J. Phys.: Condens. Matter* **10** L401.
- Hueso L E, Rivas J, Rivadulla F and López-Quintela M A 1999 *J. Appl. Phys.* **86** 3881.
- Hwang H Y, Cheong S-W, Radaelli P G, Marezio M and Batlogg B 1995 *Phys. Rev. Lett.* **75** 914.
- Hwang H Y, Cheong S W, Ong N P and Batlogg B 1996 *Phys. Rev. Lett.* **77** 2041.
- Hwang H Y and Cheong S-W 1997a *Science* **278** 1607.
- Hwang H Y and Cheong S-W 1997b *Nature (London)* **389** 942.
- Ihle D and Lorenz B 1985 *J. Phys. C: Solid State Phys.* **18** L647.
- Ihle D and Lorenz B 1986 *J. Phys. C: Solid State Phys.* **19** 5239.
- Ijiri Y, Borchers J A, Erwin R W, Lee S-H, van der Zaag P J and Wolf R M 1998a *Phys. Rev. Lett.* **80** 608.
- Ijiri Y, Borchers J A, Erwin R W, Lee S-H, van der Zaag P J and Wolf R M 1998b *J. Appl. Phys.* **83** 6882.
- Imada M, Fujimori A and Tokura Y 1998 *Rev. Mod. Phys.* **70** 1039.
- Imai H, Shimakawa Y, Sushko Yu V and Kubo Y 2000 *Phys. Rev. B* **62** 12190.
- Inoue J and Maekawa S 1995 *Phys. Rev. Lett.* **74** 3407.
- Inoue J and Maekawa S 1996 *Phys. Rev. B* **53** R11927.
- Ioffe A F and Regel A R 1960 *Prog. Semicond.* **4** 237.
- Irkhin V Yu and Katsnel'son M I 1994 *Usp. Fiz. Nauk* **164** 705 [1994 *Physics-Uspekhi* **37** 659].
- Isaac S P, Mathur N D, Evetts J E and Blamire M G 1998 *Appl. Phys. Lett.* **72** 2038.
- Ishizaka S and Ishibara S 1999 *Phys. Rev. B* **59** 8375.

- Jaime M, Salamon M B, Rubinstein M, Treece R E, Horwitz J S and Chrisey D B 1996 *Phys. Rev. B* **54** 11914.
- Jaime M, Hardner H T, Salamon M B, Rubinstein M, Dorsey P and Emin D 1997 *Phys. Rev. Lett.* **78** 951.
- Jaime M, Lin P, Salamon M B and Han P D 1998 *Phys. Rev. B* **58** R5901.
- Jaime M and Salamon M B 1999 *cond-mat/9902284* preprint.
- Jakob G, Moshchalkov V V and Bruynseraede Y 1995 *Appl. Phys. Lett.* **66** 2564.
- Jakob G, Martin F, Westerburg W and Adrian H 1998 *Phys. Rev. B* **57** 10252.
- Ji Y, Strijkers G J, Yang F Y, Chien C L, Byers J M, Anguelouch A, Xiao G and Gupta A 2001 *Phys. Rev. Lett.* **86** 5585.
- Jin S, O'Bryan H M, Tiefel T H, McCormack M and Rhodes W W 1995a *Appl. Phys. Lett.* **66** 382.
- Jin S, Tiefel T H, McCormack M, O'Bryan H M, Chen L H, Ramesh R and Schurig D 1995b *Appl. Phys. Lett.* **67** 557.
- Johnson M 1993a *Phys. Rev. Lett.* **70** 2142.
- Johnson M 1993b *Science* **260** 320.
- Jonker G and van Santen J 1950 *Physica* **16** 599.
- Ju H L, Sohn H-C and Krishnan K M 1997 *Phys. Rev. Lett.* **79** 3230.
- Julliere M 1975 *Phys. Lett.* **54A** 225.
- Kacedon D B, Rao R A and Eom C B 1997 *Appl. Phys. Lett.* **71** 1724.
- Kagan M Yu, Khomskii D I and Mostovoy M V 1999 *Eur. Phys. J. B* **12** 217.
- Kanamori J 1958 *J. Phys. Chem. Solids* **10** 87.
- Kämper K P, Schmitt W P, Güntherodt G, Gambino R J and Ruf R 1987 *Phys. Rev. Lett.* **59** 2788.
- Kapusta Cz, Riedi P C, Kocemba W, Tomka G J, Ibarra M R, de Teresa J M, Viret M and Coey J M D 1999 *J. Phys.: Condens. Matter* **11** 4079.
- Kar A K, Dhar A, Ray S K, Mathur B K, Bhattacharya D and Chopra K L 1998 *J. Phys.: Condens. Matter* **10** 10795.
- Katine J A, Albert F J, Buhrman R A, Myers E B and Ralph D C 2000 *Phys. Rev. Lett.* **84** 3149.
- Kent A D, Rüdiger U, Yu J, Thomas L and Parkin S S P 1999 *J. Appl. Phys.* **85** 5243.
- Khomskii D 2000 *Physica B* **280** 325.
- Kim T H, Uehara M, Cheong S-W and Lee S 1999 *Appl. Phys. Lett.* **74** 1737.
- Kimura T, Tomioka Y, Kuwahara H, Asamitsu A, Tamura M and Tokura Y 1996 *Science* **274** 1698.
- Kitamoto Y, Nakayama Y and Abe M 2000 *J. Appl. Phys.* **87** 7130.
- Klein L, Dodge J S, Ahn C H, Snyder G J, Geballe T H, Beasley M R and Kapitulnik A 1996 *Phys. Rev. Lett.* **77** 2774.
- Klein L, Marshall A F, Reiner J W, Ahn C H, Geballe T H, Beasley M R and Kapitulnik A 1998 *J. Magn. Magn. Mater.* **188** 319.
- Klein J, Höfener C, Uhlenbruck S, Alff L, Büchner B and Gross R 1999 *Europhys. Lett.* **47** 371.
- Kleint C A, Krause M K, Höhne R, Walter T, Semmelhack H C, Lorenz M and Esquinazi P 1998 *J. Appl. Phys.* **84** 5097.
- Kobayashi K-I, Kimura T, Sawada H, Terakura K and Tokura Y 1998 *Nature (London)* **395** 677.
- Kobayashi K-I, Kimura T, Tomioka Y, Sawada H, Terakura K and Tokura Y 1999 *Phys. Rev. B* **59** 11159.
- Kobayashi K-I, Okuda T, Tomioka Y, Kimura T and Tokura Y 2000 *J. Magn. Magn. Mater.* **218** 17.
- Kogan E and Auslender M 1988 *phys. stat. sol. (b)* **147** 613.
- Kogan E and Auslender M 1998 *cond-mat/9807069* preprint.
- Kogan E, Auslender M and Kaveh M 1999 *Eur. Phys. J. B* **9** 373.
- Korotin M A, Anisimov V I, Khomskii D I and Sawatzky G A 1998 *Phys. Rev. Lett.* **80** 4305.
- Kostic P, Okada Y, Collins N C, Schlesinger Z, Reiner J W, Klein L, Kapitulnik A, Geballe T H and Beasley M R 1998 *Phys. Rev. Lett.* **81** 2498.
- Kostopoulos D 1972 *phys. stat. sol. (a)* **9** 523.
- Kostopoulos D and Alexopoulos K 1976 *J. Appl. Phys.* **47** 1714;

- Krivorotov I N, Nikolaev K R, Dobin A Yu, Goldman A M and Dahlberg E D 2001 *Phys. Rev. Lett.* **86** 5779.
- Krupička S and Novák P in *Handbook of Magnetic Materials, Vol. 3* edited by Wohlfarth E P (North-Holland Publishing Company, Amsterdam) p. 189.
- Kubo K and Ohata N 1972 *J. Phys. Soc. Japan* **33** 21.
- Kwei G H, Booth C H, Bridges F and Subramanian M A 1997 *Phys. Rev. B* **55** R688.
- Kwon C, Kim K-C, Robson M C, Gu J Y, Rajeswari M and Venkatesan T 1997 *J. Appl. Phys.* **81** 4950.
- Kwon C, Jia Q X, Fan Y, Hundley M F, Reagor D W, Coulter J Y and Peterson D E 1998 *Appl. Phys. Lett.* **72** 486.
- Landauer R 1957 *IBM J. Res. Dev.* **1** 223.
- Lanzara A, Saini N L, Brunelli M, Natali F, Bianconi A, Radaelli P G and Cheong S-W 1998 *Phys. Rev. Lett.* **81** 878.
- Lee S, Hwang H Y, Shraiman B I, Ratcliff II W D and Cheong S-W 1999 *Phys. Rev. Lett.* **82** 4508.
- Leung L K, Morrish A H and Searle C W 1969 *Can. J. Phys.* **47** 2697.
- Levy P M and Zhang S 1997 *Phys. Rev. Lett.* **79** 5110.
- Lewis S P, Allen P B and Sasaki T 1997 *Phys. Rev. B* **55** 10253.
- Li Q, Zang J, Bishop A R and Soukoulis C M 1997a *Phys. Rev. B* **56** 4541.
- Li X W, Gupta A, Xiao G and Gong G Q 1997b *Appl. Phys. Lett.* **71** 1124.
- Li X W, Lu Y, Gong G Q, Xiao G, Gupta A, Lecoeur P, Sun J Z, Wang Y Y and Dravid V P 1997c *J. Appl. Phys.* **81** 5509.
- Li X W, Gupta A, Xiao G and Gong G Q 1998a *J. Appl. Phys.* **83** 7049.
- Li X W, Gupta A, Xiao G, Qian W and Dravid V P 1998b *Appl. Phys. Lett.* **73** 3282.
- Lind D M, Berry S D, Borchers J A, Erwin R W, Lochner E, Stoyonov P, Shaw K A and Dibari R C 1995 *J. Magn. Magn. Mater.* **148** 44.
- Lindén J, Yamamoto T, Karppinen M, Yamauchi H and Pietari T 2000 *Appl. Phys. Lett.* **76** 2925.
- Liu G-L, Zhou J-S and Goodenough J B 2001 *Phys. Rev. B* **64** 144414.
- Liu J-M, Yuan G L, Sang H, Wu Z C, Chen X Y, Liu Z G, Du Y W, Huang Q and Ong C K 2001 *Appl. Phys. Lett.* **78** 1110.
- Livesay E A, West R N, Dugdale S B, Santi G and Jarlborg T 1998 *cond-mat/9812308* preprint.
- Livesay E A, West R N, Dugdale S B, Santi G and Jarlborg T 1999 *J. Phys.: Condens. Matter* **11** L279.
- Lofland S E, Bhagat S M, Kwon C, Robson M C, Sharma R P, Ramesh R and Venkatesan T 1995 *Phys. Lett.* **209A** 246.
- Longo J M and Ward R 1961 *J. Am. Chem. Soc.* **83** 1088.
- Longo J M, Raccah P M and Goodenough J B 1968 *J. Appl. Phys.* **39** 1327.
- Lourengo A A C S, Araújo J P, Amaral V S, Tavares P B, Sousa J B, Vieira J M, Alves E, da Silva M F and Soares J C 1999 *J. Magn. Magn. Mater.* **196-197** 495.
- Lu Y, Li W, Gong G Q, Xiao G, Gupta A, Lecoeur P, Sun J Z, Wang Y Y and Dravid V P 1996 *Phys. Rev. B* **54** R8357.
- Lyanda-Geller Y, Aleiner I L and Goldbart P M 1998 *Phys. Rev. Lett.* **81** 3215.
- Lyanda-Geller Y, Chun S H, Salamon M B, Goldbart P M, Han P D, Tomioka Y, Asamitsu A and Tokura Y 2001 *Phys. Rev. B* **63** 184426.
- Lynn J W, Erwin R W, Borchers J A, Huang Q, Santoro A, Peng J-L and Li Z Y 1996 *Phys. Rev. Lett.* **76** 4046.
- MacDonald D K C 1956 *Handbuch der Physik* **14** (Springer Verlag, Berlin) p. 137.
- Mackenzie A P, Reiner J W, Tyler A W, Galvin L M, Julian S R, Beasley M R, Geballe T H and Kapitulnik A 1998 *Phys. Rev. B* **58** R13318.
- MacLaren J M, Zhang X G and Butler W H 1997 *Phys. Rev. B* **56** 11827.
- Majumdar P and Littlewood P B 1998a *Phys. Rev. Lett.* **81** 1314.
- Majumdar P and Littlewood P B 1998b *Nature (London)* **395** 479.
- Mallik R, Sampathkumaran E V and Paulose P L 1997 *Appl. Phys. Lett.* **71** 2385.

- Malozemoff A P 1986 *Phys. Rev. B* **34** 1853.
- Manako T, Izumi M, Konishi Y, Kobayashi K-I, Kawasaki M and Tokura Y 1999 *Appl. Phys. Lett.* **74** 2215.
- Manoharan S S, Elefant D, Reiss G and Goodenough J B 1998 *Appl. Phys. Lett.* **72** 984.
- Martínez B, Balcells Ll, Fontcuberta J, Obradors X, Cohenca C H and Jardim R F 1998 *J. Appl. Phys.* **83** 7058.
- Martínez B, Senis R, Fontcuberta J, Obradors X, Cheikh-Rouhou W, Strobel P, Bougerol-Chaillout C and Pernet M 1999 *Phys. Rev. Lett.* **83** 2022.
- Martínez B, Navarro J, Balcells Ll and Fontcuberta J 2000 *J. Phys.: Condens. Matter* **12** 10515.
- Mathieu R, Svedlindh P, Chakalov R A and Ivanov Z G 2000 *Phys. Rev. B* **62** 3333.
- Mathieu R, Svedlindh P, Gunnarsson R and Ivanov Z G 2001a *Phys. Rev. B* **63** 132407.
- Mathieu R, Svedlindh P, Chakalov R and Ivanov Z G 2001b *cond-mat/0109052* preprint.
- Mathur N D, Burnell G, Isaac S P, Jackson T J, Teo B-S, MacManus-Driscoll J, Cohen L F, Evetts J E and Blamire M G 1997 *Nature (London)* **387** 266.
- Mathur N D, Littlewood P B, Todd N K, Isaac S P, Teo B-S, Kang D-J, Tarte E J, Barber Z H, Evetts J E and Blamire M G 1999 *J. Appl. Phys.* **86** 6287.
- Matl P, Ong N P, Yan Y F, Li Y Q, Studebaker D, Baum T and Doubinina G 1998 *Phys. Rev. B* **57** 10248.
- Mayr M, Moreo A, Vergés J A, Arispe J, Feiguin A and Dagotto E 2001 *Phys. Rev. Lett.* **86** 135.
- Mazin I I and Singh D J 1997 *Phys. Rev. B* **56** 2556.
- Mazin I I 1999 *Phys. Rev. Lett.* **83** 1427.
- Mazin I I, Singh D J and Ambrosch-Draxl C 1999 *Phys. Rev. B* **59** 411.
- McCormack M, Jin S, Tiefel T H, Fleming R M, Phillips J M and Ramesh R 1994 *Appl. Phys. Lett.* **64** 3045.
- Merrill R L and Si Q 1999 *Phys. Rev. Lett.* **83** 5326.
- Meservey R, Paraskevopoulos D and Tedrow P M 1976 *Phys. Rev. Lett.* **37** 858.
- Meservey R, Paraskevopoulos D and Tedrow P M 1980 *Phys. Rev. B* **22** 1331.
- Meservey R and Tedrow P M 1994 *Phys. Rep.* **238** 173.
- Mieville L, Worledge D, Geballe T H, Contreras R and Char K 1998 *Appl. Phys. Lett.* **73** 1736.
- Mikheenko P, Colclough M S, Severac C, Chakalov R, Welhoffer F and Muirhead C M 2001 *Appl. Phys. Lett.* **78** 356.
- Miller D J, Lin Y K, Vlasko-Vlasov V and Welp U 2000 *J. Appl. Phys.* **87** 6758.
- Millis A J, Littlewood P B and Shraiman B I 1995 *Phys. Rev. Lett.* **74** 5144.
- Millis A J, Shraiman B I and Mueller R 1996a *Phys. Rev. Lett.* **77** 175.
- Millis A J, Mueller R and Shraiman B I 1996b *Phys. Rev. B* **54** 5389.
- Millis A J, Mueller R and Shraiman B I 1996c *Phys. Rev. B* **54** 5405.
- Millis A J, Darling T and Migliori A 1998 *J. Appl. Phys.* **83** 1588.
- Millis A J, Hu J and Das Sarma S 1999 *Phys. Rev. Lett.* **82** 2354.
- Mira J, Rivas J, Rivadulla F, Vázquez-Vázquez C and López-Quintela M A 1999 *Phys. Rev. B* **60** 2998.
- Mitani S, Fujimori H and Ohnuma S 1997 *J. Magn. Magn. Mater.* **165** 141.
- Mitani S, Takahashi S, Takanashi K, Yakushiji K, Maekawa S and Fujimori H, 1998a *Phys. Rev. Lett.* **81** 2799.
- Mitani S, Takanashi K, Yakushiji K and Fujimori H 1998b *J. Appl. Phys.* **83** 6524.
- Miyazaki T, Tezuka N, Kumagai S, Ando Y, Kubota H, Murai J, Watabe T and Yokota M 1998 *J. Phys. D: Appl. Phys.* **31** 630.
- Monsma D J, Lodder J C, Popma Th J A and Dieny B 1995 *Phys. Rev. Lett.* **74** 5260.
- Monsma D J and Parkin S S P 2000a *Appl. Phys. Lett.* **77** 720.
- Monsma D J and Parkin S S P 2000b *Appl. Phys. Lett.* **77** 883.
- Montaigne F, Nassar J, Vaurès A, Nguyen Van Dau F, Petroff F, Schuhl A and Fert A 1998 *Appl. Phys. Lett.* **73** 2829.
- Moodera J S, Kinder L R, Wong T M and Meservey R 1995 *Phys. Rev. Lett.* **74** 3273.

- Mooodera J S, Nowak J and van de Veerdonk R J M 1998 *Phys. Rev. Lett.* **80** 2941.
- Mooodera J S and Mathon G 1999 *J. Magn. Magn. Mater.* **200** 248.
- Moon-Ho Jo, Mathur N D, Todd N K and Blamire M G 2000a *Phys. Rev. B* **61** R14905.
- Moon-Ho Jo, Mathur N D, Evetts J E and Blamire M G 2000b *Appl. Phys. Lett.* **77** 3803.
- Moreo A, Yunoki S and Dagotto E 1999 *Science* **283** 2034.
- Moritomo Y, Asamitsu A, Kuwahara H and Tokura Y 1996 *Nature (London)* **380** 141.
- Moritomo Y, Xu Sh, Machida A, Akimoto T, Nishibori E, Takata M and Sakata M 2000 *Phys. Rev. B* **61** R7827.
- Morrish A H, Evans B J, Eaton J A and Leung L K 1969 *Can. J. Phys.* **47** 2691.
- Mott N F 1936 *Proc. Roy. Soc. (London)* **156A** 368.
- Mott N F 1978 *Rev. Mod. Phys.* **50** 203.
- Moutis N, Christides C, Panagiotopoulos I and Niarchos D 2001 *Phys. Rev. B* **64** 094429.
- Nadgorny B, Soulen Jr R J, Osofsky M S, Mazin I I, Laprade G, van de Veerdonk R J M, Smits A A, Cheng S F, Skelton E F and Quadri S B 2000 *Phys. Rev. B* **61** R3788.
- Nagaev E L 1996 *Usp. Fiz. Nauk* **166** 833.
- Nagaev E L 1998 *Phys. Rev. B* **58** 12242.
- Nagaev E L 1999 *Aust. J. Phys.* **52** 305.
- Nagaev E L 2001 *Phys. Rep.* **346** 387.
- Narimanov E and Varma C M 2001 *cond-mat/0110047* preprint.
- Navarro J, Frontera C, Balcells Ll, Martínez B and Fontcuberta J 2001 *Phys. Rev. B* **64** 092411.
- Niebieskikwiat D, Sánchez R D, Caneiro A, Morales L, Vásquez-Mansilla M, Rivadulla F and Hueso L E 2000 *Phys. Rev. B* **62** 3340.
- Nikolaev K R, Bhattacharya A, Kraus P A, Vas'ko V A, Cooley W K and Goldman A M 1999 *Appl. Phys. Lett.* **75** 188.
- Nikolaev K R, Krivorotov I N, Cooley W K, Bhattacharya A, Dahlberg E D and Goldman A M 2000a *Appl. Phys. Lett.* **76** 478.
- Nikolaev K R, Dobin A Yu, Krivorotov I N, Cooley W K, Bhattacharya A, Kobrinski A L, Glazman L I, Wentzovitch R M, Dahlberg E D and Goldman A M 2000b *Phys. Rev. Lett.* **85** 3728.
- Nishimura K, Kohara Y, Kitamoto Y and Abe M 2000 *J. Appl. Phys.* **87** 7127.
- Noh J S, Nath T K, Eom C B, Sun J Z, Tian W and Pan X Q 2001 *Appl. Phys. Lett.* **79** 233.
- Nowak J and Rauluszkiewicz, 1992 *J. Magn. Magn. Mater.* **109** 79.
- Obata T, Manako T, Shimakawa Y and Kubo Y 1999 *Appl. Phys. Lett.* **74** 290.
- O'Donnell J, Onellion M, Rzechowski M S, Eckstein J N and Bozovic I 1996 *Phys. Rev. B* **54** R6841.
- O'Donnell J, Onellion M, Rzechowski M S, Eckstein J N and Bozovic I 1997a *Phys. Rev. B* **55** 5873.
- O'Donnell J, Onellion M, Rzechowski M S, Eckstein J N and Bozovic I 1997b *J. Appl. Phys.* **81** 4961.
- O'Donnell J, Rzechowski M S, Eckstein J N and Bozovic I 1998 *Appl. Phys. Lett.* **72** 1775.
- O'Donnell J, Eckstein J N and Rzechowski M S 2000 *Appl. Phys. Lett.* **76** 218.
- Ogale S B, Ghosh K, Sharma R P, Greene R L, Ramesh R and Venkatesan T 1998 *Phys. Rev. B* **57** 7823.
- Ogale A S, Ogale S B, Ramesh R and Venkatesan T 1999 *Appl. Phys. Lett.* **75** 537.
- Okamoto J, Mizokawa T, Fujimori A, Hase I, Nohara M, Takagi H, Takeda Y and Takano M 1999 *Phys. Rev. B* **60** 2281.
- Okimoto Y, Katsufuji T, Ishikawa T, Arima T and Tokura Y 1997 *Phys. Rev. B* **55** 4206.
- Oliver M R, Kafalas J A, Dimmock J O and Reed T B 1970 *Phys. Rev. Lett.* **24** 1064.
- Oretzki M J and Gaunt P 1970 *Can. J. Phys.* **48** 346.
- Orozco A, Ogale S B, Li Y H, Fournier P, Li E, Asano H, Smolyaninova V, Greene R L, Sharma R P, Ramesh R and Venkatesan T 1999 *Phys. Rev. Lett.* **83** 1680.
- Osofsky M S, Nadgorny B, Soulen R J, Broussard P, Rubinstein M, Byers J, Laprade G, Mukovskii Y M, Shulyatev D and Arsenov A 1999 *J. Appl. Phys.* **85** 5567.
- Palstra T T M, Ramirez A P, Cheong S-W, Zegarski B R, Schiffer P and Zaanen J 1997 *Phys. Rev. B* **56** 5104.

- Panagiotopoulos I, Christides C, Moutis N, Pissas M and Niarchos D 1999a *J. Appl. Phys.* **85** 4913.
- Panagiotopoulos I, Christides C, Pissas M and Niarchos D 1999b *Phys. Rev. B* **60** 485.
- Paraskevopoulos D, Meservey R and Tedrow P M 1977 *Phys. Rev. B* **16** 4907.
- Park J-H, Tjeng L H, Allen J W, Metcalf P and Chen C T 1997 *Phys. Rev. B* **55** 12813.
- Park J-H, Vescovo E, Kim H-J, Kwon C, Ramesh R and Venkatesan T 1998a *Phys. Rev. Lett.* **81** 1953.
- Park J-H, Vescovo E, Kim H-J, Kwon C, Ramesh R and Venkatesan T 1998b *Nature (London)* **392** 794.
- Park M S, Kwon S K, Youn S J and Min B I 1999 *Phys. Rev. B* **59** 10018.
- Park S K, Ishikawa T and Tokura Y 1998 *Phys. Rev. B* **58** 3717.
- Patterson F, Moeller C and Ward R 1963 *Inorg. Chem.* **2** 196.
- Pénicaud M, Siberchicot B, Sommers C B and Kübler J 1992 *J. Magn. Magn. Mater.* **103** 212.
- Penney T, Shafer M W and Torrance J B 1972 *Phys. Rev. B* **5** 3669.
- Perring T G, Aeppli G, Moritomo Y and Tokura Y 1997 *Phys. Rev. Lett.* **78** 3197.
- Perring T G, Aeppli G, Kimura T, Tokura Y and Adams M A 1998 *Phys. Rev. B* **58** R14693.
- Petrov D K, Krusin-Elbaum L, Sun J Z, Feild C and Duncombe P R 1999 *Appl. Phys. Lett.* **75** 995.
- Philipp J B, Höfener C, Thienhaus S, Klein J, Alff L and Gross R 2000 *Phys. Rev. B* **62** R9248.
- Pickett W E and Singh D J 1996 *Phys. Rev. B* **53** 1146.
- Pietambaram S, Kumar D, Singh R K and Lee C B 2001 *Appl. Phys. Lett.* **78** 243.
- Pinsard-Gaudart L, Suryanarayanan R, Revcolevski A, Rodriguez-Carvajal J, Greneche J M, Smith P A I, Thomas R M, Borges R P and Coey J M D 2000 *J. Appl. Phys.* **87** 7118.
- Plaskett T S, Freitas P P, Sun J J, Sousa R C, da Silva F F, Galvao T T P, Pinho N M, Cardoso S, da Silva M F and Soares J C 1997 *Magnetic Ultrathin Films, Multilayers and Surfaces* edited by Tobin J, Chambliss D, Kubinski D, Barmak K, Dederichs P, de Jonge W, Katayama T and Schuhl A, MRS Symposia Proceedings No. 475 (Materials Research Society, Pittsburgh, 1997) 469.
- Platt C L, Dieny B and Berkowitz A E 1997 *J. Appl. Phys.* **81** 5523.
- Politzer B A and Cutler P H 1972 *Phys. Rev. Lett.* **28** 1330.
- Prellier W, Smolyaninova V, Biswas A, Galley C, Greene R L, Ramesha K and Gopalakrishnan J 2000 *J. Phys.: Condens. Matter* **12** 965.
- Prinz G A 1998 *Science* **282** 1660.
- Przyslupski P, Koleśnik S, Dynowska E, Skośkiewicz T and Sawicki M 1997 *IEEE Trans. Appl. Superconductivity* **7** 2192.
- Quijada M, Černe J, Simpson J R, Drew H D, Ahn K H, Millis A J, Shreekala R, Ramesh R, Rajeswari M and Venkatesan T 1998 *Phys. Rev. B* **58** 16093.
- Rajeswari M, Goyal A, Raychaudhuri A K, Robson M C, Xiong G C, Kwon C, Ramesh R, Greene R L, Venkatesan T and Lakeou S 1996 *Appl. Phys. Lett.* **69** 851.
- Raju N P, Greedan J E and Subramaniam M A 1994 *Phys. Rev. B* **49** 1086.
- Ramirez A P 1997 *J. Phys.: Condens. Matter* **9** 8171.
- Ramirez A P and Subramanian M A 1997 *Science* **277** 546.
- Ramirez A P, Cava R J and Krajewski J 1997 *Nature (London)* **386** 156.
- Rampe A, Hartmann D, Weber W, Popovic S, Reese M and Güntherodt G 1995 *Phys. Rev. B* **51** 3230.
- Raquet B, Coey J M D, Wirth S and von Molnár S 1999 *Phys. Rev. B* **59** 12435.
- Ray S, Kumar A, Majumdar S, Sampathkumaran E V and Sarma D D 2001a *J. Phys.: Condens. Matter* **13** 607.
- Ray S, Kumar A, Sarma D D, Cimino R, Turchini S, Zennaro S and Zema N 2001b *Phys. Rev. B* **87** 097204.
- Raychaudhuri P, Taneja P, Sarkar S, Nigam A K, Ayyub P and Pinto R 1999 *Physica B* **259-261** 812.
- Ritter C, Ibarra M R, Morellon L, Blascot J, García J and de Teresa J M 2000 *J. Phys.: Condens. Matter* **12** 8295.
- Rivadulla F, López-Qunitela M A, Mira J and Rivas J 2001 *Phys. Rev. B* **64** 052403.
- Rodbell D S, Lommel J M and DeVries R C 1966 *J. Phys. Soc. Japan* **21** 2430.
- Röder H, Zang J and Bishop A R 1996 *Phys. Rev. Lett.* **76** 1356.



- Rodriguez-Martinez L M and Attfield J P 1996 *Phys. Rev. B* **54** R15622.
- Roy M, Mitchell J F, Ramirez A P and Schiffer P 1999 *J. Phys.: Condens. Matter* **11** 4843.
- Rozenberg E, Auslender M, Felner I and Gorodetsky G 2000 *J. Appl. Phys.* **88** 2578.
- Rüdiger U, Yu J, Zhang S, Kent A D and Parkin S S P 1998a *Phys. Rev. Lett.* **80** 5639.
- Rüdiger U, Yu S, Kent A D and Parkin S S P 1998b *Appl. Phys. Lett.* **73** 1298.
- Rüdiger U, Yu J, Thomas L, Parkin S S P and Kent A D 1999a *Phys. Rev. B* **59** 11914.
- Rüdiger U, Yu J, Parkin S S P and Kent A D 1999b *J. Magn. Magn. Mater.* **198-199** 261.
- Santi G and Jarlborg T 1997 *J. Phys.: Condens. Matter* **9** 9563.
- Sarma D D, Shanthi N, Barman S R, Hamada N, Sawada H and Terakura K 1995 *Phys. Rev. Lett.* **75** 1126.
- Sarma D D, Mahadevan P, Saha-Dasgupta T, Ray S and Kumar A 2000 *Phys. Rev. Lett.* **85** 2549.
- Satpathy S, Popović Z S and Vukajlović F R 1996 *Phys. Rev. Lett.* **76** 960.
- Schiffer P, Ramirez A P, Bao W and Cheong S-W 1995 *Phys. Rev. Lett.* **75** 3336.
- Schelp L F, Fert A, Fetta F, Holody P, Lee S F, Maurice J L, Petroff F and Vaurès A 1997 *Phys. Rev. B* **56** R5747.
- Sheng P, Abeles B and Arie Y 1973 *Phys. Rev. Lett.* **31** 44.
- Searle C W and Wang S T 1969 *Can. J. Phys.* **47** 2703.
- Searle C W and Wang S T 1970 *Can. J. Phys.* **48** 2023.
- Seneor P, Fert A, Maurice J-L, Montaigne F, Petroff F and Vaurès A 1999 *Appl. Phys. Lett.* **74** 4017.
- Shang C H, Nowak J, Jansen R and Moodera J S 1998 *Phys. Rev. B* **58** R2917.
- Sharma M, Wang S X and Nickel J 1999 *Phys. Rev. Lett.* **82** 616.
- Shengelaya A, Zhao G, Keller H and Müller K A 1996 *Phys. Rev. Lett.* **77** 5296.
- Shimakawa Y, Kubo Y and Manako T 1996 *Nature (London)* **379** 53.
- Shimakawa Y, Kubo Y, Manako T, Sushko Y V, Argyriou D N and Jorgensen J D 1997 *Phys. Rev. B* **55** 6399.
- Shimakawa Y, Kubo Y, Hamada N, Jorgensen J D, Hu Z, Short S, Nohara M and Takagi H 1999 *Phys. Rev. B* **59** 1249.
- Shiozaki I, Hurd C M, McAlister S P, McKinnon W R and Strobel P 1981 *J. Phys. C: Solid State Phys.* **14** 4641.
- Simmons J G 1963 *J. Appl. Phys.* **34** 1793.
- Singh D J 1997 *Phys. Rev. B* **55** 313.
- Singley E J, Weber C P, Basov D N, Barry A and Coey J M D 1999 *Phys. Rev. B* **60** 4126.
- Sinković B, Shekel E and Hulbert S L 1995 *Phys. Rev. B* **52** R8696.
- Sleight A W, Longo J M and Ward R 1962 *Inorg. Chem.* **1** 245.
- Sleight A W and Weiher J F 1972 *J. Phys. Chem. Solids* **33** 679.
- Slonczewski J C 1989 *Phys. Rev. B* **39** 6995.
- Slonczewski J C 1996 *J. Magn. Magn. Mater.* **159** L1.
- Snyder G J, Hiskes R, DiCarolis S, Beasley M R and Geballe T H 1996 *Phys. Rev. B* **53** 14434.
- Soh Y-A, Aeppli G, Mathur N D and Blamire M G 2000 *J. Appl. Phys.* **87** 6743.
- Soh Y-A, Aeppli G, Mathur N D and Blamire M G 2001 *Phys. Rev. B* **63** 020402.
- Soulen Jr R J, Byers J M, Osofsky M S, Nadgorny B, Ambrose T, Cheng S F, Broussard P R, Tanaka C T, Nowak J, Moodera J S, Barry A and Coey J M D 1998 *Science* **282** 85.
- Srinitiwarawong C and Ziese M 1998 *Appl. Phys. Lett.* **73** 1140.
- Srinitiwarawong C and Gehring G A 2001 *J. Phys.: Condens. Matter* **13** 7987.
- Stadler S, Idzerda Y U, Chen Z, Ogale S B and Venkatesan T 1999 *Appl. Phys. Lett.* **75** 3384.
- Stadler S, Idzerda Y U, Chen Z, Ogale S B and Venkatesan T 2000 *J. Appl. Phys.* **87** 6767.
- Stearns M B 1977 *J. Magn. Magn. Mater.* **5** 1062.
- Steenbeck K, Eick T, Kirsch K, O'Donnell K and Steinbeiß E 1997 *Appl. Phys. Lett.* **71** 968.
- Steenbeck K, Eick T, Kirsch K, Schmidt H-G and Steinbeiß E 1998 *Appl. Phys. Lett.* **73** 2506.
- Steinbeiß E and Steenbeck K 1998 *Spin News, Newsletter of the Oxide Spin Electronics Network* **4** (Trinity College, Dublin) p. 3.

- Sternlieb B J, Hill J P, Wildgruber U C, Luke G M, Nachumi B, Moritomo Y and Tokura Y 1996 *Phys. Rev. Lett.* **76** 2169.
- Su Y-S, Kaplan T A, Mahanti S D and Harrison J F 2000 *Phys. Rev. B* **61** 1324.
- Sun J Z, Gallagher W J, Duncombe P R, Krusin-Elbaum L, Altman R A, Gupta A, Lu Y, Gong G Q and Xiao G 1996 *Appl. Phys. Lett.* **69** 3266.
- Sun J Z, Krusin-Elbaum L, Duncombe P R, Gupta A and Laibowitz R B 1997 *Appl. Phys. Lett.* **70** 1769.
- Sun J Z 1998 *Phil. Trans. R. Soc. Lond. A* **356** 1693.
- Sun J Z, Abraham D W, Roche K and Parkin S S P 1998 *Appl. Phys. Lett.* **73** 1008.
- Sun J Z 1999 *J. Magn. Magn. Mater.* **202** 157.
- Sun J Z, Abraham D W, Rao R A and Eom C B 1999 *Appl. Phys. Lett.* **74** 3017.
- Sun J Z 2000 *Phys. Rev. B* **62** 570.
- Suzuki K and Tedrow P M 1998 *Phys. Rev. B* **58** 11597.
- Suzuki K and Tedrow P M 1999 *Appl. Phys. Lett.* **74** 428.
- Suzuki Y, Wu Y, Yu J, Ruediger U, Kent A D, Nath T K and Eom C B 2000 *J. Appl. Phys.* **87** 6746.
- Takahashi S and Maekawa S 1998 *Phys. Rev. Lett.* **80** 1758.
- Taniyama T, Nakatani I, Namikawa T and Yamazaki Y 1999 *Phys. Rev. Lett.* **82** 2780.
- Taniyama T, Kitamoto Y and Yamazaki Y 2001 *J. Appl. Phys.* **89** 7693.
- Tatara G and Fukuyama H 1997 *Phys. Rev. Lett.* **78** 3773.
- Tatara G, Zhao Y-W, Muñoz M and García N 1999 *Phys. Rev. Lett.* **83** 2030.
- Taylor G R, Isin A and Coleman R V 1968 *Phys. Rev.* **165** 621.
- Tedrow P M and Meservey R 1971 *Phys. Rev. Lett.* **26** 192.
- Tedrow P M and Meservey R 1973 *Phys. Rev. B* **7** 318.
- Theeuwens S J C H, Caro J, Schreurs K I, van Gorkom R P, Wellock K P, Gribov N N, Radelaar S, Jungblut R M, Oepts W, Coehoorn R and Kozub V I 2001 *J. Appl. Phys.* **89** 4442.
- Thomson W 1857 *Proc. Roy. Soc. (London)* **8** 546.
- Todo S, Siratori K and Kimura S 1995 *J. Phys. Soc. Japan* **64** 2118.
- Tokura Y, Urushibara A, Moritomo Y, Arima T, Asamitsu A, Kido G and Furukawa N 1994 *J. Phys. Soc. Japan* **63** 3931.
- Tokura Y and Tomioka Y 1999 *J. Magn. Magn. Mater.* **200** 1.
- Tomioka Y, Okuda T, Okimoto Y, Kumai R, Kobayashi K-I and Tokura Y 2000 *Phys. Rev. B* **61** 422.
- Tomioka Y, Asamitsu A and Tokura Y, 2001 *Phys. Rev. B* **63** 024421.
- Trajanovic Z, Kwon C, Robson M C, Kim K-C, Rajeswari M, Lofland S E, Bhagat S M and Fork D 1996 *Appl. Phys. Lett.* **69** 1005.
- Troyanchuk I P, Khalyavin D D, Hervieu M, Maignan A, Michel C and Petrowski K 1998 *phys. stat. sol. (a)* **169** R1.
- Tsujioka T, Mizokawa T, Okamoto J, Fujimori A, Nohara M, Takagi H, Yamaura K and Takano M 1997 *Phys. Rev. B* **56** R15509.
- Tsymbal E Yu and Pettifor D G 1997 *J. Phys.: Condens. Matter* **9** L411.
- Tsymbal E Yu and Pettifor D G 1998 *Phys. Rev. B* **58** 432.
- Uehara M, Mori S, Chen C H and Cheong S-W 1999 *Nature (London)* **399** 560.
- Uotani M, Taniyama T and Yamazaki Y 2000 *J. Appl. Phys.* **87** 5585.
- Upadhyay S K, Palanisami A, Louie R N and Buhrman R A 1998 *Phys. Rev. Lett.* **81** 3247.
- Urushibara A, Moritomo Y, Arima T, Asamitsu A, Kido G and Tokura Y 1995 *Phys. Rev. B* **51**, 14103.
- van den Brom W E and Volger J 1968 *Phys. Lett.* **26A** 197.
- van der Heijden P A A, Swüste C H W, de Jonge W J M, Gaines J M, van Eemeren J T W M and Shep K M 1999 *Phys. Rev. Lett.* **82** 1020.
- van der Zaag P J, Bloemen P J H, Gaines J M, Wolf R M, van der Heijden P A A, van de Veerdonk R J M and de Jonge W J M 2000 *J. Magn. Magn. Mater.* **211** 301.
- van Gorkom R P, Brataas A and Bauer G E W 1999 *Phys. Rev. Lett.* **83** 4401.
- van Gorkom R P, Caro J, Theeuwens S J C H, Wellock K P, Gribov N N and Radelaar S 1999 *Appl.*

- Phys. Lett.* **74** 422.
- van Hoof J B A N, Schep K M, Brataas A, Bauer G E W and Kelly P J 1999 *Phys. Rev. B* **59** 138.
- Varma C M 1996 *Phys. Rev. B* **54** 7328.
- Vas'ko V A, Larkin V A, Kraus P A, Nikolaev K R, Grupp D E, Nordman C A and Goldman A M 1997 *Phys. Rev. Lett.* **78** 1134.
- Vas'ko V A, Nikolaev K R, Larkin V A, Kraus P A and Goldman A M 1998 *Appl. Phys. Lett.* **73** 844.
- Venimadhav A, Hegde M S, Prasad V and Subramanyam S V 2000 *J. Phys. D: Appl. Phys.* **33** 2921.
- Ventura C I and Gusmão M A 2001 *cond-mat/0106319* preprint.
- Versluijs J J, Ott F and Coey J M D 1999 *Appl. Phys. Lett.* **75** 1152.
- Versluijs J J, Bari M, Ott F, Coey J M D and Revcolevschi A 2000 *J. Magn. Magn. Mater.* **211** 212.
- Versluijs J J, Bari M A and Coey J M D 2001 *Phys. Rev. Lett.* **87** 026601.
- Verwey E J W 1939 *Nature (London)* **144** 327.
- Viret M, Vignoles D, Cole D, Coey J M D, Allen W, Daniel D S and Gregg J F, 1996 *Phys. Rev. B* **53** 8464.
- Viret M, Drouet M, Nassar J, Contour J P, Fermon C and Fert A 1997a *Europhys. Lett.* **39** 545.
- Viret M, Ranno L and Coey J M D 1997b *Phys. Rev. B* **55** 8067.
- Viret M, Nassar J, Drouet M, Contour J P, Fermon C and Fert A 1999 *J. Magn. Magn. Mater.* **198-199** 1.
- Viret M, Samson Y, Warin P, Marty A, Ott F, Søndergård E, Klein O and Fermon C 2000 *Phys. Rev. Lett.* **85** 3962.
- Volger J 1954 *Physica* **20** 49.
- von Helmolt R, Wecker J, Holzapfel B, Schultz L and Samwer K 1993 *Phys. Rev. Lett.* **71** 2331.
- Wagner P, Gordon I, Trappeniers L, Vanacken J, Herlach F, Moshchalkov V V and Bruynseraede Y 1998 *Phys. Rev. Lett.* **81** 3980.
- Walter T, Dörr K, Müller K-H, Holzapfel B, Eckert D, Wolf M, Schläfer D, Schultz L and Grötzschel R 1999 *Appl. Phys. Lett.* **74** 2218.
- Wang H S and Li Q 1998 *Appl. Phys. Lett.* **73** 2360.
- Wang L, Yin J, Huang S, Hunag X, Xu J, Liu Z and Chen K 1999 *Phys. Rev. B* **60** R6976.
- Wang X and Zhang X-G 1999 *Phys. Rev. Lett.* **82** 4276.
- Wang X L, Dou S X, Liu H K, Ionescu M and Zeimet B 1998 *Appl. Phys. Lett.* **73** 396.
- Wegrowe J-E, Kelly D, Franck A, Gilbert S E and Ansermet J-Ph 1999 *Phys. Rev. Lett.* **82** 3681.
- Wegrowe J-E, Comment A, Jaccard Y, Ansermet J-Ph, Dempsey N M and Nozières J-P 2000 *Phys. Rev. B* **61** 12216.
- Wei J Y T, Yeh N-C and Vasquez R P 1997 *Phys. Rev. Lett.* **79** 5150.
- Wei J Y T, Yeh N-C, Vasquez R P and Gupta A 1998 *J. Appl. Phys.* **83** 7366.
- Weiß A, Loos J and Fehske H 2001 *Phys. Rev. B* **64** 104413.
- West R N 1995 *Proc. Int. School of Physics, 'Enrico Fermi'- Positron Spectroscopy of Solids* edited by Dupasquier A and Mills A P (IOS Press, Amsterdam).
- Westerburg W, Martin F, Friedrich S, Maier M and Jakob G 1999 *J. Appl. Phys.* **86** 2173.
- Westerburg W, Reisinger D and Jakob G 2000 *Phys. Rev. B* **62** R767.
- Wiesmann H, Gurvitch M, Lutz H, Ghosh A, Schwartz B, Strongin M, Allen P B and Halley J W 1977 *Phys. Rev. Lett.* **38** 782.
- Wolfman J, Prellier W, Simon Ch and Mercey B 1998 *J. Appl. Phys.* **83** 7186.
- Wollan E O and Koehler W C 1955 *Phys. Rev.* **100** 545.
- Worledge D C and Geballe T H 2000a *Appl. Phys. Lett.* **76** 900.
- Worledge D C and Geballe T H 2000b *Phys. Rev. Lett.* **85** 5182.
- Wu Y, Suzuki Y, Rüdiger U, Yu J, Kent A D, Nath T K and Eom C B 1999 *Appl. Phys. Lett.* **75** 2295.
- Xu R, Husmann A, Rosenbaum T F, Saboungi M-L, Enderby E J and Littlewood P B 1997 *Nature (London)* **390** 57.
- Yamada Y, Hino O, Nohdo S, Kanao R, Inami T and Katano S 1995 *Phys. Rev. Lett.* **77** 904 (1996).
- Yamaguchi S, Taniguchi H, Takagi H, Arima T and Tokura Y 1995 *J. Phys. Soc. Japan* **64** 1885.

- Yamanaka M and Nagaosa N 1996 *J. Phys. Soc. Japan* **65** 3088.
- Yamamoto R, Moritomo Y and Nakamura A 2000 *Phys. Rev. B* **61** R5062.
- Yanase A and Siratori K 1984 *J. Phys. Soc. Japan* **53** 312.
- Yanase A and Hamada N 1999 *J. Phys. Soc. Japan* **68** 1607.
- Yang Z, Tan S, Chen Z and Zhang Y 2000 *Phys. Rev. B* **62** 13872.
- Yeh N-C, Vasquez R P, Fu C C, Samoilov A V, Li Y and Vakili K 1999 *Phys. Rev. B* **60** 10522.
- Yin H Q, Zhou J-S, Zhou J-P, Dass R, McDevitt J T and Goodenough J B 1999 *Appl. Phys. Lett.* **75** 2812.
- Yin H Q, Zhou J-S and Goodenough J B 2000 *Appl. Phys. Lett.* **77** 714.
- Yoon S, Liu H L, Schollerer G, Cooper S L, Han P D, Payne D A, Cheong S-W and Fisk Z 1998 *Phys. Rev. B* **58** 2795.
- Yuan C L, Wang S G, Song W H, Yu T, Dai J M, Ye S L and Sun Y P 1999 *Appl. Phys. Lett.* **75** 3853.
- Zandbergen H W, Freisem S, Nojima T and Aarts J 1999 *Phys. Rev. B* **60** 10259.
- Zang J, Bishop A R and Röder H 1996 *Phys. Rev. B* **53** R8840.
- Zener C 1951 *Phys. Rev.* **82** 403.
- Zeng Z, Greenblatt M and Croft M 1998 *Phys. Rev. B* **58** R595.
- Zeng Z, Greenblatt M, Subramanian M A and Croft M 1999 *Phys. Rev. Lett.* **82** 3164.
- Zhang J and White R M 1998 *J. Appl. Phys.* **83** 6512.
- Zhang J, Dai P, Fernandez-Baca J A, Plummer E W, Tomioka Y and Tokura Y 2001 *Phys. Rev. Lett.* **86** 3823.
- Zhang S and Yang Z 1996 *J. Appl. Phys.* **79** 7398.
- Zhang S, Levy P M, Marley A C and Parkin S S P 1997a *Phys. Rev. Lett.* **79** 3744.
- Zhang N, Ding W, Zhong W, Xing D and Du Y 1997b *Phys. Rev. B* **56** 8138.
- Zhao G, Hunt M B and Keller H 1997 *Phys. Rev. Lett.* **78** 955.
- Zhao G, Smolyaninova V, Prellier W and Keller H 2000a *Phys. Rev. Lett.* **84** 6086.
- Zhao G, Wang Y S, Kang D J, Prellier W, Rajeswari M, Keller H, Venkatesan T, Chu C W and Green R L 2000b *Phys. Rev. B* **62** R11949.
- Zhao G, Keller H, Prellier W and Kang D J 2001 *Phys. Rev. B* **63** 172411.
- Zhou J P, McDevitt J T, Zhou J-S, Yin H Q, Goodenough J B, Gim Y and Jia Q X 1999 *Appl. Phys. Lett.* **75** 1146.
- Zhou J-S, Goodenough J B, Asamitsu A and Tokura Y 1997 *Phys. Rev. Lett.* **79** 3234.
- Zhou J-S and Goodenough J B 1998 *Phys. Rev. Lett.* **80** 2665.
- Zhou J-S and Goodenough J B 1999 *Phys. Rev. B* **60** R15002.
- Zhou J-S and Goodenough J B 2000 *Phys. Rev. B* **62** 3834.
- Zhou J-S and Goodenough J B 2001 *Phys. Rev. B* **64** 024421.
- Zhou J-S, Yin H Q and Goodenough J B 2001 *Phys. Rev. B* **63** 184423.
- Zhu J-X, Friedman B and Ting C S 1999 *Phys. Rev. B* **59** 9558.
- Zhu T, Shen B G, Sun J R, Zhao H W and Zhan W S 2001 *Appl. Phys. Lett.* **78** 3863.
- Ziese M, Sena S P, Shearwood C, Blythe H J, Gibbs M R J and Gehring G A 1998a *Phys. Rev. B* **57** 2963.
- Ziese M, Srinitiwawong C and Shearwood C, 1998b *J. Phys.: Condens. Matter* **10** L659.
- Ziese M and Sena S P 1998 *J. Phys.: Condens. Matter* **10** 2727.
- Ziese M and Srinitiwawong C 1998 *Phys. Rev. B* **58** 11519.
- Ziese M 1999 *Phys. Rev. B* **60** R738.
- Ziese M and Srinitiwawong C 1999 *Europhys. Lett.* **45** 256 .
- Ziese M, Heydon G, Höhne R, Esquinazi P and Dienelt J 1999a *Appl. Phys. Lett.* **74** 1481.
- Ziese M, Sena S P and Blythe H J 1999b *J. Magn. Magn. Mater.* **202** 292.
- Ziese M, Sena S P and Blythe H J 1999c *J. Appl. Phys.* submitted.
- Ziese M 2000a *Phil. Trans. R. Soc. Lond. A* **358** 137.
- Ziese M 2000b *Phys. Rev. B* **62** 1044.
- Ziese M and Blythe H J 2000 *J. Phys.: Condens. Matter* **12** 13.

Ziese M 2001a *J. Phys.: Condens. Matter* **13** 2919.  
Ziese M 2001b *phys. stat. sol. (b)* **228** R1.  
Ziese M and Thornton M J (Eds.) 2001 *Spin Electronics* (Springer, Heidelberg).